

NASA CONTRACTOR REPORT



NASA CR-255

NASA CR-255

FACILITY FORM 602

N65-28054

(ACCESSION NUMBER)

204

(PAGES)

(NASA CR OR TMX OR AD NUMBER)

(THRU)

(CODE)

28

(CATEGORY)

DEVELOPMENT OF A HYDROGEN-OXYGEN INTERNAL COMBUSTION ENGINE SPACE POWER SYSTEM

by *N. E. Morgan and W. D. Morath*

Prepared under Contract No. NAS 3-2787 by

VICKERS, INC.

Detroit, Mich.

for

GPO PRICE \$

CFSTI PRICE(S) \$ 6.50

Hard copy (HC)

Microfiche (MF) 1.25

ff 653 July 65

DEVELOPMENT OF A HYDROGEN-OXYGEN INTERNAL COMBUSTION
ENGINE SPACE POWER SYSTEM

By N. E. Morgan and W. D. Morath

Distribution of this report is provided in the interest of information exchange. Responsibility for the contents resides in the author or organization that prepared it.

Prepared under Contract No. NAS 3-2787 by
VICKERS, INC.
Detroit, Mich.

for

NATIONAL AERONAUTICS AND SPACE ADMINISTRATION

TABLE OF CONTENTS

<u>Section</u>	<u>Title</u>	<u>Page</u>
1.0	INTRODUCTION - SUMMARY AND CONCLUSIONS	1
1.1	Introduction	1
1.2	Summary	2
1.2.1	Prototype Engine	2
1.2.2	Prototype Compressor	5
1.3	Conclusion and Recommendations	6
1.3.1	Conclusions	7
1.3.2	Recommendations	9
1.3.2.1	Engine	9
1.3.2.2	Compressor	11
2.0	POWER SYSTEM DESCRIPTION	14
2.1	System Concept	14
2.2	Proposed Flight System	14
3.0	PROTOTYPE ENGINE DEVELOPMENT	22
3.1	Design Evolution and Description	22
3.1.1	Summary	22
3.1.2	Oxygen Injector	27
3.1.2.1	Mounting and Lubricated Drive Section	27
3.1.2.2	Quill Shaft and Internal Pivot Bearings	39
3.1.2.3	Poppet and Seat Guide	40
3.1.2.4	Rocker Arm and Poppet	44
3.1.3	Cylinder, Piston, and Cylinder Head Ring	47
3.1.4	Hydrogen Valve	56
3.1.5	Cylinder Head Insert and Seal	62
3.1.6	Starting	68
3.1.7	Lubrication	70
3.2	Mechanical Problem Summary	73
3.3	Engine Testing	74

TABLE OF CONTENTS (Continued)

<u>Section</u>	<u>Title</u>	<u>Page</u>
3.3.1	Test Equipment and Instrumentation	76
3.3.2	Endurance Test Results	88
3.3.3	Engine Performance Tests	100
4.0	PROTOTYPE COMPRESSOR DEVELOPMENT	131
4.1	Design, Description and Evolution	131
4.2	Test Equipment and Instrumentation	140
4.3	Prototype Compressor Testing	144
4.3.1	Endurance Test	145
4.3.2	Calibration Tests	151
4.3.2.1	First Stage Compressor Calibration Test Results	151
4.3.2.2	Two-Stage Calibration Results	161
4.3.3	Accuracy of Compressor Test Results	166
4.3.4	Discussion of Compressor Test Results	169
	REFERENCES	178
	APPENDIX A - Failure Report and Summary Sheets	179
	APPENDIX B - Derivation of Engine Input Energy	186
	APPENDIX C - Analysis Letter	194
	APPENDIX D - Performance Graph	195
	APPENDIX E - Sample Data Sheets and Data Reduction Forms	196

I. 0 INTRODUCTION ~ SUMMARY AND CONCLUSIONS

1. 1 Introduction

This report describes the results of work accomplished under NASA Contract NAS 3-2787 between July 1, 1963 and August 31, 1964. The basic objectives of the program were to conduct engineering studies, design studies, fabrication, performance testing, and endurance testing leading to the design of an auxiliary power generation unit capable of operating in a space environment, utilizing hydrogen and oxygen as reactants. The work was performed under the technical management of Harry M. Cameron, Lewis Research Center, Cleveland, Ohio.

This program was a continuation of work previously conducted under NASA Contract NAS 3-2550 which in turn was based on feasibility demonstrations performed under USAF-ASD Contract AF 33(616)8406. Under the ASD contract, the feasibility of operating an internal combustion engine on hydrogen and oxygen was demonstrated, and the oxygen injection type engine was determined to have performance characteristics superior to the carburetted type. During the program conducted under NASA Contract NAS 3-2550, development testing of the oxygen injection type engine was continued and development testing was initiated on a cryogenic hydrogen compressor and a recuperative heat exchanger. Concurrently with the component development work, analytical and design studies were conducted to provide, in conjunction with the test program, a sound basis for the preliminary design of a space auxiliary power system. The results of that program are reported in Reference 1.

The program described in this report, conducted under NASA Contract NAS 3-2787, included continuation of development testing of the components and endurance test demonstrations on

the hydrogen-oxygen I. C. engine. During the first part of the program the major portion of effort was devoted to modification and performance improvement of the prototype engine and compressor and to building up the necessary new test facilities. During the latter part of the program, the emphasis was entirely on engine endurance testing.

1.2 Summary

- 1.2.1 Prototype Engine - The prototype engine development effort consisted of design studies, hardware modifications, performance and endurance test evaluation, and the fabrication and procurement of new test equipment and instrumentation. Major re-design effort was concentrated on the oxygen injector, the hydrogen valve, the piston and cylinder, and the combustion chamber. The new test equipment consisted of: an electric dynamometer; an electric hydrogen heater for each of the two test stands; a closed loop cylinder cooling system (using Dowtherm A coolant) shared by both test stands; an exhaust vacuum pump and associated plumbing shared by both test stands; and a balanced pressure transducer system for obtaining cylinder pressure data.

Engine performance development resulted in a marked reduction in specific propellant consumption (BSPC) compared with past experience. The lowest BSPC consistently observed during this program was 1.6 lbs/hp-hr, which was 30% less than the 2.3 lb/hp-hr achieved during the previous contract. Figure 1-1 shows minimum BSPC versus horsepower curves for each of the two programs.

The curve shown in Figure 1-1 for the present contract represents performance with a hydrogen inlet temperature of approximately 500°F, and an exhaust pressure of less than 6 psia, whereas

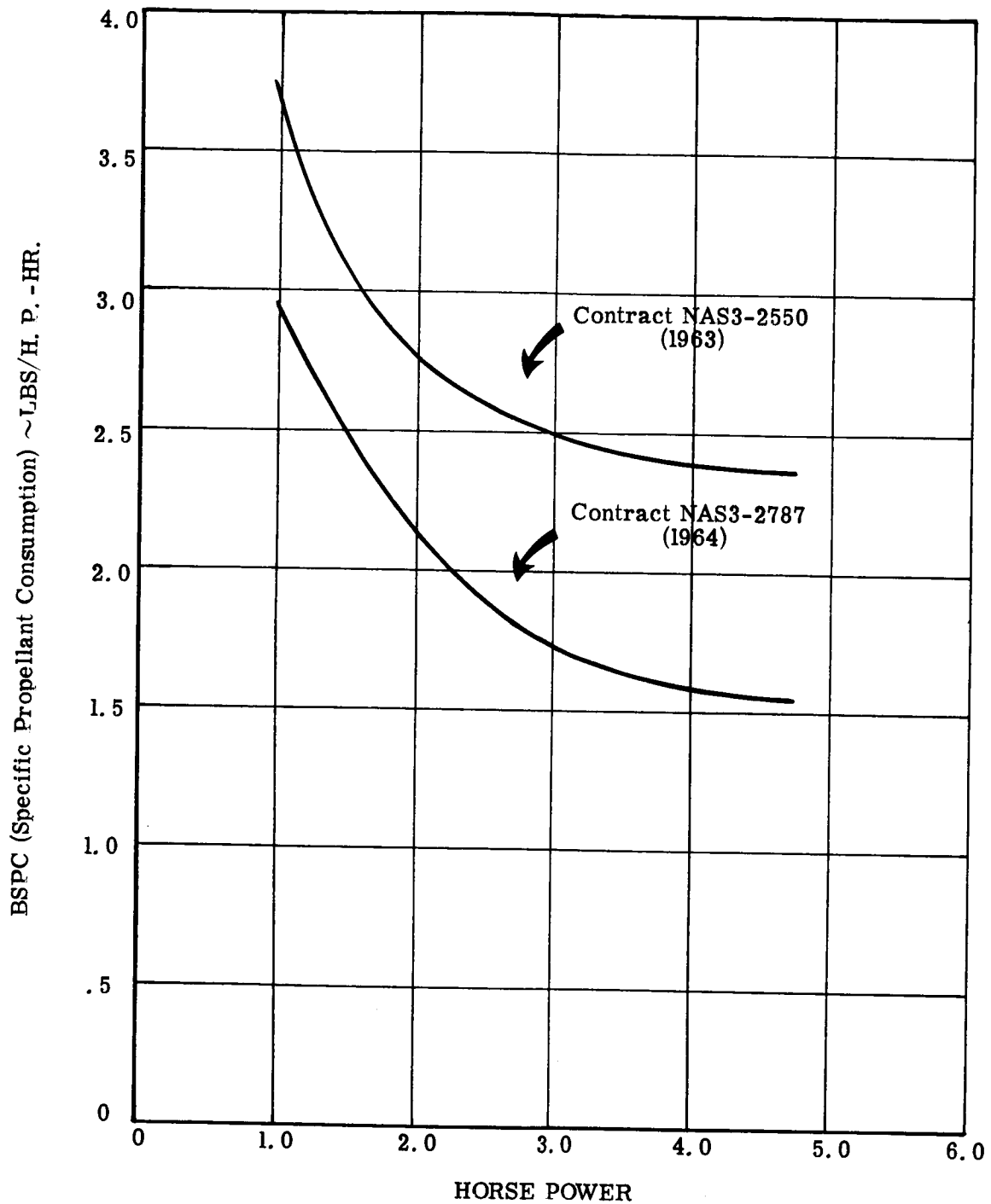


Fig. 1-1 - Improvement in Specific Propellant Consumption

the curve shown for the previous contract is for conditions of ambient hydrogen inlet temperature and ambient exhaust. Of equal importance to the more realistic operating conditions in improving performance were mechanical refinements such as reducing exhaust port restriction, reducing cylinder leakage through use of better piston rings, and piston and cylinder design improvements.

A total of 619 hours of endurance testing was accumulated on two engines with the longest continuous run being 120 hours. Five runs in excess of 65 hours were made. In addition to the endurance testing, approximately 108 hours of engine performance type testing were logged, consisting of numerous tests up to about 2 hours duration each.

The major accomplishment of extended engine endurance life has resulted primarily from mechanical design refinements and materials selection in the oxygen injector. At the beginning of the program, injector life was limited to 1 to 2 hours because of excessive wear, galling, and fatigue failures of injector parts. By the end of the program it appeared that oxygen injector life problems had been mainly resolved and engine life would now be limited by more conventional problems such as valve spring fatigue life and valve lifter wear. Problems of this latter type are common to all long life internal combustion engines and can normally be resolved within the limits of available technology.

Other major problems still unresolved at the end of the program include excessive oil consumption and difficulties of reliable restarting. The major portion of the oil loss appears to be from leakage past the oil control ring on the piston directly out the exhaust ports into the exhaust system. Modifications to the cylinder lubrication system to reduce the amount of oil supplied to the cylinder, in conjunction with revised oil control ring

configuration, is expected to reduce oil consumption to acceptable values.

Tests show that the palladium catalyst used for initiating combustion during engine start-up loses its effectiveness after about 3 hours of engine operation. Reliable restart capability is dependent upon achieving a much longer catalyst life or developing an alternate type of ignition system, such as spark or glow-plug ignition.

1. 2. 2 Prototype Compressor - Approximately 12% of the overall program effort was devoted to development of the prototype compressor. Extensive design changes were made on the drive system and the piston seals of the prototype compressor previously fabricated under NASA Contract NAS 3-2550. The test setup and instrumentation were greatly improved as the level of the compressor performance was improved.

The compressor development effort was primarily concentrated on solutions to two problems. One problem was the development of a dynamic piston-to-cylinder seal that would effectively seal hydrogen gas over a wide temperature and pressure range without incurring high friction losses; the other, to select a material for use as a low friction, non-lubricated drive system bearing operating in a hydrogen atmosphere with a wide temperature range. These two problems were solved and the results demonstrated were as good as could reasonably be expected within the limitations of the test equipment and budget.

All testing was done with gas temperatures between -320°F and room temperature. Both Rulon A and Rulon LD were demonstrated to be suitable bearing materials. The final piston-to-cylinder seal design is a hybrid design which incorporates the advantages and eliminates the disadvantages of two different

approaches. The use of piston rings allows for fluctuating dimensions due to temperature change, but high friction losses were incurred in obtaining a good seal. A good seal can be obtained with low friction by using a ringless piston with very small clearance with the bore, but this design will not readily tolerate temperature changes. The piston design developed during the program is ringless, has a sufficient clearance with the bore to tolerate temperature change, and incorporates a continuous flexible sealing edge which results in excellent sealing with only moderate friction. The integrity of the piston and internal bearing design was demonstrated during a 100 hour endurance run.

In spite of these improvements the achievement of satisfactory compressor performance was limited by inadequate valve response and flow area, and by deflections in the internal drive linkage and in the external linkage of the test stand. Insight has been gained as to how to solve these problems, but effort was not directed in these areas because personnel and funds were more urgently needed for the engine endurance test effort.

The highest overall thermal efficiency achieved on the compressor was 46% with two stage operation at 2500 rpm and a pressure ratio of 11:1. The highest overall efficiency at a pressure of 20:1 (which will result in the design value of 300 psia discharge pressure), was 42% at 3000 rpm with two stage operation.

1.3 Conclusion and Recommendations

The results of this program, and the insight gained by the development effort to date, strongly indicate that a prototype engine can be developed that will operate continuously for its design life of 500 hours without adjustment or degradation

of performance and that by further reduction of heat losses and friction losses and improvements in combustion, a lower specific propellant consumption can be achieved.

1.3.1 Conclusions - Specific conclusions resulting from the work conducted on the prototype components are:

1. The increased endurance capability of the oxygen injector demonstrated during this program makes future improvement look promising. Basically, the ultimate endurance life of the engine now depends on the wear rates at two points in the oxygen injector and the solution of conventional engine development problems; specifically, hydrogen valve spring and lifter life.
2. Further reductions in specific propellant consumption should be achievable, particularly at low horsepower levels, by increasing hydrogen inlet temperature, by improving combustion chamber design, by reducing heat rejection from the cylinder and/or by recuperating the heat rejected from the cylinder and cylinder head to the incoming hydrogen.
3. The catalyst pellets now being used are not suitable for re-starting the engine.
4. The loss of oil from the engine during vacuum exhaust operation is high and requires further development efforts.
5. The compressor piston seal is satisfactory at liquid nitrogen temperature and above, but its operational characteristics must still be ascertained at liquid hydrogen temperatures.
6. While Rulon has proved to be a satisfactory material for use in the piston and in the compressor internal drive linkage,

its use for bearing construction is unsatisfactory because of its excessive resiliency.

7. The valves, now incorporated in the compressor head, have inadequate frequency response and flow area, which results in excessive heat transfer from discharge to inlet gas. This seriously limits compressor performance.
8. While retaining the present Rulon piston seal design, further increases in compressor overall efficiency, operating speed range, and operating temperature range should be achieved by redesigning for single stage compression with: a springless inlet valve-in-piston; a discharge valve in the cylinder head with a seating diameter equal to or larger than the cylinder bore, and with as few rubbing surfaces as possible in contact with the incoming fluid.
9. When fully developed, a space power system employing the hydrogen-oxygen internal combustion engine promises to provide a number of unique features which make it attractive for many space applications. Among its advantages are low specific dry weight, particularly at power levels of several kilowatts; mechanical shaft power without conversion equipment; multiple output capability such as ac and dc electrical power, shaft power, and hydraulic power, all from the same machine; self-cooling without significant penalty in propellant consumption; the ability to utilize cryogenic propellant boil-off, even contaminated boil-off; quick starting and restarting; and relative insensitivity to environmental extremes.

1.3.2 Recommendations

1.3.2.1 Engine

The engine has been developed to the point where a flight-type design study could be started, if it were required for a specific application. Some of the remaining development problems are of the type which could best be solved with redesigned flight-type hardware although many of them can be solved or partially solved by continued development of the existing prototype hardware. It is recommended that the development of the prototype engine be continued, concurrent with the design of a flight system. The following tasks must be accomplished before a flight system can be finalized:

A. Oxygen Injector

1. Balance the wear rates at each end of the poppet so that the poppet lift adjustment does not change greatly during its operational life.
2. Modify the oxygen cam cover so that the poppet lift and lash adjustment can be made without its removal.

B. Hydrogen Valve

1. Reduce the working stress level of the valve springs to insure that they will not fail during a 500 hour mission. (Basically, a new engine design will be required to accomplish this; however, stress levels can be reduced sufficiently in the prototype engine to make a 500 hour test without much risk of failure).

B. Hydrogen Valve, cont.

2. Modify the design of the outer valve lifter to reduce wear.
3. Evaluate methods of hard surfacing (such as flame plating) valve stems as insurance against the possibility that prolonged engine operation will cause excessive lubricating oil consumption due to valve stem and guide wear.

C. Delay selection of a final cylinder material until a fair evaluation can be made. Both T-15 tool steel and cast iron cylinders have been used. Running time on the cast iron cylinder was too short to evaluate wear. Cast iron offers the advantages of good lubrication retention and easy machineability.

D. Combustion Chamber

1. Continue combustion chamber experimentation as long as other engine developmental testing is being done. It is a trial and error process which may result in substantial performance improvements.
2. Try to replace the "K" seal between the combustion chamber and the cylinder head ring with a seal which has less free volume and lower unit cost. (The "K" seal functioned satisfactorily during the latter part of the program but its replacement each time the combustion chamber was removed may be an unnecessary expense. An alternate sealing method functioned satisfactorily during 5 hours of test).

E. Restart Capability

1. Evaluation of catalytic methods of starting and re-starting the engine should be continued.
2. As a back-up to catalytic approach, develop an ignition system incorporating a glow plug in the cylinder head.

F. Lubrication System

1. Develop a lubrication system to minimize oil consumption and evolve a flight system lubrication concept suitable for zero G operation (initial work can be accomplished with the prototype hardware).

G. Control

1. Establish the optimum method of power control. This will depend on the load profile of the specific mission for which the flight-type power system is designed.

H. Preheating and Engine Cooling

1. Establish the optimum method of preheating propellants, and cooling the engine, based on the requirements of the mission for which the flight-type system is designed.

1.3.2.2 Compressor

The inadequacies of the prototype compressor drive linkage and

valving, and the fact that single stage compression appears to be desirable, dictate that a new compressor design must eventually be developed. However, the operational characteristics of the piston seal and the Rulon bearing material must yet be determined at liquid hydrogen temperatures. Also, sizing of a new compressor will depend upon accurately predicting its performance characteristics. Therefore, it is recommended that the present hardware be modified to evaluate the performance of new valving concepts and to determine the characteristics of the Rulon piston seal and bearing materials at liquid hydrogen temperatures as outlined in the following steps:

A. Modify Prototype Hardware

1. Rework the first stage end of the prototype piston to incorporate a springless inlet valve.
2. Fabricate a new first stage cylinder head incorporating a discharge valve with a seating diameter equal to or greater than the cylinder bore diameter. This will allow minimum clearance volume to be achieved, since the valve may be hit by the piston without damage when the compressor speed and discharge pressure are low.

B. Adjust and Test Modified Prototype Compressor

1. Statically adjust the piston stroke so that when the piston is at TDC it extends beyond the end of the cylinder by an amount which will compensate for the deflection of drive linkage, and result in a minimum clearance volume when operating at a desired speed and pressure.

2. Bring inlet H_2 in through the drive case, and evaluate performance at LN_2 and LH_2 temperatures.

C. Design New Compressor

1. Design a new single stage compressor based upon the data collected in Step B, which incorporates a rigid drive linkage with few rubbing parts in contact with or conducting heat to the incoming gas.

2.0 POWER SYSTEM DESCRIPTION

2.1 System Concept

For the requirements of this program, parametric studies have shown that the best system configuration consists of a H_2-O_2 internal combustion engine driving an alternator directly at engine speed. A recuperative heat exchanger, which pre-heats incoming propellants with engine exhaust waste heat, contributes to the low propellant consumption of the system. Propellant is supplied to the system from either supercritical tankage or as boil-off gases from propulsion tanks. When operating on boil-off, an engine driven compressor boosts the propellant pressure to that required for engine operation. Relevant background material describing the evolution of this power system concept may be found in References 1, 2, 3, and 4.

A schematic diagram representing the recuperative system concept is shown in Figure 2-1. This figure also illustrates the multiple output capabilities of the system such as the possibility of providing electrical, mechanical or hydraulic outputs, either singly or in combination. Possible applications indicated are electrical power generation, portable power source for tools and mechanical equipment, and propulsion for lunar surface vehicles. The schematic also shows how a system could be arranged to utilize propellant from either supercritical storage tanks or from rocket propulsion tankage boil-off.

2.2 Proposed Flight System

Preliminary design studies conducted previously under NASA Contract NAS 3-2550 resulted in a power plant configuration

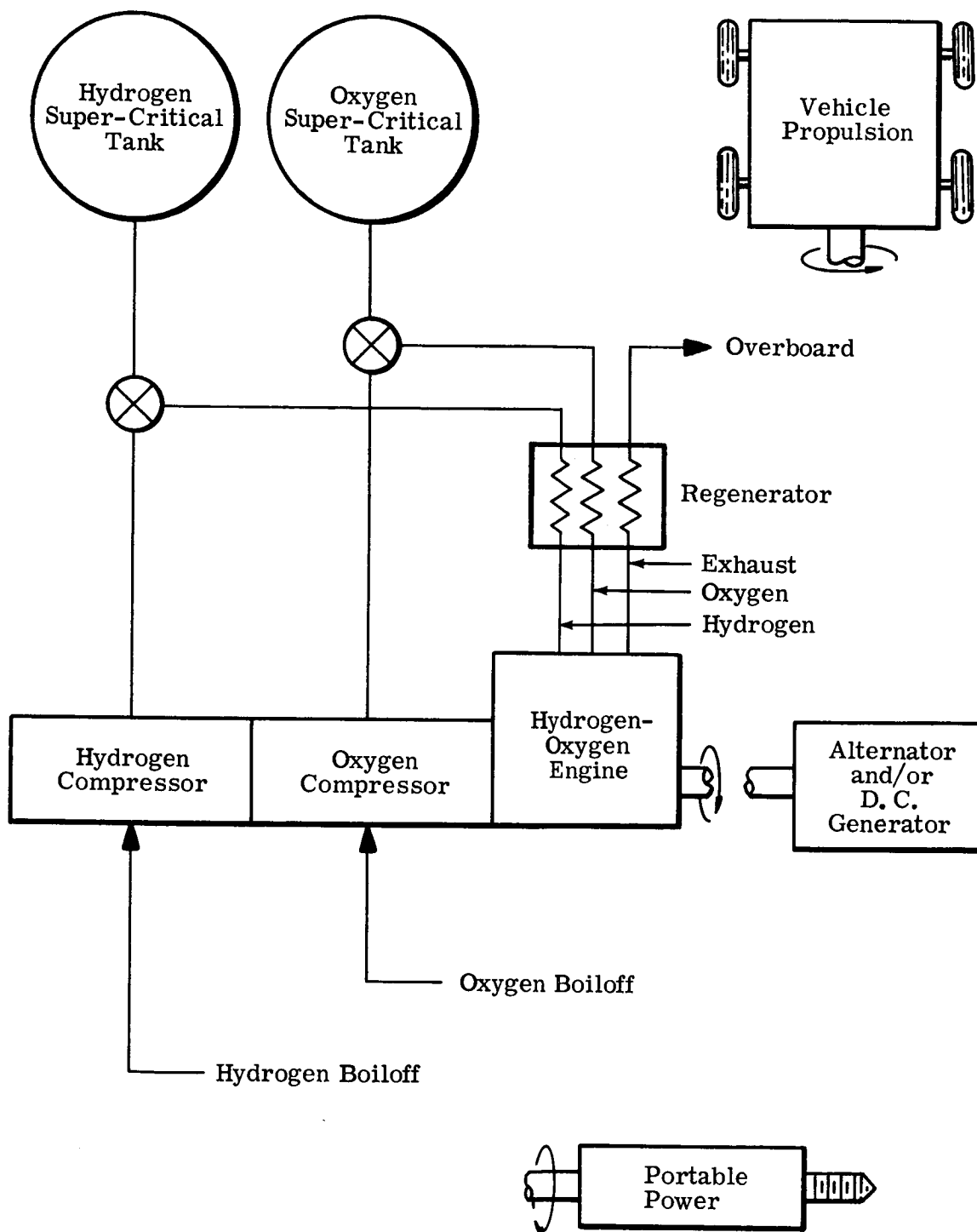


Fig. 2-1 - Hydrogen-Oxygen Power System Concept

shown in Figure 2-2. This is a conceptual drawing of how the engine, alternator and boil-off compressors might be arranged into a compact integrated power unit. In this design, the alternator rotor is arranged outside of the stator to act as a large flywheel for the single cylinder engine. The excitation windings are arranged in the conventional manner and are located inside the main stator. This arrangement has the further advantage of allowing very stable speed regulation with a relatively simple speed control system. For starting, AC power from a battery and inverter is supplied to the alternator, causing it to operate as an induction motor, thus rotating the engine. This system is described in detail in Reference 1.

The estimated dry weight (excluding propellants and tankage) of power systems employing the hydrogen-oxygen engine is shown in Figure 2-3 as a function of power. At 2 kw it will be noted that the system's specific weight is much lower than current fuel cells and about equal to the specific weight predicted for future lightweight fuel cells. At higher power levels, the specific weight of the mechanical power system is even lower. An estimated weight breakdown for a 3 kw system is shown in Table 2-1.

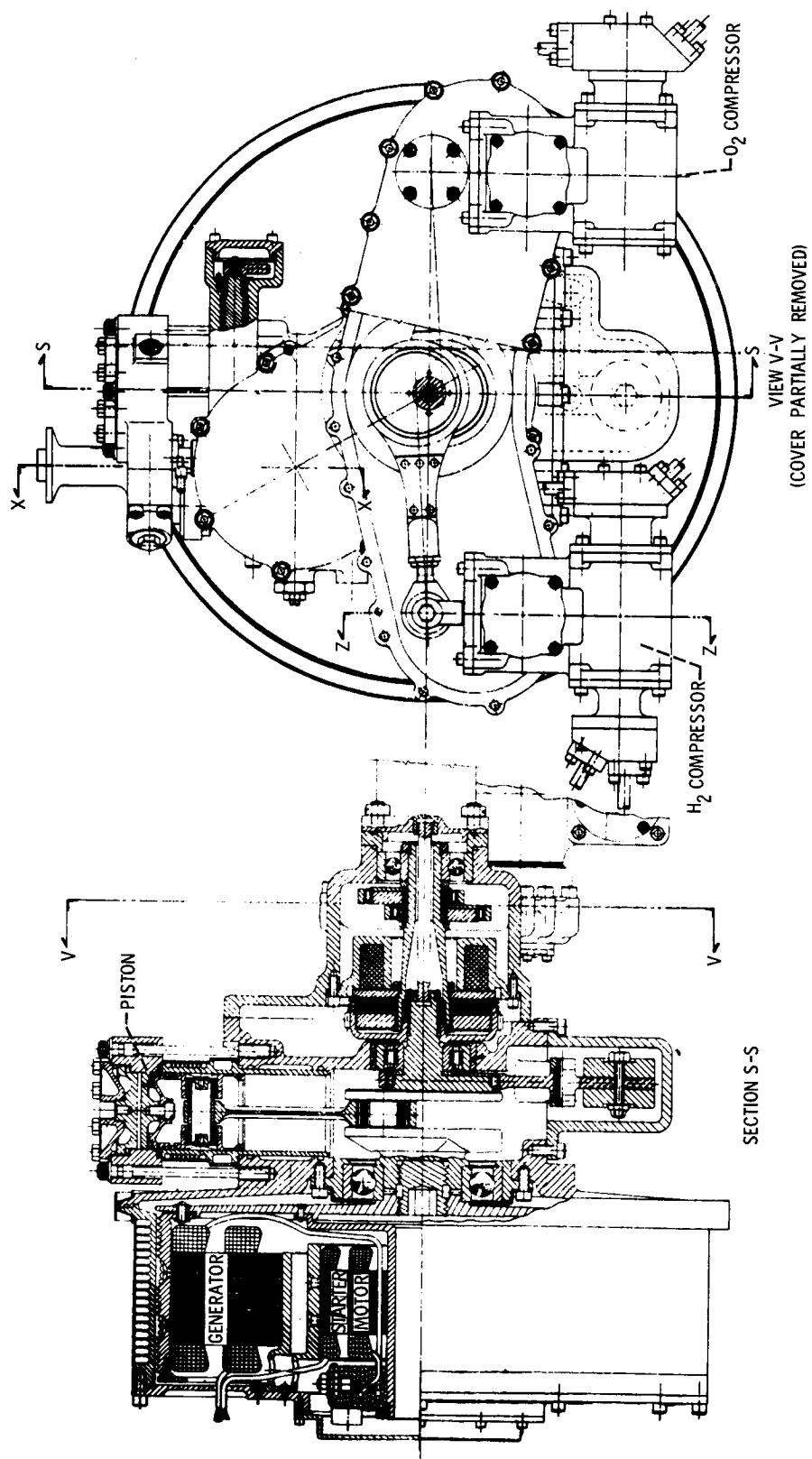


Fig. 2-2(A) - Conceptual Drawing of H_2-O_2 I. C. Power System.

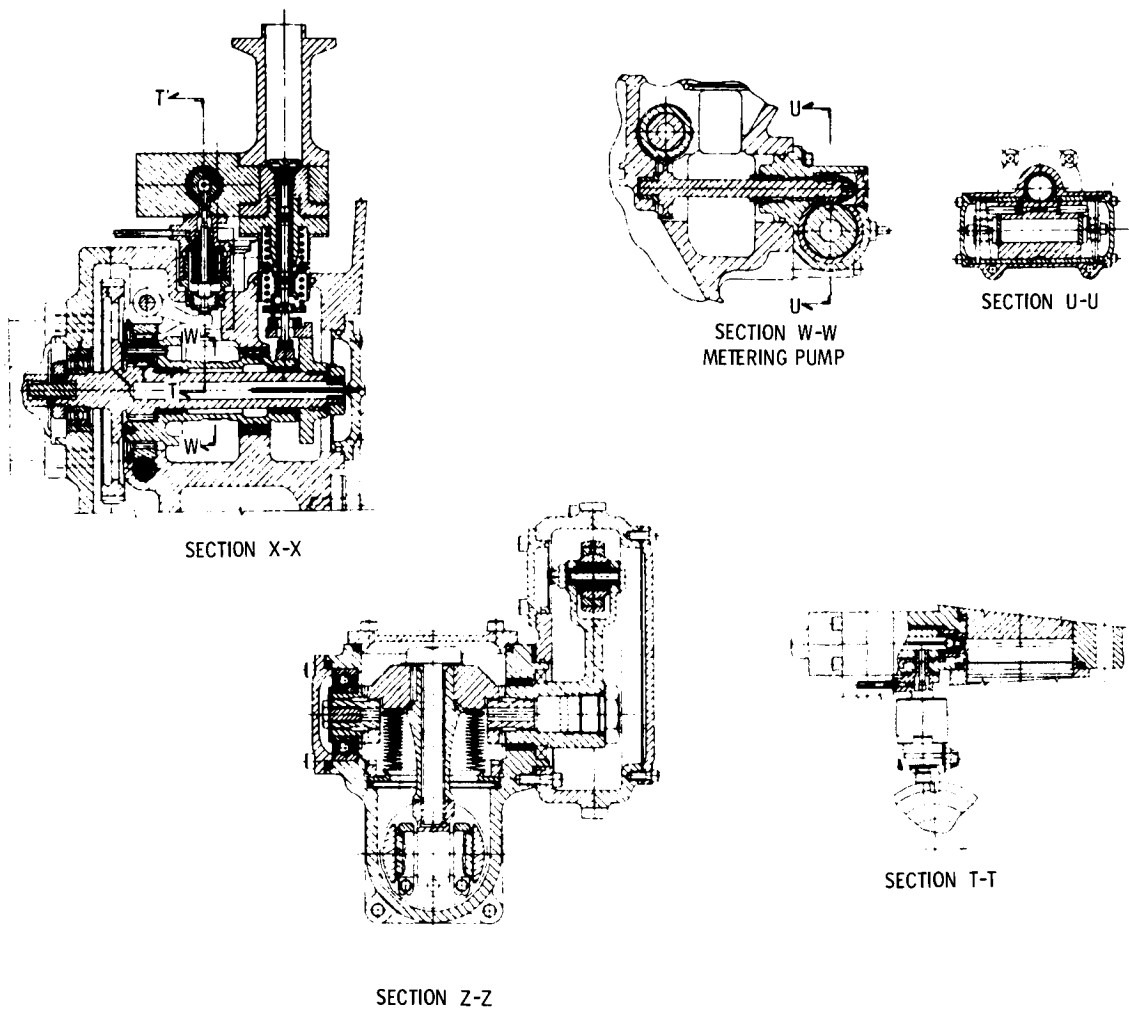


Fig. 2-2(B) - Assembly Drawing of H_2-O_2 I. C. Power System.

TABLE 2-1
3 kw System Dry Weight*

H ₂ -O ₂ Engine	14 lbs
Regenerator	12
Alternator & Exciter	35
H ₂ Compressor	6 **
O ₂ Compressor	4 **
Voltage Regulator	1
Inverter	9
Controls	6
Plumbing	5
Battery	8
<hr/>	
Total	100 lbs

* Radiator weight is not included because the power system may share heat rejection elements with other vehicle systems which must be cooled. Common radiator usage may be accomplished without significant radiator weight being charged to the power system, since the system can probably raise the average radiator rejection temperature and thus allow the additional heat to be rejected without a major increase in radiator area.

** Required only for operation with boil-off gases.

The total system weight including reactants and supercritical tankage is shown as a function of mission duration for 2 kw and 3 kw in Figure 2-4. These curves are based on currently demonstrated consumption rates of 2.2 lb/kw hr. Since this value has been measured at the engine shaft, it does not make allowance for generator inefficiency and other parasitic losses (e.g., power requirements for controls and pumps). It is expected, however, that improvement in fuel consumption rates can be achieved to make up for the parasitic losses. Hence, these curves represent conservative system weight estimates.

Another factor to be considered in a flight system is heat dissipation. When operating with an O/F ratio less than 1.3, there is sufficient heat capacity in the hydrogen fuel to absorb all of the waste heat of the power system. Thus, the need for a radiator to dissipate power system waste heat would be avoided. This could be a significant advantage for emergency power applications, re-entry vehicles, and wherever a lightweight, easily portable power plant is required. Since the design point for the O/F ratio is 2, this would, however, result in increased hydrogen consumption and tankage weight. Therefore, for any specific application the alternative of using excess hydrogen or radiative heat rejection must be carefully weighed.

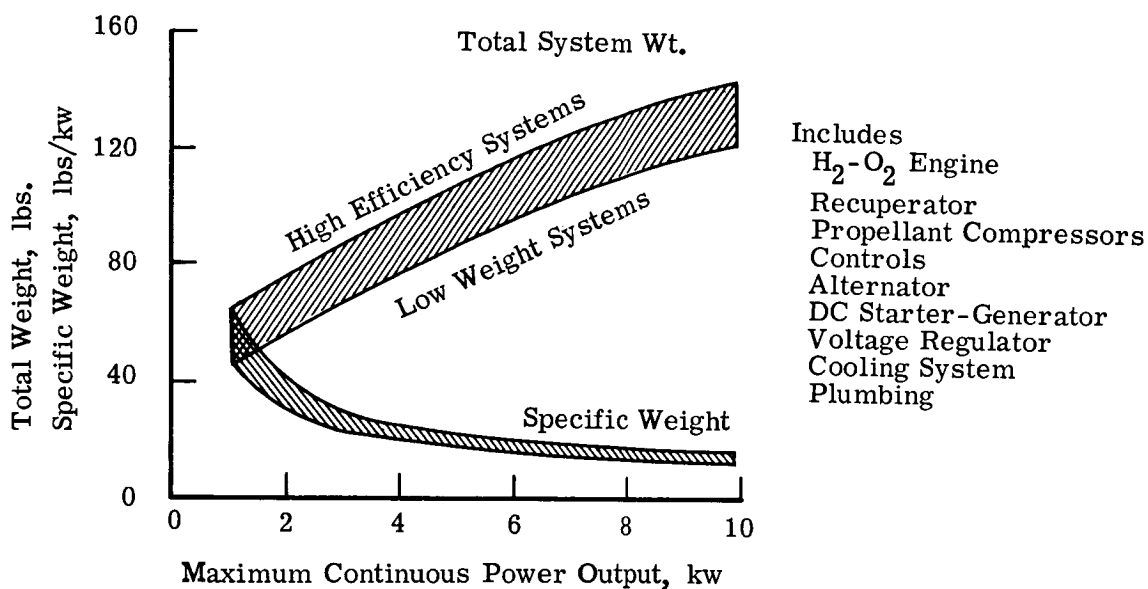


Fig. 2-3 - Power System Dry Weight

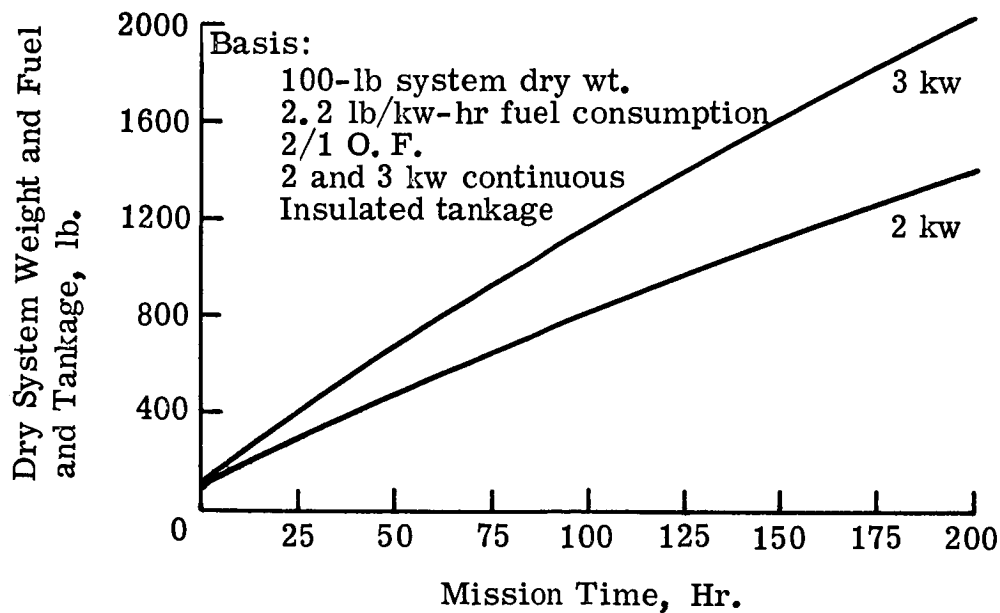


Fig. 2-4 - System Weight vs. Mission Time

3.0 PROTOTYPE ENGINE DEVELOPMENT

3.1 Design Evolution and Description

3.1.1 Summary - Figure 3-1 is a photograph showing the prototype engine. The external appearance of the engine was not greatly altered during the course of the program. The basic operating principles were adhered to while integrity of the hardware was improved by making design changes based upon the evaluation of test results.

A comparison of Figures 3-2 and 3-3, which are sections of assembly drawings of the initial and final configuration respectively, show the overall degree to which the hardware was changed. As was anticipated at the beginning of the program, the oxygen injector presented the most difficulties, since its design and application were the greatest departure from state-of-the-art technology. It went through the greatest design evolution and as a result of this effort demonstrated the most outstanding degree of improvement of any engine components. The injector is no longer the critical component which limits the useful engine life. However, further effort is required to minimize and make self-compensating the wear rates of internal contact surfaces so that the lift adjustment of the injector does not change significantly with running time.

Next to the oxygen injector, the cylinder, piston, combustion chamber, and associated seals presented the greatest departure from state-of-the-art technology because of their elevated operating temperatures, direct oxygen impingement, and the problems of sealing hydrogen gas. The piston has been developed to a satisfactory configuration except for the requirement of

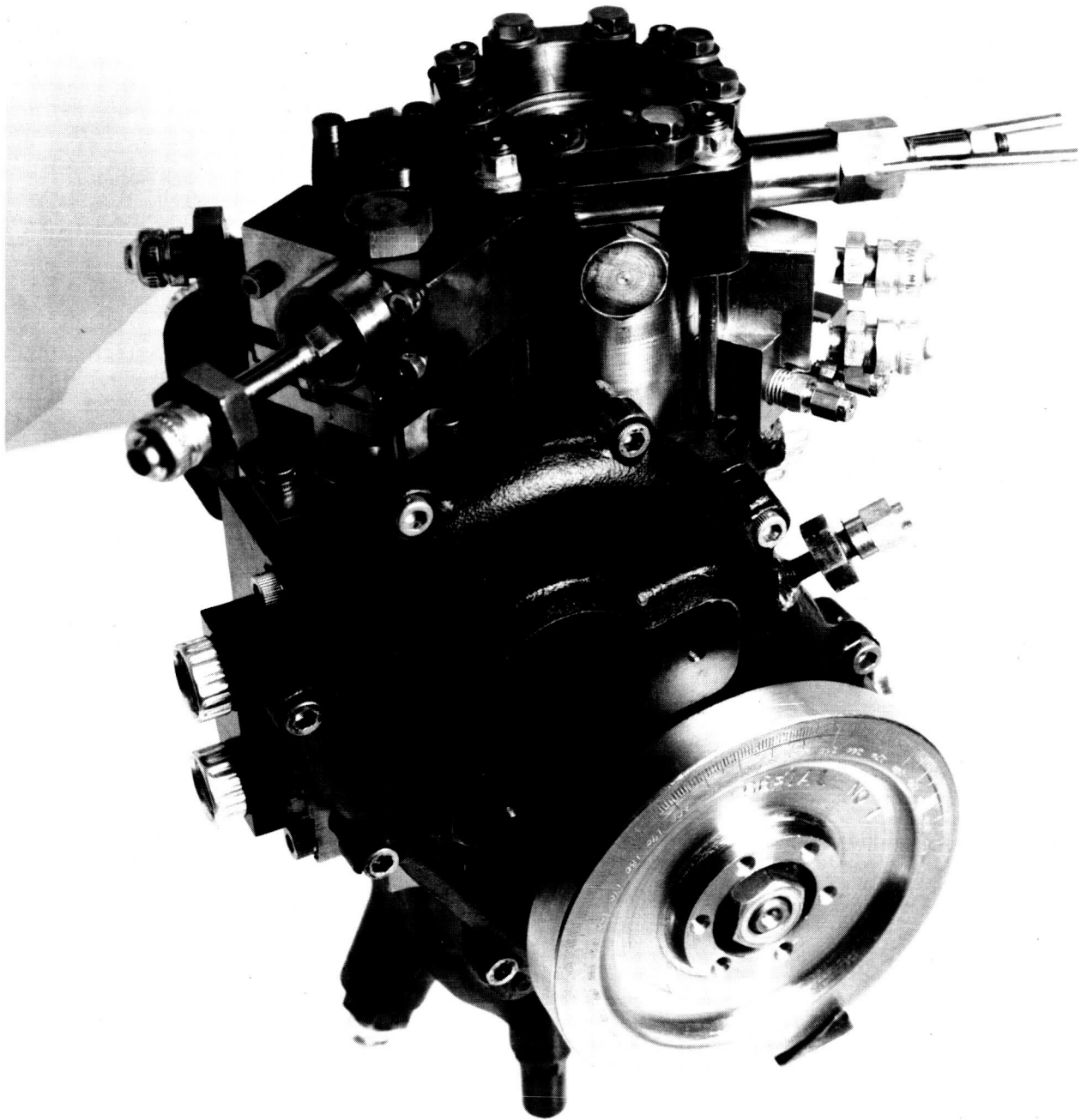


Fig. 3-1 - Prototype Engine at End of Program

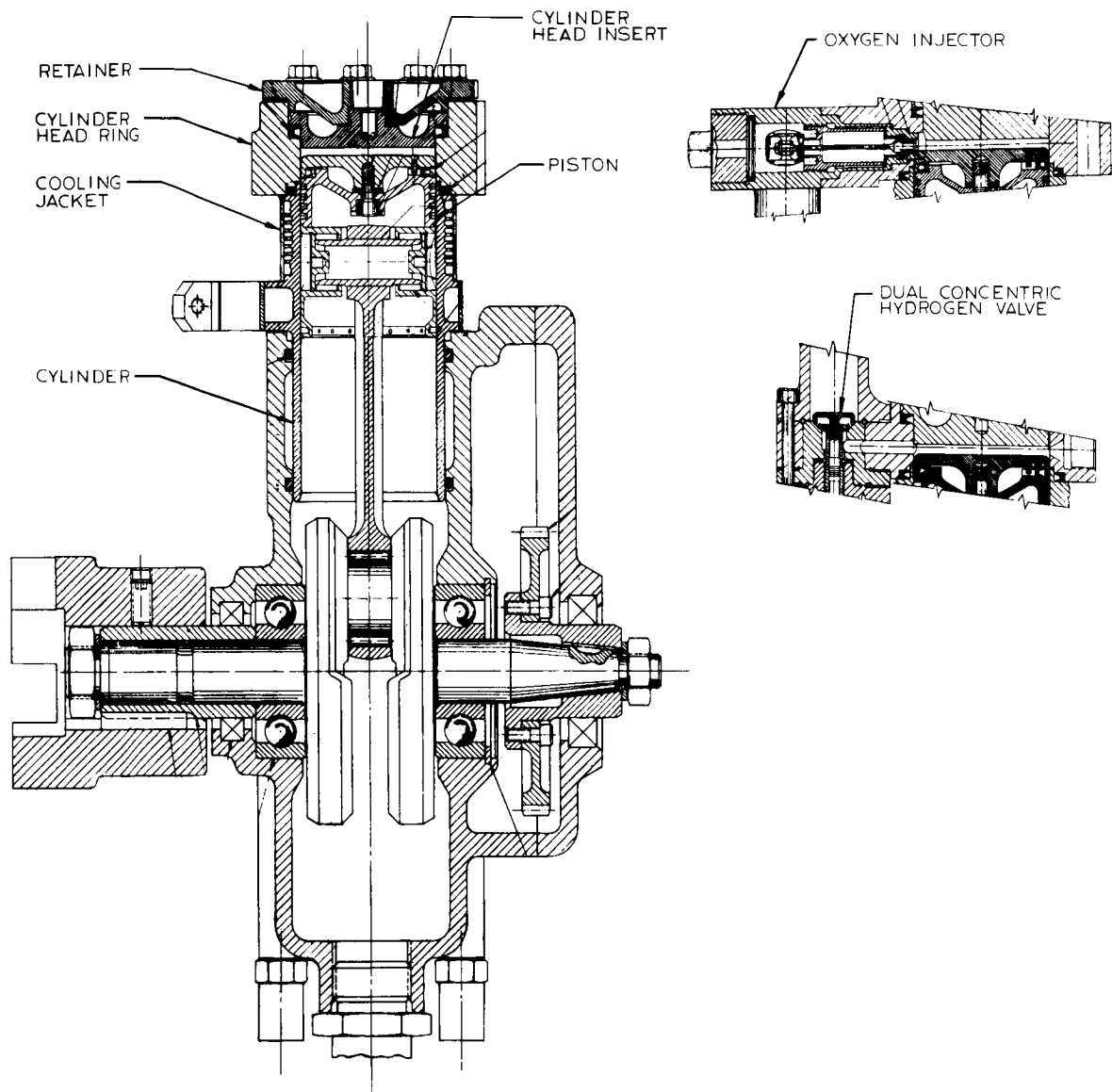


Fig. 3-2 - Engine at Beginning of Program

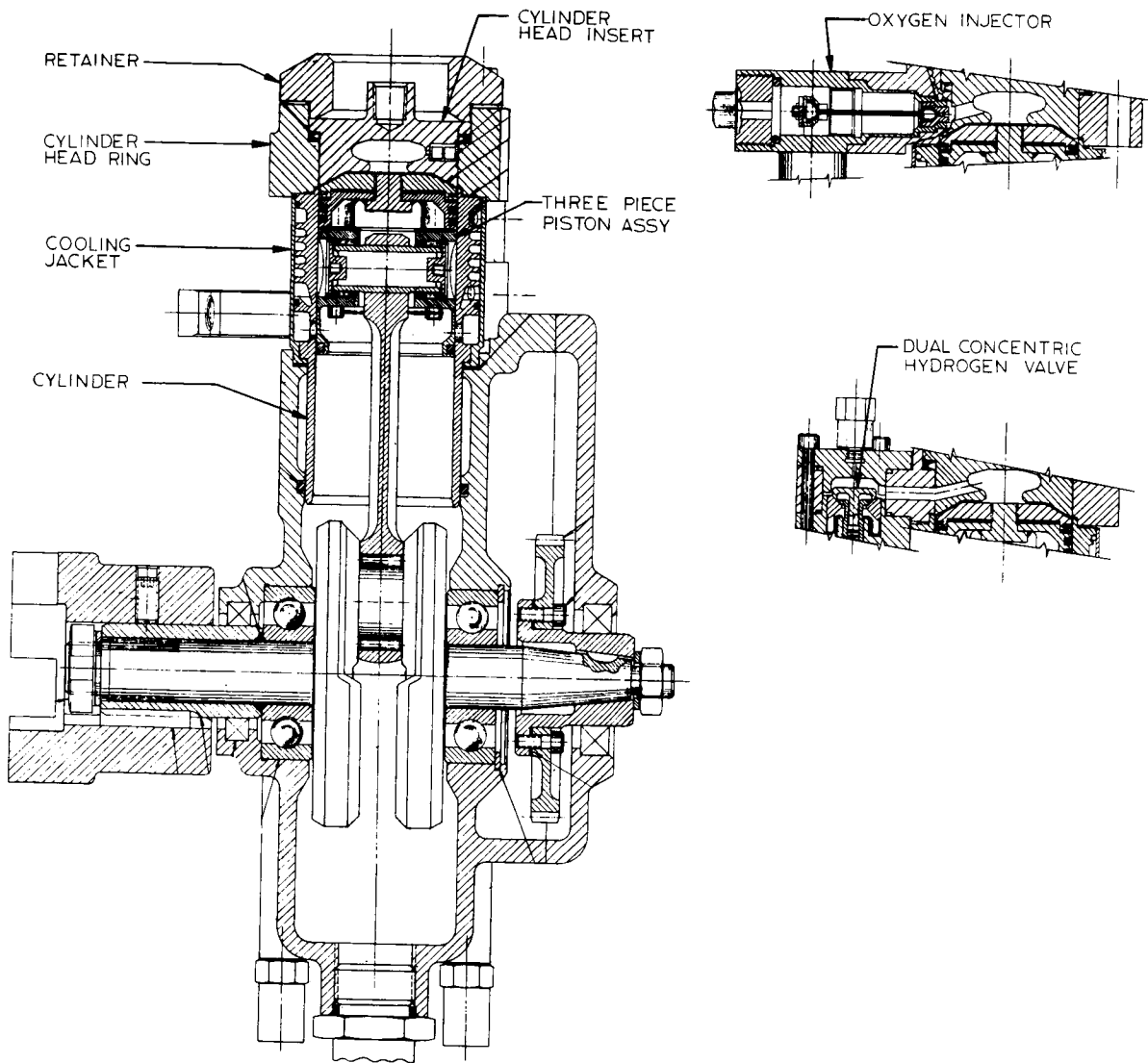


Fig. 3-3 - Engine at End of Program

further oil control ring development in conjunction with lubrication system improvement. It is also felt that the cylinder and cooling jacket assembly is developed to a satisfactory configuration. The final selection of the cylinder material, however, should be delayed until after further endurance evaluation of candidate materials.

Two static seals presented the most problems; one between the oxygen injector nose and the cylinder head ring and one between the cylinder head insert and the cylinder head ring. Failure of these seals (which were changed each time the injector was removed) has not occurred during the last 361 hours of endurance testing. However, it cannot be said with certainty that these problems have been solved until further testing has been accomplished.

The hydrogen valve underwent a design revision, which changed it from a configuration in which the valve stems were always exposed to the combustion chamber to one in which they are not exposed. However, several problem areas remain to be solved: Hydrogen valve spring failures have been a major cause of endurance test stoppage during the longer duration tests. Calculations show that the springs are stressed too highly for the high frequency cycling application. The high spring stress is the result of a space limitation imposed by the engine crankcase design which was carried over from earlier work under Air Force contract. By increasing spring coil diameter to the greatest extent possible with the present crankcase, the spring stresses can be lowered to a value which appears adequate for a 300 to 500 hour life. However, for a flight-type design the crankcase can be modified to allow the use of even longer springs with correspondingly lower stress, as discussed later. Failures of the lifter of one hydrogen valve poppet has been encountered.

However, these failures can be eliminated by a minor redesign.

Because of the time required to design, fabricate, evaluate and develop various critical parts of the engine, significant improvement in the endurance life of the engine was not achieved until the last few months of the program.

The materials used in the final engine configuration are listed in Table 3-I.

3.1.2 Oxygen Injector - Figure 3-4 is a functional perspective drawing of the oxygen injector. The operating principles of the injector were not changed by the development effort. A fundamental part of the injector design concept is the hermetic sealing torque tube. No problems with this tube have occurred and it is considered to be satisfactory. One end of the torque tube is welded to the cam follower end of the quill shaft and the other to a body attachment flange. The tube deflects in torsion as the quill shaft is rotated by action of the cam and cam follower. It forms a hermetic seal between the oxygen atmosphere section of the injector and the lubricated cam chamber. Figures 3-5, 3-6, and 3-7 are sectional views of the injector in its initial, intermediate, and present configurations. Figures 3-5 and 3-7 show the extent to which the oxygen injector was changed. Figures 3-8 and 3-9 are photographs of the old and present injector hardware. The following paragraphs describe the detail changes.

3.1.2.1 Mounting and Lubricated Drive Section - The nose of the oxygen injector body pilots in the cylinder head ring (see Figure 3-10), and the body is held in place by three screws and a dowel pin.

TABLE 3-I
Engine Material List

Description	Material	Special Treatment or Notes
<u>ENGINE COMPONENTS - X611440</u>		
Crank Case Subassy.	Cast iron AMS 5316	- - -
Crank Shaft & Conn. Rod Assembly	- - -	"Honda" Crank Shaft. No material analysis was made.
Cylinder Assembly	Handy- Harmon Easy Flow	Induction brazed X613008
Jacket - Coolant	AISI 347	- - -
Cylinder	T-15 tool steel	R _c 61-65
Cylinder to Head Gasket	AISI 302	Dead soft
Cylinder Head	Rene 41	Annealed cond.
Cylinder Head Stud	Rene 41	R _c 40 min.
Cylinder Head to Comb. Chamber Seal	Inconel X	Silver plated QQS-365
Head Combustion Chamber	Inconel X	Alternate: Inconel 702
Retainer Comb. Chamber	AISI 304	- - -
Housing Piston Pin (Skirt)	T-15 tool steel	R _c 61-65
Piston Ring Belt	Inconel X	Alternate: Inconel 702
Piston Dome	Inconel X	Alternate: Inconel 702
Piston Heat Shield	Stainless Steel	Shim stock

TABLE 3-I (Continued)

Engine Material List

Description	Material	Special Treatment or Notes
Screw Piston Skirt to Ring Belt	Inconel X	Alternate: Inconel 702
Piston Pin	M-50 tool steel	R _c 58-62
Retainer Piston Pin	AISI 440 C	R _c 55-60
Roller Bearing	M-50 tool steel	R _c 58-62
Oil Ring - Piston	Pearlitic Gray - Cast Iron	Hard chrome plate .003 in.
Ring Piston - Fire Ring	17-4 stainless steel	Hard chrome plate .002-.003 in.
Ring Piston Comp. 3-piece	17-4 stainless steel	Hard chrome plate .002-.003 in.
Gear - Crank Shaft	Nitraloy 135 Medium carbon	Nitride .005-.010 deep 15N-91 case hardness R _c 32-36 core
Gear - Crank Shaft	Nitraloy 135 Medium carbon	Nitride .005-.010 deep 15N-91 case hardness R _c 32-36 core
Shaft - Cam	Nitraloy 135 Medium carbon	Nitride .005-.010 deep 15N-91 case hardness R _c 32-36 core
Cam O ₂ Injector	AISI 8620 or AISI 4620	Carburize .030-.035 deep Case R _c 60-63. Core R _c 28-35
Cam H ₂ Valve	AISI 8620 or AISI 4620	Carburize .030-.035 deep Case R _c 60-63. Core R _c 28-35

TABLE 3-I (Continued)

Engine Material List

Description	Material	Special Treatment or Notes
Cam - H ₂ Valve	AISI 8620 or AISI 4620	Carburize .030-.035 deep Case R _c 60-63. Core R _c 28-35
Rockerarm - H ₂ Outer Valve	AISI 4620	Case .020-.030 deep Case R _c 58-62. Core R _c 28-35.
Rockerarm - H ₂ Outer Valve	AISI 4620	Case .020-.030 deep Case R _c 58-62. Core R _c 28-35.
<hr/> O ₂ INJECTOR - X612218 <hr/>		
Cam Follower - O ₂ Injector	AISI 52100	R _c 60-63
Body - Oxygen Injector	Inconel 702	- - -
Torque Tube - O ₂ Injector	RENE 41 AMS 5712	- - -
Quill Shaft - O ₂ Injector	RENE 41 AMS 5712	Journal flame plated. Linde Co. - LA-2 99% Al ₂ O ₃
Flange - O ₂ Injector	RENE 41 AMS 5712	- - -
Rocker Shaft - O ₂ Injector	AISI 4620 Steel	Case .020-.030 deep. Case R _c 58-62. Core R _c 28-35
Bushing - Quill Shaft - O ₂ Injector	Haynes 25	Cobalt base alloy
Rockerarm - O ₂ Injector Poppet	Stellite 6B	Cobalt base alloy
Poppet - O ₂ Injector	Stellite 6B	Cobalt base alloy. Flame plated Linde LW-1 N4D (WC + 15% Co)

TABLE 3-I (Continued)

Engine Material List

Description	Material	Special Treatment or Notes
Seat - O ₂ Injector Poppet	Haynes 25	Cobalt base alloy
Rockerarm - O ₂ Injector Poppet	Haynes 25 *	Cobalt base alloy
Poppet - O ₂ Injector	Haynes 25 *	Cobalt base alloy. Flame plated Linde LW-IN 40 (WC + 15% Co)
Retainer - O ₂ Injector Poppet	Haynes 25	Cobalt base alloy
* Alternate Material		

H₂ VALVE - X611414

Cap - Inner Valve (Follower)	AISI H-11 Tool Steel	R _c 48-52
Ring - Outer Valve (Follower)	AISI 52100	R _c 55-60
Spider - Inner Valve (Follower)	AISI 4130	R _c 28-32
Valve - Inner	AISI H-11 Tool Steel	R _c 48-52
Valve - Outer	AISI H-11 Tool Steel	R _c 48-52
Guide - Valve	AISI H-11 Tool Steel	R _c 52-56
Valve Seat	AISI H-11 Tool Steel	Nitride case .010-.015 in. Core hardness R _c 48-52
Spring - Inner Valve	Elgiloy	Material of Elgin Watch Co.
Spring - Outer Valve	Elgiloy	Material of Elgin Watch Co.

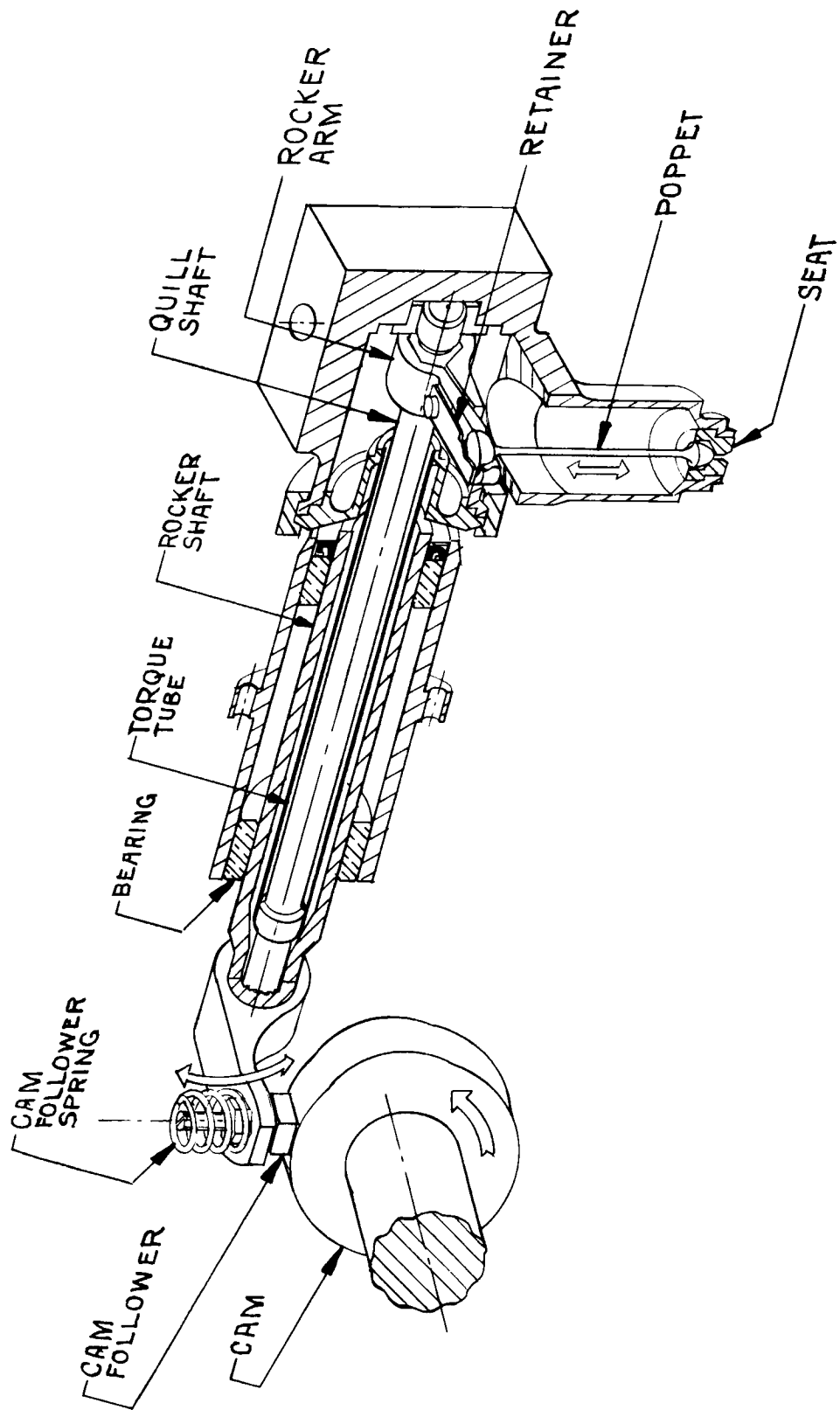


Fig. 3-4 - Oxygen Injector

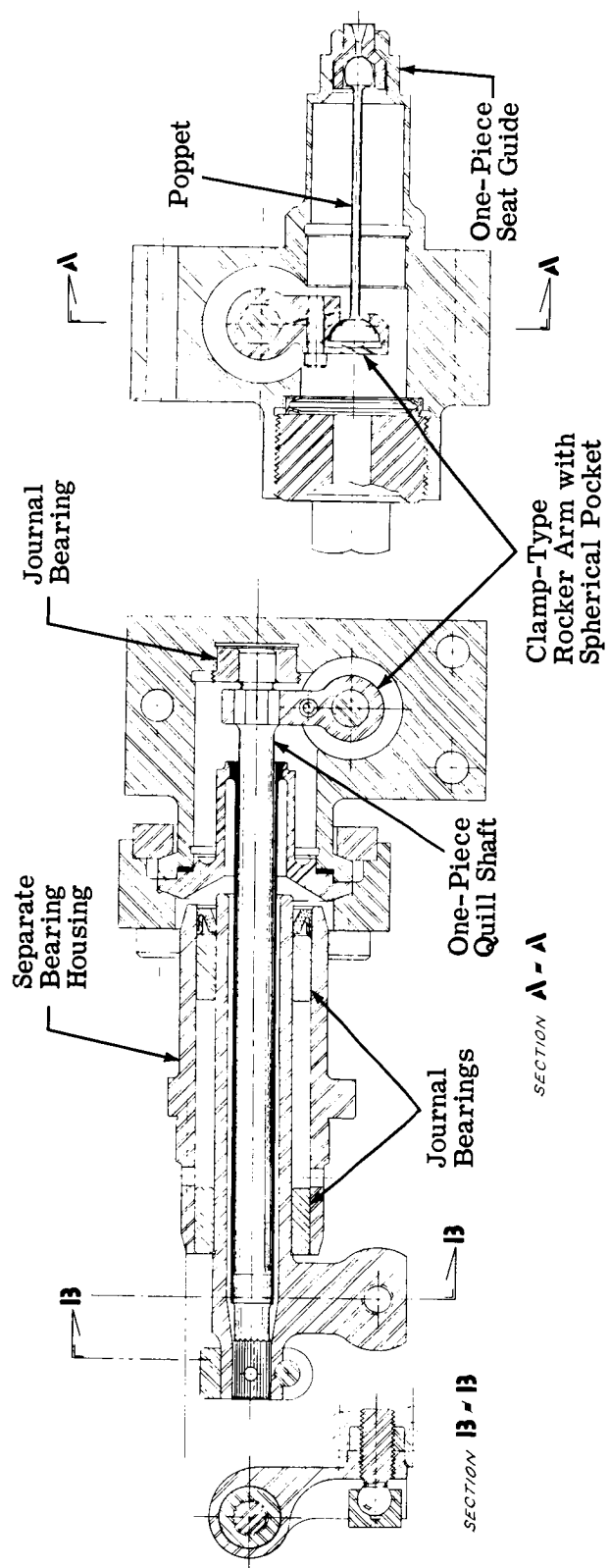


Fig. 3-7 - Section Views of Final Oxygen Injector Assembly

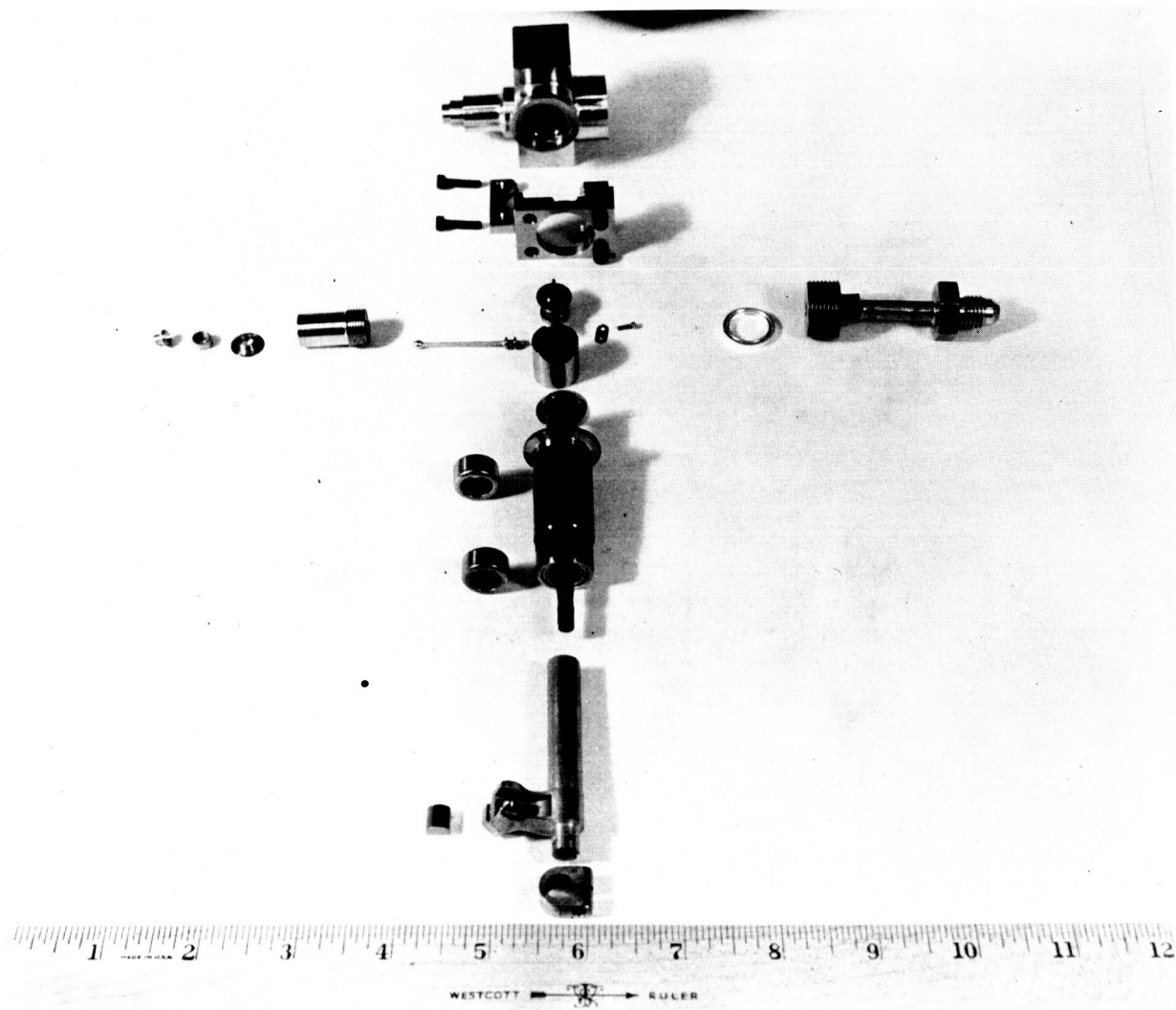


Fig. 3-8 - Initial Oxygen Injector Disassembled

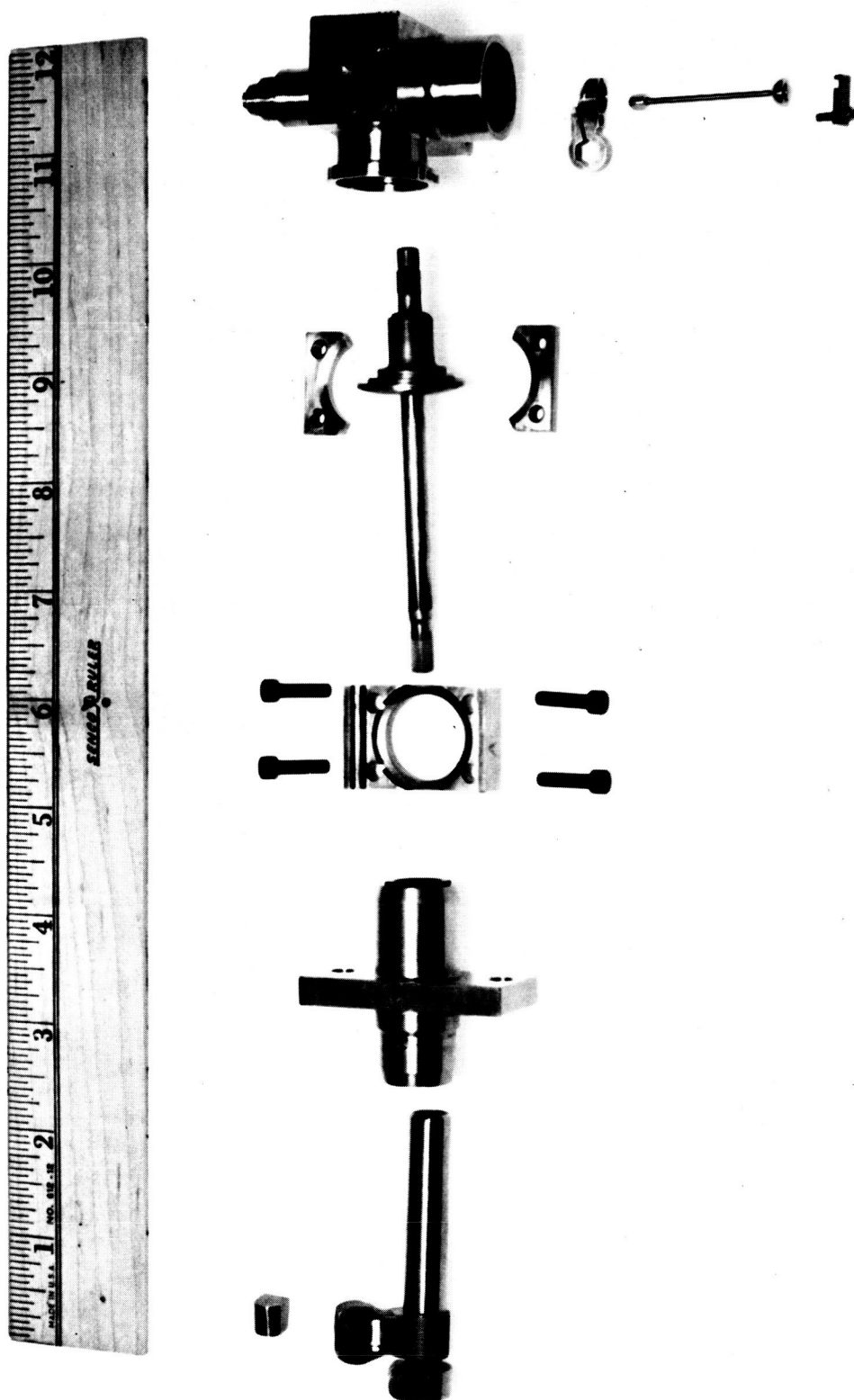


Fig. 3-9 - Final Oxygen Injector Disassembled

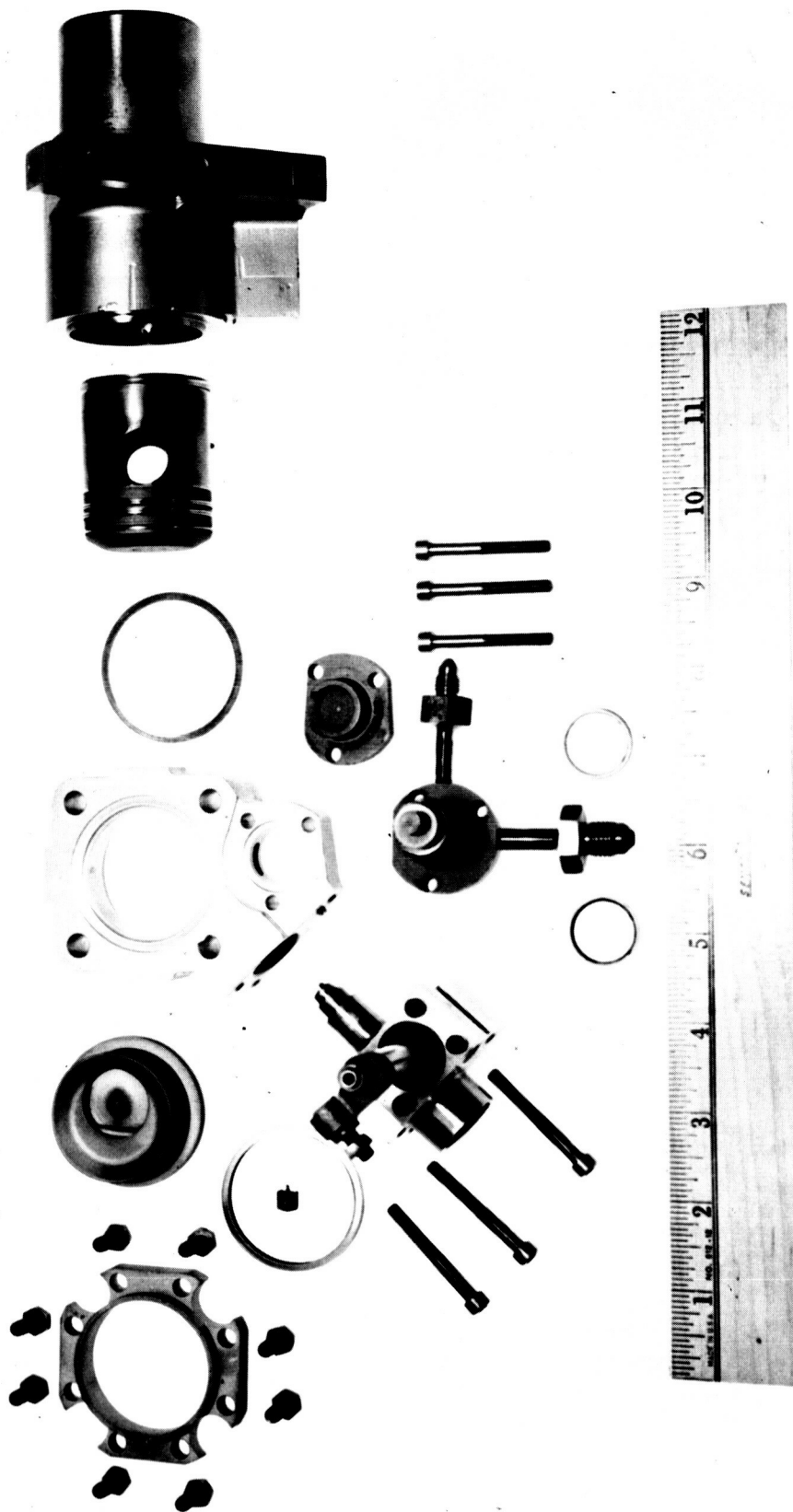


Fig. 3-10 - Engine Cylinder, Piston, Cylinder Head,
and Valve Assemblies

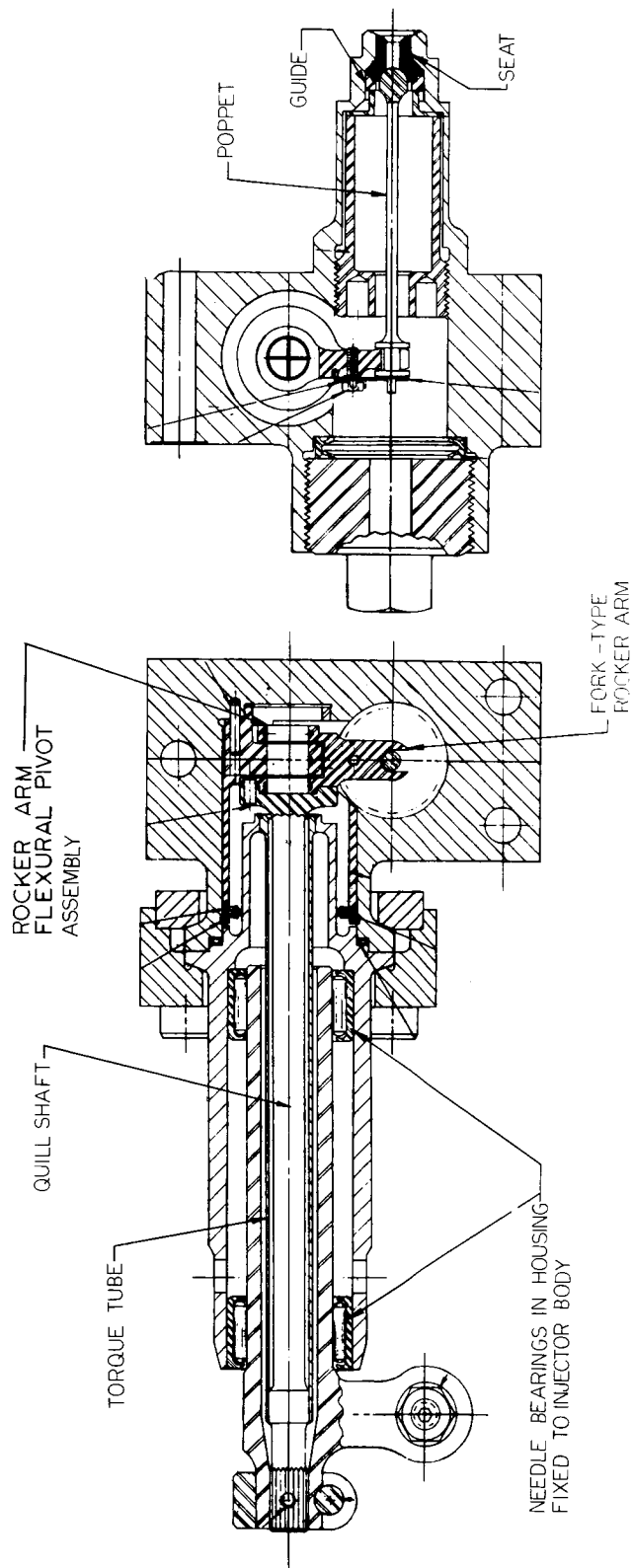


Fig. 3-5 - Section Views of Initial Oxygen Injector Assembly

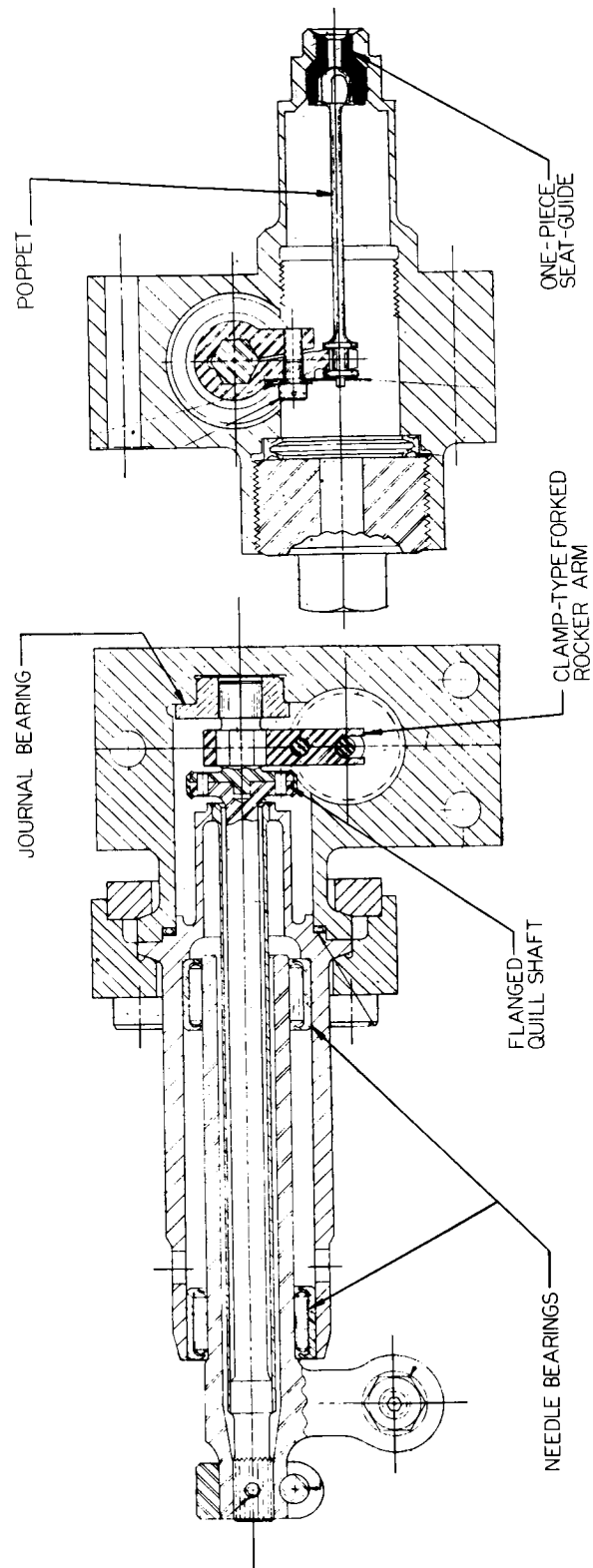


Fig. 3-6 - Section Views of Intermediate Oxygen Injector Assembly

As can be seen in Figure 3-5, the cam follower rocker shaft bearing housing was originally attached to the oxygen injector body and thus attached rigidly to the cylinder head ring. This arrangement allowed thermal expansion to change the axis of rotation of the cam follower rocker arm with respect to the cam shaft, which is mounted in the crankcase. This problem was corrected by splitting the injector body so that cam follower rocker shaft bearings could be fixed rigidly to the crankcase as shown in Figures 3-4 and 3-7. This arrangement allowed the injector body to shift, relative to the crankcase, without changing adjustment, by allowing the torque tube and quill shaft to deflect in bending.

Originally the cam follower rocker shaft was supported by needle bearings. These bearings were satisfactory for short performance tests, probably because of a shift in location of the needles with respect to the rocker shaft during assembly between tests. After the first 12-hour endurance test, Brinell damage of the rocker shaft by the needles was observed. The damage was attributed to the high frequency small angle fretting motion of the rocker shaft.

This problem was corrected by replacing the needle bearings with journal bearings. A number of different bearing materials were procured as back-up, but only "Bronze Oilite" and "Iron Oilite" were used. Both proved to be satisfactory.

- 3.1.2.2 Quill Shaft and Internal Pivot Bearings - The evolution of the quill shaft can be seen in Figures 3-5, 3-6, and 3-7. The original design had a flange on the upper end which drove the rocker arm by means of a torque transmitter pin. The rocker arm was supported by a Bendix flexural pivot. A photograph of a flexural pivot is shown in Figure 3-11. The rocker arm-flexural

pivot assembly can be seen in Figures 3-5, 3-8, and 3-12. The disadvantages of this design were:

1. Short pivot life
2. The pivot deflected radially and cocked during operation, causing erratic operation
3. Axial dimensions were critical.

These problems were eliminated by replacing the flex pivot with a journal bearing. The bushing material is Haynes 25 cobalt-base alloy. The journal, integral with the Rene' 41 quill shaft, is flame-plated with Linde LA-2 aluminum oxide and polished to a mirror finish. As backup to the flame-plated journal, two journals were coated with calcium fluoride. Also, molybdenum bushings, coated with molybdenum dioxide, were fabricated to run with a plain Rene' 41 shaft. However, the aluminum oxide flame-plated journal with the Haynes 25 bushing proved so successful that it was unnecessary to evaluate the backup combinations.

- 3.1.2.3 Poppet and Seat Guide - Figure 3-12 is a photograph showing the evolution of the rocker arm, poppet, and seat guide with the older hardware to the left. Initially, the valve seat and poppet guide were two separate pieces. The guide was cylindrical with three scallops at 120° apart. The guide contact surface of the poppet was cylindrical. Small differences in the concentricity, due to the guide and seat being separate pieces, caused a high wear rate and galling of the contact surfaces of the poppet and guide. The first step in correcting this condition was to make a one-piece seat guide and to grind flats 120° apart on the poppet guide contact surfaces to allow the gas to flow between

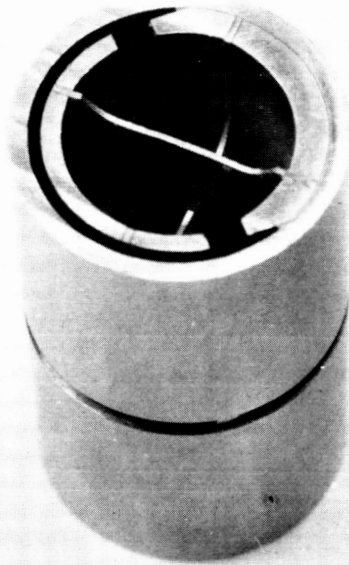


Fig. 3-11 - Flexural Pivot

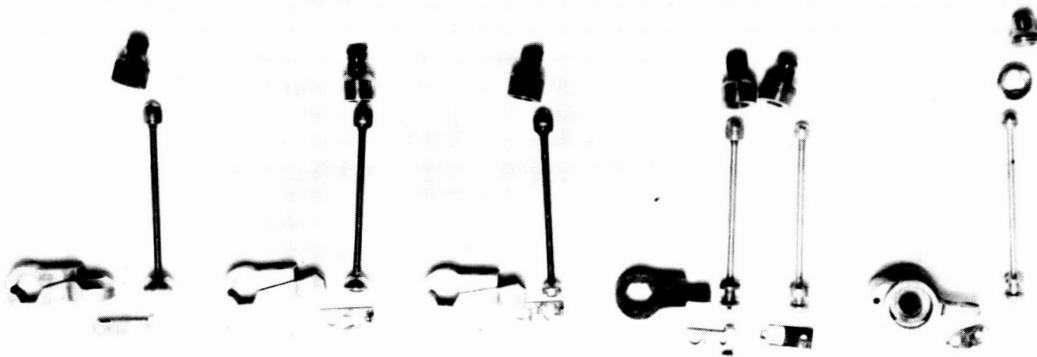


Fig. 3-12 - Evolution of Oxygen injector Rocker Arm,
Poppet, and Seat

the poppet and cylindrical guide. This design showed considerable promise and evolved to the present seat guide and poppet configuration. The diameter of the guide contact surfaces of the poppet was increased and barrel shaped to allow for its rocking motion. The diameter of the spherical seating surface of the poppet nose was increased. Seats and poppets of both Haynes 25 and Haynes 6B have been used. The seating and guide surfaces of poppets have been evaluated with calcium fluoride and with lead monoxide coatings. Viewed under a microscope, these coatings appeared to have worn off after a short running time. However, poppets so treated showed less wear with the guide contact surface of the seat than did noncoated poppets during longer duration runs. This would tend to indicate that the coatings are beneficial in aiding break-in.

Tests were also run with two poppets flame-plated with tungsten carbide. The results of these tests were not encouraging. During a cold gas test on the injector test stand, the plating chipped at the seat contact surface. During a short, hot run on the engine the plating appeared to gall or smear off of the guide contact surface. By use of cobalt-base alloys with lead monoxide or calcium fluoride coatings, the wear rate between the seat and guide has been reduced to the point where it has not been a serious problem during endurance testing.

The present problem is to reduce the amount of wear between the poppet and its seating surface. This wear rate for the last several endurance tests can be seen in Table 3-II, under the column "Wear, Poppet Moved Into Seat." Several approaches may be taken toward solving this problem. The poppet's seat contact surface may be increased; different coatings and materials may be applied; the cam contour can be altered to reduce seating loads, or the impact load may be reduced by spring-

TABLE 3-II

OXYGEN INJECTOR ENDURANCE HISTORY SUMMARY

Test Dates Start & Stop	Data Sheets Start & Stop	Hours Of Test	Seal		Poppet			Rocker Arm		Retainer Type	Lift		Lash Chg. Inches	Wear						Poppet-Seal Increase
			Type	Mtl.	Type	Mtl.	Coating	Type	Mtl.		Chg. + or - Inches	Rate in. hr.		Poppet Moved Into Rocker	Poppet Moved Into Seal	In Rocker By Poppet	On Poppet By Rocker	On Poppet By Retainer	In Retainer By Poppet	
5/19-23/64	2-16	100.1	0.032 Straight Cone	H-25	1	H-25	None	1	H-25	1	H-25	-0.008 -51 hr.	-0.00016	0.0265						
6/2-3/64	19-25	24.6	0.032 Straight Cone	H-25	1	H-25	C _a F ₂	1	H-25	1	H-25	-0.0087 50.1 hr.	-0.00017							
6/11-12/64	28-33	32.0	0.045 Straight Cone	H-25	2	H-25 6B	C _a F ₂	2	H-25	2	H-25	-0.0038 24 hr.	-0.00016	0.004						
6/15-18/64	34-44	65.5	0.045 Straight Cone	H-25	2	H-25 6B	C _a F ₂	2	H-25	2	H-25	-0.0058 58.7 hr.	-0.00009	0.006						
6/24-25/64	45-53	34.4	0.045 Straight Cone	H-25	2	H-25 6B	C _a F ₂	2	H-25	2.1	H-25	-0.0032 32 hr.	-0.0001	Broken Leaf Spring						
7/1-3/64	57-62	30.4	0.045 Straight Cone	H-25	3	H-6B	None	3	H-6B	3	H-25	-0.0017 13.37 hr.	-0.00001	0.002	0.001	0.001				
7/6-10/64	63-74	80.1	0.032 Straight Cone	H-25	3	H-6B	P _b O	3	H-6B	3	H-25	-	-		0.0085	0.0039	0.0075	0.002		
7/11-17/64	75-90	120.0	0.032 Straight Cone	H-25	3	H-6B	P _b O	3	H-25	3	H-25	-0.0031 114 hr.	-0.00003	0.021	0.0065	0.0032	0.0033	0.0125	0.0032	0.0043
7/28-7/64	94-110	95.9	0.032 Straight Cone	H-6B	3	H-25	None	3	H-6B	3.1	H-25	+0.0035 89 hr.	+0.00003	0.0048	0.0011	0.0057	0.0002	0.0003	0.002	0.0035

H-25 - Haynes Alloy 25

* H-6B - Haynes Stellite 6B

* H-25 Stellite 6B brazed to Haynes 25 6B

mounting the tail end of the poppet, as discussed in the following paragraph.

- 3.1.2.4 Rocker Arm and Poppet - The evolution of the poppet and rocker may also be seen in Figure 3-12 (left to right). After the flex pivot bearing was replaced with a journal bearing, new rocker arms were made, using the same poppet connection principle as was used with the flex pivot type rocker arm.

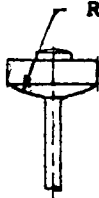
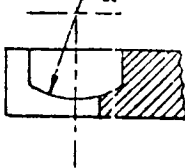

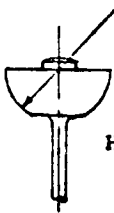
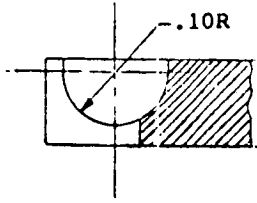
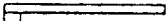
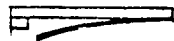
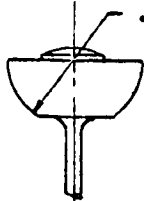
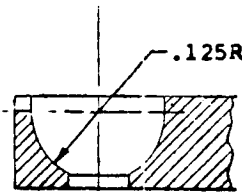

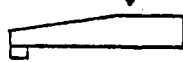
When longer performance tests were run, and at the start of endurance testing, it became apparent that this means of lifting the poppet would be unsatisfactory and would result in excessive wear due to impact loads on the small contact area of the rocker. Also, the hole in the thin cantilever spring retainer became enlarged by contact with the mating tip of the poppet. A non-spring plate type retainer was tried, but it rapidly wore away the contacting tip of the poppet. The rocker-poppet contact joint was redesigned so that the rocker end of the poppet was trapped in a spherical pocket within the rocker and retained by a flat cover plate.

The contact surface between the poppet and rocker was made spherical so that accurate angular alignment was no longer required. This new design evolved through three different configurations as shown in Table 3-III. The Type 1 configuration shown in Table 3-III was a vast improvement over earlier designs but the wear rate between the rocker and poppet contact surfaces was still too high. After endurance tests of 100.1 and 24.6 hours, the contact surface of the poppet was worn to a concave configuration, as shown in Figure 3-13.

The next step was to provide a full hemispherical seat in the rocker arm and a mating hemispherical surface on the poppet

TABLE 3-III

O₂ Injector Poppet & Rocker Arm Design Types

<p>1</p> <p>Poppet</p>  <p>Partial Sphere Part No. SK14621</p>	<p>1</p> <p>Rocker Arm</p>  <p>Slotted Partial Sphere Part No. X612212</p>	<p>1</p> <p>Retainer</p>  <p>Flat Part No. X612211</p>
<p>2</p>  <p>Small Hemisphere Part No. SK 15847</p>	<p>2</p>  <p>Small Hemisphere Slotted Part No. SK15846</p>	<p>2</p>  <p>Flat Part No. X612211</p>
		<p>2.1</p>  <p>Flat with Cant.Spring Part No. X612211</p>
<p>3</p>  <p>Large Hemisphere Haynes Part No. 6B X612215 25B SK 15851 Flame SK 16261 Plated</p>	<p>3</p>  <p>Large Hemisphere Haynes Part No. 6B X612214 25B SK 15849</p>	<p>3</p>  <p>Flat-Thin Part No. X612216</p>
		<p>3.1</p>  <p>Flat-Thick Part No. SK 16267</p>

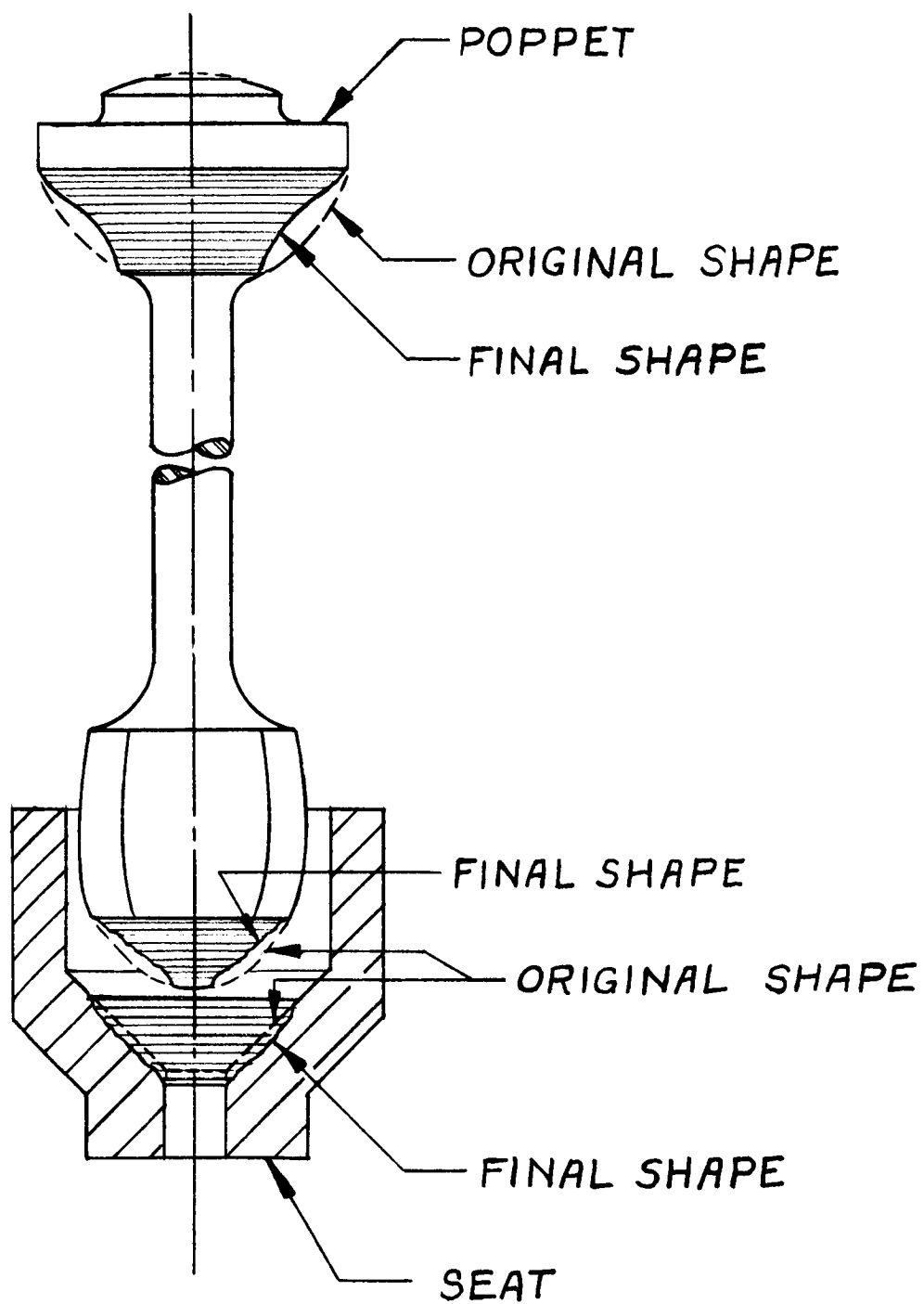


Fig. 3-13 - Poppet and Seat Wear Pattern

by brazing a larger piece of material onto the stem of the existing poppets. This configuration is shown as Type 2 on Table 3-III and was used in the interim while the Type 3 configuration of Table 3-III was fabricated. Configuration 3 eliminated the slot in the rocker arm, the sharp edge of which may have contributed to wear on the poppet. Type 2 and Type 3 configurations were run with various combinations of Haynes Stellite 6B and Haynes 25 materials with the hemispherical surface on the poppet coated with lead oxide or calcium fluoride, or flame-plated with tungsten carbide (Linde Flame Plate LW-1 N40), as can be seen in Table 3-II.

Best results have been shown with a Haynes 25 poppet, flame-plated with tungsten carbide, running with a Stellite 6B uncoated rocker arm. A wear rate of .0048 inch in 96 hours was observed with this combination. The wear between the rocker and poppet configuration was less than that between the seat and poppet, thus causing the injector lift to increase with time. Matching of the wear rates at each end of the poppet would result in no change in poppet lift.

The spring loaded poppet configuration shown in Figure 3-14 was scheduled to be tested next but the program came to an end before this could be accomplished. It is expected that the spring will reduce the impact loads between the poppet and the seat and between the poppet and rocker arm, and hence, reduce wear and tend to balance the wear rate at the two ends of the poppet.

- 3.1.3 Cylinder, Piston, and Cylinder Head Ring - The differences between the initial and the present cylinder, piston, and combustion chamber designs can be seen by comparing Figures 3-2 and 3-3.

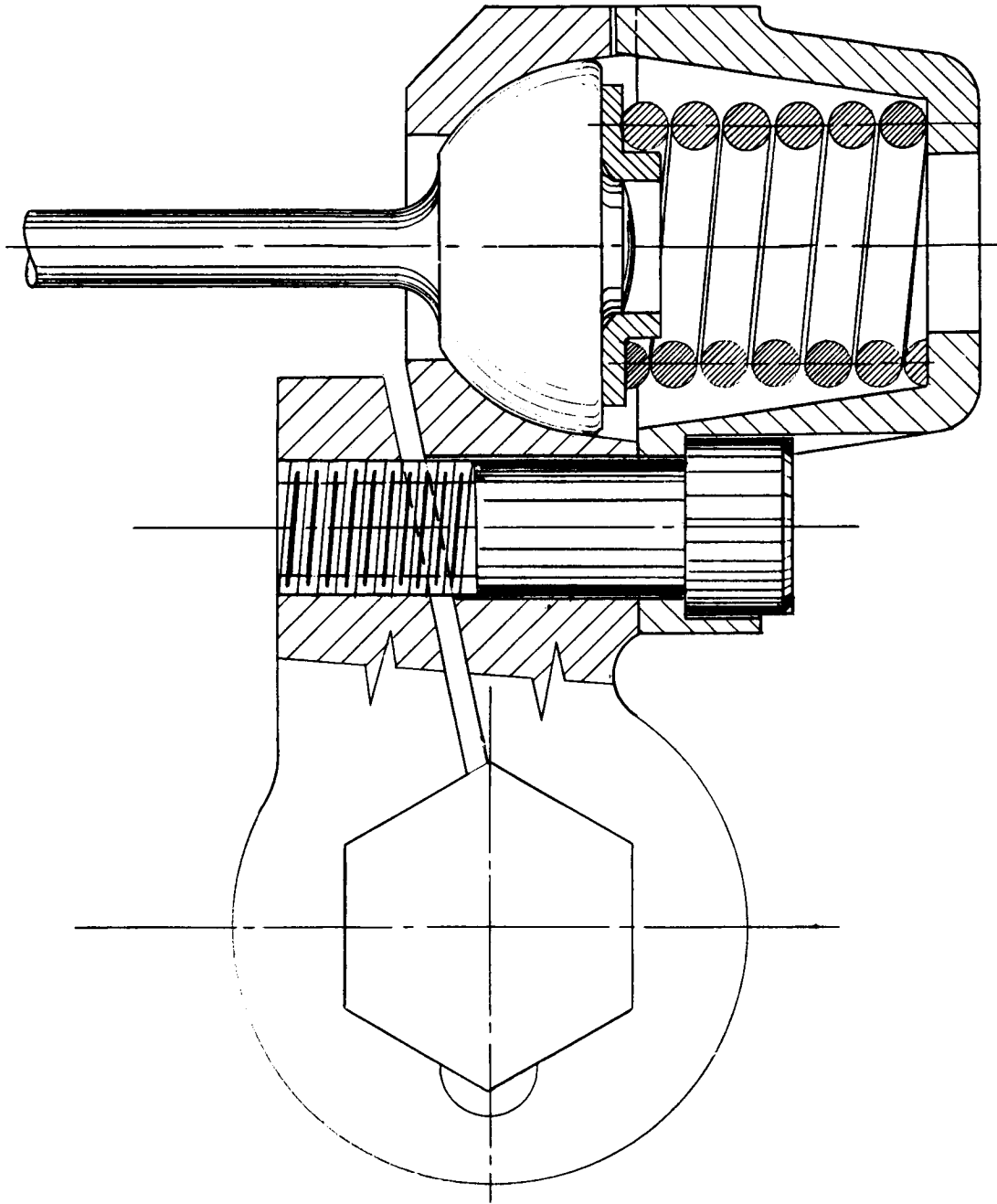


Fig. 3-14 - Oxygen Injector Poppet Retainer
Incorporating Coil Spring

From the experience gained by the 15.7 hours of engine testing during Contract NAS 3-2550, and from the work done during the early part of this contract, it was evident that the existing piston and cylinder hardware would be inadequate for completion of the scheduled performance and endurance testing of the present contract. Since new hardware was required, there was an opportunity to modify the design and eliminate a number of functional problems. Problems encountered with the original design were:

1. The original cylinder design required a long fabrication time and experienced a 50% scrap rate when originally fabricated during Contract NAS 3-2550. Furthermore, the bore dimensions of the two existing usable cylinders had been distorted during fabrication and were badly worn by testing.
2. At TDC position, the top edge of the piston was exposed to direct oxygen impingement, the cylinder head ring was exposed to high velocity combustion gas, and the design of the piston dome and combustion chamber insert limited the possibilities of experimentation with combustion chamber shapes.
3. The "K" seal (acting as a cylinder head gasket) between the cylinder and the cylinder head ring was repeatedly the source of leakage.
4. The metal O-Ring seal between the piston dome and the piston often leaked after test, and even when it did not leak after test, it was not certain that it did not leak during test.

5. Wear occurred between the piston pin and its needle bearings and needles rubbed and scored the needle retainers. Also, the clearance fit (free floating) between the pin and the connecting rod caused the pin bore in the rod to elongate.
6. Magnaflux and Zyglow inspections of the piston showed the beginning of cracks in the brazed joint between piston body and ring belt.
7. The evaluation of pressure time traces and gas flow analysis, based upon layout drawings of actual hardware dimensions, indicated that the exhaust port area was too restrictive.

The design study of a new cylinder and piston design was started early in the program, and the existing hardware was refurbished so testing could begin. The old cylinders were honed and the old pistons were hard chromium plated and reground in the piston ring area.

Figure 3-15 shows views from the layout drawing from which detail drawings were made and from which new hardware was fabricated. Some rework of upper crankcase castings and the cylinder head ring was required to incorporate the new hardware.

The major changes incorporated in the new cylinder and piston designs are enumerated below:

1. The axial and radial structural rigidity of cylinder and jacket were increased, as can be seen by comparing the cylinders in Figure 3-2 and Figure 3-3. The cylinder wall thickness and the cooling jacket diameter were increased.

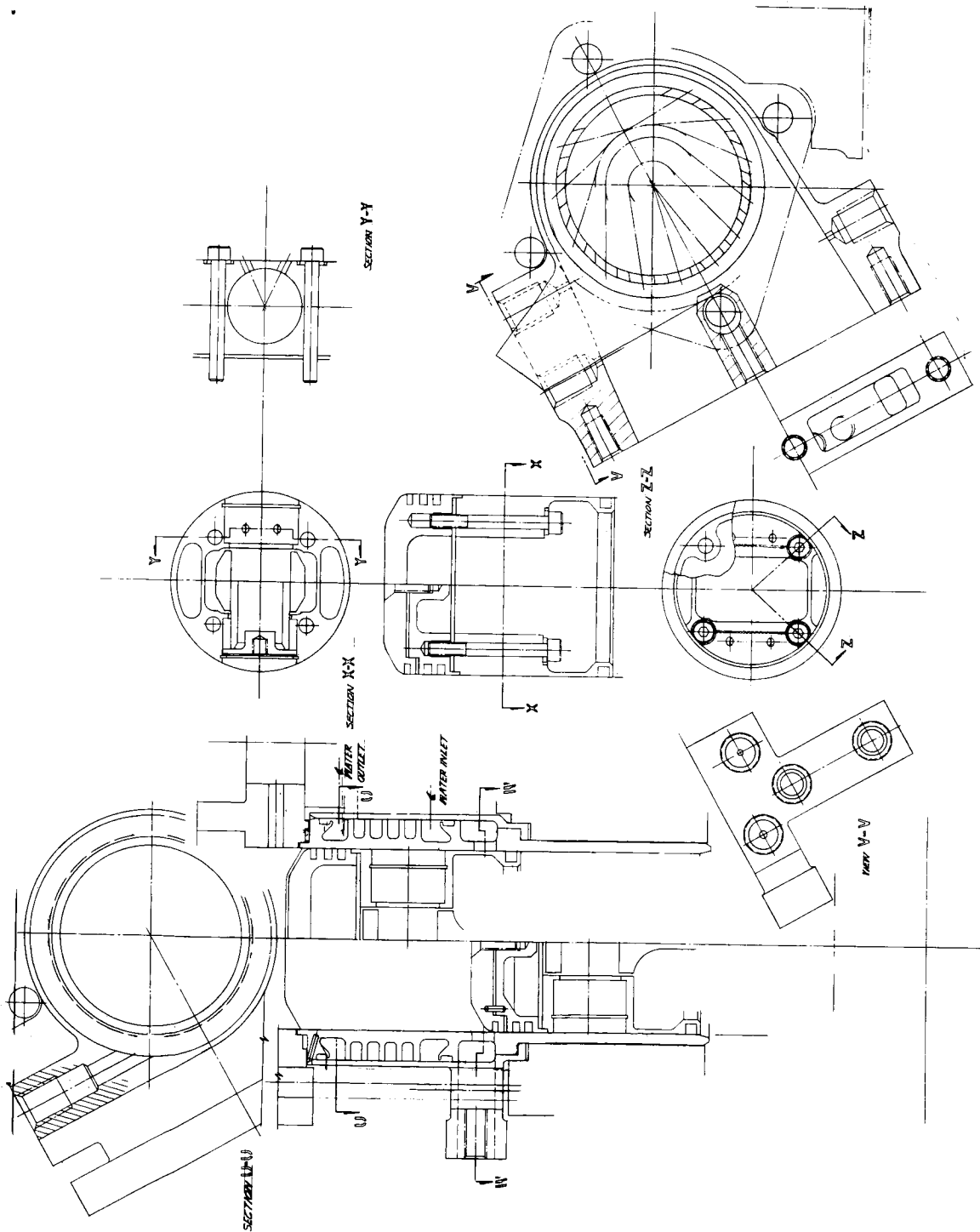


Fig. 3-15 - New Piston and Cylinder Design

2. The coolant flow area of the cylinder was increased and the cooling jacket was extended to a higher location to provide better cooling of the cylinder wall adjacent to the upper limit of travel of the top compression ring.
3. The exhaust manifold area was increased. Exhaust ports were re-directed to provide a smoother flow passage. The BDC position of the piston exhaust timing ring (or fire ring) exposes greater port area. A bevel on the piston dome also increased flow area to exhaust ports.
4. The TDC position of the piston has been lowered with respect to the combustion chamber so that the cylinder head insert may be extended downward to protect the cylinder head ring, seal, and the top lip on the cylinder barrel, and to provide room for various combustion chamber shapes. Oxygen injection occurs across the top surface of the piston with this design.
5. The piston body, containing the piston pin bearings and oil ring, is held to the compression ring belt by four screws. This design allows the use of a laminated stainless steel heat dam between the two parts and allows for experimentation with piston dome shapes and piston ring configurations.
6. The leakage path through the piston and the associated seal was eliminated. Two approaches were taken. In one approach, a two-piece piston was used in which the ring belt and dome with the fire ring groove are one piece. This placed the joint between the piston body and ring belt in the low pressure area below the compression rings. In the other approach, a three-piece piston was used in which

the dome is attached by a screw inserted through a hole in the top of the dome into a blind hole in the ring belt. A laminated stainless steel heat dam is used between the dome and the ring belt.

7. The "K" seal between the cylinder and the cylinder head ring was replaced with a flat crush gasket. A number of different types of seals were designed, but only a solid annealed copper and annealed stainless steel seals were fabricated and tested. The flat seal reduced the clearance volume and lowered the cost of seal replacement during experimentation.

As a result of subsequent experimental evaluation, some of the design changes had to be modified. The two-piece piston assembly with the one-piece ring belt and dome was rejected because the compression rings were damaged by overheating, and because a seizure occurred between the piston and cylinder at the points nearest, and directly opposite, the point of oxygen injection (highest temp.). It was concluded that the heat transfer rate down the piston was too high and that the temperature distribution of the ring belt was uneven. Figure 3-16 shows a piston ring which has taken a set of approximately 40%, due to high temperature next to a new ring. The three-piece piston was retained. With this design, heat transfer to the ring belt is reduced and the dome piece can be run with a large clearance and may distort without affecting the lower parts of the piston.

The means of connecting the dome of the three-piece piston to the ring belt was changed because the retaining screw was found to have yielded after several tests. As shown in Figure 3-3, a large diameter Inconel X stud was inserted through the bottom of the ring belt, the dome turned on to it, and the top of the

threads was staked. Initially, the stud was silver brazed to the ring belt; later it was welded on.

Two types of compression rings were evaluated; the thin rail ring, and the three-piece ring shown in Figure 3-17. In the latest piston configuration, the three-piece compression rings are used in the lower two ring grooves and the thin rail ring is used as in the top ring groove. The top ring acts as a fire ring to protect the lower two rings from heat and to control exhaust timing. The advantages of the three-piece rings are their ability to conform to an out-of-round cylinder and to reduce leakage by staggering the ring gaps. All rings are of 17-4 ph stainless steel with the cylinder contact surfaces hard chromium plated.

The drain holes on the inside diameter of the oil ring groove were eliminated. The double edged wiper ring used with the old piston was replaced with a solid, hard chrome plated pearlitic cast iron ring with the top edge chamfered. These changes were made to prevent crankcase oil from leaking to the exhaust during vacuum operation; however, additional work in conjunction with the lubrication system development will be required to solve this problem.

Safe diametral clearances between the piston and the cylinder were established as follows:

Dome	.030 inches
Ring Belt	.010 inches
Skirt	.002 inches at the bottom, tapering to .005 inches at the top

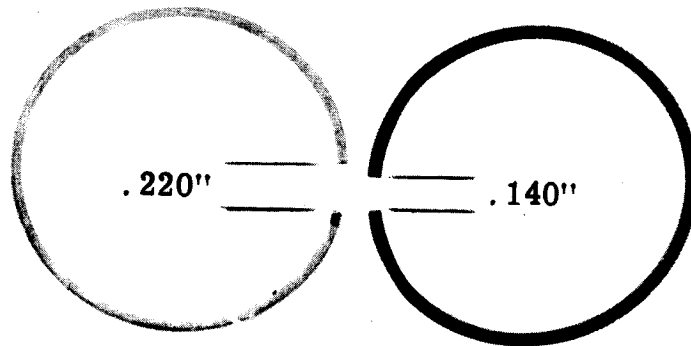


Fig. 3-16 - Comparison of New and Heat-Set Ring

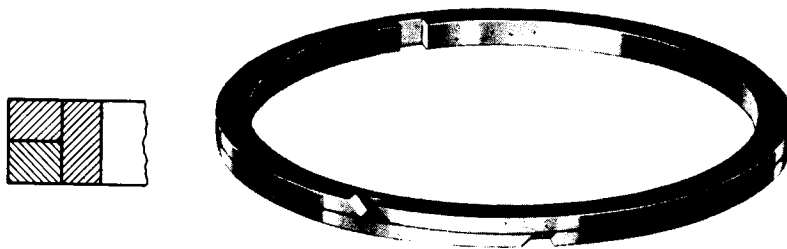


Fig. 3-17 - Three Piece Piston Ring

These values were calculated using temperature test data from two tests when seizures occurred.

The seal between the cylinder and cylinder head ring was perfected, using both the copper and the stainless steel gasket, by grinding three raised ridges onto the sealing surface of the cylinder directly under the loading ridge of the head ring.

Silicon rubber O-rings, Viton A O-rings, and Handy and Harmon Easy Flow 45 Silver solder induction brazing were evaluated as sealing methods between the cooling jacket portion of the cylinder and the jacket. The silicon O-rings resulted in repeated failures. The Viton A O-rings were successful during a limited amount of testing but were rejected in favor of brazing because of its obvious reliability advantages. The brazed joint has been successful.

Both T-15 tool steel with a vapor-honed bore finish, and cast iron cylinders with a conventional cross-hatch hone pattern bore finish were fabricated. All but about five hours of testing have been with T-15 tool steel cylinders. Since the cylinder bores were finished prior to brazing the cooling jacket to the cylinder barrel, some distortion of the cylinder bore resulted. The cast iron cylinder suffered no observable deterioration during the five hours it was tested; however, extensive testing will be required to determine if its wear rate is acceptable. If it is found to be acceptable, the cast iron would be a preferable cylinder material because of ease of fabrication, as well as being able to offer a better retention of lubrication.

- 3.1.4 Hydrogen Valve - The original hydrogen valve design is shown in Figure 3-18 and the present configuration is shown in Figure 3-19. While in the original design the valve stems were exposed

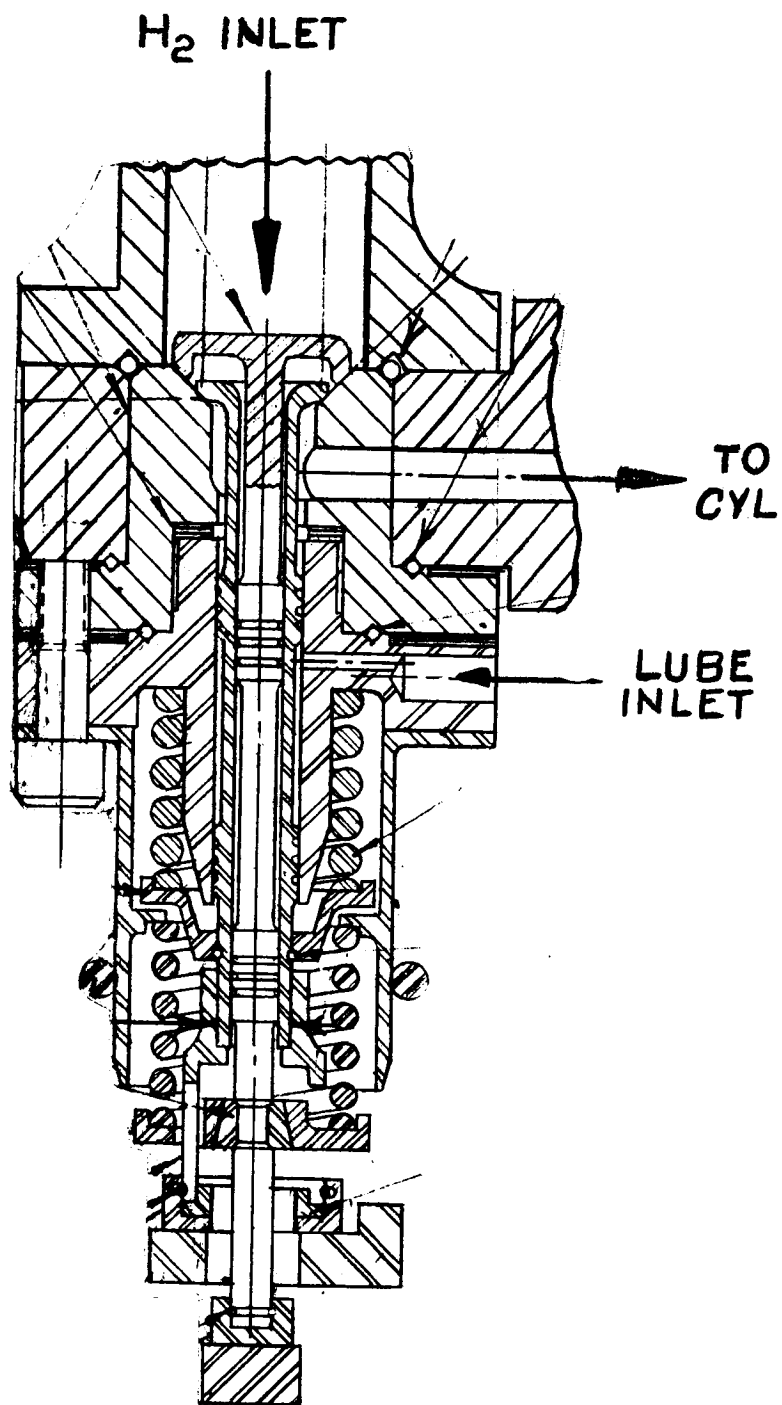


Fig. 3-18 - Initial Hydrogen Valve Design

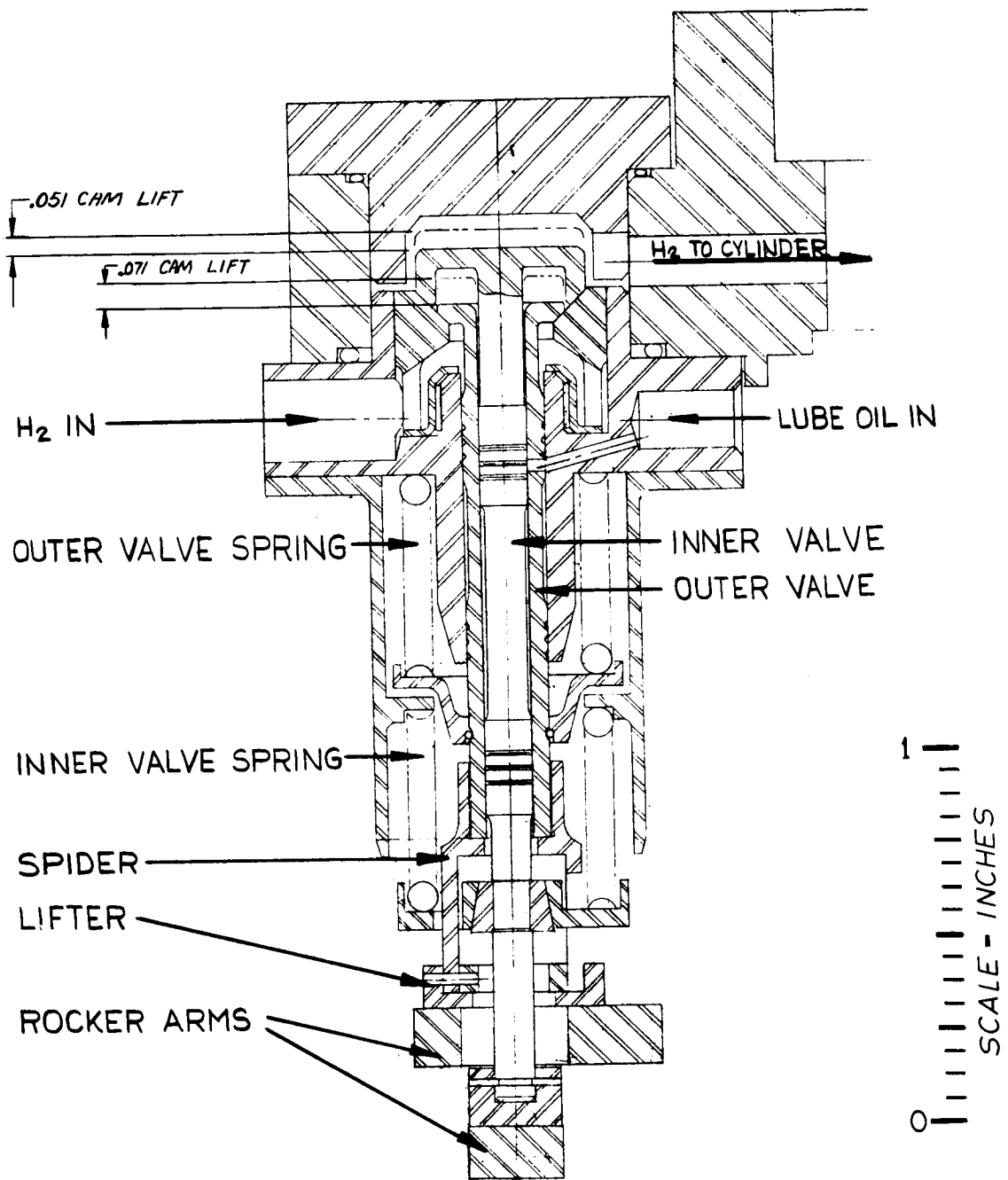


Fig. 3-19 - Final Hydrogen Valve Design

to the combustion chamber, they are exposed to the hydrogen supply in the present design. A heat shield was added to protect the valve guide from direct impingement of high temperature hydrogen gas flow. The reasons for changing the design were:

1. Exposure of the stems to the combustion chamber had resulted in high stem and guide wear and valve leakage due to thermal distortion.
2. There was the possibility that the valves could be opened by combustion pressure peaks.
3. Chances of assuring proper lubrication, effecting a hydrogen seal, and minimizing oil loss to the combustion chamber will be better with a constant gas pressure balancing the oil pressure.

While the present hydrogen valve hardware was being fabricated, interim higher load hydrogen valve springs were used with the original valve so that higher peak combustion chamber peak pressures would not result in the valves blowing open.

The composite test experience with the valve shown in Figure 3-19 has revealed a number of deficiencies which must still be overcome. These, together with recommended fixes, are discussed below:

1. Valve Springs

Inner and outer valve springs of both Music wire and Elgiloy have been used. The maximum working stress of the inner valve spring is approximately 120,000 psi,

and the maximum working stress of the outer is approximately 130,000 psi. These working stresses are too high for this type of application and failures of both springs have resulted. Music wire springs took permanent sets and Elgiloy springs fractured. As previously mentioned, the crankcase casting design has imposed a space limitation on the hydrogen valve spring. A layout drawing, conforming to the present crankcase, by which the maximum valve stresses can be reduced to approximately 116,000 psi for the outer valve, and 96,000 psi for the inner valve, has been made. The design requires new retainers and rework of the spring housing. With these stress levels, failure should not occur within the required design life. However, the stress level should be further reduced for a flight-type design.

2. Outer Valve Spider and Lifter

The outer valve lifter rides on the outer valve rocker arm which is in contact with the outer valve cam. The lifter transmits the lift motion to the spider and the spider transmits it to the outer valve stem. The legs of the spider pass through three holes in the lower spring retainer of the inner valve. A few spider failures, as shown in Figure 3-20, have occurred. In addition, wear between the spider and the lifter has occurred during some, but not all, of the endurance test runs. Figure 3-21 shows a worn lifter, a worn spider, and a failed outer valve spring. Even when wear and spider failure occurred the assembly held together and did not directly result in test stoppage. However, when the life of the valve springs has been increased, this wear will eventually result in failure. The wear problem is attributed to rocking and turning between the two parts with

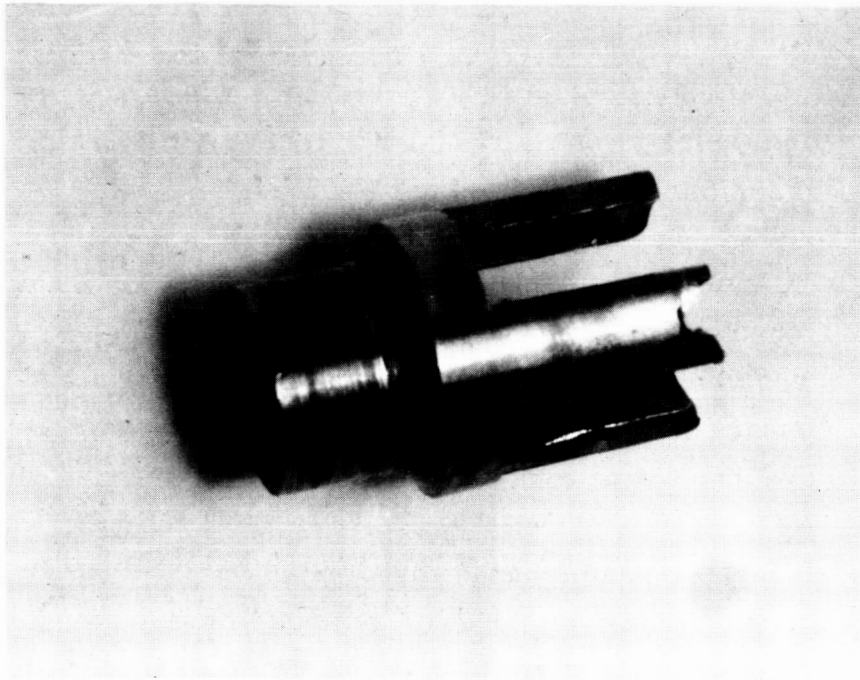


Fig. 3-20 - Failed Hydrogen Valve Spider

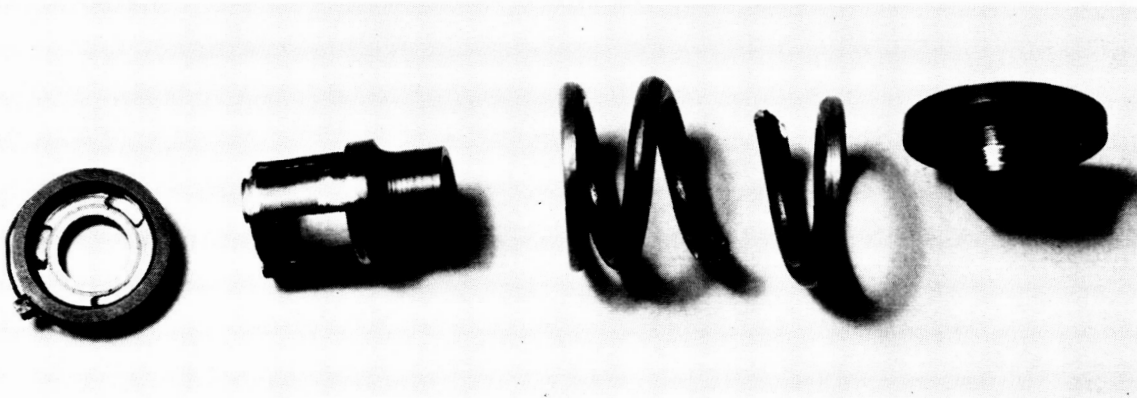


Fig. 3-21 - Failed Spring, Spider, and Worn Lifter

a fretting motion. This problem will be corrected by redesign of the two parts. One possible approach would be to replace the spider legs with pins which are press-fitted into holes in one part and which have a tight slip fit in the other part.

3. If, during the development of the lubrication system, it is found that oil consumption is extensively increased due to wear between the valve stems and guide, it may be necessary to hard surface these surfaces. It is recommended that hard surfacing be evaluated initially.
4. If further performance tests indicate that performance of an acceptable level can be achieved by fixed hydrogen valve timing and varying power by controlling hydrogen pressure, it may be desirable to use a single poppet valve.
5. During some tests, valve sticking, due to carbon deposits built up above the poppets, has been suspected. The remedy for this problem is to improve the lubrication system so that less lubrication oil is carried into the combustion chamber.

3.1.5 Cylinder Head Insert and Seal - The cylinder head insert fits into the cylinder head ring and forms the engine's combustion chamber (see Figures 3-2 and 3-3). Figure 3-22 shows how the thickness of the cylinder head insert was increased during the program. The cylinder head insert "A" in Figure 3-22 was used with the original cylinder and piston design shown in Figure 3-2. This insert provided no space for combustion chamber experimentation. Insert "B" in Figure 3-22 was used with the old cylinder design, but with a piston of reduced height, which allowed the insert thickness to be increased. Insert "C" in

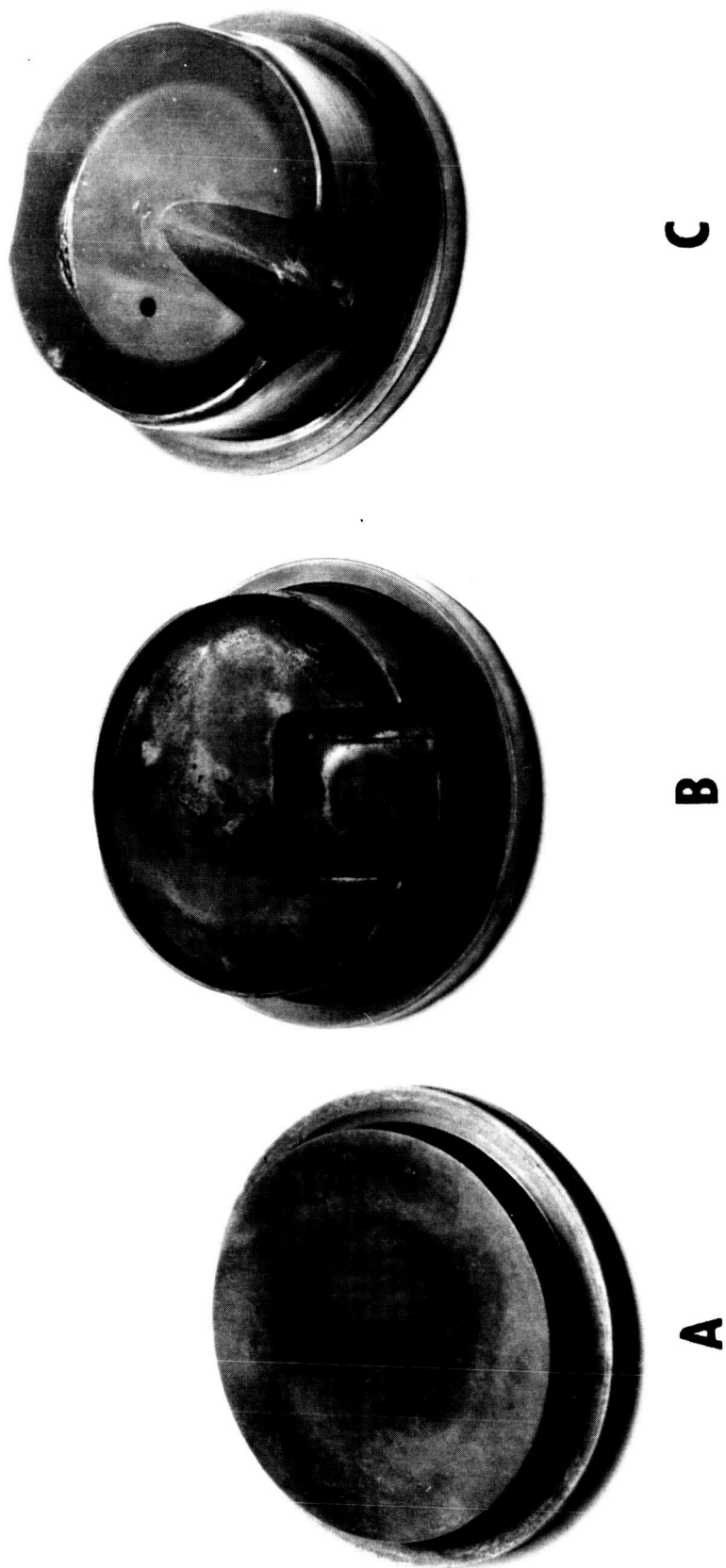


Fig. 3-22 - Cylinder Head - Combustion Chamber Evolution

Figure 3-22 was used with the present engine configuration shown in Figure 3-3. It is the thickest of the three inserts and allows the most space for combustion chamber experimentation. In addition, the thick cylinder head insert design protects the cylinder head ring from direct impingement of combustion gas as can be seen in Figure 3-3.

During engine tests with the new piston and cylinder design, thick cylinder head inserts with a "mushroom" (Figure 3-23), a "Mexican Hat" (Figure 3-24), and a "Figure Eight" (Figure 3-25) combustion chamber shape were used. Cross-sectional sketches of these chamber shapes are shown in Figure 3-41, in Section 3.3.3.

The objective of combustion chamber experimentation was to improve combustion efficiency by creating turbulence to speed the combustion process and the mixing of combustion gas with the unburned hydrogen.

The Inconel X "K" seal between the head insert and cylinder head ring has leaked on numerous occasions. However, no leak has occurred during approximately the last 361 hours of endurance testing. The elimination of the leak problem is attributed to the practice of lapping the insert to the head ring and using the more rigid retainer ring.

Though the "K" seal may now be successful, it would be desirable to replace it with a seal that has less dead gas volume and is less expensive.

The gasket and load ring sealing arrangement shown in Figure 3-26 was fabricated as a possible replacement of the cylinder head insert "K" seal. The load ring is of Inconel X and is re-



Fig. 3-23 - "Mushroom" Combustion Chamber



Fig. 3-24 - "Mexican Hat" Combustion Chamber



Fig. 3-25 - "Figure 8" Combustion Chamber

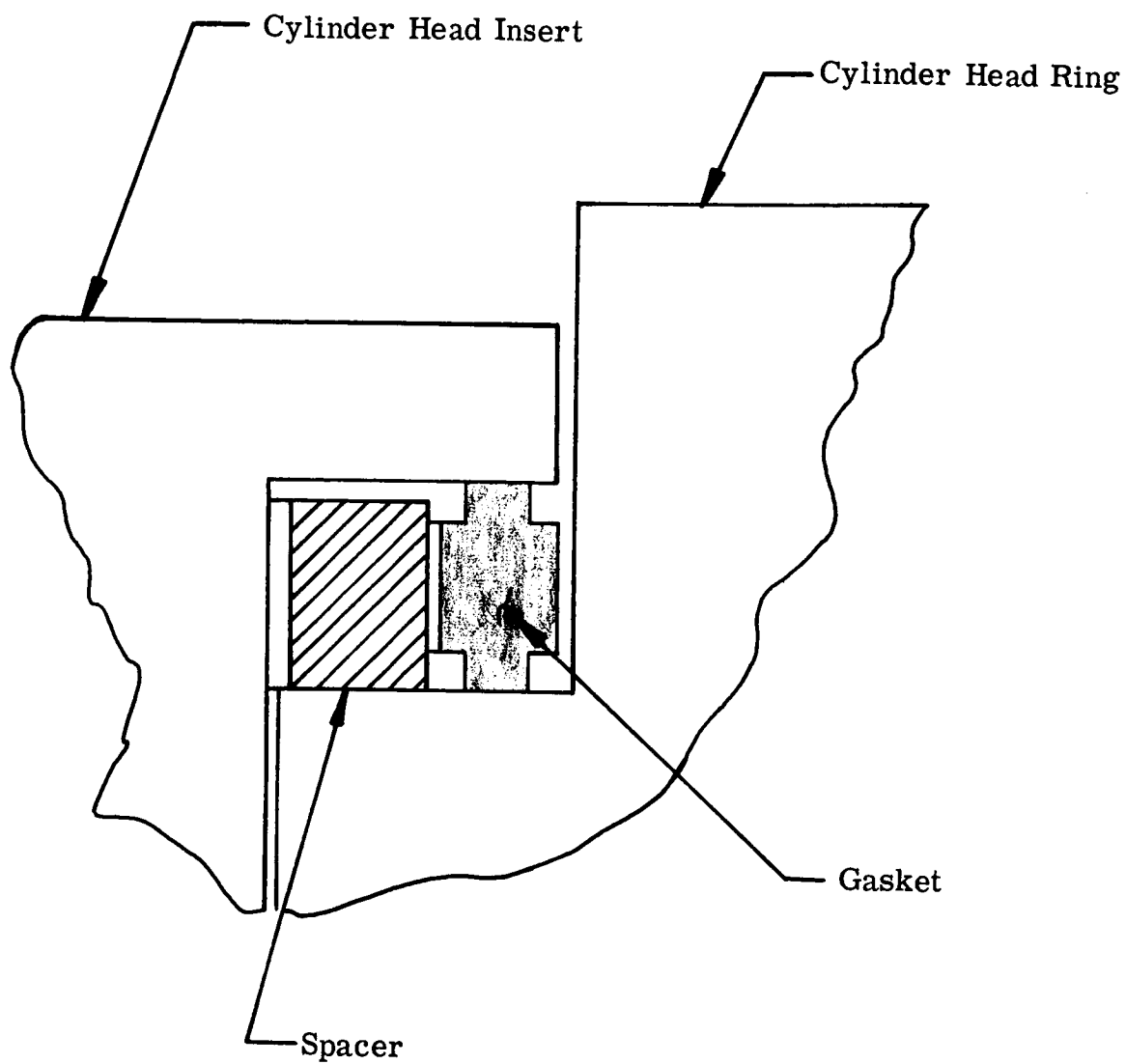


Fig. 3-26 - Alternate Cylinder Head Seal

useable. The gasket is of soft copper and is not re-useable. Figure 3-26 shows the gasket in the unloaded condition. When the cylinder head retainer screws are torqued down the gasket is crushed to the thickness of the load ring. The gasket did not leak during five hours of performance testing, but more test time will be required to prove its integrity.

- 3.1.6 Starting - Throughout this program the engine was started by means of catalyst pellets contained in a cavity adjacent and connected to the combustion chamber. The pellets, supplied by Baker & Company, Newark, New Jersey, consist of a layer of palladium deposited on a substrate of aluminum oxide and are .125 inch diameter by .125 inch long. Two to six pellets are required for starting, depending on combustion chamber shape and catalyst location. During a few tests, the pellets were retained in drilled pockets in the cylinder head insert. In most cases, for testing convenience, they were retained in plugs which screwed into the combustion chamber from the outside of the cylinder head ring. After some tests, depending on the hardware configuration, the pellets were observed to have been worn from vibration. In cases where they remained intact, it was sometimes possible to stop and restart the engine after it had run for three hours or less. After the engine had run for longer than three hours, it was usually necessary to use new pellets. It was also observed that new pellets, when soaked with engine oil, would not start the engine unless the oil was removed by washing the pellets with solvent. Pellets used for more than three hours would not start the engine regardless of being cleaned in solvent.

Used pellets turn black in color, whereas the new pellets are light gray. When new and old pellets were cut open and compared under the microscope it was found that the black of the used pellets extended into the porous cross-section of the aluminum oxide

for the same distance as did the palladium in a new pellet, even though oil had apparently been absorbed by the aluminum oxide to a greater distance.

An X-ray analysis was made at the Lewis Research Center of catalyst pellets, both new and used in an extended engine run. Analysis of the new pellets showed patterns of Chi Alumina, Beta Al (OH)₃ and palladium.

Analysis of the pellets run in the engine for 7.4 hours showed patterns of Chi Alumina and Gamma Alumina. No palladium patterns were found, indicating that it somehow had disappeared during the engine operation. Since no carbon patterns were found, the possibility that carbon deposits might have obscured the palladium must be discounted.

In any event, the experienced inability to restart the engine after a long run is readily explained by the disappearance of the palladium catalyst.

It was concluded that with time, oil was absorbed by the pellets and that it reacted in some way with the palladium to make the palladium ineffective, and that these catalyst pellets are not suitable for applications where restart capability is required unless they can be protected from contact with oil and damage from vibration.

Three other catalyst starting methods, two without success and one uncertain, were evaluated. Attempts to start the engine with a solid 1/8 inch diameter bar of palladium and with a platinum plated nichrome wire were unsuccessful. This was probably due to their small surface area and large heat sink capacity, as compared to the palladium coated alumina pellets.

Because the effectiveness of catalyst pellets is very dependent on the manufacturing process, particularly with regard to the method of distribution of the catalyst on the substrate, one other type of pellet, supplied by Harshaw Chemical Company, was tried. An unsuccessful attempt to start the engine with Harshaw Catalyst PD-0509T 1/8 pellets was made; however, this test is not considered conclusive because starting difficulty had previously been experienced with the combustion chamber shape used during the test, and the engine may have started if a larger number of pellets were used. These pellets are of the same material, size, and shape as the pellets described above except they are of a harder consistency and particles of palladium are distributed homogenously through them.

The effort which has been devoted to improving the method of starting and restarting the engine has not been intensive because of more urgent engine development problems. It is felt that engine development is now at the stage that efforts can and should be directed toward starting improvements.

Catalytic restart capability is highly desirable because of its simplicity and catalyst research should be continued, but because it has been demonstrated that the engine can be started by a spark plug or hot surface with certainty (even though it is more complex), a glow plug or a similar type of system should be fabricated and perfected as a backup.

- 3.1.7 Lubrication - The effort to improve the lubrication system was not started until the last few weeks of the program because of more urgent engine development work. During the major part of the program the only requirement of the lubrication system was to supply sufficient oil to specific locations to avoid problems from lack of lubrication. All testing during this program was

conducted with MIL-L-6086B oil, with extreme pressure additives, supplied to the engine through two lines from an external lubricant supply system which was part of the test stand and included the pump. One of the supply lines provided oil to the hydrogen valve guide and valve stems at a pressure that was adjusted to match hydrogen gas engine inlet pressure in order to prevent hydrogen leakage into the crankcase. The other supply line distributed oil directly to:

1. Each of the two hydrogen valve cams
2. Each of the hydrogen valve cam follower pivot bearings
3. The oxygen cam
4. The cam shaft drive gears
5. A crankcase jet which directly impinged on the crankpin bearings, and connecting rod.

The cylinder, the oxygen cam follower rocker arm bearings, and the anti-friction main bearings and cam shaft bearings are lubricated by splash and mist, caused by impingement of the crankcase jet on the rotating crank shaft.

During endurance testing, oil losses were excessively high (approximately 1 liter per hour) when operating with vacuum exhaust. Ambient exhaust pressure operation greatly reduced the losses (to approximately 0.1 liter per hour) but the loss rate was still too high for flight application. The oil loss can only occur through two paths, other than external leakage. Oil from the hydrogen valve guide supply can be carried into the combustion chamber by the hydrogen gas, or oil from the crankcase can pass

across the oil control ring and through the clearance between the piston and cylinder, directly to the exhaust ports. It is believed that the major portion of the oil loss comes from the crankcase. The oil loss from the hydrogen valve can be minimized by maintaining a balance between hydrogen inlet pressure and oil pressure. The pressure relationship between the hydrogen and oil depends on the clearance existing between the valve guide and stem and on the oil viscosity. Preliminary tests have shown that with close clearances, oil pressure can be 50 to 100 psi below hydrogen pressure, depending upon speed. Additional analysis and test work will be required before the design of the hydrogen valve lubrication system can be finalized.

The oil lost past the piston depends on the amount of oil applied to the cylinder and the configuration of the oil ring used. This problem is aggravated when the exhaust pressure is less than the crankcase pressure. The amount of oil lost past the piston can be minimized by reducing the amount of oil applied to the cylinder and by experimentation with methods of application, oil control ring configuration, and crankcase pressure level relative to exhaust pressure.

Whether the lubrication system of the final flight type engine is of the recycling or throw-away type, it will be important to reduce the amount of oil metered to the engine and the amount of oil lost from the engine through the exhaust ports to the minimum safe limit. The engine has been developed to the point where the next phase of the development effort can and should include a concerted effort to reduce oil consumption and determine minimum quantities required for adequate lubrication. Shortly before the end of the current contract, a breadboard oil supply manifold was set up by which the oil flow to each application point (except to the hydrogen valve) could be individually

adjusted and measured.

It is recommended that efforts to reduce oil flow and consumption be continued by:

1. Analyzing and studying flow requirements separately for each lubricated area, and performing engine evaluations under motoring and firing conditions.
2. Designing and testing various oil application methods that will minimize oil waste and function under zero gravity conditions.
3. Evaluating the effects of different crankcase pressure levels (less than sea level ambient) upon oil loss and lubrication effectiveness by connecting the crankcase to the vacuum pump line through a throttle valve and running motoring and firing tests.
4. Some of the new oil application methods that may be tried are: To supply oil to the cylinder through fine holes drilled through the cylinder wall below the exhaust ports; to lubricate the cams with follower-type wipers; and to alter the design of the jet lubricating the cylinder wall from a continuous to a periodic flow. This can be accomplished if the oil is brought in through a drilled hole in the crank pin, which matches a port in the connecting rod once each revolution.

3.2 Mechanical Problem Summary

As part of the reliability and quality assurance effort, a tabulation of all engine failure reports was maintained and a failure mode

code number was assigned to each new type of failure as it occurred. A complete list of failures experienced on this program is in the Failure Report and Summary Sheets in Appendix A. As a summary of engine design integrity, improvement effort information and comments concerning each of the engine failure modes are presented in Table 3-IV.

It can be seen from Table 3-IV that of the 24 types of failures that occurred during the program, all but four appear to have been solved. One may be solved, and three remain as problems. The three unsolved are concerned with the hydrogen valve's springs and lift mechanism. Design concepts by which these problems may be resolved have been devised and are discussed in Section 3.1.4.

3.3 Engine Testing

Engine testing was divided into two major categories; endurance testing, and performance testing.

The primary objective of the endurance testing was to run the engine until a malfunction occurred so that design modifications could be made that would reduce the possibility of a recurrence of a similar malfunction. The secondary objective of the endurance test was to determine if wear of engine parts would cause performance to degrade; if so, steps could be taken to reduce wear in those areas.

A total of 727 hours of engine running were accumulated and more than 1500 data points were taken during the course of the program.

TABLE 3-IV

FAILURE MODES AND CORRECTIVE ACTIONS

Code No.	Failure Mode Description 1. O ₂ Injector 2. Engine (excluding O ₂ injector)	No. Failures	Date of Last Failure	Corrective Action	Corr. Action Effectiveness
1A	Broken Flex Pivot	4	10/12/63	New design eliminates flex pivot	R
1B	Static Seal Leak - O ₂ Inlet Plug	1	10/8/63	Silicon rubber seal used	T
1C	Quill Shaft Bushing Seizure	2	10/21/63	Clearance increased	R
1D	Poppet Retainer Spring Deformed	3	12/12/63	Spring heat treated to make harder (later eliminated from design)	R
1E	Flame Plated Valve Worn	3	11/23/63	Eliminated flame plating	R
1F	Rocker Shaft Brinelled	1	2/6/64	Needle bearings replaced with oilite bushings	R
1G	Rocker Shaft Galled	1	3/12/64	Shaft hardened	R
1H	Rocker Arm and Poppet Wear - Type 1	1	5/23/64	Design modified to Types 2 & 3	R
1I	Broken Poppet Retainer Spring - Type 2, 1	1	6/29/64	Spring eliminated from design	R
1J	Broken Poppet Retainer - Type 3	1	7/10/64	Used thicker retainer - Type 3. 1	R
2A	H ₂ Valve Guide to Cyl. Head Seal	3	12/20/63	Seal design revised when H ₂ valve redesigned	R
2B	Catalyst Plug Gasket Leak			Use new spark plug gasket each time plug removed	U
2C	H ₂ Valve Lifter Retainer Ring Broke	1	12/12/63	New thicker ring installed	R
2D	Piston Dome Retaining Screw Broke	1	1/17/64	Replaced screw with stud welded to piston body	R
2E	Piston Seized in Cylinder	2	3/31/64	Clearance increased	R
2F	Top Cylinder-To-Cooling Jacket "O" ring failure	7	4/28/64	"O" rings eliminated - braising substituted	R
2G	Copper Head Gasket Leaked	6	5/13/64	Stainless steel gasket used	R
2H	Combustion Chamber Seal Leakage	7	6/11/64	Stainless steel gasket used	P
2I	Top of Cylinder Cracked	1	6/5/64	Failure was due to overheating during test caused by cooling system failure	R
2J	Broken H ₂ Valve Spring (inner)	1	6/18/64	Spring must be redesigned for lower stress	U
2K	Broken H ₂ Valve Spring (outer)	1	6/28/64	Spring must be redesigned for lower stress	U
2L	Broken H ₂ Valve Spider	3	7/27/64	New design conceived but not tested	U
2M	Lockwire Failed on Piston Body Bolts	1	7/3/64	Modify assembly procedure	T
2N	Piston Dome Stud Braze Failed	1	7/3/64	Stud Heliarc welded to piston body	R

*Corrective Action Effectiveness:

R = Resolved

P = Probably Resolved

U = Unresolved

T = Temporarily resolved but correction not suitable for flight type design

3.3.1 Test Equipment and Instrumentation - Test facilities consisted of two engine test stands in separate test cells, each with its own controls and instrumentation. A Kinney Model KD-850 vacuum pump for controlling exhaust pressure, and a recirculating Dowtherm-A cylinder cooling system were shared by the two test stands. In addition to an engine test stand, one of the test cells also contained a stand for testing the oxygen injector. Figure 3-27 shows the engine mounted on the endurance test stand in its test cell and Figure 3-28 shows the engine mounted on the performance test stand. Figure 3-29 shows the oxygen injector mounted on the oxygen injector test stand in the performance test cell.

Figure 3-30 is a schematic of the engine performance test stand. The schematic of the endurance test stand is identical, except that the engine load is absorbed by a D-C generator instead of a hydraulic pump.

Hydrogen and oxygen gas are supplied to the engine from high pressure storage bottles through remote control pressure regulators and metering orifices. Engine power is absorbed and measured by an electrical or a hydraulic dynamometer. Engine rpm is read by a direct-current tachometer for an approximate reading and by an electronic counter for an exact speed count. Temperatures are sensed with Chromel-Alumel and Iron Constantan thermocouples and are recorded on strip chart recorders and observed on direct reading indicators.

Temperatures recorded include cylinder head temperature, exhaust gas temperature, oxygen and hydrogen inlet temperatures, inlet and outlet temperatures of the coolant flowing through the cylinder cooling jacket, wall temperatures on the top and the bottom of the cylinder, and lubricant inlet and outlet temperatures.

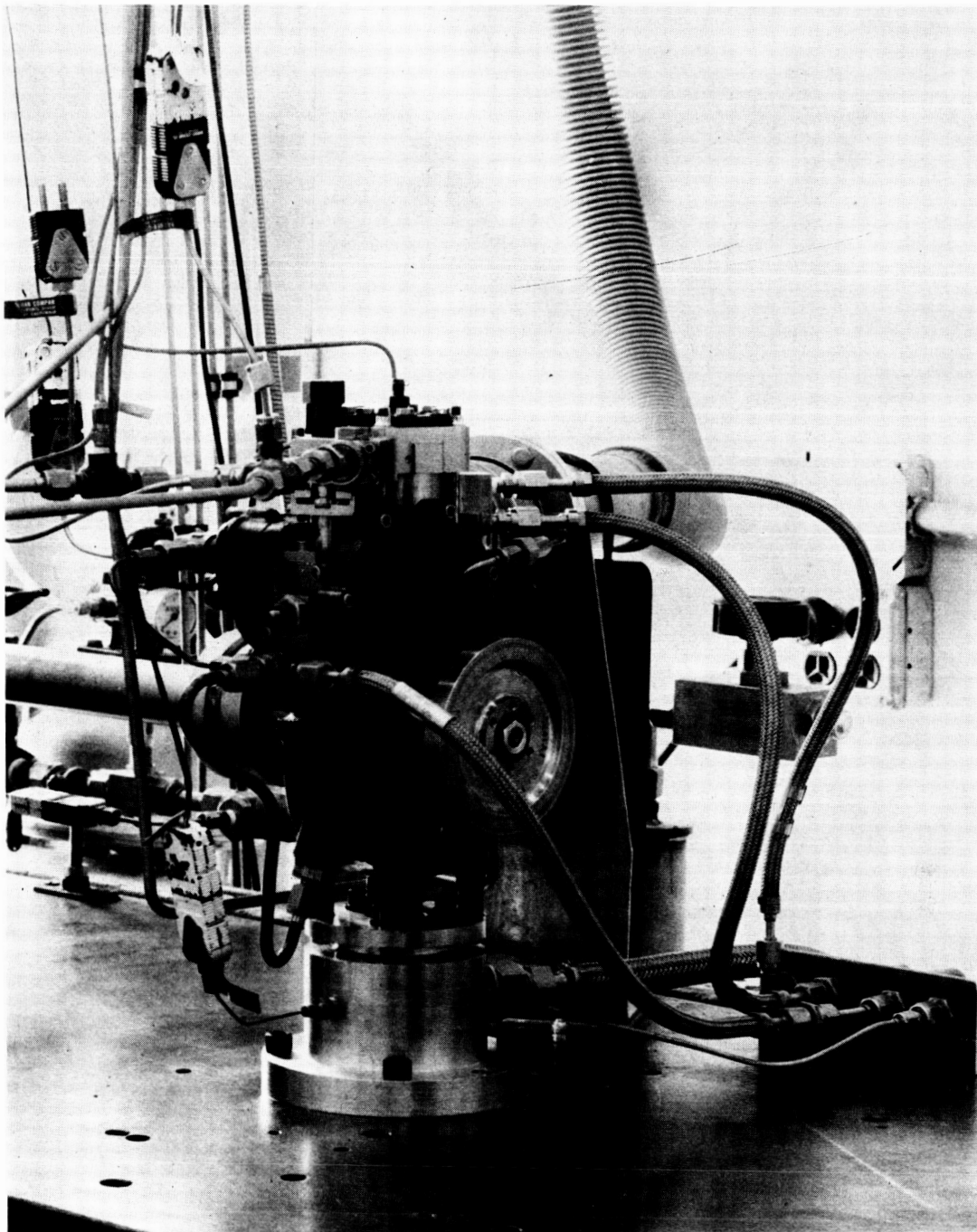


Fig. 3-27 - Engine on Endurance Test Stand

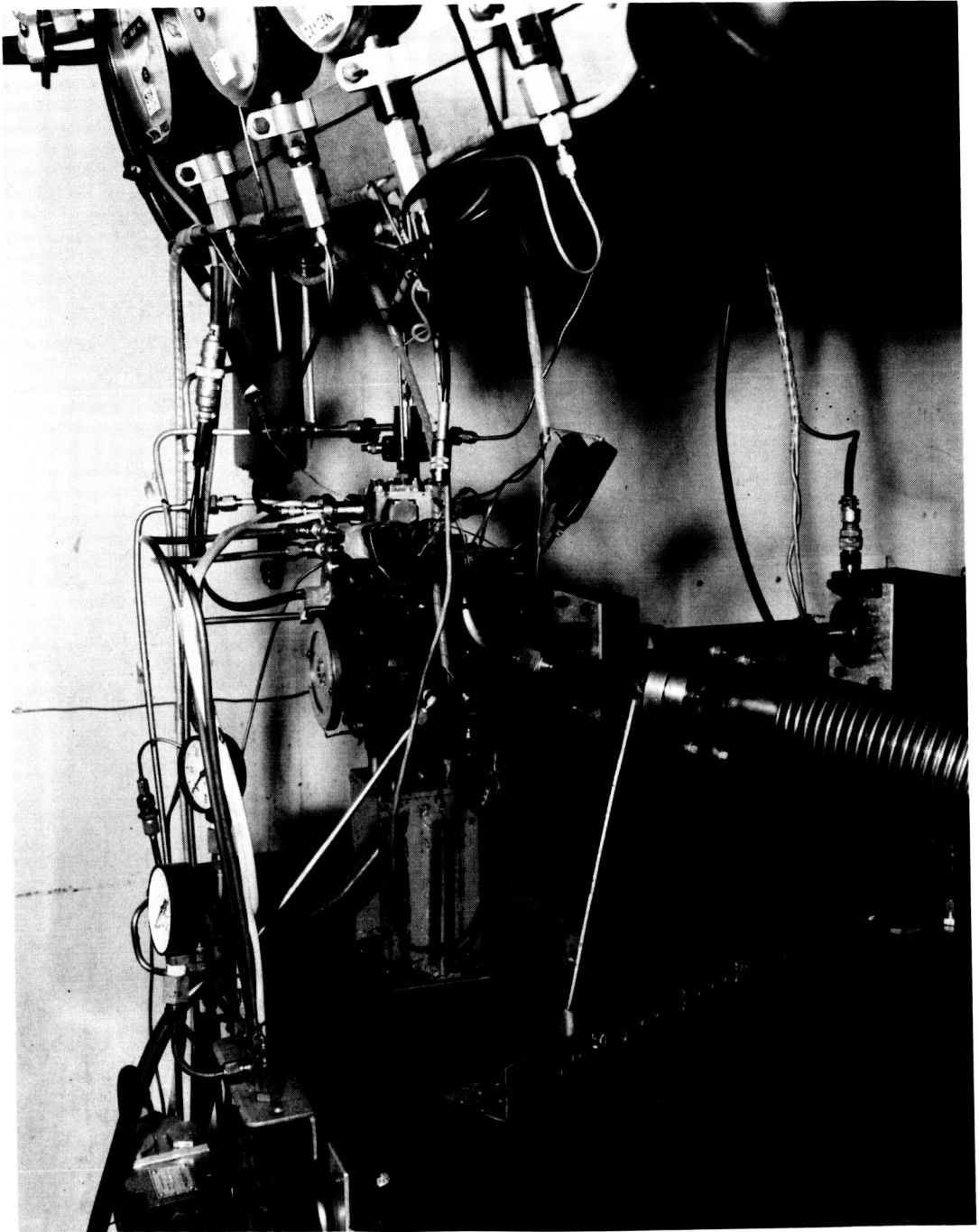


Fig. 3-28 - Engine on Performance Test Stand

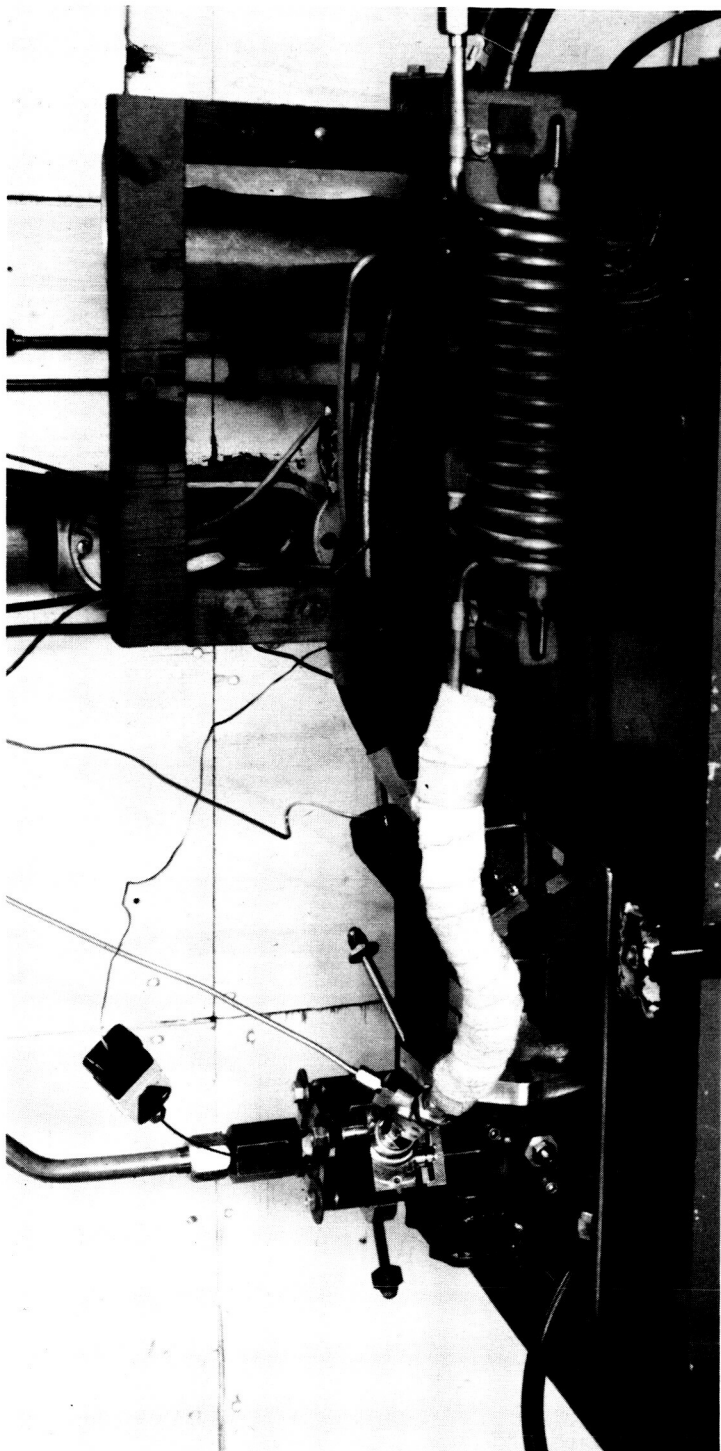


Fig. 3-29 - Oxygen Injector Test Stand and Oxygen Heater

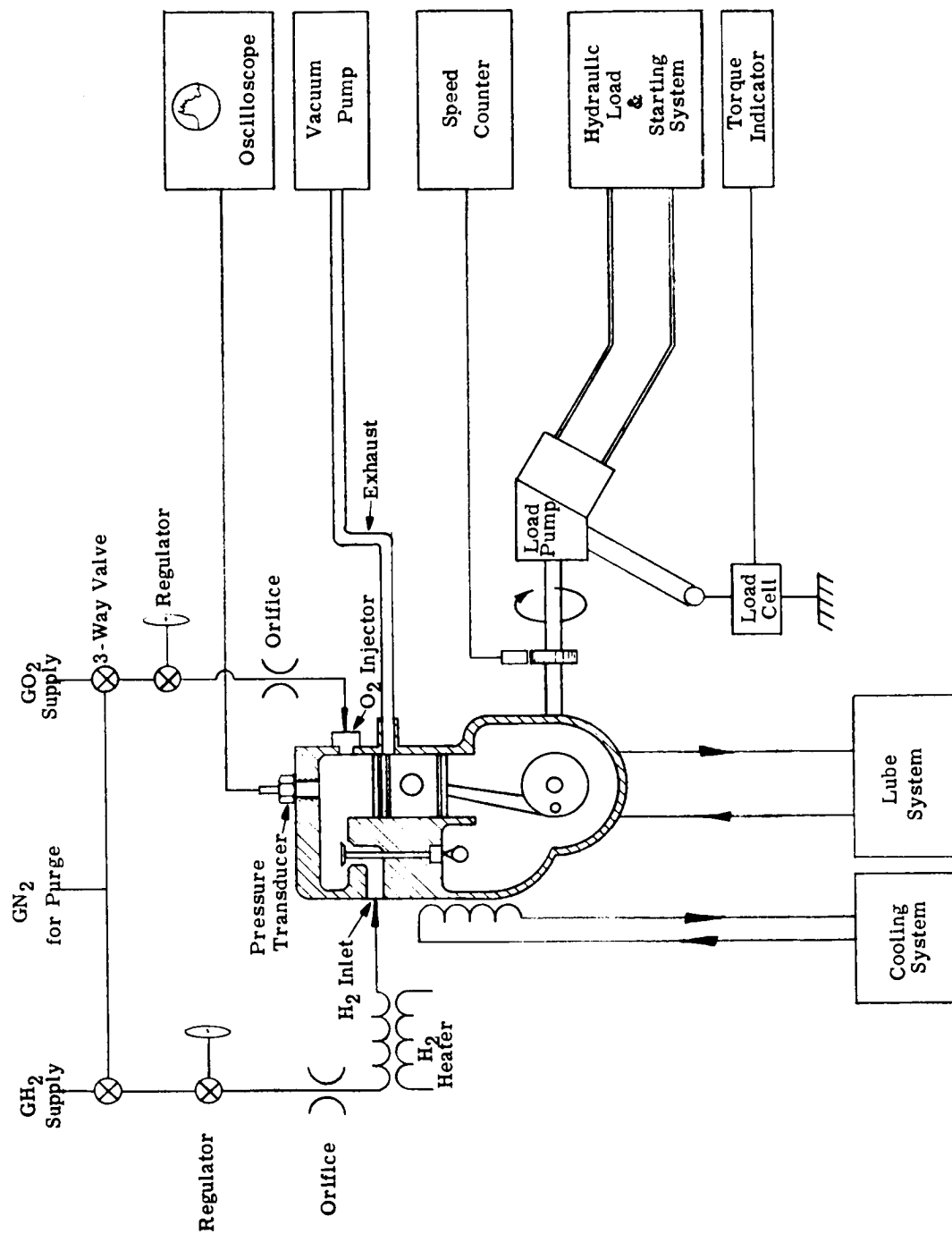


Fig. 3-30 - Engine Performance Test Stand Schematic

The coolant flow is measured so that heat rejection to the coolant can be calculated. The temperature of the hydrogen gas at the engine inlet can be maintained by a controllable electric heater.

A Kistler Model 601 pressure transducer is employed for combustion chamber pressure measurements. This is a miniaturized quartz crystal transducer that is widely used in internal combustion engine research. It is installed in an adapter that fits any of the three ignition plug ports in the cylinder head ring, or in a port above the hydrogen valve poppets. The signal from the pressure transducer is fed to the vertical input of an oscilloscope that is calibrated directly in units of pressure (psi). A horizontal time sweep corresponding to one crank shaft revolution results in a pressure-time trace that is photographed by a Polaroid camera for later comparison with performance data. A typical time trace is shown in Figure 3-31A.

In the interest of safety, the test cells are completely open at one end and have ceiling vents to prevent accumulation of hydrogen gas in case of a leak. Remote control pressure regulators are used for controlling gas pressure to the engine in order to avoid high pressure gas lines passing through the control room. Also, all gas pressure gages are located in the test cell to avoid hydrogen leakage in the control room. Gages are read through a window of safety glass from the control room. Other instrumentation readout equipment is located within the control room, shown in Figure 3-32.

The gas supply system is shown schematically in Figure 3-30. Both the hydrogen and oxygen lines can be purged with nitrogen. Propellant flow rates are calculated from the upstream pressure, differential pressure, gas temperature, area, and flow coefficient

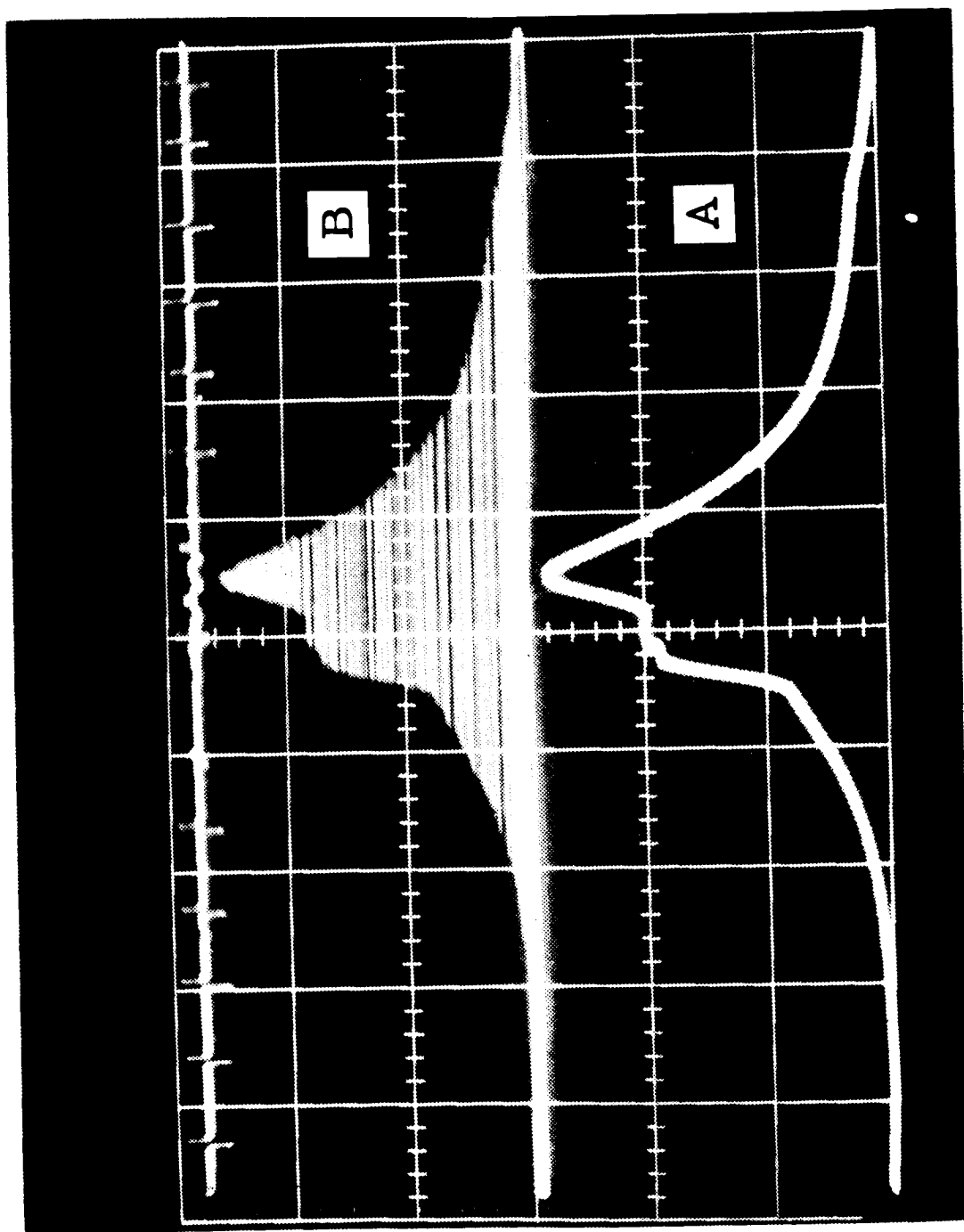


Fig. 3-31 - Cylinder Pressure Time Traces



Fig. 3-32 - Engine Control Room

of the flow nozzles using the equation:

$$\dot{W} = KA \sqrt{\frac{P \Delta P}{T}}$$

Where K is a constant, including all constants, conversion factors, and the nozzle flow coefficient.

The flow nozzles were calibrated against accurate sonic orifices. Also, the flow nozzles and the instrumentation system (pressure gage, ΔP gage and temperature readout) were calibrated as a unit against a certified Rotometer flow meter. This was done for the oxygen and hydrogen flow nozzles used on the endurance test.

On the performance test stand, where the load is absorbed hydraulically, power is computed from the direct torque readout of a trunnion-mounted strain gage load-cell and the speed reading of the electronic counter. The complete torque indication system is calibrated with a series of dead weights at a known lever arm prior to test.

On the endurance test stand, where the load is absorbed with a direct current electric generator, power is calculated with the equation:

$$\text{WATTS (Output Power)} = IV + IV_b + I^2R + S. L.$$

Where:

I = Output current of the generator

V = Voltage across the generator

R = Known resistance of the portion
generator through which I is flowing

V_b = Calibrated, brush voltage drop

S. L. = Stray losses (all other losses), calibrated, and plotted as function of speed and current through an excitation field. Field current is controlled by a separate direct-current power supply.

Although the piezoelectric transducer has proven to be very useful for qualitative purposes, it has not produced data sufficiently accurate for quantitative analysis of engine performance. For precise cylinder pressure data, the technique commonly used in internal combustion engine research employs a balanced-pressure diaphragm pickup with a controlled reference pressure on one side and cylinder pressure on the other side of the diaphragm. When cylinder pressure equals the reference pressure, the pickup generates a signal due to diaphragm motion. By varying reference pressure over the full range of cylinder pressure, a history of cylinder pressure over a large number of cycles can be obtained. Reference 5 describes the technique and equipment used for this purpose. The primary disadvantage of this technique is that it requires point-by-point plotting of many individual data points to obtain a complete picture of the cyclic cylinder pressure variation.

In order to avoid the laborious point by point technique, a new unique method was developed for rapid accumulation of cylinder pressure data by means of a balanced pressure pickup. The equipment used for this purpose is shown schematically in Figure 3-33. The balanced pressure pickup (a Photocon diaphragm switch) is used to switch the electric output of the pressure transducer in the reference pressure line. The magnitude of the cylinder pressure, as well as the crank angle at which the switch opened and closed, is displayed on the scope and photo-

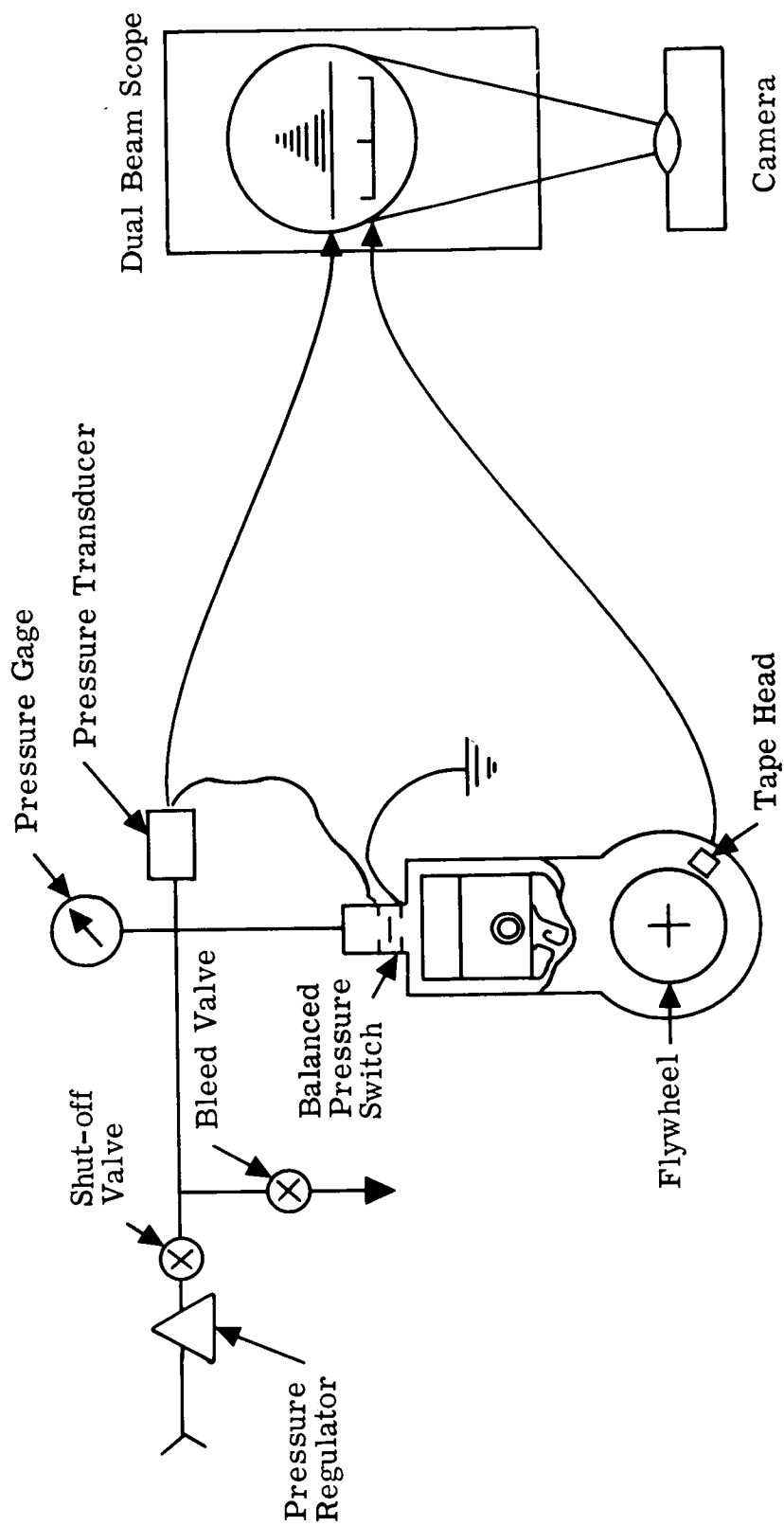


Fig. 3-33 - Schematic of Balanced Pressure Indicator System

graphed. The other beam of the scope displays crank angle position blips picked up by a tape recorder head from a magnetic tape mounted on the engine flywheel.

The reference pressure side of the balanced pressure switch is initially pressurized to a level above peak cylinder pressure. The pressure is then allowed to decay (with the engine running) while a time exposure photograph of the oscilloscope display is taken. The decaying reference pressure changes the crank angle at which the switch opens and closes. This change is due to the changing pressure unbalance between the reference pressure and cylinder pressure. The resulting photograph consists of a series of horizontal lines whose extremities represent points of cylinder pressure equal to reference pressure. The envelope of this series of lines thus provides a pressure-time history of cylinder pressure over the number of cycles which occur while the camera shutter is open (usually about 2 seconds). A typical photo of the results is shown in Figure 3-31B, with the output of the piezoelectric transducer on the lower trace for comparison purposes (A). This photo also contains timing blips on the top trace.

The balanced pressure was particularly useful in the evaluation of the exhaust blowdown portion of the engine cycle because it was possible to accurately determine pressure in the low pressure region.

Although considerably more accurate, temperature sensitivity of the balanced pressure switch has limited the application of this instrumentation. Water cooling the transducer gives rise to a substantial heat sink in the cylinder head. This is an unrealistic test condition when running tests to evaluate performance with the head uncooled. For these reasons, the Kistler

transducer was used during the majority of performance test runs.

3.3.2 Endurance Test Results - A summary of the results of the 13 endurance tests performed during the program are summarized in Table 3-V. Oxygen injector configurations and wear rates during Tests 5 through 13 are summarized in Table 3-VI. Table 3-VII schematically defines the oxygen injector hardware-type codes of Tables 3-V and 3-VI. Table 3-VIIIA and Table 3-VIIIB tabulate dimensional changes of hydrogen valve, piston and cylinder. Inspections were made at convenient times during endurance testing and therefore, the time between inspections does not correspond exactly with test times. Additional hardware and test conditions are listed below:

1. Cylinder and Piston Configuration

Tests 1 through 4

Original cylinder design (nitralloy) and original piston design reworked for increased exhaust blow-down area.

Tests 5 through 10

New design T-15 tool steel cylinder and new design three-piece piston with brazed piston dome stud.

Tests 11 through 13

Same as Tests 5 through 10, except that the piston dome stud was welded to the ring belt.

TABLE 3-V

ENGINE ENDURANCE TEST SUMMARY

Test No.	Date 1964	Hrs. Per Test *	Accum. Hrs *	HP	BSPC Lbs. / Hp-Hr.	Reason for Terminating Test	Comments	O ₂ Rocker Arm Type **	O ₂ Valve Lift Adjusted
1	2/5	8.1	8.1	2.2-2.5	2.1-2.3	Scheduled - shut down		Interim	No
2	2/6	6.1	14.2	2.2-2.7	2.0-2.2	Scheduled - shut down		Interim	No
3	2/24	12.2	26.4	2.3-2.7	1.9-2.3	Scheduled - shut down		Interim	No
4	2/28	9.4	35.8	2.2-2.6	1.7-2.0	O ₂ Injector, port plug	Not a serious problem	Interim	No
5	5/19-23	100.1	135.9	0.9-2.1	1.8-3.1	Scheduled - shut down		#1	@51.2 HRS
6	6/2-3	24.9	160.8	2.2-2.4	2.0-2.2	Fire at hydrogen supply line fitting	Not part of engine	#1	No
7	6/11-12	32.0	192.8	2.4-2.6	1.6-1.9	H ₂ valve sticking due to carbon deposit	Oil consumption too high	#2	No
8	6/15-18	65.5	258.3	2.4-2.7	1.6-1.9	H ₂ spring failure	Spring over stressed. Requires re-design.	#2	No
9	6/24-25	34.4	292.7	2.5-2.7	1.7-2.0	H ₂ spring failure	Spring over stressed. Requires re-design.	#2.1	No
10	7/1-3	30.4	323.1	2.2	1.7	Failure of safety wire on piston body bolt	Assembly error	#3	@21.6 HRS
11	7/6-10	80.1	403.2	2.2-2.6	1.7-1.9	O ₂ poppet retainer failure	Part damage inadjustment also re-designed	#3	No
12	7/11-17	120.4	523.6	2.2-2.5	1.7-1.9	Slippage of clamp locating O ₂ cam follower.	Part not to print	#3	@ 6 HRS
13	7/24 -	95.9	619.5	2.3-2.5	1.7-1.9	H ₂ valve spring failure	Springs over stressed. Requires re-design.	#3.1	@7.2 HRS

* Test time includes pre-endurance checkout time provided no wearing or moving parts are replaced.

** See Table 3-VII

TABLE 3-VI

OXYGEN INJECTOR ENDURANCE HISTORY SUMMARY

Test Dates Start & Stop	Data Sheets Start & Stop	Hours Of Test	Seat		Poppet				Rocker Arm		Retainer Type, Mtl.	Lift		Lash Chg. Inches	Wear							
			Type	Mtl.	Type	Mtl.	Coating	Guide	Rocker Contact	Type		Mtl.	Coating		Chg. in. - Inches	Rate in. hr.	Poppet Moved Into Rocker	Poppet Moved Into Seal	In Poppet By Rocker	On Poppet By Retainer	In Retainer By Poppet	Poppet-Seal Guide Clearance Increase
5/19-23 /64	2-16	100.1	0.032 Straight Cone	H-25	1	H-25	C _a F ₂	None	1	H-25	None	1	H-25	-0.008 51 hr.	-0.00016	0.0265						
6/2-3 /64	19-25	24.6	0.032 Straight Cone	H-25	1	H-25	C _a F ₂	C _a F ₂	1	H-25	None	1	H-25	-0.0052 24.6 hr.	-0.00022	0.0155						
6/11-12 /64	28-33	32.0	0.045 Straight Cone	H-25	2	H-25 6B	C _a F ₂	None	2	H-25	None	2	H-25	-0.0038 24 hr.	-0.00016	0.004						
6/15-18 /64	34-44	65.5	0.045 Straight Cone	H-25	2	H-25 6B	C _a F ₂	None	2	H-25	None	2	H-25	-0.0058 58.7 hr.	-0.00009	0.006						
6/24-25 /64	45-53	34.4	0.045 Straight Cone	H-25	2	H-25 6B	C _a F ₂	P _b O	2	H-25	None	2.1	H-25	-0.0032 32 hr.	-0.0001	Broken Leaf Spring						
7/1-3 /64	57-62	30.4	0.045 Straight Cone	H-25	3	H-6B	None	None	3	H-6B	None	3	H-25	+0.0017 13.37 hr.	+0.00001	0.002	0.001					
7/6-10 /64	63-74	80.1	0.032 Straight Cone	H-25	3	H-6B	P _b O	P _b O	3	H-6B	None	3	H-25	-	-		0.0085	0.0039	0.0075	0.002		
7/11-17	75-90	120.0	0.032 Straight Cone	H-25	3	H-6B	P _b O	P _b O	3	H-25	None	3	H-25	-0.0031 114 hr.	-0.00003	0.021	0.0065	0.0063	0.0032	0.0125	0.0032	0.0043
7/28- /64	94-110	95.9	0.032 Straight Cone	H-6B	3	H-25	None	WC	3	H-6B	None	3.1	H-25	+0.0035 89 hr.	+0.00003	0.0048	0.0011	0.0057	0.0002	0.0003	0.002	0.0035

H-25 - Haynes Alloy 25
 * H-6B - Haynes Stellite 6B

* H-25 Stellite 6B brazed to Haynes 25
 6B

TABLE 3-VII

O₂ Injector Poppet & Rocker Arm Design Types


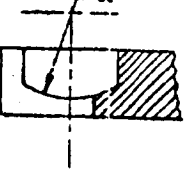
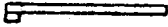
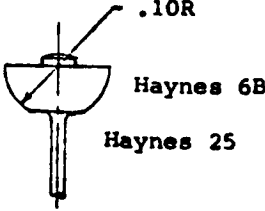
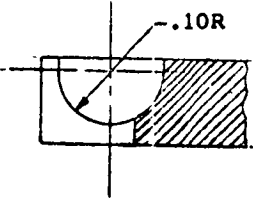
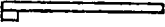
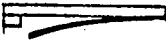
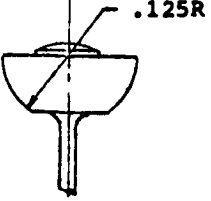
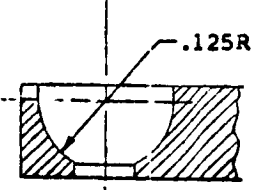
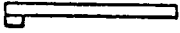
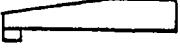
<p>1</p> <p>Poppet</p>  <p>Partial Sphere Part No. SK14621</p>	<p>1</p> <p>Rocker Arm</p>  <p>Slotted Partial, Sphere Part No. X612212</p>	<p>1</p> <p>Retainer</p>  <p>Flat Part No. X612211</p>
<p>2</p>  <p>Small Hemisphere Part No. SK 15847</p>	<p>2</p>  <p>Small Hemisphere Slotted Part No. SK15846</p>	<p>2</p>  <p>Flat Part No. X612211</p> <p>2.1</p>  <p>Flat with Cant.Spring Part No. X612211</p>
<p>3</p>  <p>Large Hemisphere Haynes Part No. 6B X612215 25B SK 15851 Flame SK 16261 Plated</p>	<p>3</p>  <p>Large Hemisphere Haynes Part No. 6B X612214 25B SK 15849</p>	<p>3</p>  <p>Flat-Thin Part No. X612216</p> <p>3.1</p>  <p>Flat-Thick Part No. SK 16267</p>

TABLE 3-VIII A

B = Before Operation
 A = After Operation (Tear Down)
 W = Wear (B - A, Or Change)

HYDROGEN VALVE ASSEMBLY												
Date Assem. Inspect.	Acc. Hot Hours	Inner Valve			Outer Valve				Guide			
		Stem Top land	OD	Stem Bott. land	Stem Top ID	Stem Bott. ID	Stem Top land	Stem OD Bott. land	Top ID	Bott. ID		
2-12-64	35.8	B-, 1247	B-, 1247	B-, 1247	B-, 12520	B-, 12510	B-, 21745	B-, 21750	B-, 21810	B-, 21810		
3-6-64		A-, 1243	A-, 1246	A-, 1246	A-, 12515	A-, 12500	A-, 21730	A-, 21740	A-, 21800	A-, 21810		
		W-, 0004	W-, 0001		W-, 00005	W-, 00010	W-, 00015	W-, 00010	W-, 00010	W-, 00000		
4-16-64	100.1	B-, 12460	B-, 12470	B-, 12470	B-, 12495	B-, 12495	B-, 2177	B-, 21760	B-, 21819	B-, 21807		
6-8-64		A-, 12460	A-, 12470		A-, 12510	A-, 12500	A-, 2175	A-, 21760	A-, 21820	A-, 21810		
		W-, 00000	W-, 00000		W-, 00015	W-, 00005	W-, 0002	W-, 00000	W-, 00001	W-, 00003		
5-23-64	24.9	B-, 1244	B-, 1245		B-, 1251	B-, 1251	B-, 2177	B-, 2177	B-, 2181	B-, 2181		
6-3-64												
6-4-64	97.5	A-, 1240	A-, 1243		A-, 1253	A-, 1251	A-, 2175	A-, 2176	A-, 2183	A-, 2181		
6-19-64		W-, 0004	W-, 0002		W-, 0002	W-, 0000	W-, 0002	W-, 0001	W-, 0002	W-, 0000		
6-22-64	34.4	B-, 1246	B-, 1247		B-, 1251	B-, 1250	B-, 2175	B-, 2176	B-, 2182	B-, 2181		
6-26-64		A-, 1237	A-, 1244		A-, 1253	A-, 1252	A-, 2173	A-, 2175	A-, 2183	A-, 2181		
		W-, 0009	W-, 0003		W-, 0002	W-, 0002	W-, 0002	W-, 0001	W-, 0001	W-, 0000		
6-29-64	30.4	B-, 1237	B-, 1244		B-, 1253	B-, 1252	B-, 2173	B-, 2175	B-, 2183	B-, 21810		
7-3-64												
7-3-64	296.4	A-, 1234	A-, 1243		A-, 1263	A-, 1253	A-, 2164	A-, 2173	A-, 2184	A-, 21816		
8-18-64		W-, 0003	W-, 0001		W-, 0010	W-, 0001	W-, 0011	W-, 0002	W-, 0001	W-, 00006		

TABLE 3-VIII B

B = Before Operation
 A = After Operation (Tear Down)
 W = Wear (B - A, Or Change)

PISTON ASSEMBLY													
Date Assem. Inspect	Acc. Hot Hours	RING END GAP				RING SIDE C/L.				Skirt & Housing Dimensions			
		#1	#2	#3	#4	#1	#2	#3	#4	BODY	Ring Housing		
2-12-64 3-6-64	35.8	B. 030 A. 130 W. 100	B. 030 A. 030 W-0-	B. 030 A. 030 W-0-	B. 027 A. 027 W-0-	B. 008 A. 008 W-0-	B. 004 A. 004 W-0-	B. 005 A. 005 W-0-	B. 002 A. 002 W-0-	B 1.495 A 1.495 W-0-	Same		
4-16-64 6-8-64	100.1	B. 080 A. 081 W. 001	B. 016 A. 016 W-0-	B. 016 A. 016 W-0-	B. 007 A. 007 W-0-	B. 004 A. 004 W-0-	B. 004 A. 004 W-0-	B. 004 A. 004 W-0-	B. 0025 A. 0025 W-0-	B 1.495 A 1.495 W-0-	Same		
5-23-64 6-3-64	24.9	B. 080 A. 093 W. 013	B. 017 A. 017 W-0-	B. 017 A. 017 W-0-	B. 005 A. 005 W-0-	B. 002 A. 002 W-0-	B. 005 A. 005 W-0-	B. 005 A. 005 W-0-	B. 0025 A. 0025 W-0-	B 1.4985 A 1.4985 W-0-	B 1.490 A 1.490 W-0-		
6-4-64 6-19-64	97.5	B. 064 A. 097 W. 033	B. 1.009 2.007 A	B. 1.009 2.008 A	B. .007 A .010	B. 004 A. 020 W=.016	B. 004 A. 014 W. 010	B. 004 A. 010 W=006	A. 0025 B. 0108 .0083	B 1.4985 A 1.4985 W-0-	B 1.490 A 1.490 W-0-		

TABLE 3-VIII B (Continued)

B = Before Operation
A = After Operation (Tear Down)
W = Wear (B - A, Or Change)

Date Assem. Inspect	Acc. Hot Hours	PISTON ASSEMBLY									
		RING END GAP				RING SIDE CL.				Skirt & Housing Dimensions	
		#1	#2	#3	#4	#1	#2	#3	#4	BODY	Ring Housing
6-22-64 6-26-64	34.4	B. 050 A. 057 W. 007 65hr	B 1. 011 2. 011 A 1. 012 2. 012 W=001 65hr	B 1. 019 2. 017 A 1. 019 2. 017 W=0 65hr	B .005 A. 005 O 65hr	B. 005 A. 005 W=0- 65hr	B. 005 A. 005 W=0- 65hr	B. 0055 A. 0055 W=0- 65hr	.002 .002 W=0- 65hr	B 1. 4983 P. 4983 W-0-	B 1. 490 A 1. 490
6-29-64 7-3-64	30.4	B. 050 A. 057 W. 007	B 1. 012 2. 014 A 1. 013 2. 017 W 1. 001 2. 003	B 1. 013 A 1. 013 2. 014 W-0-	B .0065 A. 0065 W=0	B .005 A. 010 W=. 005	B .004 A. 008 W=. 004	B .004 A. 006 W. 002	B .0025 A. 0035 W. 0010	B 1. 4983 A 1. 4983 W-0-	B 1. 490 A 1. 490 W-0-
7-3-64 8-18-64	296.4	B. 050 A. 082 W. 032	B 1. 012 2. 014 A 1. 018 2. 021 W 1. 006 2. 007	B 1. 013 2. 014 A 1. 017 2. 022 W 1. 004 2. 008	B .0065 A. 012 W. 0055	B .005 A. 008 W. 003	B .004 A. 007 W. 003	B .004 A. 006 W. 002	B .0025 A. 003 W. 0005	B 1. 4985 A 1. 4985 W-0-	B 1. 490 A 1. 490 W-0-

TABLE 3-VIIB (Continued)

B = Before Operation
 A = After Operation (Tear Down)
 W = Wear (B - A, Or Change)

Date Assem. Inspect.	Acc. Hot Hours	CYLINDER ASSEMBLY			
		X & Y Dimensions			
		X 1/4" from top	Y 1/4" from top	X Exhaust Port	Y - Exhaust Port
2-12-64 3-6-64	35.8	B 1.5051 A 1.5056 W=.0014	B 1.5054 A 1.5065 W=.0011	B 1.5035 A 1.5037 W=.0002	B 1.5035 A 1.5038 W=.0003
4-16-64 6-8-64	100.1	B 1.5009 A 1.5014 W=.0005	B 1.5008 A 1.5013 W=.0005	B. 1.5001 A. 1.5012 W=.0001	B. 1.5009 A. 1.5024 W=.00015
5-23-64 6-3-64	24.9	B. 1.5000 A. 1.5000 W=-0-	B. 1.5000 A. 1.4999 W=.0001	B. 1.4997 A. 1.5005 W=.0008	B. 1.4997 A. 1.5005 W=.0008
6-4-64 6-26-64	97.5	B. 1.5014 A. 1.503 W=0.0016	B. 1.5013 A. 1.503 W=0.0017	B. 1.5012 A. 1.5015 W=0.0003	B. 1.5024 A. 1.5025 W. 0.0001
6-22-64 6-26-64	34.4	B. 1.503	B. 1.503	B. 1.5015	B. 1.5025
6-29-64 7-3-64	30.4	A. 1.5026 W. .0004+	A. 1.5028 W.0002	A. 1.5014 W.0001	A. 1.5024 W.0001
7-3-64 8-18-64	296.4	B. 1.5026 A. 1.504 W.0014	B. 1.5028 A. 1.5038 W.001	B. 1.5014 A. 1.5018 W.0004	B. 1.5024 A. 1.5021 W.0003

2. Valve Timing

Tests 1 and 2

H₂ 5° BTDC to 35° ATDC
O₂ 15° ATDC to 55° ATDC

Tests 3 and 4

H₂ 5° BTDC to 40° ATDC
O₂ 19° ATDC to 59° ATDC

Test 5

H₂ 10° BTDC to 20° ATDC
O₂ 5° ATDC to 45° ATDC

Tests 6 through 13

H₂ 10° BTDC to 35° ATDC
O₂ 15° BTDC to 55° ATDC

3. Oxygen Injector Configuration

The one piece seat-guide design and journal-type internal bearing designs were used for all endurance tests. The split-drive design (cam follower rocker arm bearings mounted to the crankcase) was used during Tests 5 through 13. Different versions of the new rocker-to-poppet joint design were also used during Tests 5 through 13, as shown in Table 3-V.

4. Cylinder Heads and Clearance Volume

Tests 1 through 3

8.5% clearance volume, Dowtherm A cooled head

Test 4

9% clearance volume, channel-type combustion chamber with uncooled head

Tests 5 through 13

9% clearance volume - Mushroom-type head, uncooled

5. All tests were at 3000 rpm with a nominal 500°F hydrogen temperature, 300 psig hydrogen pressure, and with the exhaust pressure below 300 mm of hg absolute. Oxygen pressure was varied, depending on the oxygen injector orifice size used, to compensate for changes in lift adjustment.

By evaluation of the reasons for forced termination of the tests in Table 3-V, it is determined that the malfunction that now limits engine life, and which requires a redesign, is failure of the hydrogen valve spring. As explained in Section 3.1.4, the hydrogen valve springs were overstressed. Redesign was in process at the end of the program. Also described in Section 3.1.4, is the fact that post-test inspection indicates that the outer valve lifter and spider would most likely be the next problem requiring solution after the spring problem is solved. A possible redesign of these parts is described in Section 3.1.4. Test No. 7 was stopped because the hydrogen valve stuck because

of thick carbon deposits on the top side of the poppets. The possibility of this type of malfunction can be eliminated by maintaining better control of the hydrogen valve lubrication pressure, and will be eliminated by further development of the lubrication system.

Test No. 10 was stopped because the lockwire on the piston body bolts was cut by a sharp corner on the connecting rod. The future possibility of this type of failure was eliminated by breaking the sharp edge of the rod to a smooth radius and establishing piston assembly procedures in which the heads of the four piston assembly screws are torqued to a specified value (4 in-lb) plus an amount necessary to locate safety holes in line, in pairs, to avoid having the safety wire extend over the rod cavity in the piston body.

Test 11 was stopped because of failure of the Type 3 oxygen injector poppet retainer (Table 3-VI). This retainer had previously been weakened by bending for lash adjustment. This practice has been discontinued and, in addition, a thicker retainer 0.10 inch (Table 3-VII), is now being used. It is not anticipated that this type of failure will reoccur.

Test 4 was stopped because the oxygen injector inspection plug was not installed tight enough and, therefore, loosened during the test. Test 7 was stopped because of a test stand failure.

Test No. 12 was stopped because the oxygen injector rocker shaft slipped with respect to the quill shaft, causing the cam follower to change position with respect to the cam. The slippage was attributed to excessive clearance between the male spline of the quill shaft and the female spline of the rocker shaft. Be-

cause of the excess spline clearance, the clamp ring around the split rocker shaft spline did not provide for sufficient friction between the splines. This type of malfunction can be eliminated by proper selection of parts.

During the longer endurance runs, it was learned that differential wear rates in the oxygen injector caused the injector lift to change with time.

During the tests, power output was maintained constant, within limits, by varying oxygen supply pressure to compensate for lift change. Initially, the wear rate between the poppet and rocker arm was higher than the wear rate between poppet and seat, and lift was lost with time.

By development effort, the wear rate between poppet and rocker arm has been reduced below that between the poppet and the seat, and during Tests 10 and 13 the injector gained lift with time. During Test 13 the wear between the rocker arm and poppet was only .001 of an inch in 96 hours, and it appeared that the poppet had just properly seated itself in the rocker. As is explained in Section 3.1.2, the next development effort should be to reduce the wear rate between the poppet and seat by a like amount, and if this effort is not wholly successful, again increase the rate between the poppet and rocker arm to match the poppet-seat wear rate.

Data taken during the endurance test and comparison of pre-test and post-test performance runs did not indicate that performance changes resulted from wear, except for the necessity of changing oxygen pressure to compensate for oxygen injector lift.

3.3.3 Engine Performance Tests

Extensive performance tests were performed during the early part of the program using engine hardware developed mainly under the previous contract. When the new design hardware became available, the urgency of endurance testing limited performance testing of the new hardware to calibration tests at only a few selected valve timings with 300 psi inlet hydrogen pressure. Although the early performance tests do not represent the high level of performance which could be obtained with the new hardware, the data is still suitable for comparative purposes to demonstrate some of the generalizations which were drawn from the test program.

General observations and conclusions, resulting from performance tests with both the old and new hardware, are discussed below:

The Effect of Heated Hydrogen and Reduced Back Pressure

BSPC was greatly decreased by reducing the exhaust back pressure and raising hydrogen inlet temperature. Figure 3-34 shows the difference in BSPC versus horsepower. The top curve is for ambient hydrogen temperature and ambient exhaust pressure. The lower curve is for a 220 mm of Hg absolute exhaust pressure and a 500°F hydrogen inlet temperature. The data are for comparison and do not represent the best performance configuration. Sufficient runs at different power levels were not made to permit the two effects to be shown separately.

The following tabulation of data points is presented to show how the engine reacts to hot hydrogen and to vacuum exhaust:

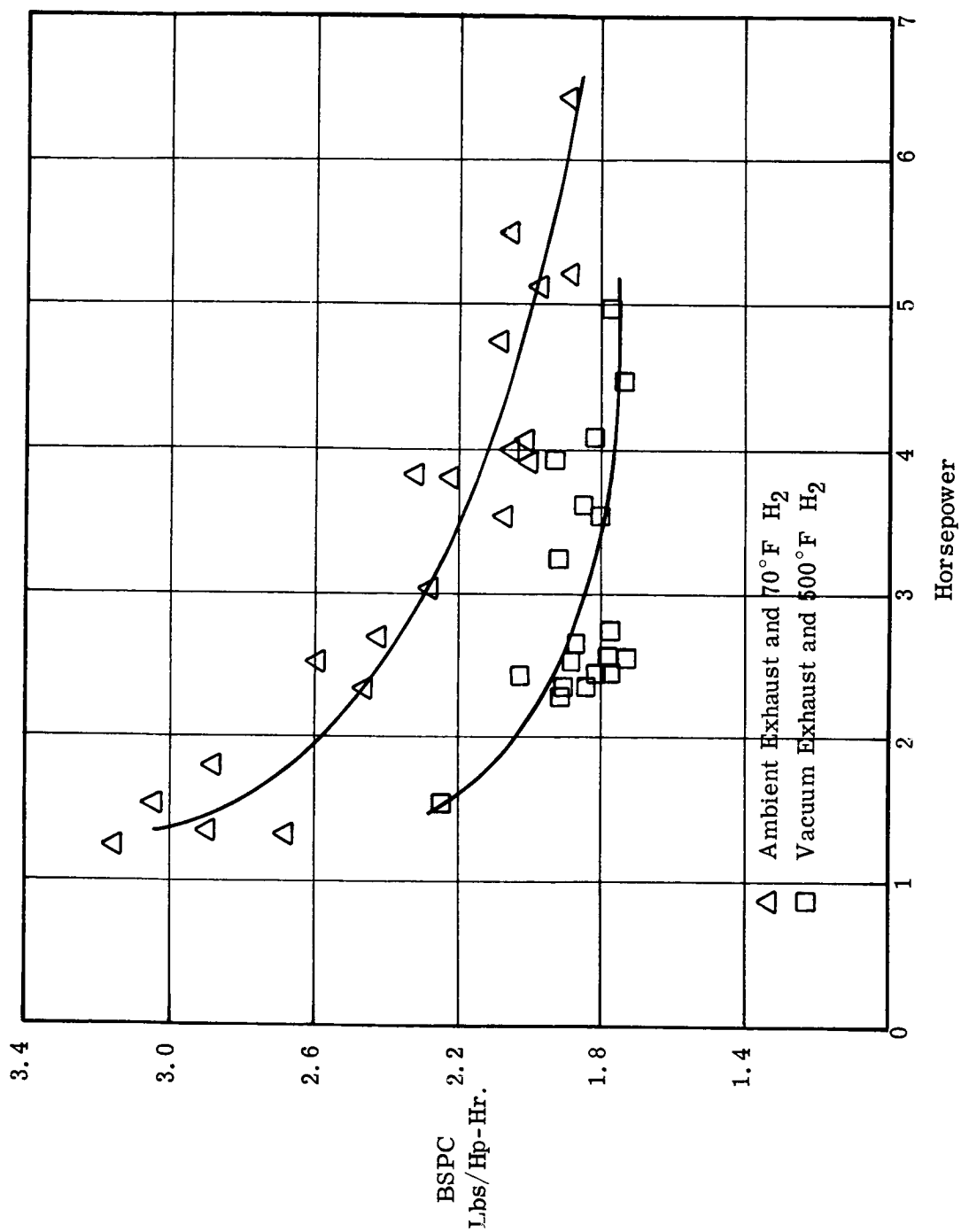


Fig. 3-34 - Effect of Vacuum Exhaust and Heated Hydrogen on BSPC

<u>RPM</u>	<u>Exhaust Pressure</u>	<u>H₂ Temp</u>	<u>HP</u>	<u>BSPC LB/HP HR</u>	<u>O/F</u>	<u>Cyl. Head Temp °F</u>	<u>η_{th}</u>
3000	Ambient	Ambient	2.16	2.10	1.68	1510	26.2
3000	Vacuum	Ambient	2.95	1.90	1.60	1555	29.7
3000	Vacuum	500°F	2.83	1.69	1.66	1555	27.9

From the above table, it can be seen that when the exhaust pressure is lowered the power increases and BSPC decreases, as would be expected. When heated hydrogen is supplied to the engine the BSPC again drops but the power also decreases slightly.

When heated hydrogen is supplied to the engine, and adjustments are made to hold the speed and head temperature constant, the hydrogen mass flow decreases and the oxygen flow is also lower. The net result is a reduction in BSPC and horsepower and no significant change in O/F ratio. A comparison of Figures 3-35 and 3-36, which are pressure-time traces for the ambient and heated hydrogen data points (both with vacuum exhaust) shown in the tabulation above, shows that there is a significant difference in the pressure characteristics from TDC through the combustion process. These differences can be seen more clearly in Figures 3-37 and 3-38, which are linear P-V diagrams reduced from the pressure time photographs shown in Figures 3-35 and 3-36. With heated hydrogen, the cylinder pressure decreased more rapidly prior to combustion and the combustion pressure rise was less than with ambient hydrogen. Figure 3-37 (ambient hydrogen) shows a 10 psi drop prior to combustion and a combustion pressure rise of 70 psi to a peak pressure of 350 psia. Figure 3-38 (heated hydrogen) shows a 20 psi drop prior to combustion, and a 45 psi combustion rise to a peak pressure of 320 psia.

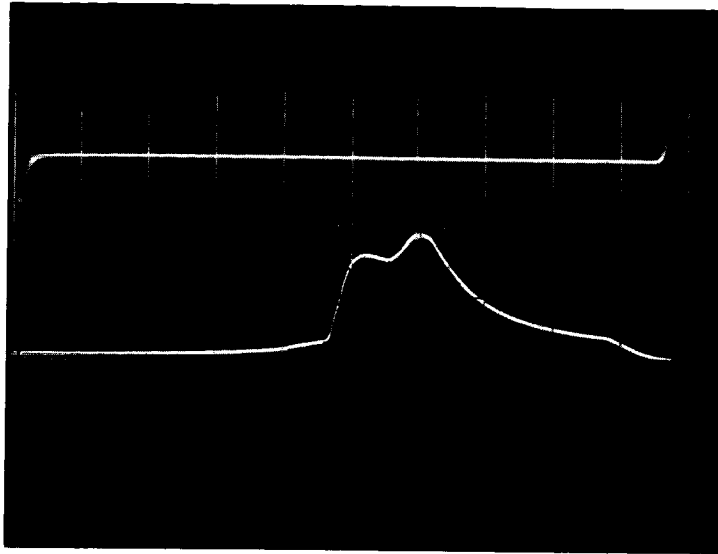


Fig. 3-35 - Pressure vs. Time Trace with Ambient Temperature Hydrogen and Vacuum Exhaust



Fig. 3-36 - Pressure vs. Time Trace with 500° F Hydrogen and Vacuum Exhaust

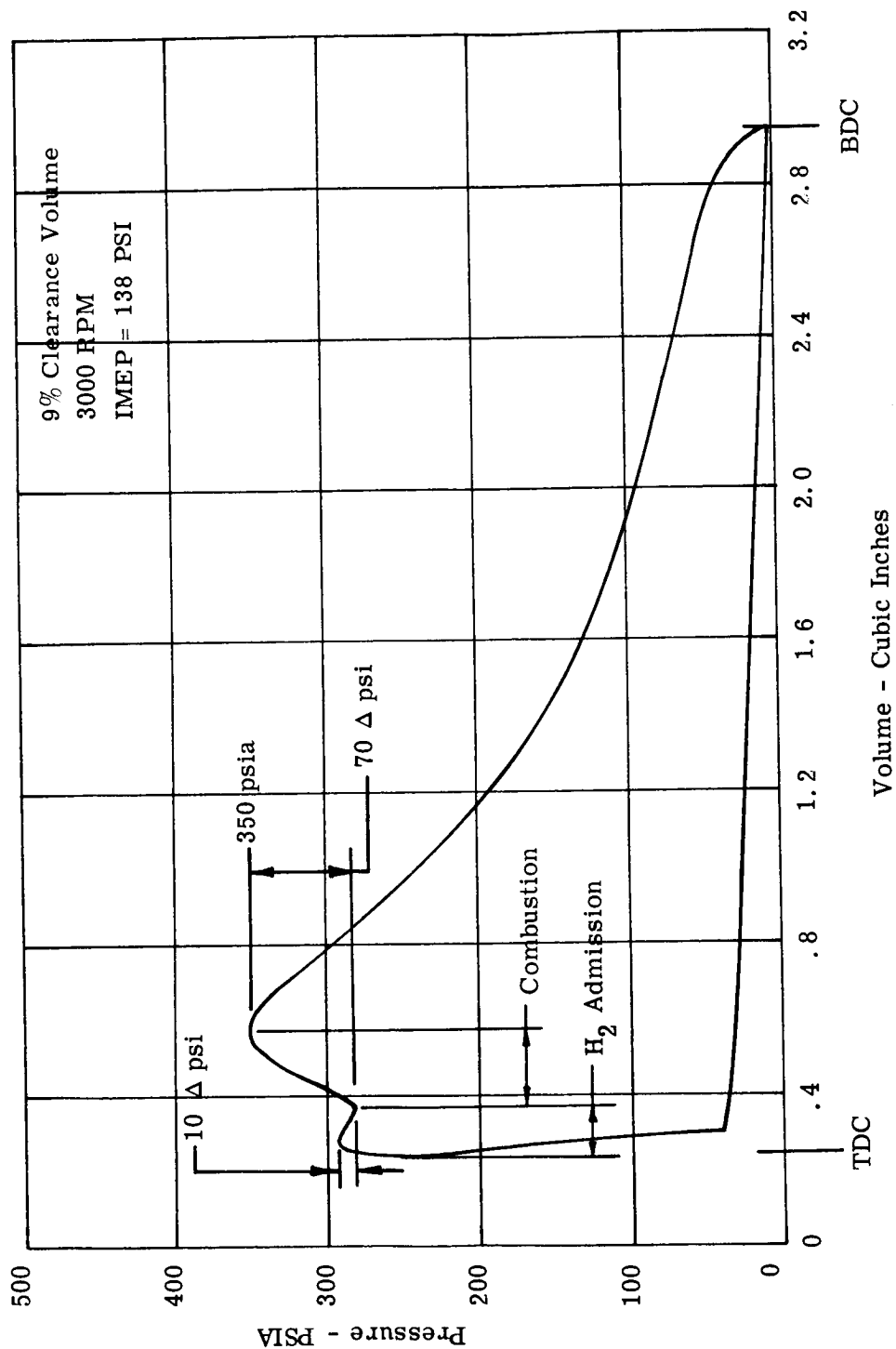


Fig. 3-37 - Linear P-V Indicator Diagram with Ambient Temperature Hydrogen and Vacuum Exhaust

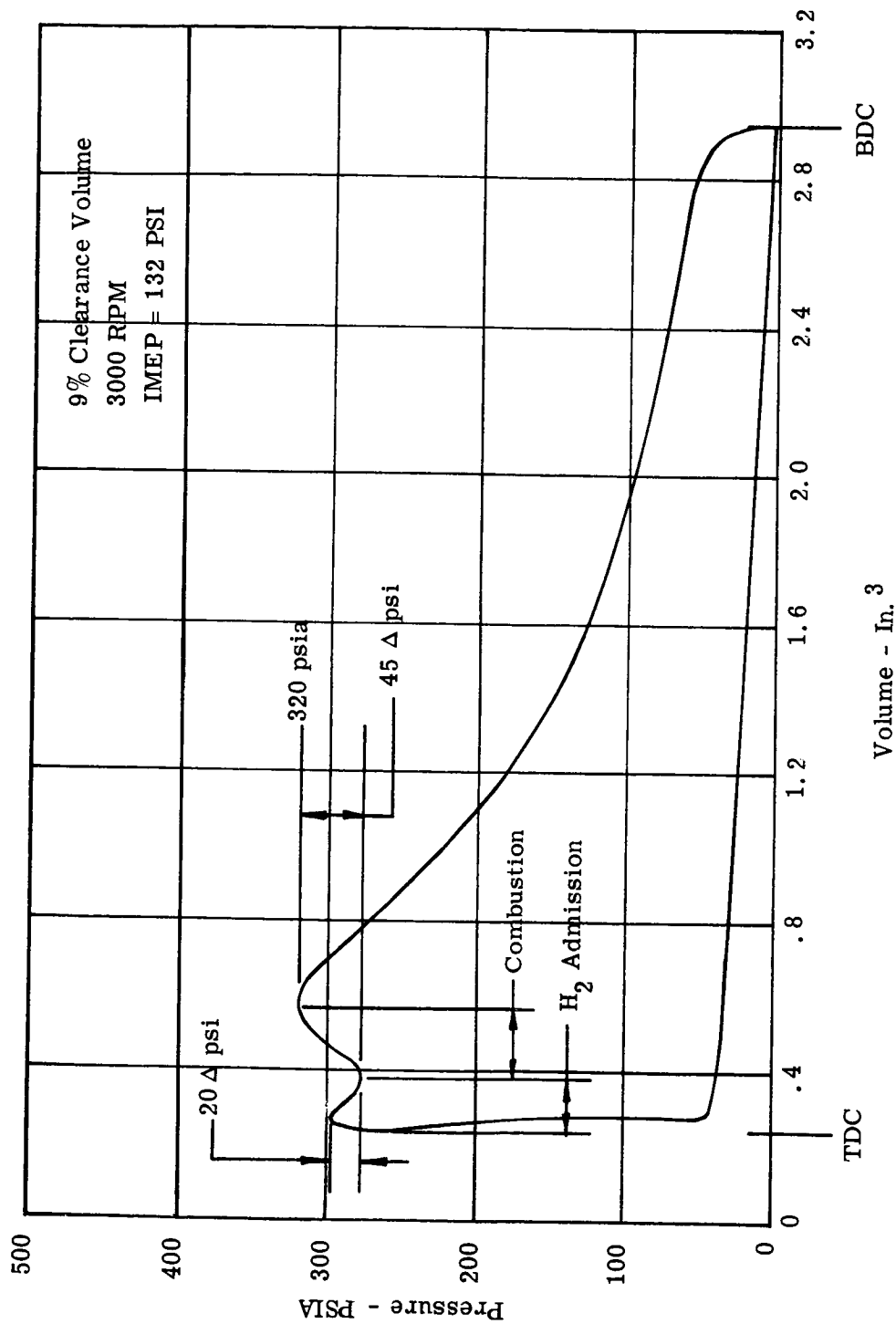


Fig. 3-38 - Linear P-V Indicator Diagram with 500° F Hydrogen and Vacuum Exhaust

The smaller P-V diagram area is attributed to increased heat losses due to the higher theoretical peak combustion temperature resulting from the higher initial temperature of the heated hydrogen. This conclusion is supported by the drop in thermal efficiency, from 29.7% to 27.9% (see table above), resulting from heating the hydrogen (the analysis upon which the thermal efficiencies are based are in Appendix B). The BSFC was lower with heated hydrogen because the input energy per pound of propellant was sufficiently increased to compensate for the higher heat losses and still provide a greater output power per pound of propellant. For given hydrogen temperature, it may be possible to increase the thermal efficiency and reduce the BSFC by increasing the overlap between the hydrogen and oxygen values, i. e., injecting the oxygen closer to TDC and/or increasing speed. This may result in more rapid combustion and reduce the time in which heat transfer may occur.

Figure 3-39 is a log-log P-V diagram reduced from the heated hydrogen pressure-time trace, Figure 3-36. The log-log P-V curve is used to determine the actual polytropic expansion coefficient of the cycle. The slope of the straight part of the expansion stroke in Figure 3-39 is approximately 1.25. This is slightly less than the adiabatic exponent for the combustion products at the measured O/F ratio.

The Effect of Heated Oxygen

Figure 3-40 shows the results of a test during which inlet oxygen was heated. BSFC, BMEP, and O/F are plotted versus oxygen inlet temperature. The BMEP (and power) remained constant. The BSFC increased slightly and the O/F decreased slightly with increased oxygen temperature. No significant result was observed. This could be expected since the heat capacity of the oxygen is small compared to that of hydrogen. Heated oxygen injection was tried because it was felt that it might increase turbulence

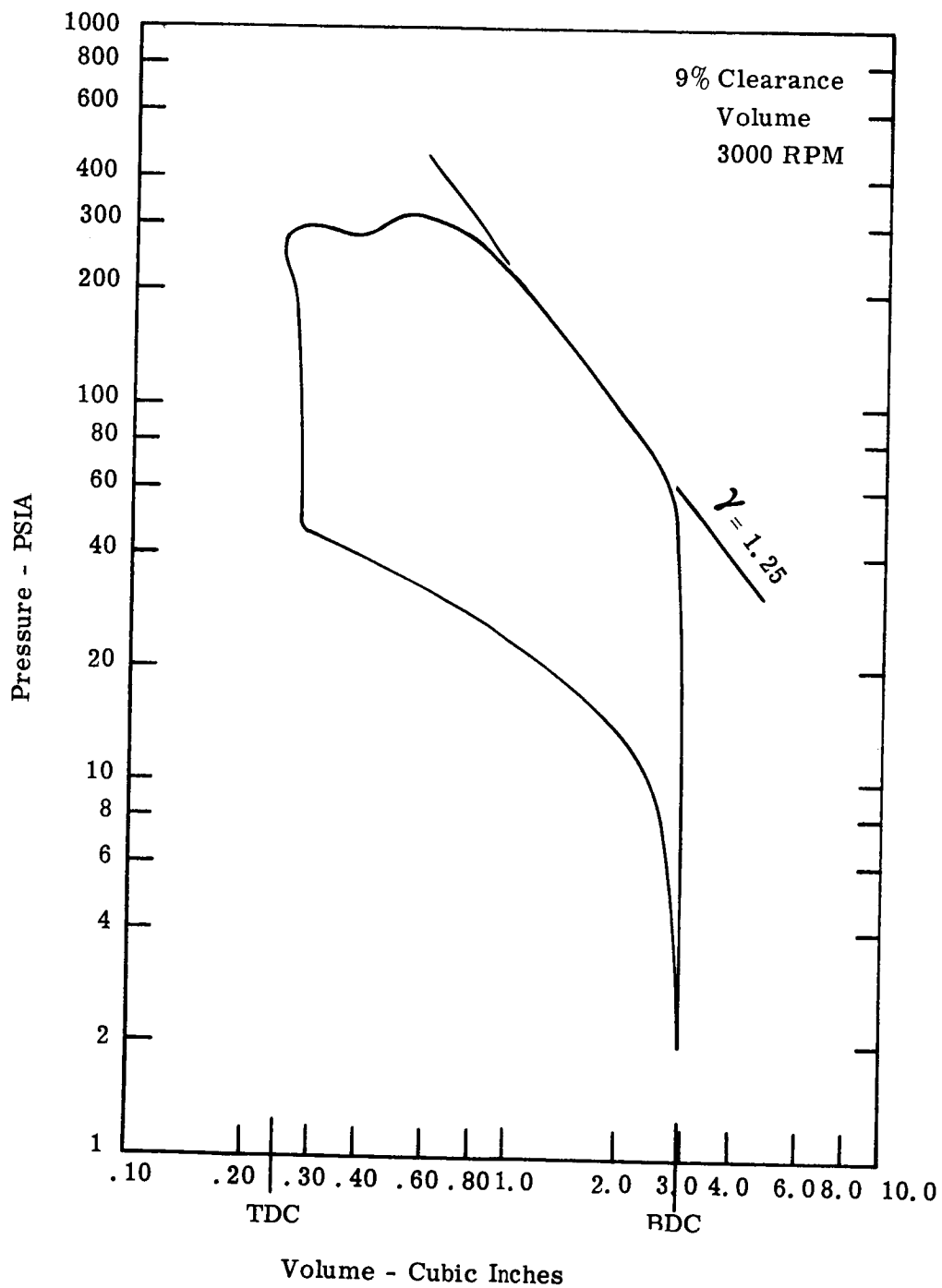


Fig. - 3-39 - Log-Log P-V Indicator Diagram with 500°F
Hydrogen and Vacuum Exhaust

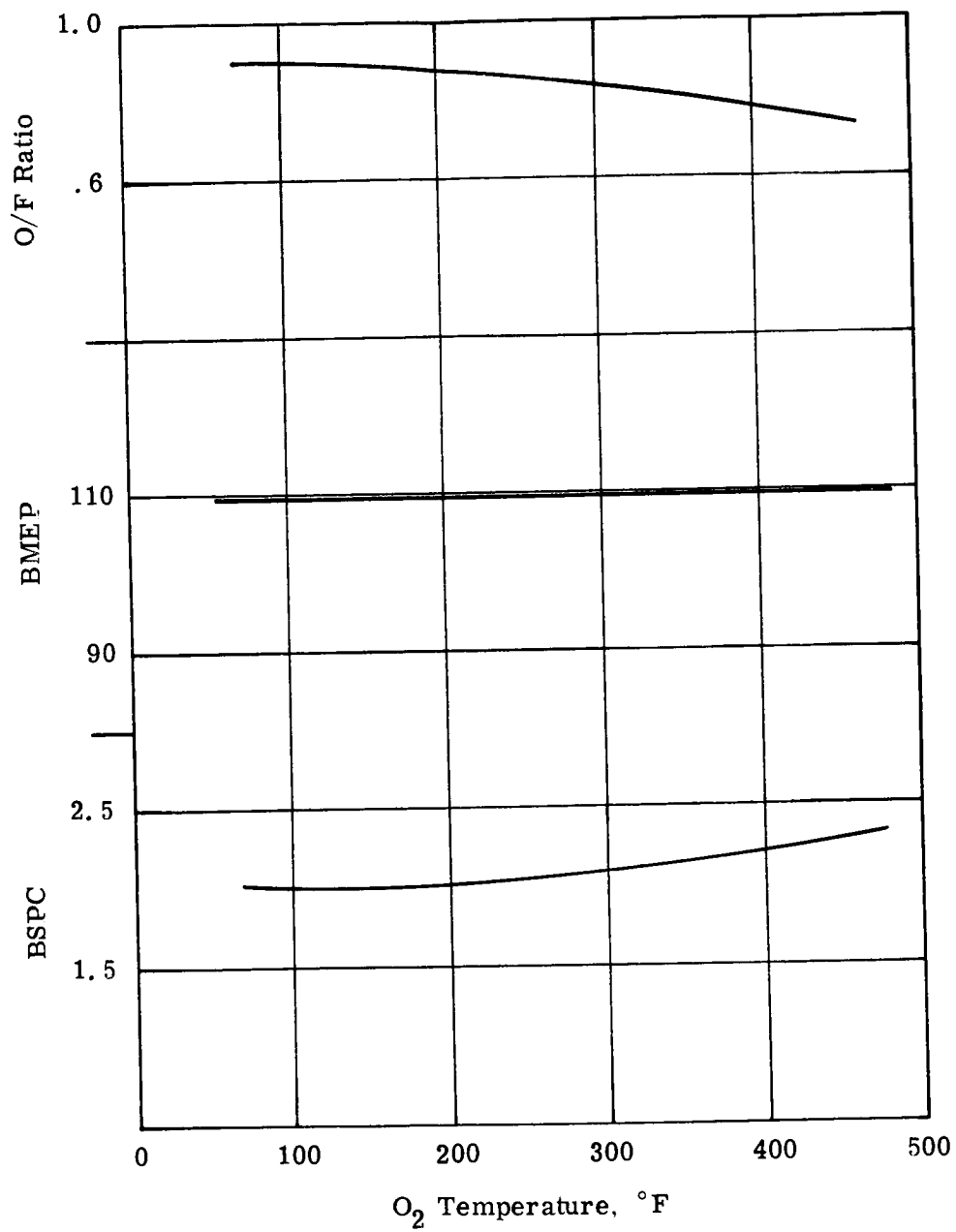


Fig. 3-40 - Results of Heated Oxygen Tests

and improve combustion efficiency.

Though handling problems may be difficult, and high cylinder head temperature gradients may result, the effect of injecting cryogenic oxygen should be considered as another possible means of improving combustion efficiency. The high density of the cryogenic oxygen would reduce the time required to inject a given mass of oxygen into the cylinder. The short injection time may result in a sharper combustion spike.

The Effect of Combustion Chamber Shape

Figure 3-41 shows BSPC data points vs. BMEP for 3 different combustion chamber configurations. The data was all taken with the same valve timing, exhaust pressure, and hydrogen inlet conditions. The performance of the "Mexican Hat" and "Mushroom" chambers was superior to that of the "Figure 8."

The problem of improving combustion efficiency is a trial and error process. The objective of the experimentation is to find a chamber shape which causes combustion and the mixing of combustion products with unburned hydrogen to occur as early in the cycle as possible. This type of experimentation should be continued throughout the engine development effort.

Since late combustion reduces efficiency, exhaust gas samples were analyzed to determine whether or not any of the oxygen remained unburned by the time it left the cylinder.

Exhaust gas samples were taken at ambient back pressure, since the sampling techniques did not permit the use of a vacuum exhaust. Samples were taken in evacuated bottles at a point about 6 feet from the engine exhaust manifold. Exhaust temperature was nearly ambient. A spectrographic analysis of the samples was

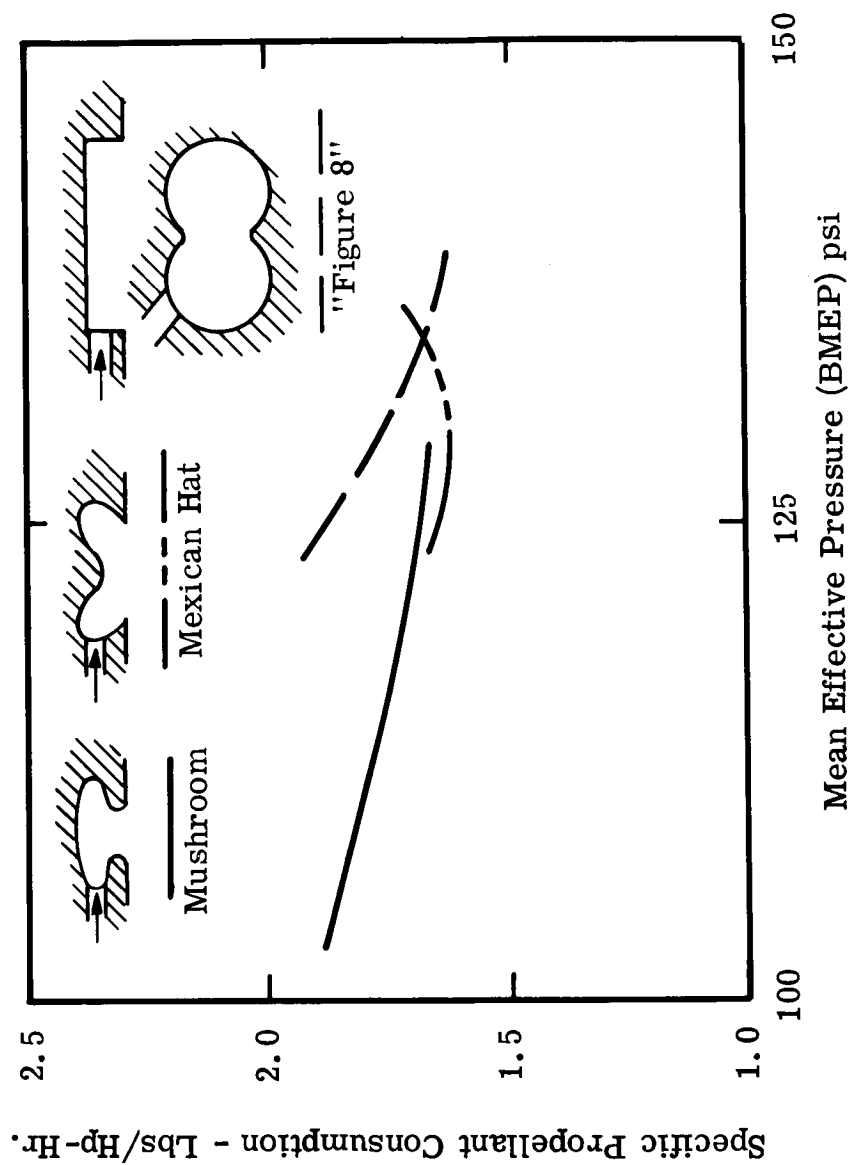


Fig. 3-41 - Effect of Combustion Chamber Shape on BSPC

accomplished by an outside laboratory. The results are given in Table 3-IX and the laboratory report is shown in Appendix C.

The oxygen and nitrogen correspond, within the limits of accuracy stated by NESCO, to about 1% air by volume. This is reasonable considering the sampling technique. The water vapor is approximately half of the amount generated by the engine according to the calculated O/F ratio. This is also reasonable since the exhaust was actively condensing at sample conditions, and appeared as a fog containing water droplets.

The test results only prove that combustion was complete at a point 6 feet away from engine exhaust ports and do not preclude the possibility of combustion in the exhaust duct up to that point. However, the results do indicate that incomplete combustion is not a major problem.

The Effect of Heat Rejection and Other Losses

Figure 3-42 shows the results of a cooled cylinder head test. Total heat rejection to coolant and cylinder barrel heat rejection to coolant, expressed as percent of shaft power, are shown as a function of O/F ratio. The curve shows the proportion of the total heat loss which is rejected to the cylinder cooling jacket. As O/F ratio is increased, an increasing portion of the available energy goes to waste heat.

Figure 3-43 shows bands of data points from tests with both cooled and uncooled cylinder heads. The heat rejection is again plotted in percent of shaft power versus O/F ratio. The data show that in the O/F ratio range where the uncooled and cooled head data cross, heat rejection to the cylinder alone during the uncooled head tests was an equal or greater percent of shaft power than of the total rejection to the coolant for the tests with the cooled head. This effect tends to be compensated for by

TABLE 3-IX

MASS SPECTROMETER ANALYSIS OF EXHAUST GAS

Run	Engine Speed	Constituent	Volume %	Weight %
3:45	3000	O ₂	.14	1.5
		N ₂	.95	9.0
		H ₂ O	4.1	25.0
		H ₂	94.8	64.5
3:50	4300	O ₂	.17	1.7
		N ₂	.93	8.3
		H ₂ O	5.3	30.4
		H ₂	93.6	59.6
4:00	3000	O ₂	.09	1.0
		N ₂	.92	9.3
		H ₂ O	3.2	20.5
		H ₂	96.8	69.2

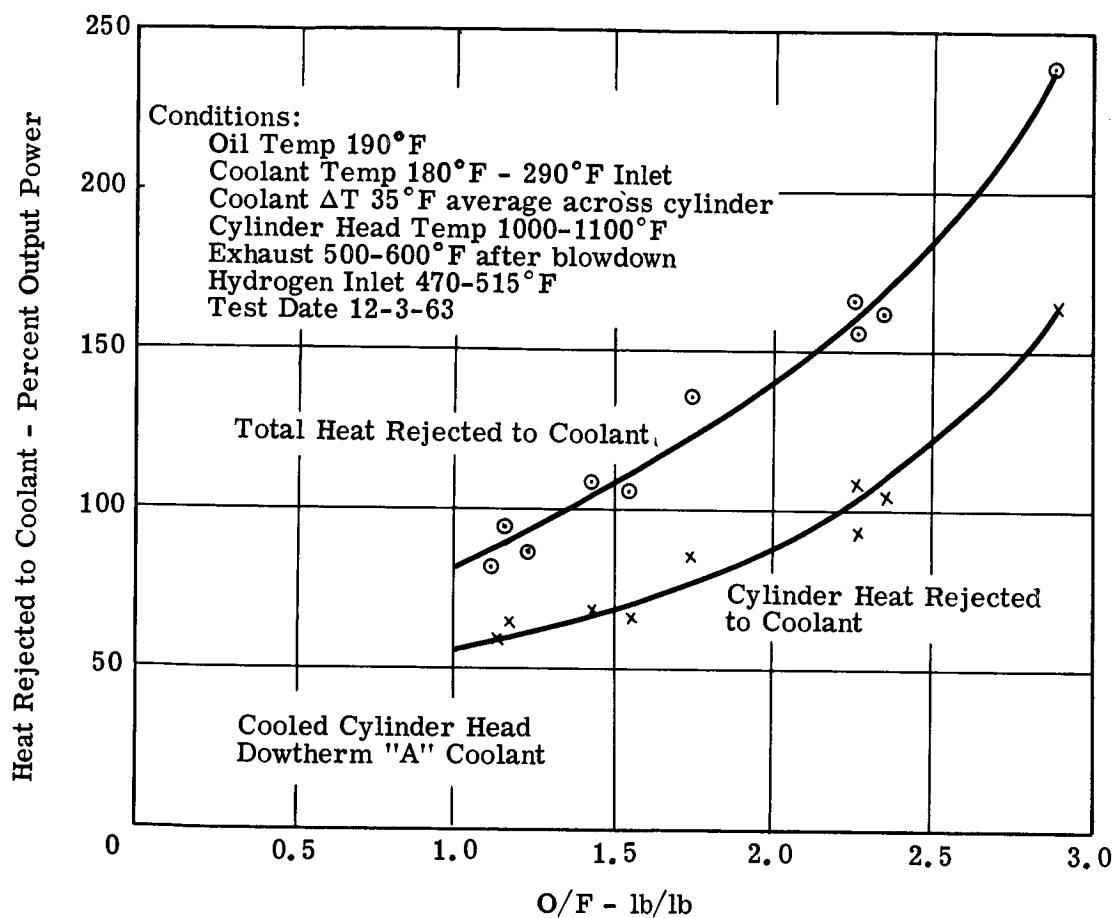


Fig. 3-42 - Heat Rejection with Cooled Cylinder Head

Cooled Cylinder Head

- Total heat rejected to coolant
- Heat rejected to cylinder cooling jacket

Uncooled Cylinder Head

- △ Heat rejected to cylinder jacket

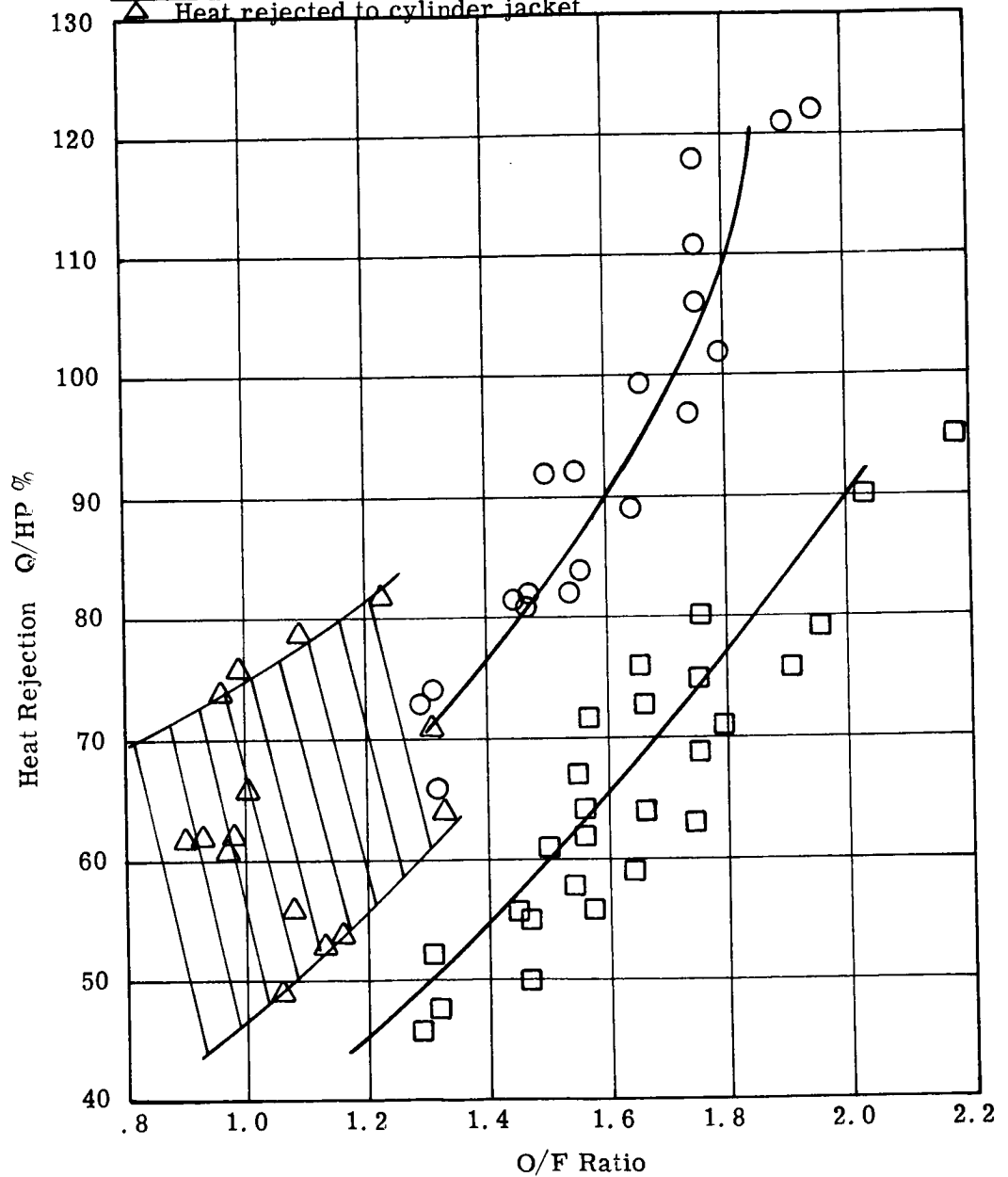


Fig. 3-43 - Heat Rejection with Cooled and Uncooled Cylinder Head

the fact that BSPC is lower with the uncooled head, i. e. , more shaft power is delivered per pound of propellant and thus allowing a higher percent of shaft power to be lost in the cylinder. Considering that additional heat is lost from the uncooled head by radiation, the data tends to show that use of an uncooled head is less of a benefit than was originally expected.

Figure 3-44 shows Brake Mean Effective Pressure (BMEP) versus total Input Mean Effective Pressure (EMEP) for 300 psi 500° F inlet hydrogen and vacuum exhaust.

The slope of a line through the origin and a data point represents the overall thermal efficiency of the engine. The best efficiency, shown in Figure 3-44 is 32.2%. The total EMEP represents the total input energy to the engine and includes the energy available from expansion of hydrogen through the pressure ratio across the engine, as well as from combustion of hydrogen and oxygen. The analysis upon which the total EMEP calculation is based appears in Appendix B.

Figure 3-45 shows BMEP versus EMEP for tests run at different hydrogen inlet pressures. These tests were run to study the feasibility controlling power with hydrogen supply pressure. A large number of tests at different valve timing will be required to obtain a comparable set of data for variable admission power control. The 300 psi data points on Figure 3-45 are not directly comparable with Figure 3-44.

By subtracting the measured BMEP values from the calculated total EMEP values a loss MEP (or LMEP) value is obtained. The LMEP values represent all loss from heat rejection, energy in the exhaust, leakage, and friction. The LMEP and BMEP values, divided by hydrogen supply pressure, are plotted versus O/F ratio in Figure 3-46 for the data points shown in Figures 3-44 and 3-45.

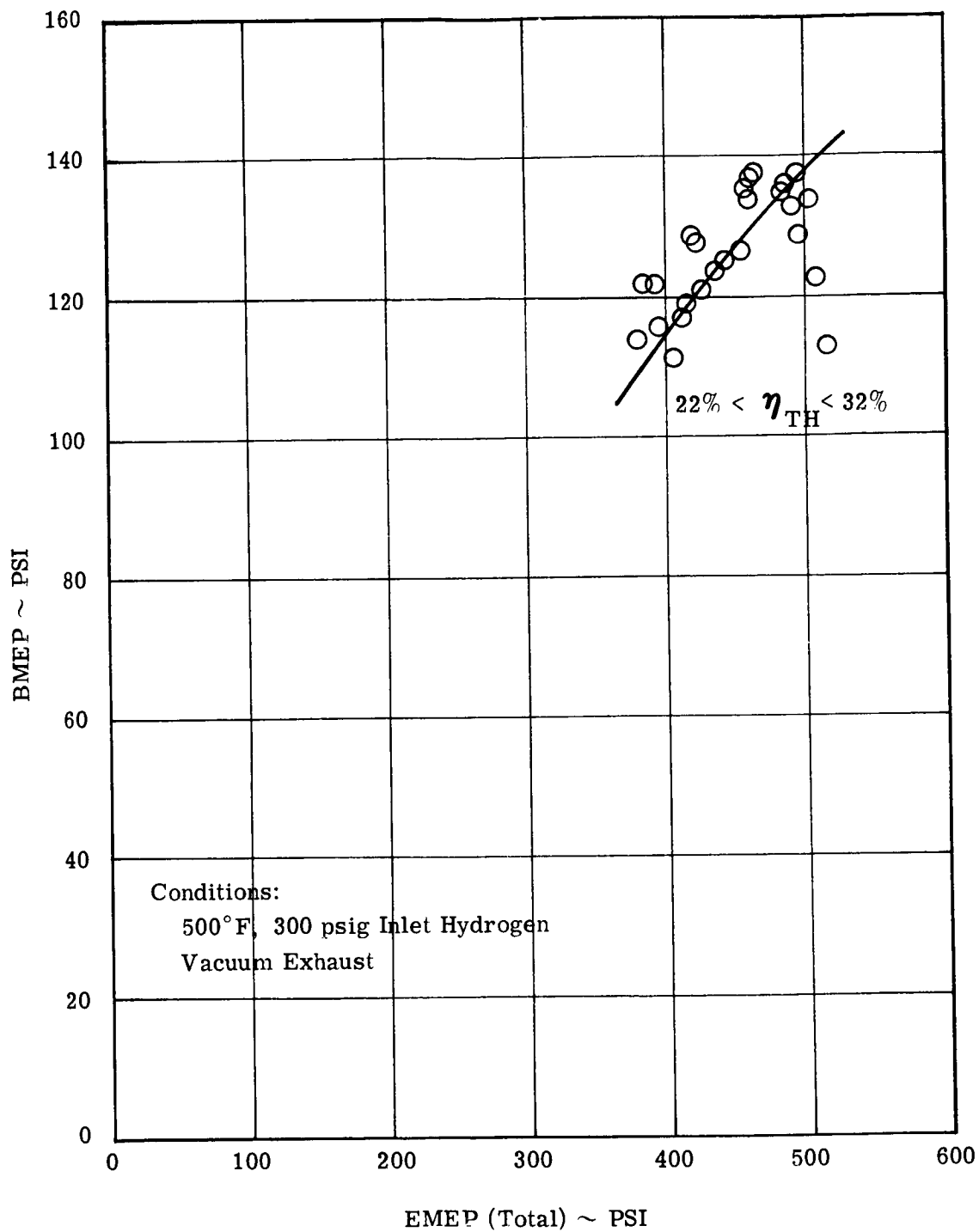


Fig. 3-44 - BMEP vs. Input MEP for 300 PSIG
Hydrogen Inlet Pressure

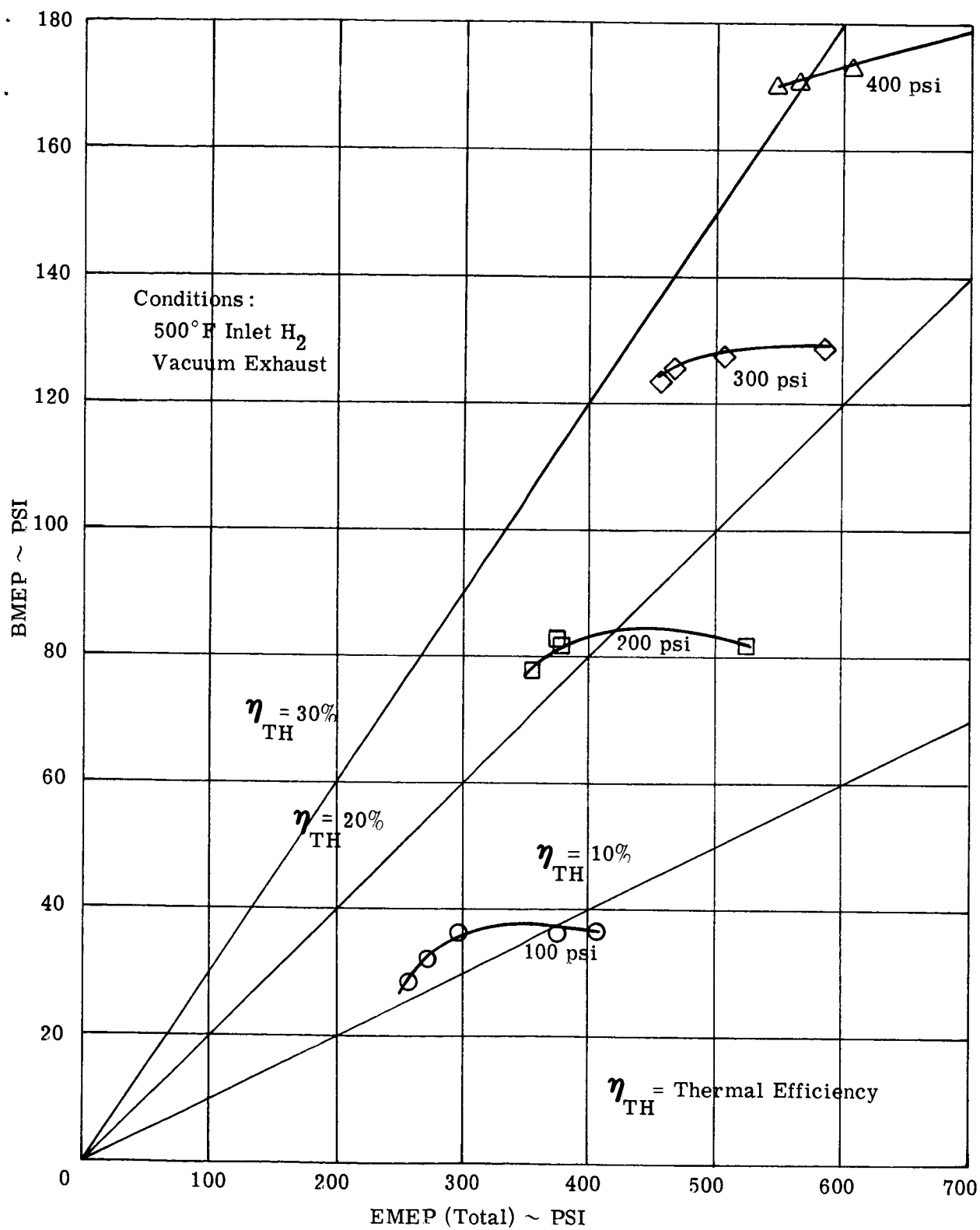


Fig. 3-45 - BMEP vs. Input MEP for Various Hydrogen Inlet Pressures

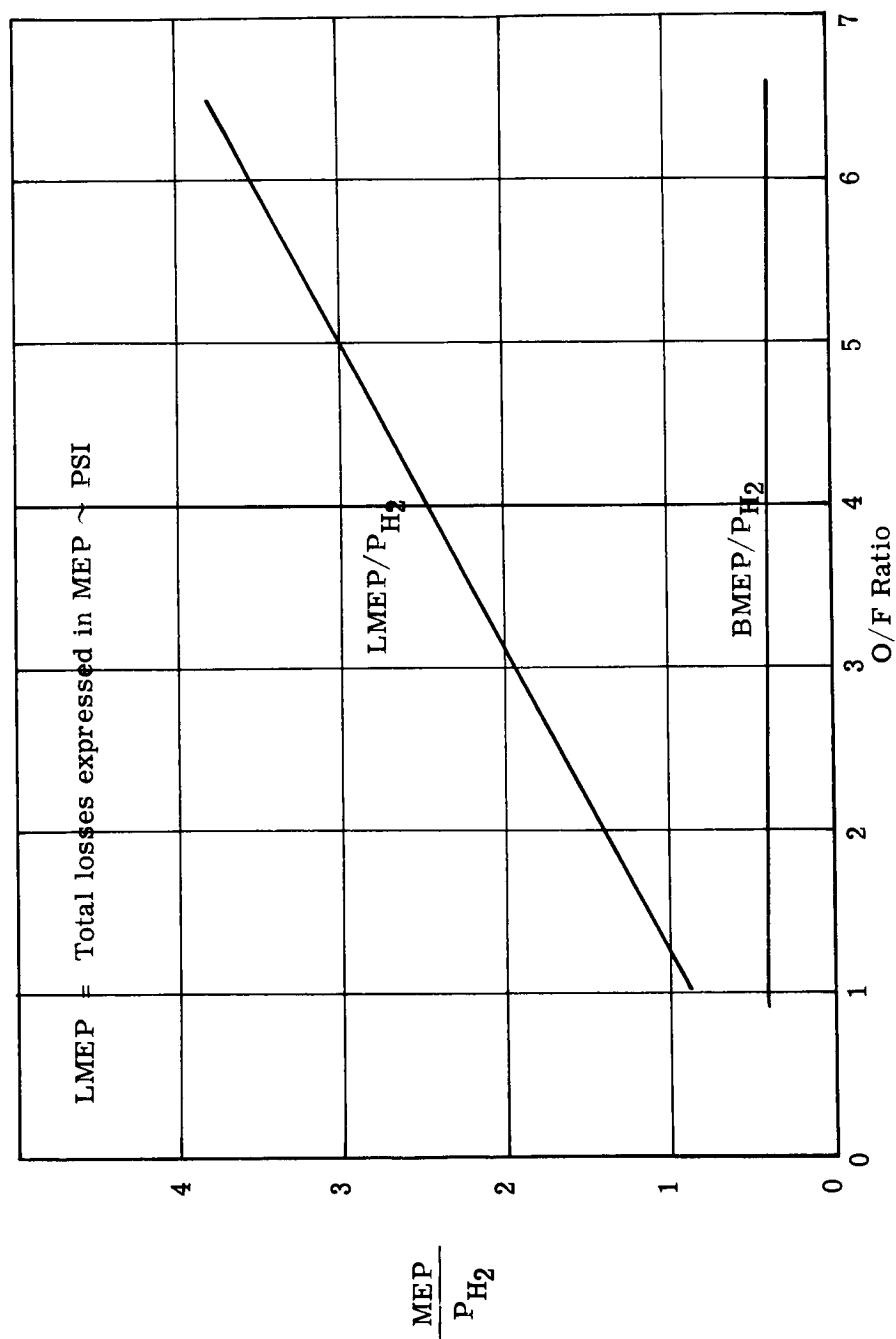


Fig. 3-46 - $\frac{BMEP}{P_{H_2}}$ and $\frac{LMEP}{P_{H_2}}$ vs. O/F Ratio

Figure 3-46 shows that $\text{BMEP}/P_{\text{H}_2}$ remains constant as O/F ratio is changed and that $\text{LMEP}/P_{\text{H}_2}$ increases linearly with O/F ratio. Since all the test data was taken at same valve timing with 500°F inlet H_2 , and since the density of H_2 is directly proportional to pressure when the temperature is held constant, the weight of the hydrogen per cycle is directly proportional to the H_2 supply pressure P_{H_2} . At a fixed O/F ratio, the total weight of the gas added to the cylinder per cycle is proportional to P_{H_2} . In summary, Figure 3-46 shows that at the valve timing and 500°F hydrogen inlet temperature of the tests, at a fixed O/F ratio, both power per cycle and total loss per cycle were a direct function of P_{H_2} (and therefore approximately a direct function of propellant charge per cycle), and that for a fixed P_{H_2} , the total loss per cycle was a direct function of O/F ratio, while the power per cycle was not effected by O/F ratio.

Figure 3-47 shows BSFC, BSFC, BSOC, and O/F ratio versus horsepower for the sets of data where inlet hydrogen pressure was varied to control power at a given speed. This data shows that the BSFC remains relatively constant as the power varies, while the BSOC is high at low power levels and increases rapidly as power is decreased. Comparison of Figures 3-46 and 3-47 shows that the higher O/F values on Figure 3-46 resulted at low power and low P_{H_2} .

This leads to the conclusion that BSFC could be improved at the lowest power levels by reducing heat rejection through control of coolant flow in proportion to power output, or by incorporating a thermostatic control to maintain the desired level of cylinder head temperature through control of coolant flow instead of O/F ratio. Another more promising possibility which suggests itself is regeneratively cooling the cylinder jacket and cylinder head with the incoming hydrogen. This would tend to increase hydrogen inlet temperature at low power levels when the hydrogen

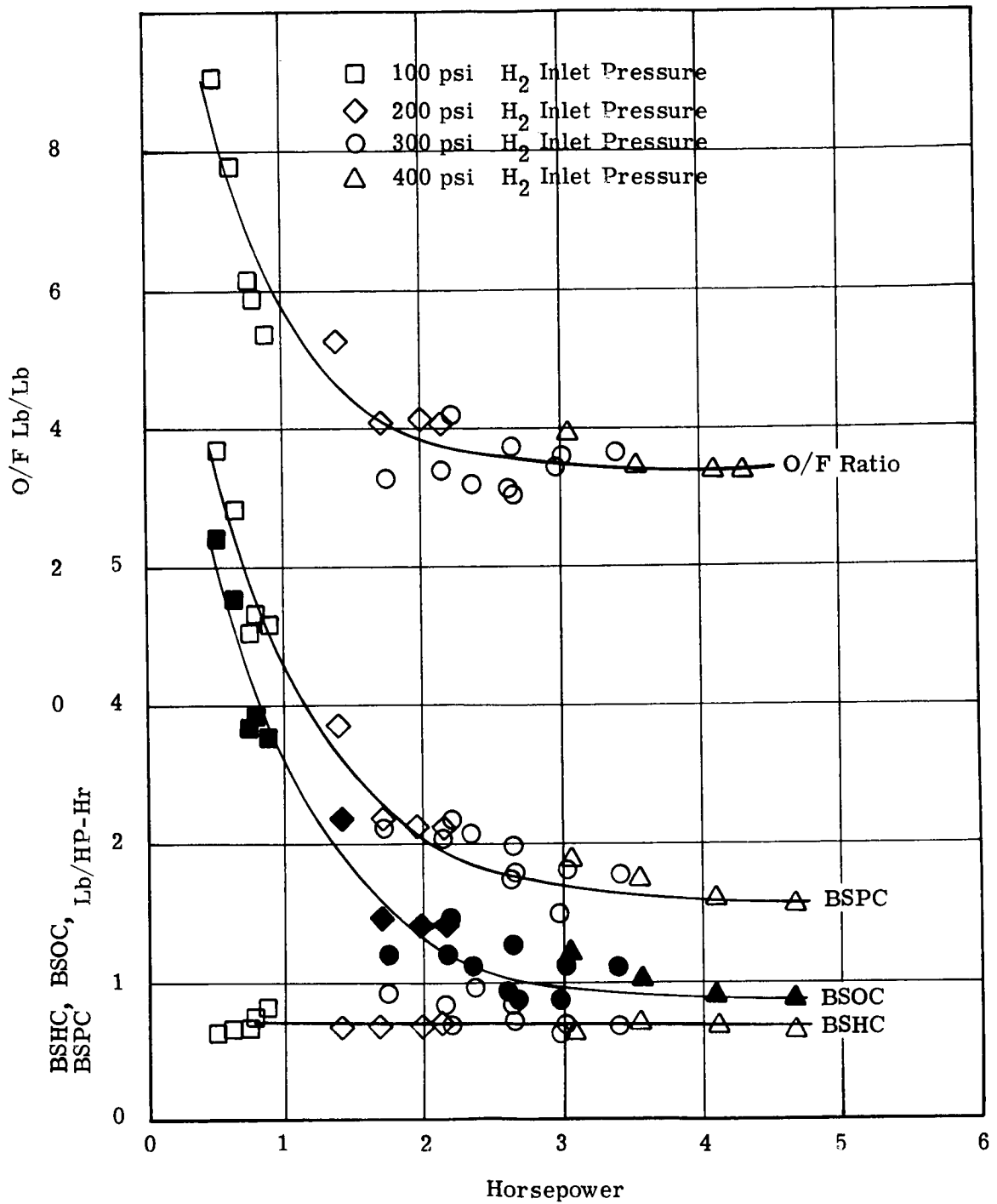


Fig. 3-47 - BSOC, BSHC, BSFC and O/F vs. Horsepower

flow is low, and hence, reduce the amount of oxygen required to maintain the desired operating temperatures.

Figure 3-48 shows the average motoring friction power observed during the program expressed as FHP and as FMEP versus engine speed. The friction data were taken by motoring the engine with the cylinder head removed. Therefore, the actual friction losses during engine operation will be somewhat higher due to pressure loading on the piston rings and the bearings. At any rate, the friction losses are primarily a function of speed and at any given speed cause BSFC to increase as power is reduced.

In summary, all the data on losses presented here indicate that BSFC increases at low power levels and that the increase is due to an increase in BSOC (O/F ratio) which is required to provide energy to make up losses which are much greater than can be attributed to friction alone.

The flattening out of the BSFC vs. HP curve also indicates that the chamber is sized for maximum economy near, if not at, a somewhat higher power level than the 4.75 HP which was the peak power produced in this test series.

Power Control by Hydrogen Pressure

Figures 3-49 through 3-53 show the results of tests where hydrogen inlet pressure was varied as a means of controlling power to determine the feasibility of this method of power control with fixed valve timing. Figure 3-49 shows shaft power, BSFC, and O/F ratio vs. hydrogen supply pressure for different engine speeds. Figures 3-50 through 3-53 show BSFC, shaft horsepower, torque, and O/F ratio vs. speed for different speeds. The curves show that for a given speed, power is a

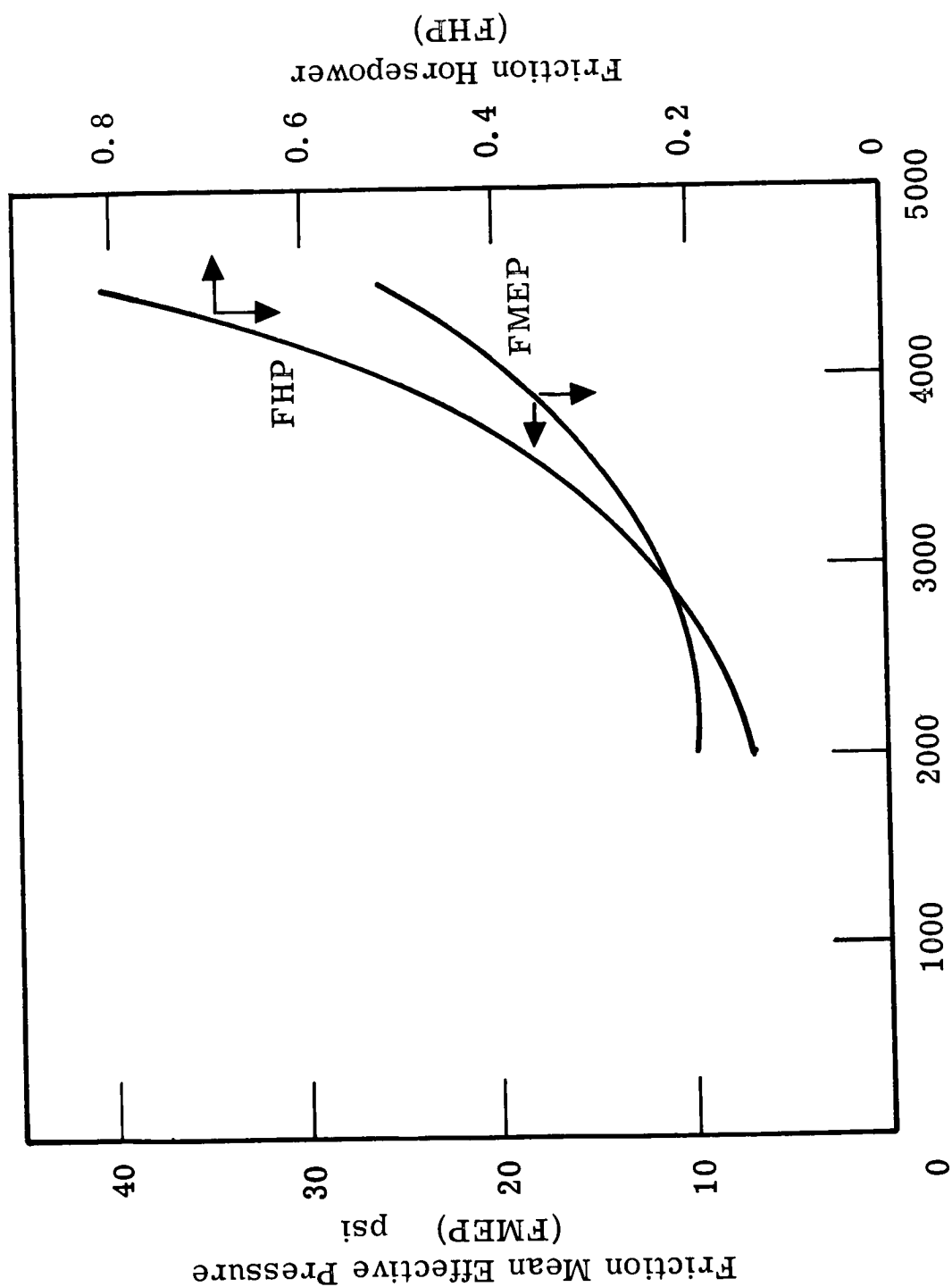


Fig. 3-48 - Engine Friction vs. Engine Speed

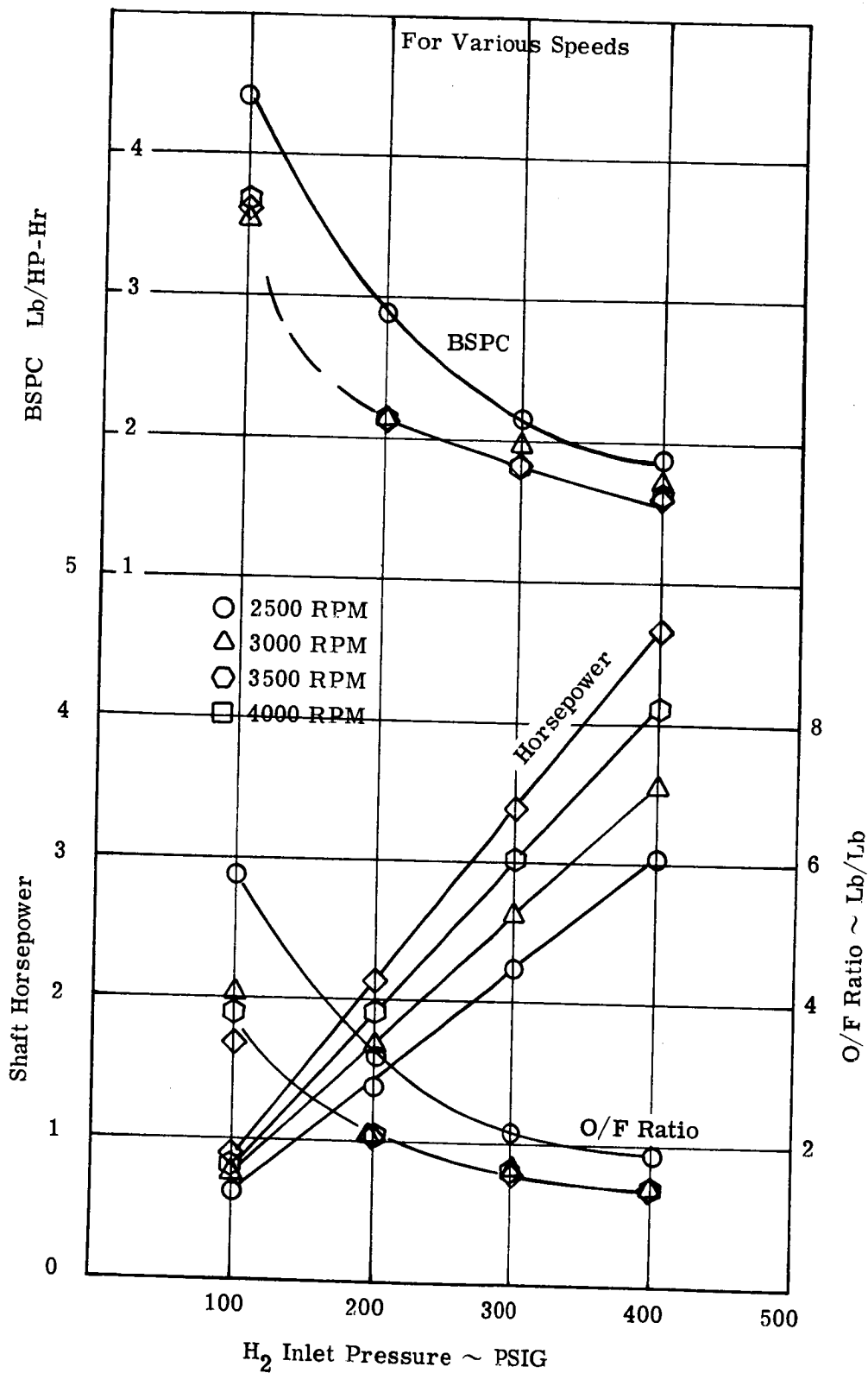


Fig. 3-49 - BSPC, Horsepower and O/F vs. Hydrogen Supply Pressure at Various Speeds

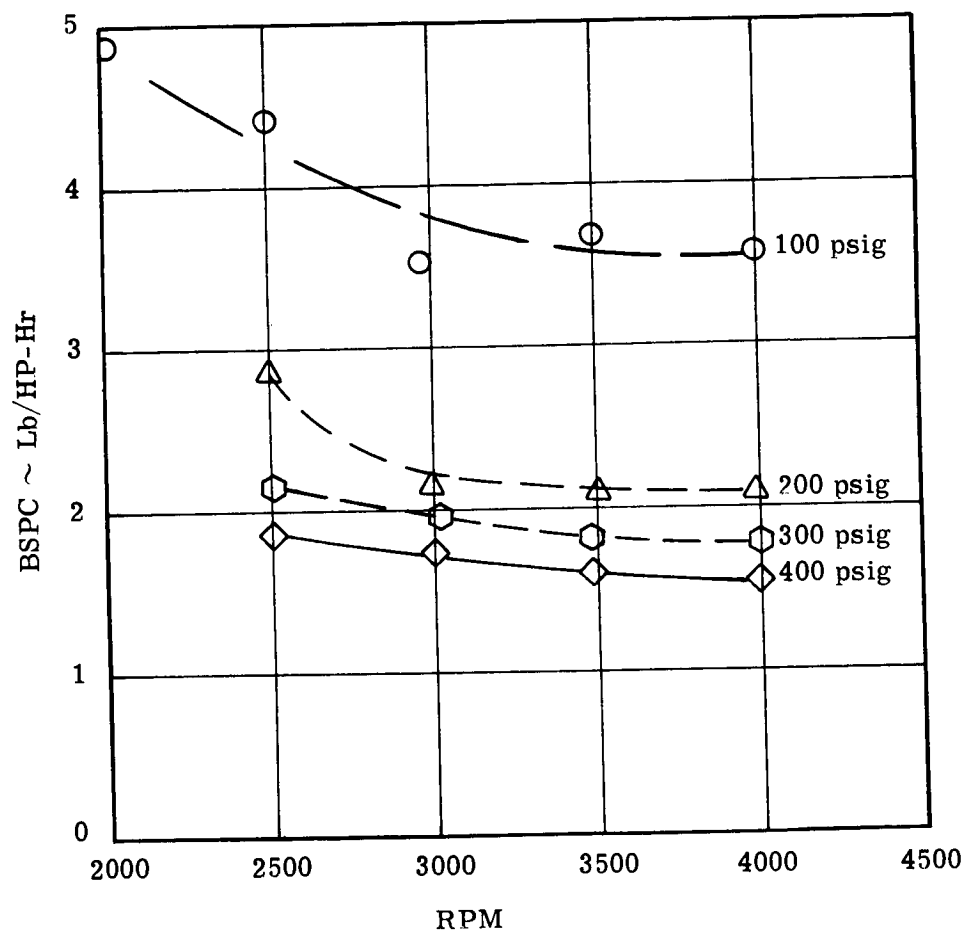


Fig. 3-50 - BSPC vs. Speed at Various Hydrogen Supply Pressures

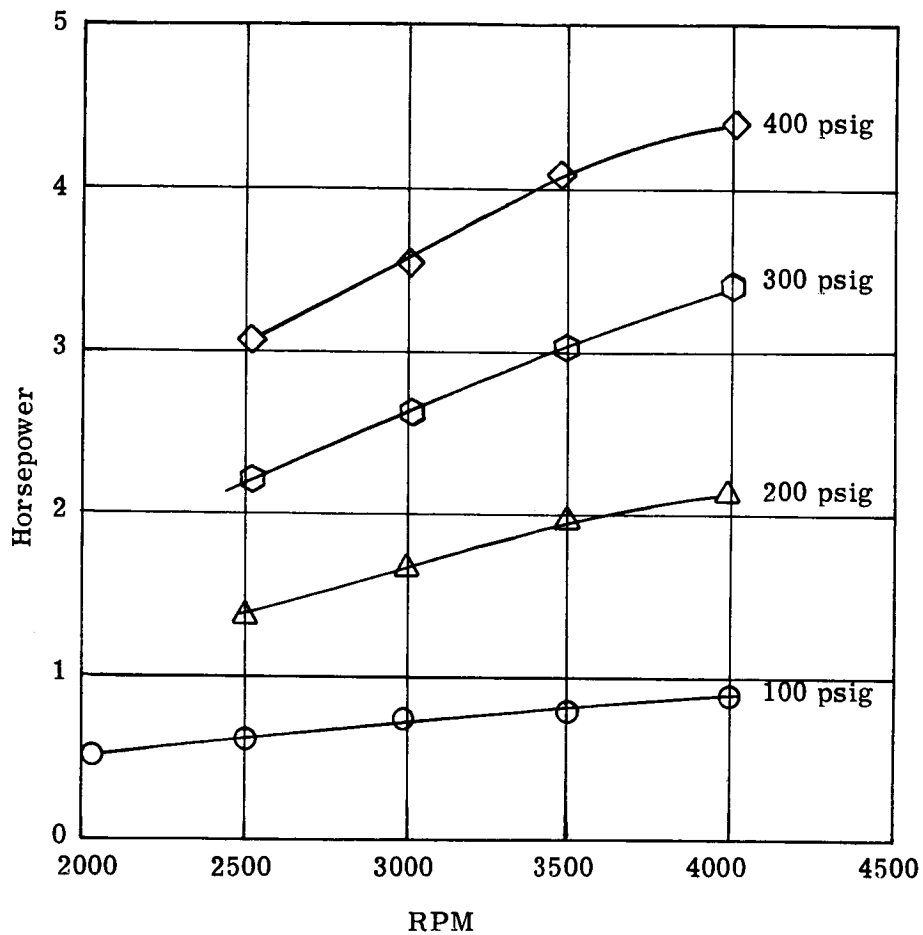


Fig. 3-51 - Horsepower vs. Speed at Various Hydrogen Supply Pressures

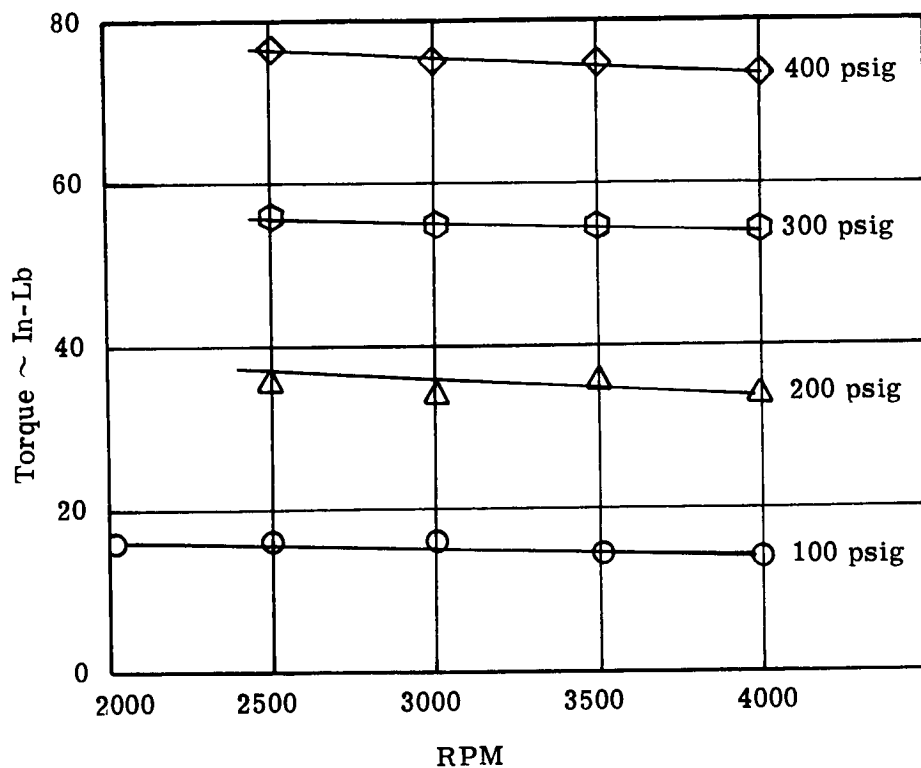


Fig. 3-52 - Torque vs. Speed at Various Hydrogen Supply Pressures

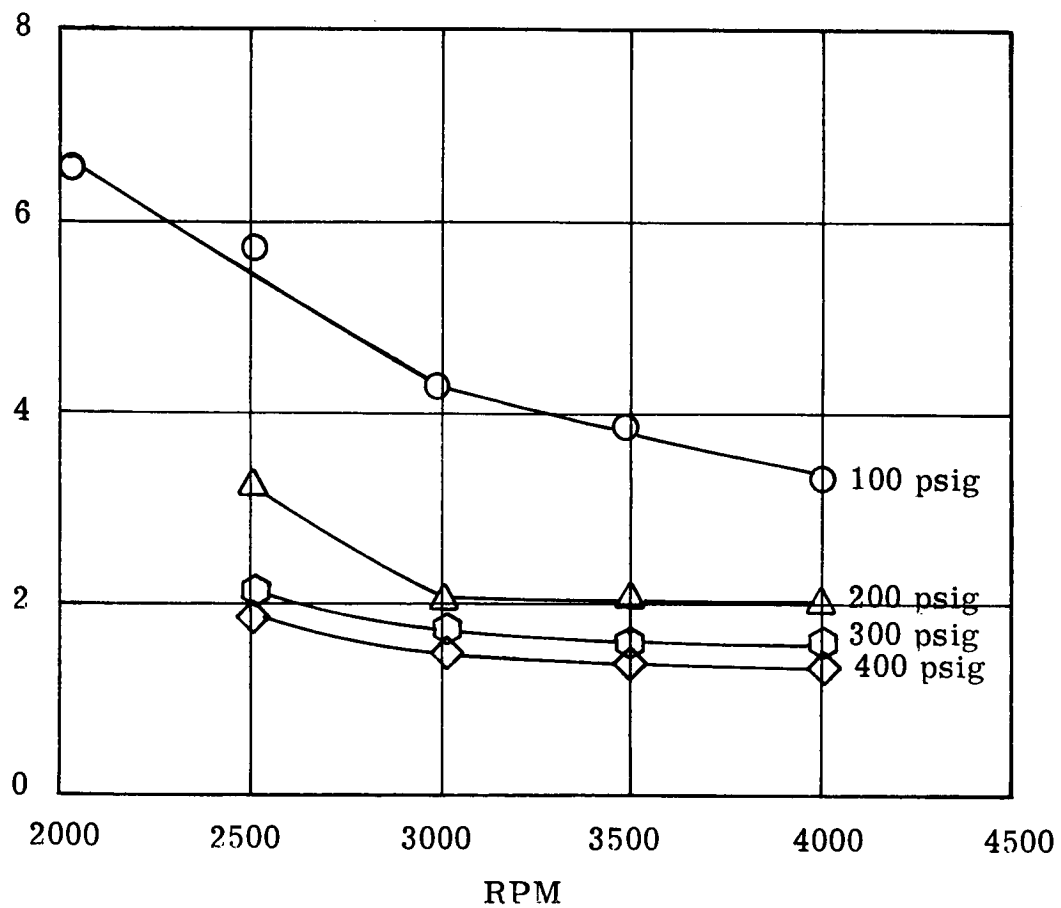


Fig. 3-53 - O/F Ratio vs. Speed at Various Hydrogen Supply Pressures

linear function of hydrogen supply pressure. For a given inlet pressure range, the range of useful power regulation is greater when operating at higher speeds.

In order to make a fair comparison of BSPC versus power performance for the variable pressure control method with the variable admission control method, a large number of runs at different valve timings must be made. Disregarding any performance differences between the two control methods, the variable hydrogen pressure approach is the most straightforward and requires less complex hardware. Only a single hydrogen valve with a fixed phase cam shaft and an inlet pressure throttle would be required, as compared to the dual concentric hydrogen valve and variable phase (advance-retard relative to the crankshaft) camshaft drive mechanism required for power control through variable opening duration of the hydrogen valve.

A careful design study must be completed before the decision is made to use a single poppet valve. Acceleration forces may be too high with a single poppet valve. Thus it may be desirable to retain the dual poppet with a fixed phase relationship, for the variable pressure control system.

Summary of Performance Testing

The reduction in BSPC accomplished during this program is attributed to hardware improvement, the reduction in exhaust pressure, and the use of heated hydrogen. The hardware improvements which contributed to improved performance were:

1. The improved exhaust system design.
2. The improved dimensional relationship of the combustion chamber with respect to the hydrogen valve and oxygen injector.

3. The cylinder, piston and piston ring redesigns which directly reduced leakage and indirectly reduced the possibility of leakage due to heat distortion and wear.
4. A more reliable oxygen injector with less leakage during the unproductive portion of the cycle.

It is believed additional BSFC reduction will result from the use of heated hydrogen when the optimum phase relationship between the hydrogen valve and the oxygen injector is found. By increasing the amount of overlap between hydrogen and oxygen admission, and thus injecting oxygen nearer to TDC, more rapid combustion and mixing may result. This may result in a higher pressure peak and less time for heat transfer.

The difference in performance between combustion chamber configurations, and the shape of pressure-time traces indicate that additional BSFC reduction can result from experimentation with combustion chamber shape and injection methods.

Evaluation of test data indicates that with the present engine configuration, the use of high O/F ratios will not result in as large a reduction in BSFC as was originally predicted. This fact, in conjunction with the fact that as power is reduced the ratio of heat loss to output power increases, indicates that a lower and flatter BSFC versus power curve can be obtained by completely regenerating the rejected heat from the engine (as shown schematically in Figure 3-54), so that it is not necessary to increase the O/F ratio at low power levels. In addition, this system would eliminate the fixed weight penalty of a radiator for the cylinder heat rejection. By using the completely regenerated cycle, the high heat loss at low power levels can be recuperated by the hydrogen so that it is not necessary to add large amounts of oxygen to make up for these losses.

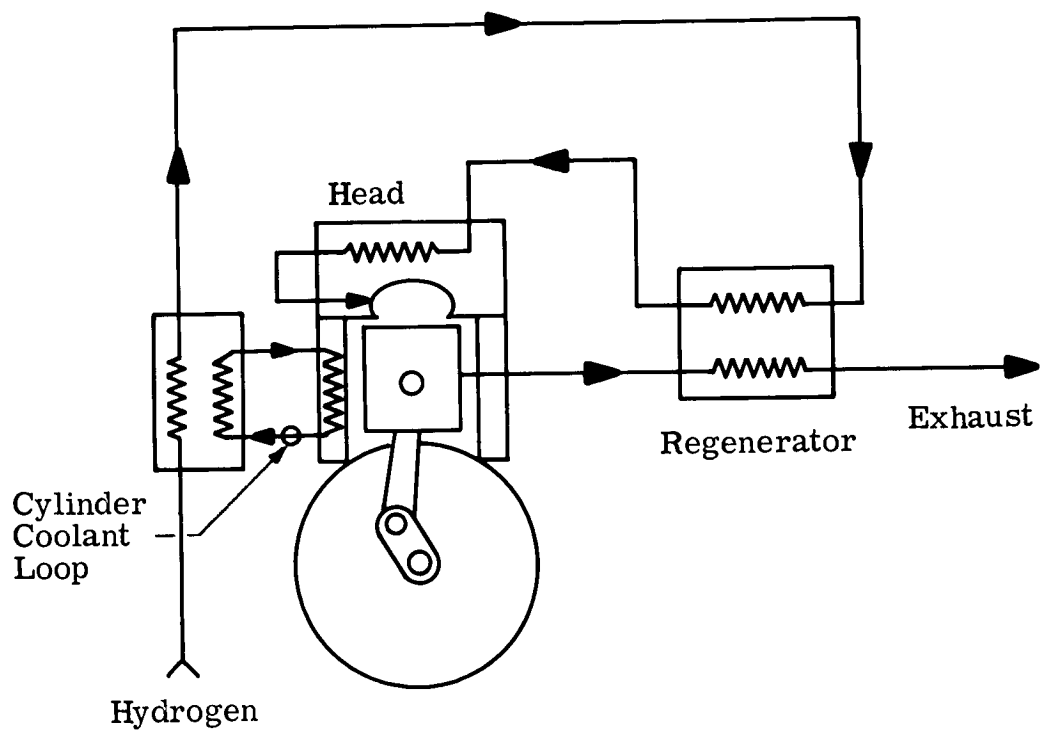


Fig. 3-54 - Completely Regenerated Engine

4.0 PROTOTYPE COMPRESSOR DEVELOPMENT

4.1 Design, Description and Evolution

Work previously performed under NASA Contract NAS 3-2550 disclosed deficiencies in the compressor design shown in Figure 4-1. This compressor's drive mechanism was designed to eliminate sliding motion between members exposed to cryogenic hydrogen. The oscillating arm driving the piston was connected to it by means of a Bendix flexural pivot and a flexural wire cage. These members did not lend themselves to stress calculation and failed during the first attempt at two-stage testing. The first stage cylinder head design contained an internal static seal between the inlet and outlet ports which could not be checked for leakage. The performance of this design was too low to be measurable. During the present program, the design of the internal drive linkage, the piston to cylinder seal and the first stage head were developed to the configurations shown in Figure 4-2.

A photograph of the present internal drive components is shown in Figure 4-3. While retaining the kinematics of the drive system the flexural members were replaced with more conventional sliding members. The rubbing surfaces of the mechanism consist of the cylindrical hole in the center of the piston and its mating piston pin, and the cylindrical hole in the center of the pin and the mating surface of the rocker arm shaft. The piston pin allows for the angular motion between the rocker arm and the piston. The bearing surface between the rocker arm and the piston pin allows for change in the effective radius arm length, with respect to the piston. Bearing surfaces of Fluoroloy (1),

- (1) Fluoroloy is a teflon base material with glass, iron oxide, and molybdenum sulfide fillers supplied by Mace Corp., San Gabriel, California.

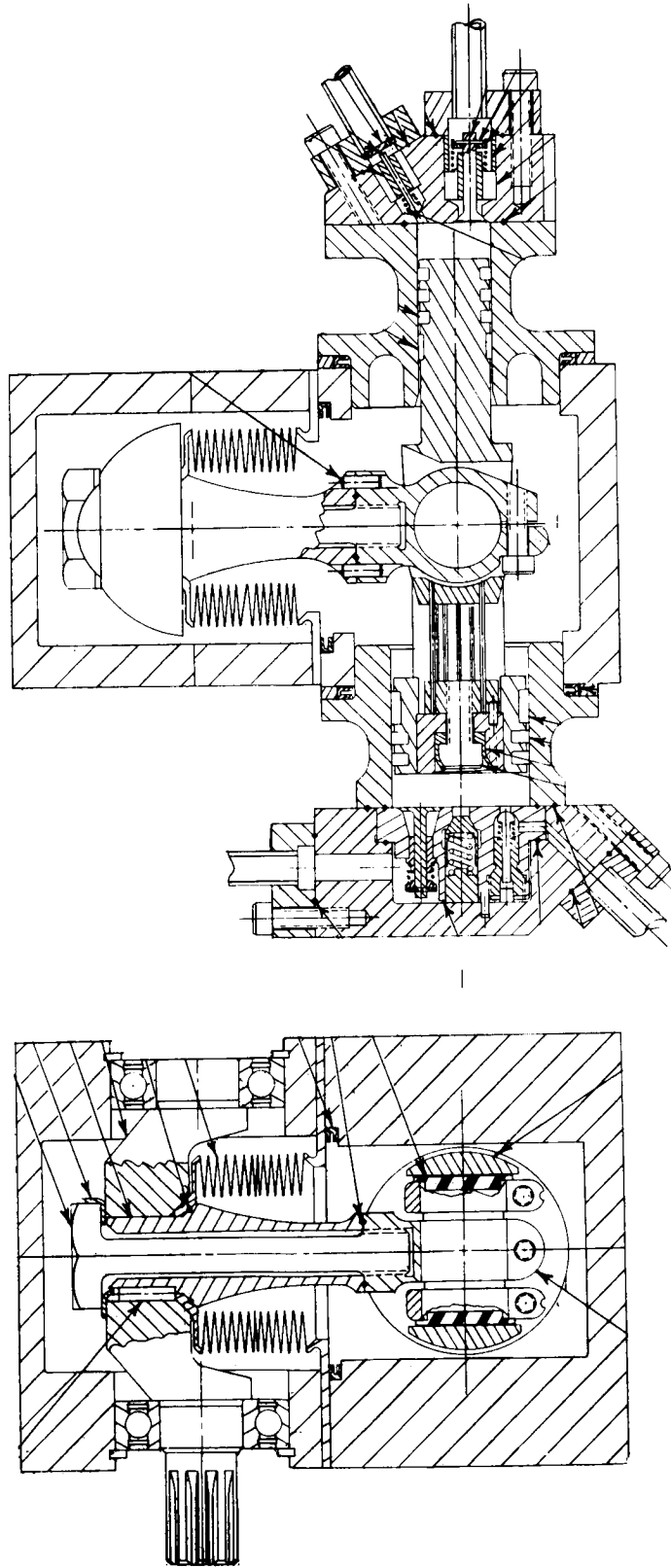


Fig. 4-1 - Initial Compressor Design

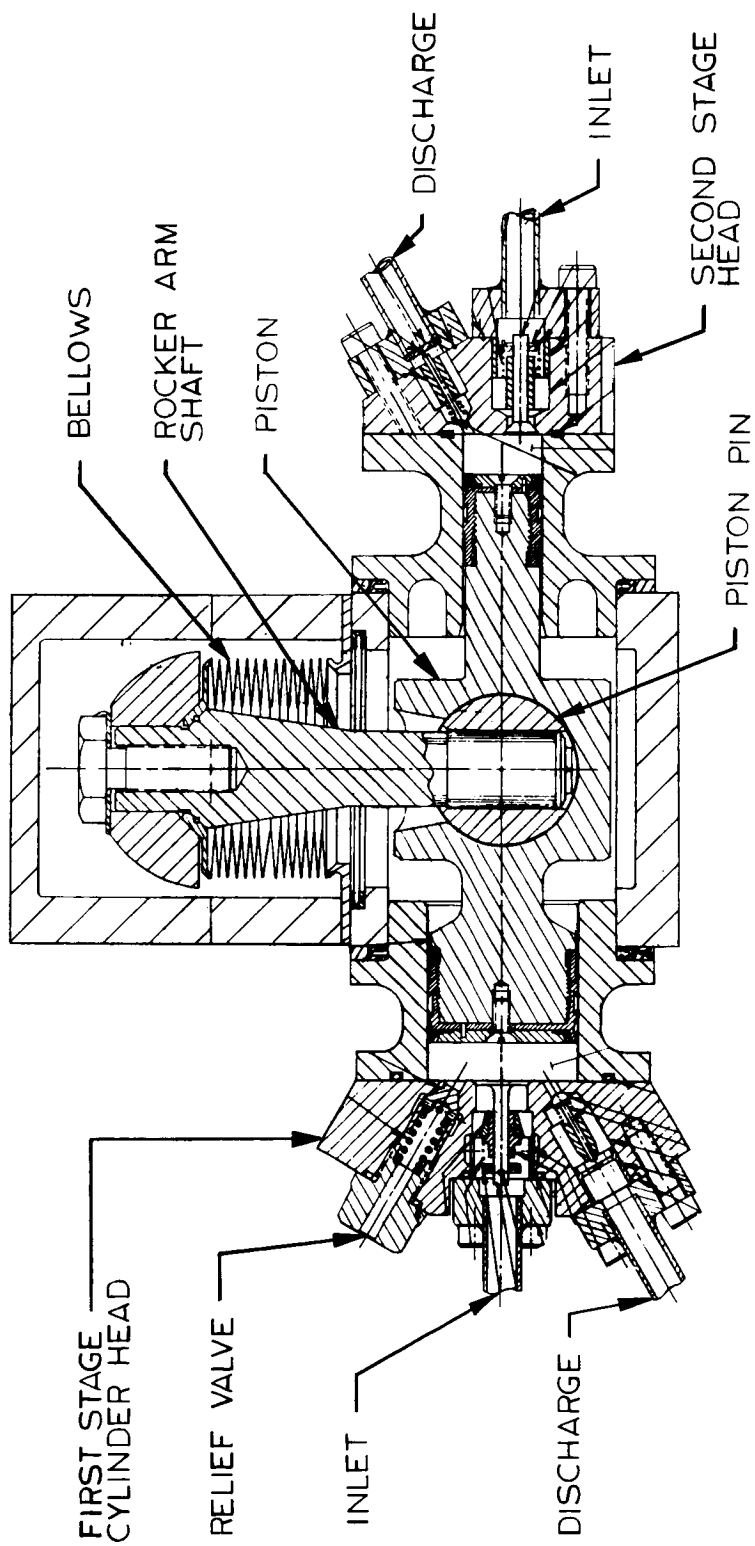


Fig. 4-2 - Final Compressor Design

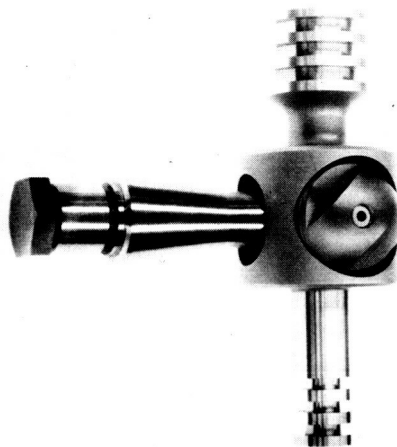
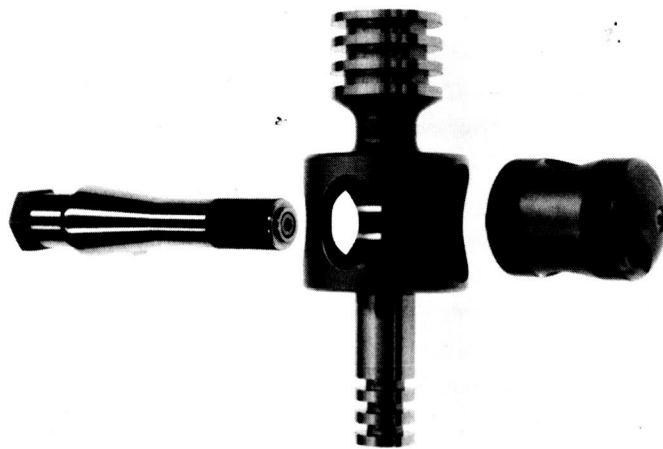


Fig. 4-3 - Present Drive Linkage

Rulon A (2) and Rulon LD (2) materials were evaluated on the piston pin and on the rocker arm. The Fluoroloy was unsatisfactory. Both Rulon A and Rulon LD were successful.

Prior to the development of the present piston configuration a three-piece piston ring was tested. It consisted of a "T" shaped expander of Kel-F and two Fluoroloy compression rings. Also, a one-piece Rulon A compression ring with a metallic expander was tested. The Rulon A ring was the better of the two.

The present piston design is shown in Figure 4-4. A thread was machined on the ends of the basic stainless steel piston and oversize Rulon A caps were screwed onto the piston and epoxy-bonded in place. The Rulon was then finished to the final configuration.

A lip on the leading edge of the piston forms a seal with the cylinder. A serrated disc-spring preloads the lip to improve sealing during the low pressure portion of the compression cycle.

Since valving deficiencies became apparent during the test program, preliminary layouts were made for two new first stage inlet valve designs. These designs are presented and discussed in Section 4.3.4, as they are best described and understood after reading the performance test section. The new valving concepts were not explored further than the sketch layout stage because of the emphasis on engine endurance testing during the later part of the program.

Materials used in the final compressor configuration are listed in Table 4-I.

- (2) Rulon is a reinforced TFE fluorocarbon material of proprietary composition supplied by Dixon Corp., Bristol, Rhode Island.

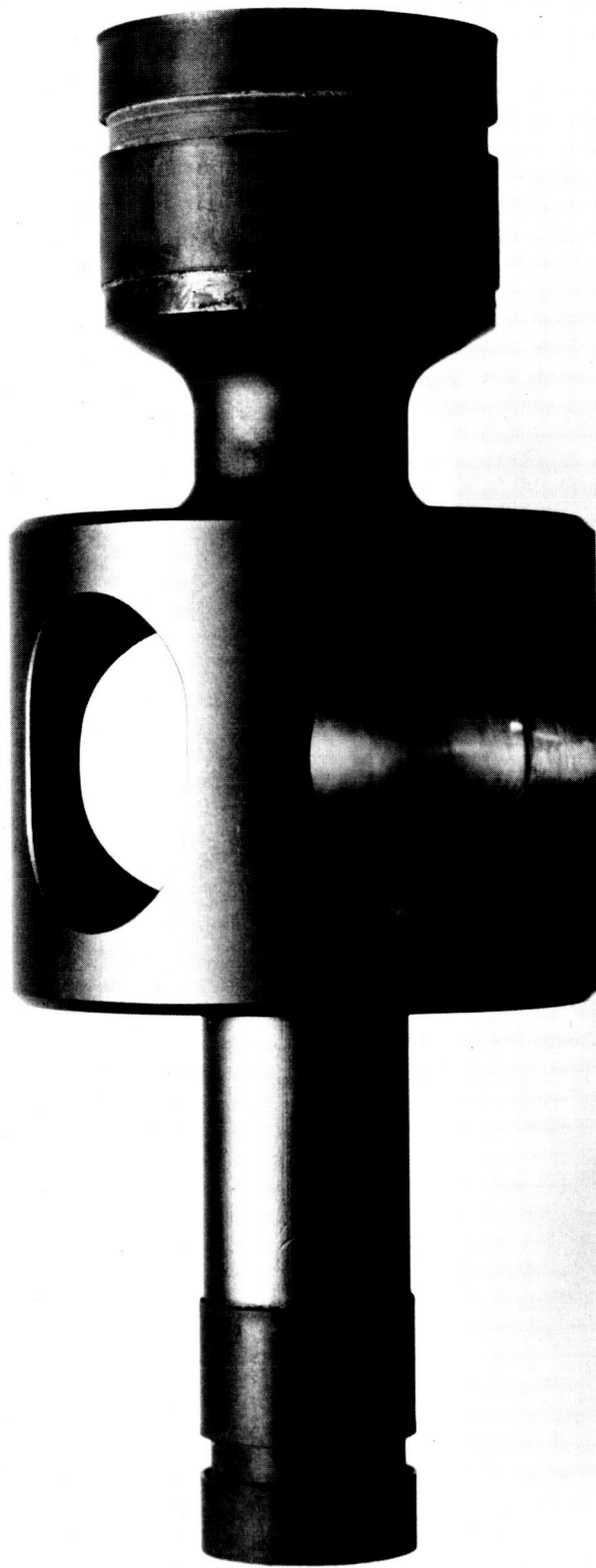


Fig. 4-4 - Present Piston Design (After 100 hr.
Endurance Test)

Table 4-I
Material List - H₂ Compressor

Description	Material	Special Treatment or Notes
Housing Assembly	Stainless AISI 304	- - -
Crank Shaft	18% Ni. 300 Mar Aging Stl.	Aged to R _c 50 min.
Bellows Assembly	Stainless 347	Alternate Mat'l. Inconel X
Rockerarm	18% Ni. 300 Mar Aging Stl.	Aged to R _c 50 min.
Bushing - Rockerarm	Rulon L.D.	Filled teflon. Composition not released. Dixon Corp., Rhode Island.
Screw Rockerarm	18% Ni. 300 Mar Aging Stl.	Aged to R _c 50 min.
Face Seal - Housing	17-4 Ph. Stainless Stl.	Teflon coated
Face Seal - Housing	17-4 Ph. Stainless Stl.	Teflon coated
Cylinder - 1st Stage	Stainless AISI 347	Nitrided bore - case .003-.004 Rockwell 15N91 (TVS 1002)
Cylinder - 2nd Stage	Stainless AISI 347	Nitrided bore - case .003-.004 Rockwell 15N91 (TVS 1002)
Piston Pin	Stainless AISI 347	Nitrided bore - case .003-.004 Rockwell 15N91 (TVS 1002)
Bushing - Piston Pin	Rulon LD.	Filled teflon. Composition not released. Dixon Corp., Rhode Island.

Table 4-I (Continued)
Material List - H₂ Compressor

Description	Material	Special Treatment or Notes
Flange - Piston Pin	Stainless AISI 347	Nitrided case .003-.004 Rockwell 15N91 (per TVS 1002)
Piston	Stainless AISI 347	Nitrided case .003-.004 Rockwell 15N91 (per TVS 1002)
Cap - Piston - 1st Stage	Rulon L.D.	Filled teflon. Composition not released. Dixon Corp., Rhode Island.
Cap - Piston - 2nd Stage	Rulon L.D.	Filled teflon. Composition not released. Dixon Corp., Rhode Island.
Expander - Piston Cap	Stainless AISI 304	Shim stock full hard
Washer - Expander	Aluminum 2024	T 4 condition
Valve Housing - 1st Stage	AMS 5643 17-4 Ph.	Cond. H 900 R _C 45
Valve Relief - 1st Stage	Virgin Teflon	- - -
Valve Inlet - 1st Stage	17-4 Ph.	Cond. H 900 R _C 45
Guide Valve Inlet - 1st Stage	Teflon filled bronze	65% bronze by weight. Remainder teflon.
Spring-Inlet Valve - 1st Stage	302 Cres.	- - -
Valve Outlet - 1st Stage	17-4 Ph. H 900 R _C 45	These components were replaced by a reworked std. stainless steel check valve to reduce valve sealing problems that existed with the original design.
Guide Valve Outlet-1st Stg.	65% teflon filled bronze	
Spring Outlet - 1st Stage	302 Cres.	

Table 4-I (Continued)
Material List - H₂ Compressor

Description	Material	Special Treatment or Notes
Valve Inlet - 2nd Stage	17-4 Ph.	Cond. H 900 R _c 45
Guide Inlet - 2nd Stage	Teflon filled bronze	65% bronze by weight, remainder teflon.
Spring Inlet Valve - 2nd Stage	302 Cres.	- - -
Valve Outlet - 2nd Stage	17-4 Ph.	Cond. H 900 R _c 45
Guide Outlet Valve - 2nd Stage	Teflon filled bronze	65% bronze by weight, remainder teflon.
Spring Outlet Valve - 2nd Stage	302 Cres.	- - -
Metal "O" Ring	Stainless Stl. - Teflon coated	Typical static seal at the different joints.

The compressor control room with instrumentation is shown in Figure 4-5. Figure 4-6 shows the test cell, and Figure 4-7 is a photograph of the compressor mounted on the test stand. Figure 4-8 is a schematic of the test set-up.

The compressor is driven with a fixed displacement hydraulic motor. The speed of the drive motor is set by adjusting the flow of the hydraulic power supply. Either hydrogen or nitrogen gas is supplied to the compressor inlet from high pressure storage bottles through remote control valves and regulators. The inlet gas is cooled by passing it through a coil of tubing submerged in liquid nitrogen contained in an insulated Dewar. The inlet pressure is controlled by two regulators in series, upstream of the cooling Dewar. The inlet gas temperature is controlled by adjusting one or both of two control valves. One valve bleeds a portion of the LN_2 cooled gas to ambient, for cooling down the lines, and the other valve allows ambient temperature gas to be mixed with LN_2 cooled gas upstream of the compressor inlet to provide control of compressor inlet temperature.

A set of gas manifolds allows for either first stage only, or two-stage, operation. The compressor discharge pressure is controlled by throttling the gas flow with a bellows-type hermetically sealed valve. The discharge flow is measured with a certified Rotometer-type flow meter discharging to atmosphere. A sufficient length of uninsulated tubing upstream of the flow meter allows the gas to reach ambient temperature before it enters the flow meter.

Input torque is measured with a 1,000 inch-ounce, in-shaft type strain gage torque pickup and a direct read-out indicator.

Compressor speed is determined with an electric counter with



Fig. 4-5 - Compressor Control Room

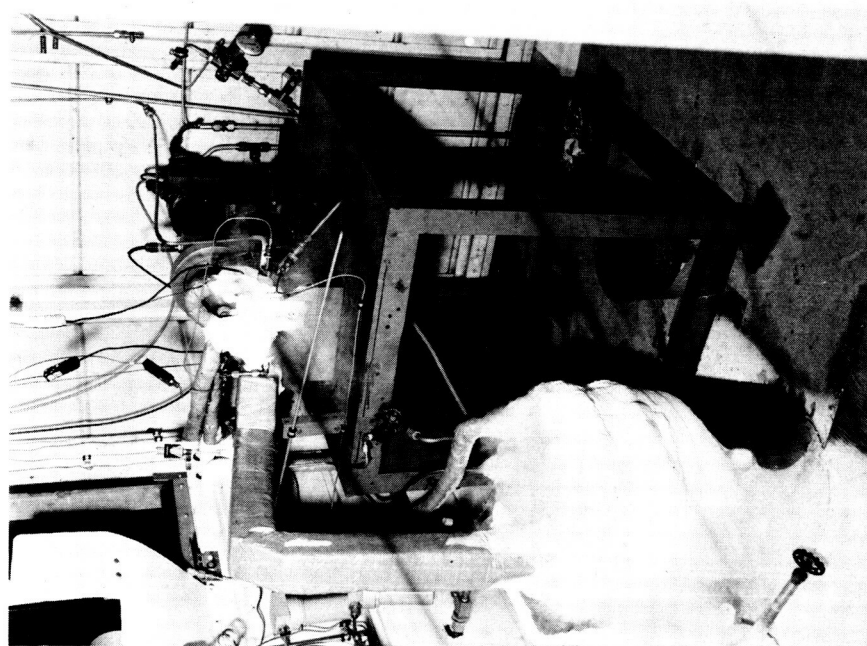


Fig. 4-6 - Compressor Test Cell

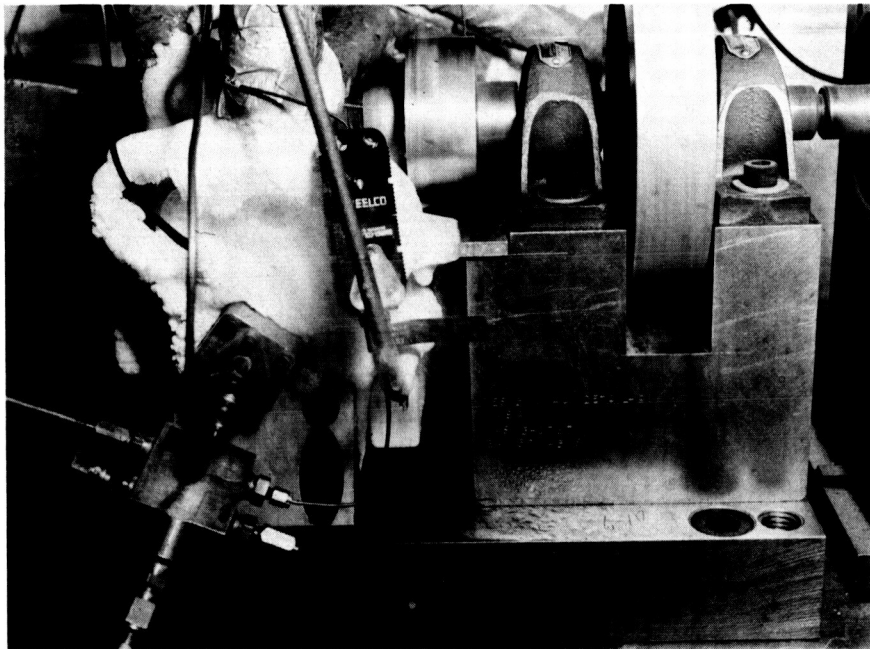


Fig. 4-7 - Compressor Mounted on Test Stand

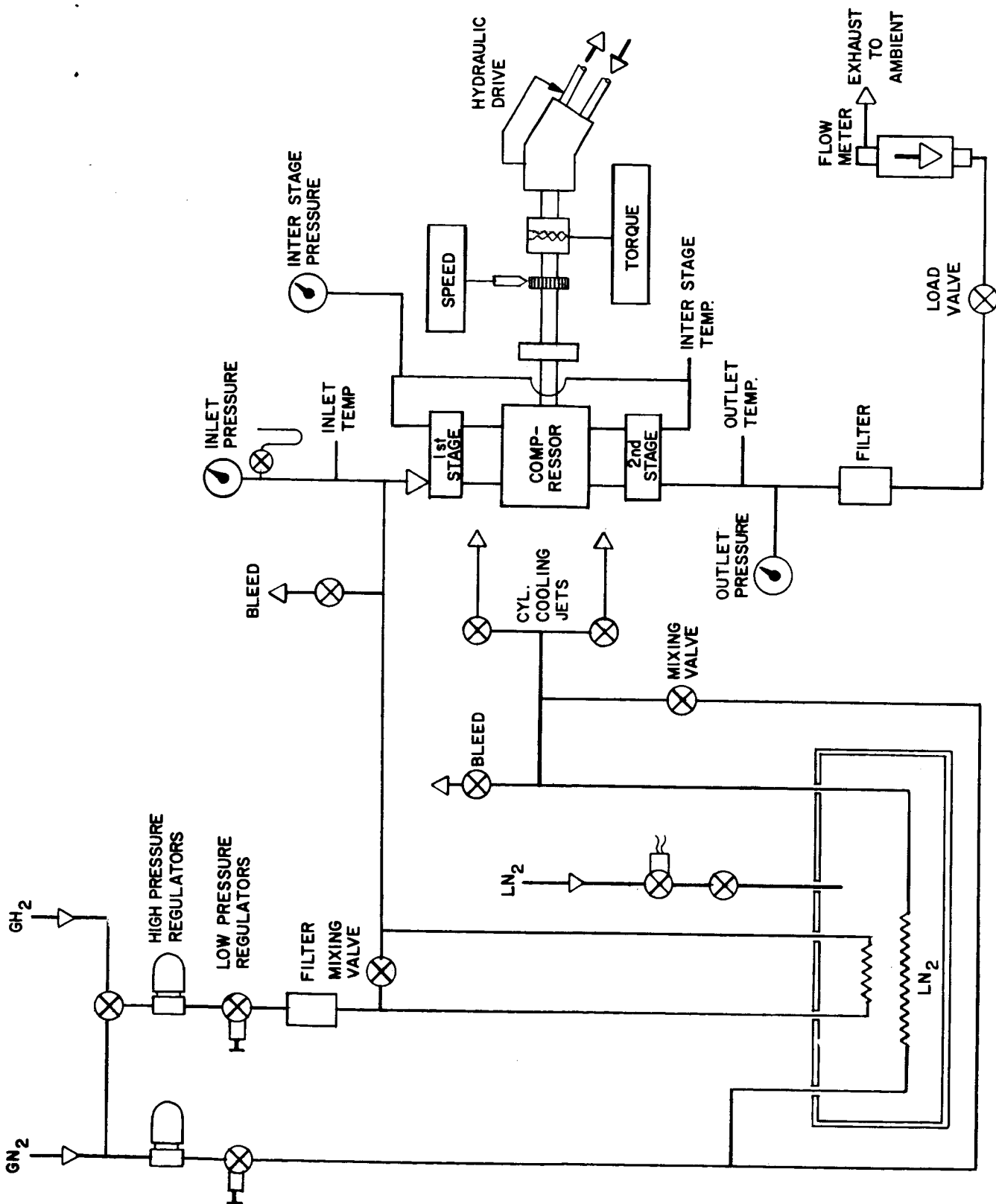


Fig. 4-8 - Schematic of Compressor Test Set-up

a direct rpm read-out. Temperatures are sensed with copper-constantan and iron-constantan thermocouples and are observed on direct read-out instruments or recorded by strip chart recorders. Temperature measurements include inlet temperatures, outlet temperature of each stage, cylinder temperatures, body temperatures, and the flow meter temperature. The cylinder temperatures are controlled by cooling with cold N₂ gas.

The first stage inlet pressure is measured with a mercury manometer. Interstage pressure and discharge pressure are measured with bourdon tube pressure gages.

The sample data sheet and reduction sheet shown in Appendix E show the detail steps of data collection and reduction.

The compressor test set-up and instrumentation were improved along with the development of the prototype compressor. The instrumentation has been sufficiently sensitive to observe changes in performance when design changes were made. For example, marked changes were observed between different methods of sealing, between the piston and the cylinder, and minor changes were detected during minor valve modifications. The present instrumentation, with the addition of a cylinder pressure indicator, will be adequate for the development of new valving at liquid nitrogen temperature, which is the next logical development task. For final evaluation and calibration of the compressor at liquid hydrogen temperatures, additional refinements will be required.

4.3 Prototype Compressor Testing

A total of 174 hours of compressor testing was conducted using two compressor assemblies. Compressor No. 1 was subjected to a 100-hour endurance test. Compressor No. 2 was run for a

total of 74 hours, consisting of extensive development testing and the final calibration test runs. Development testing included evaluation of several piston ring configurations, of minor valve modifications, of different bearing materials, and of different Rulon-capped piston designs and piston-to-cylinder seals. The last 44 hours of test time on Compressor No. 2 (including the calibration test runs) were made using the Rulon A capped piston lip seal spring loaded against the cylinder wall. The 100-hour endurance test on Compressor No. 1 was run without the use of the sealing lip preload spring. The most significant test results were obtained during the 100-hour run and during the final calibration tests.

4.3.1 Endurance Test - The objective of the endurance test was to determine:

1. The endurance capability and wear rate of the Rulon capped piston.
2. The endurance capability and wear rate of the Rulon bearing surfaces of the internal drive linkage.
3. The endurance capability of the metal bellows.

The endurance test time was accumulated at a rate of one shift per day. Nitrogen gas was used for reasons of economy. Maximum and minimum values for the test data recorded during the test were as follows:

Stroke	.478 inches
First Stage Clearance (piston to cyl. head)	.0195 inches
Second Stage Clearance (piston to cyl. head)	.0200 inches
First Stage Inlet Temp.	-115°F to -175°F
First Stage Inlet Press.	2.0 to 4.5 inches of Hg gage
Interstage Temperature	30°F to +100°F
Interstage Pressure	46 to 62 psig
Second Stage Discharge Temperature	145°F to 200°F
Second Stage Discharge Pressure	410 to 500 psig
Weight Flow Rate	1.20 to 1.45 lb/hr
Speed	2524 to 2874 rpm

At the end of the test period, accumulated time on the parts was:

Piston, Rulon A	101:07 hours
Internal Drive Linkage	107:33 hours
Metal Bellows	107:33 hours

The results of pre and post-test inspections are listed below:

1. Test Set-up:

The 0.0195 clearance between the piston top and the cylinder head remained unchanged during the 100-hour test.

2. First stage piston diameter showed no wear or scoring (see Figure 4-4).

3. First stage cylinder bore showed no wear.

4. First stage piston-to-cylinder diametral clearance remained 0.0012 inch.
5. Second stage piston wore 0.0005 inch (see Figure 4-4).
6. Second stage cylinder showed no wear.
7. Second stage piston to cylinder diametral clearance increased from 0.0008 to 0.0013 inch.

The wear of the second stage is attributed to the higher gas loads on the piston.

8. Piston pin O. D. wear was 0.0002 inch (see Figure 4-9).
9. Piston pin bore in piston showed no wear.
10. Piston pin-to-piston clearance increased from 0.0010 to 0.0012 inch.
11. Rocker arm bore in piston pin showed no wear.
12. Rocker arm O. D. wear was 0.0001 inch (see Figure 4-10).
13. Rocker arm-to-piston pin clearance increased from 0.001 to 0.0011.
14. First Stage Valving:
 - a. Inlet valve: Contaminated with Rulon residue.
Opening pressure: 5 psi full flow.
*Pressure holding: 120 bubbles/min. at 30 psi.

* The term "Pressure Holding" means the valve is pressurized from the reversed flow direction.

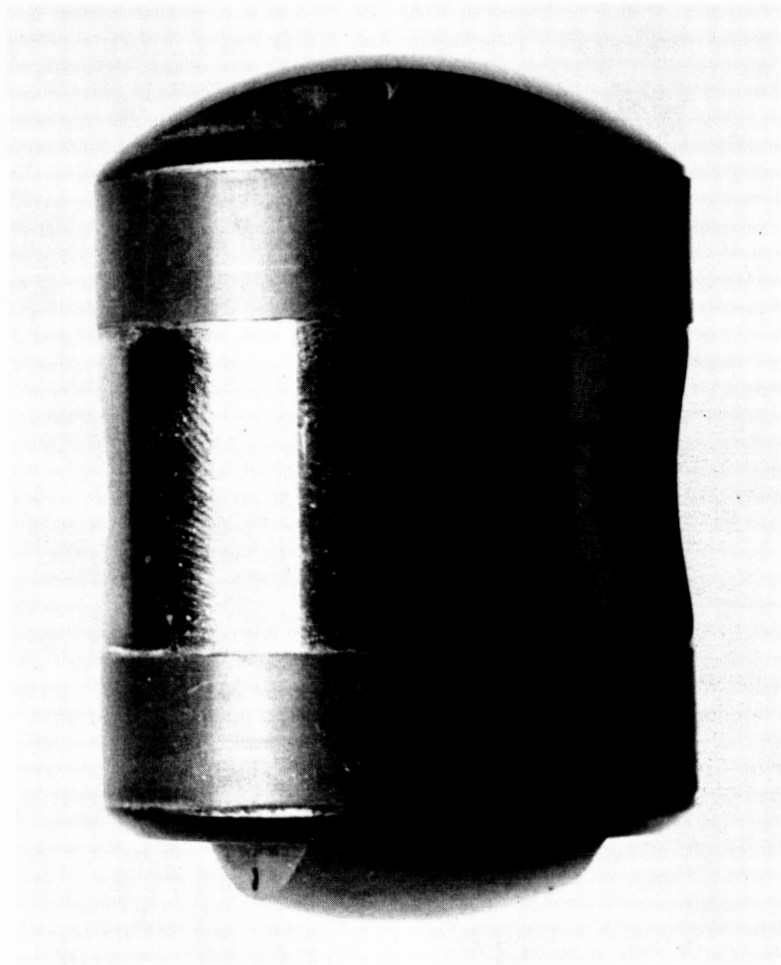


Fig. 4-9 - Compressor Piston Pin (After 100 hr.
Endurance Test)

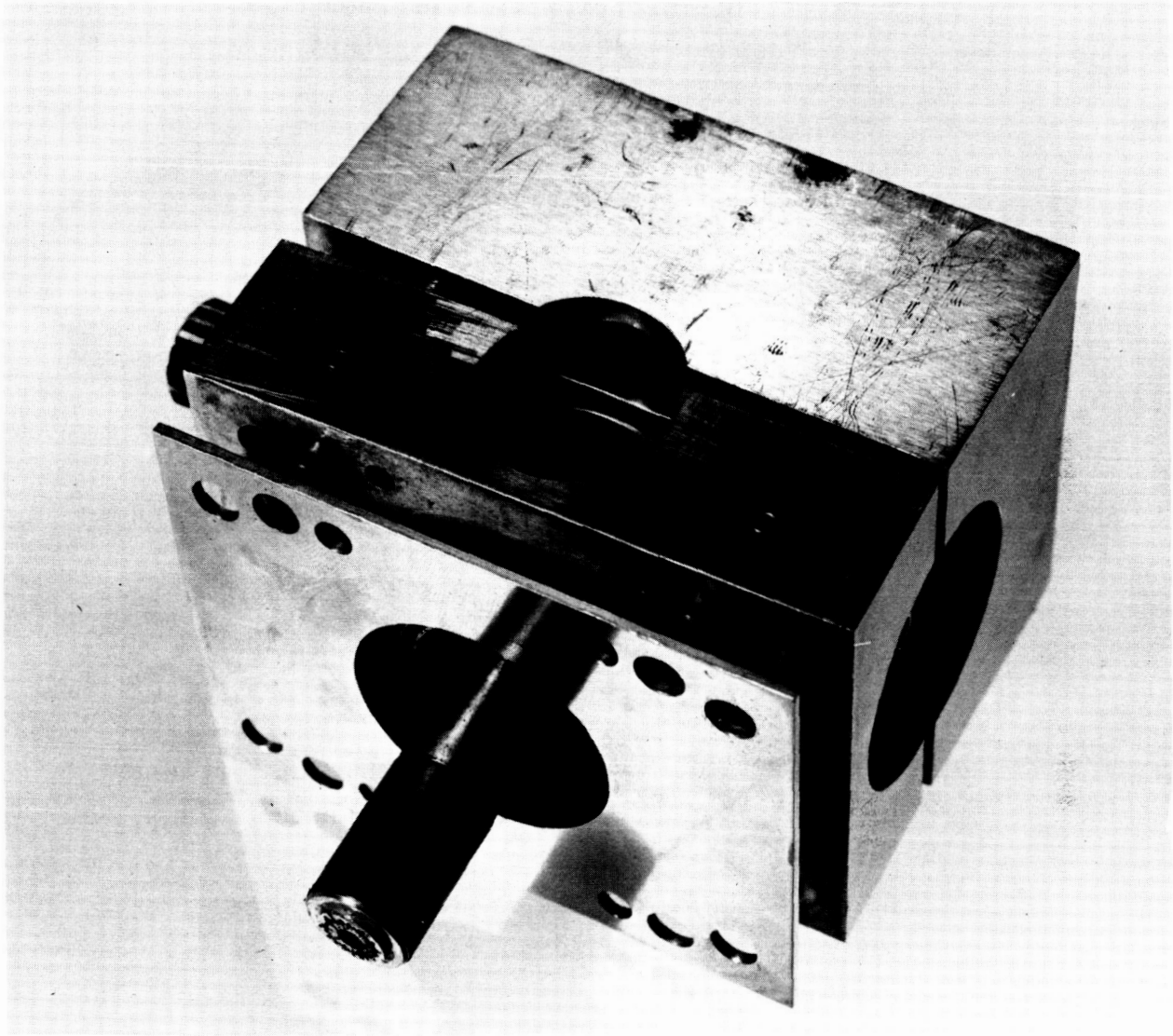


Fig. 4-10 - Compressor Rocker Arm Pin (After 100 hr.
Endurance Test)

- b. Discharge valve: Contaminated with Rulon residue.
Opening pressure: 3 psi full flow.
Pressure holding: 5 psi, 140 bubbles/min.
- c. Relief valve opens at 250 psi.

15. Second Stage Valving:

- a. Inlet valve: Contaminated with Rulon residue.
Opening pressure: 3 psi.
Pressure holding: 50 psi, 50 bubbles/min.
- b. Discharge valve:
Opening pressure: 4 psi.
Pressure holding: 50 psi, 46 bubbles/min.

16. Metal Bellows:

The first convolution nearest the crank shaft developed a leak. The time of the failure is not known because the compressor was not disassembled during the test period. This failure is not conclusive, since the bellows previously received a permanent set due to a pressure regulator failure when it was leak tested before installation. No leak was found, but the weld joint could have been weakened, resulting in failure during the endurance test.

An accurate cycle record was kept on another bellows during subsequent compressor tests, and it was periodically removed from the assembly and checked for leaks. This bellows failed after about 5 million cycles. (This would represent 27.8 hours of operation at 3000 rpm.) Approximately 15 million cycles were accumulated during the 100-hour test. Therefore, it is

probable that the bellows failed within the first 30 hours of operation.

Since the operating conditions, such as inlet and outlet pressure and temperature, as well as the speed, were changing from time to time during the 100-hour test, the expression

$$\frac{\eta_v}{CF} = \frac{\text{Volumetric efficiency}}{\text{Clearance factor}} \quad \text{was used to}$$

compare performance with elapsed time regardless of different operating conditions. (Volumetric efficiency η_v and the clearance factor CF are defined in Appendix D.)

The $\frac{\eta_v}{CF}$ values for both the first and second stages are

shown as a function of elapsed time in Figure 4-11. The diagram shows that although there was some performance fluctuation, there was no appreciable performance degradation during the 100-hour test.

4. 3. 2 Calibration Tests - Calibration tests were run on the first stage alone, then by running with the second stage cylinder head removed, and on the two stages in series. During each calibration test run the inlet pressure, inlet temperature, and speed were maintained constant. The discharge pressure was set at different values by adjusting a throttle in the discharge line. Data obtained from runs at different speeds were reduced and plotted versus the pressure ratio across the compressor.

4. 3. 2. 1 First Stage Compressor Calibration Test Results - Figures 4-12 and 4-13 show η_v/CF (overall volumetric efficiency), and η_o (overall thermal efficiency), versus pressure ratio.

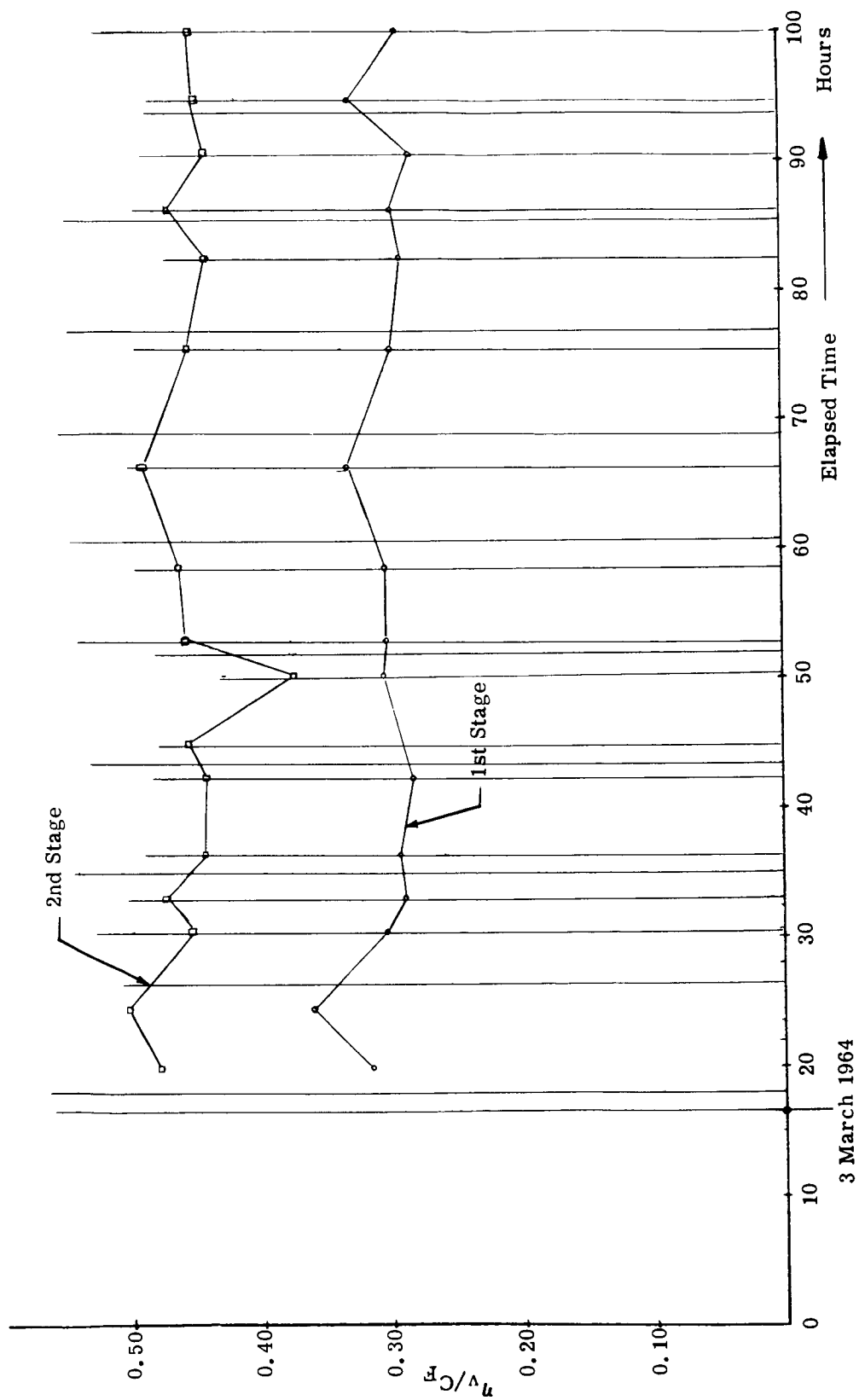


Fig. 4-11 - Compressor η_v/CF vs. Test Time for
100 hr. Endurance Test

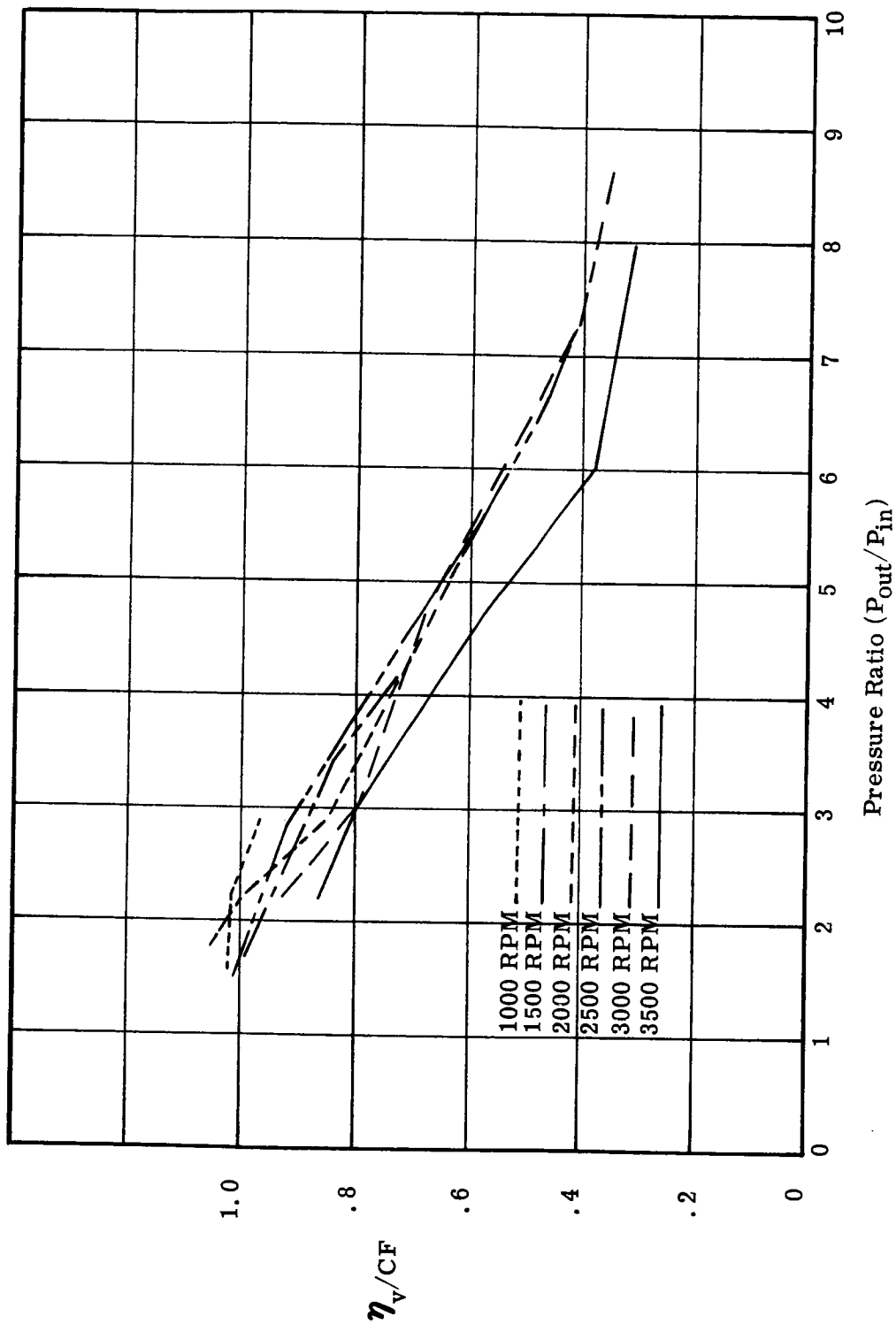


Fig. 4-12 - η_v/CF vs. Pressure Ratio for First Stage Calibration
Test with 15.65 PSIA Inlet Pressure

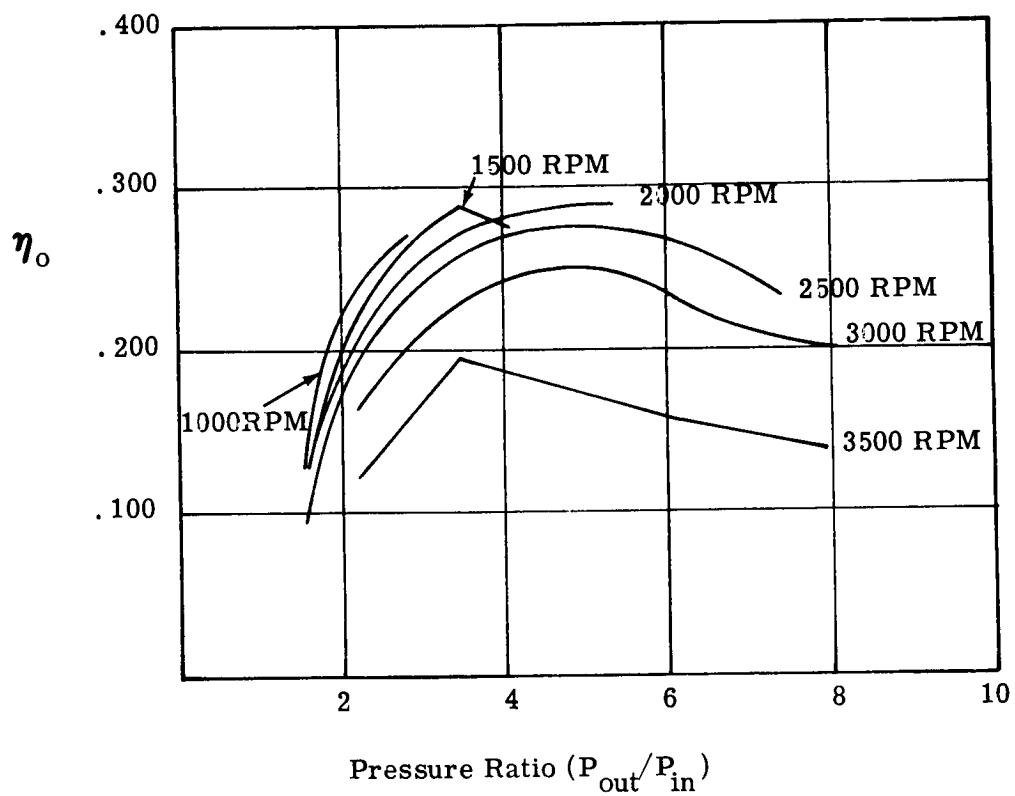


Fig. 4-13 - η_o vs. Pressure Ratio for First Stage Calibration
Test with 15.65 PSIA Inlet Pressure

Figure 4-14 is a nomogram plot showing measured mass flow rate, calculated mass flow rate for a 60°R inlet temperature (assuming volume flow rate will not change with inlet temperature), and measured input power; all versus pressure ratio. The data were taken from tests run at 1000, 1500, 2000, 2500, 3000 and 3500 rpm, during which:

Inlet pressure was maintained at 15.65 psia.

Inlet temperature was maintained at $-111^{\circ}\text{F} \pm 14^{\circ}\text{F}$.

Discharge pressure was varied between 10 and 120 psig.

Discharge temperature varied from 40°F to 72°F.

Statically measured clearance volume was 5.08% of displacement.

The cylinder was cooled to an outside temperature of 0°F.

Figure 4-12 shows that η_v/CF is primarily a function of pressure ratio and that it is influenced to a lesser extent by speed. The drop of η_v/CF with increasing pressure ratio can result from some combination of leakage (valve or piston seal), deficient inlet temperature indication, and deflections in the internal and external drive linkages. It is felt the deflection and deficient temperature indications are the predominant effects. These effects are discussed in more detail in Section 4.3.3. The fact that η_v/CF did not vary greatly with speed for speeds below 3000 rpm, and that it dropped significantly at 3500 rpm, indicates that leakage is not great since the effect of leakage is to reduce η_v/CF as speed is reduced. The lower η_v/CF at 3500 rpm is attributed to valve pressure drop and valve opening and closing dynamics, since the effect of deflection should act the other way at higher speed.

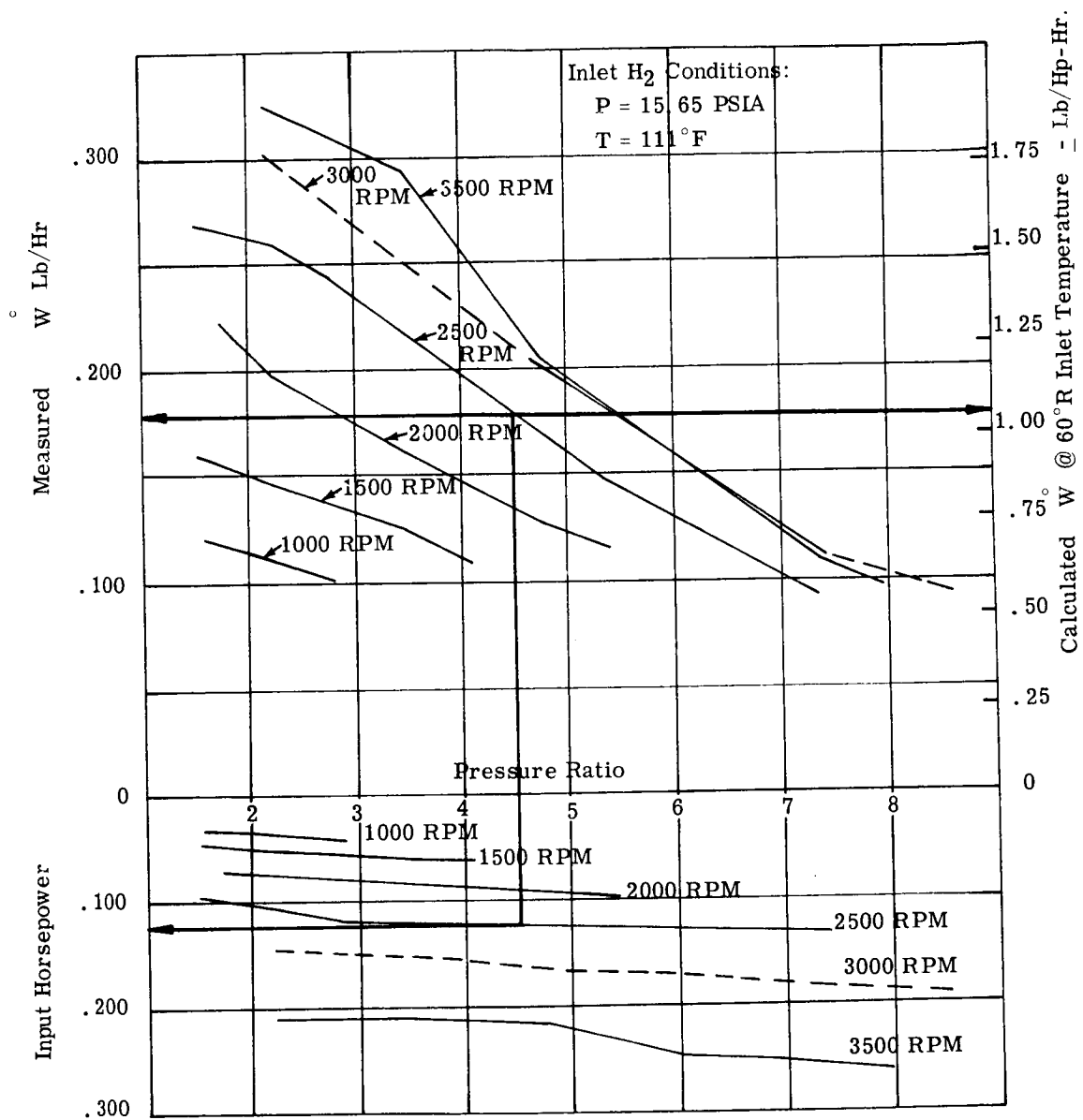


Fig. 4-14 - First Stage Calibration Nomogram of Weight Flow and Input Horsepower vs. Pressure Ratio

The η_o shown in Figure 4-13 is the ratio of ideal isentropic work done on the measured weight flow divided by the input shaft power. It should be noted that input work includes second stage friction and that only the first stage was performing useful work. The η_o is very low at low pressure ratios because little work is being done on the gas. The drop in η_o at higher pressure ratios is due to some combination of drop-off in η_v/CF with pressure and increased piston to cylinder friction with increased pressure. A comparison of this data with data from calibration tests run at a high inlet pressure, indicates that η_v/CF is the predominant factor in decreasing η_o at high pressure ratios.

Figures 4-15 and 4-16 show η_v/CF and η_o versus pressure ratio for a 19.63 psia inlet pressure. Both η_v/CF and η_o were lower for this set of tests than for the 15.65 psia inlet tests. The fact that the pressure load on the piston is higher for a given pressure ratio with a higher inlet pressure, and that the percent differences between the η_v/CF values for the two different inlet pressures tends to be higher than the percent difference between the η_o values, indicates that low η_o at high pressure ratios is due to a low η_v/CF . The lower performance of the 19.63 psia inlet test also indicates loss of stroke and increased clearance volume due to deflection of the internal and external drive linkages. Figure 4-17, which is a plot of "Dead Head" pressure ratio (pressure ratio at zero discharge flow) versus speed for the 15.65 psig inlet test, shows that achievable pressure ratio increases with speed. This again indicates deflection. The theoretical isentropic "Dead Head" pressure ratio for the statically measured clearance is 51 (the isothermal pressure ratio is 19.4).

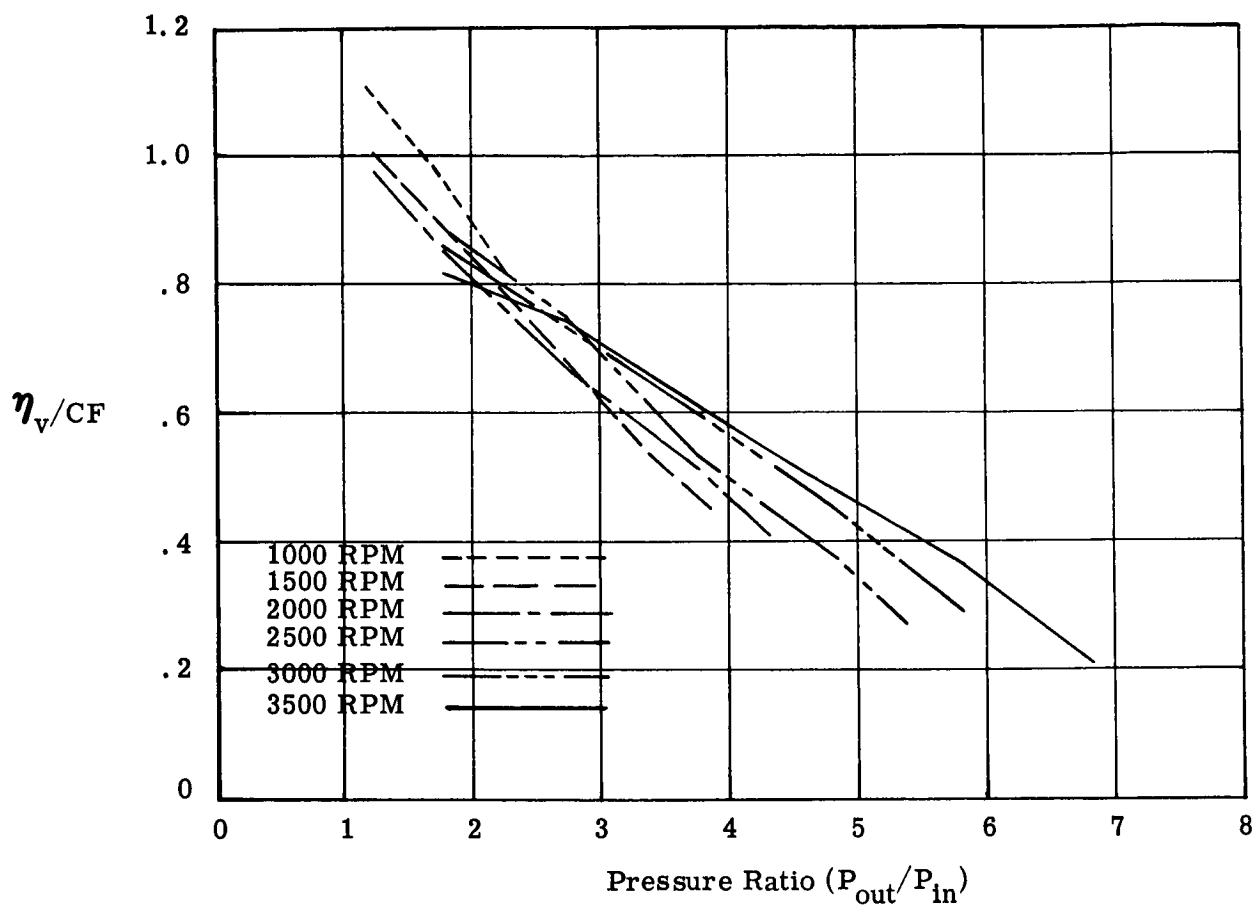


Fig. 4-15 - η_v/CF vs. Pressure Ratio - First Stage Calibration
Test with 19.63 PSIA Inlet Pressure

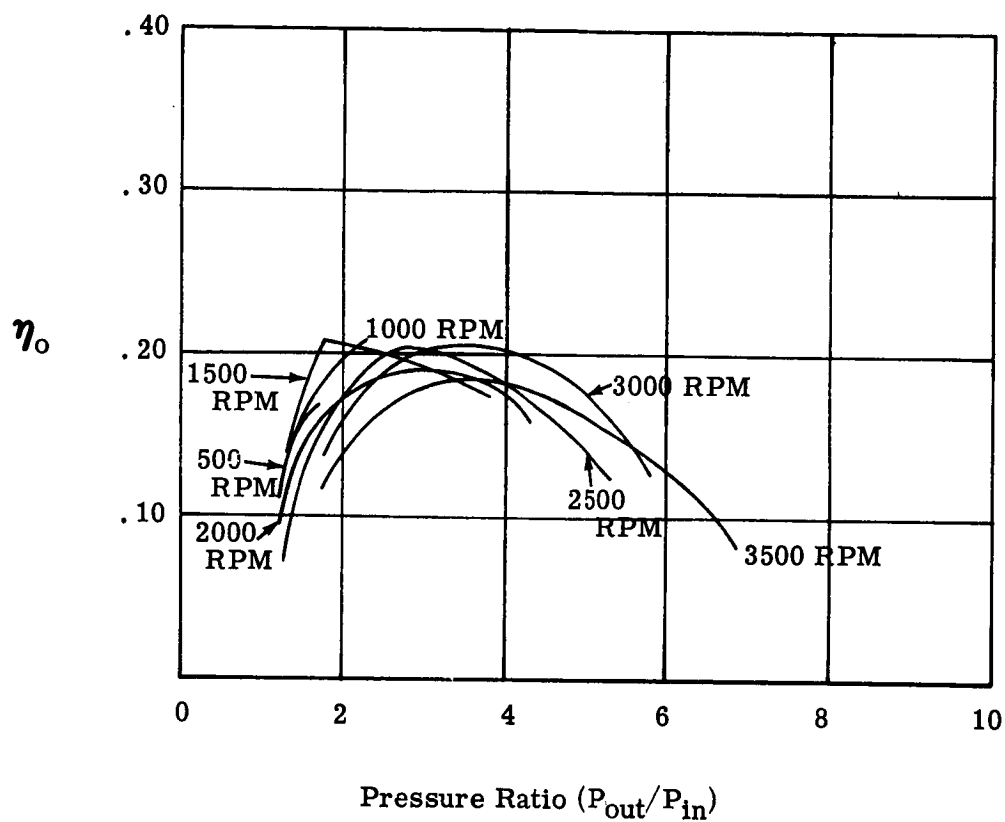


Fig. 4-16 - η_o vs. Pressure Ratio - First Stage Calibration Test with 19.63 PSIA Inlet Pressure

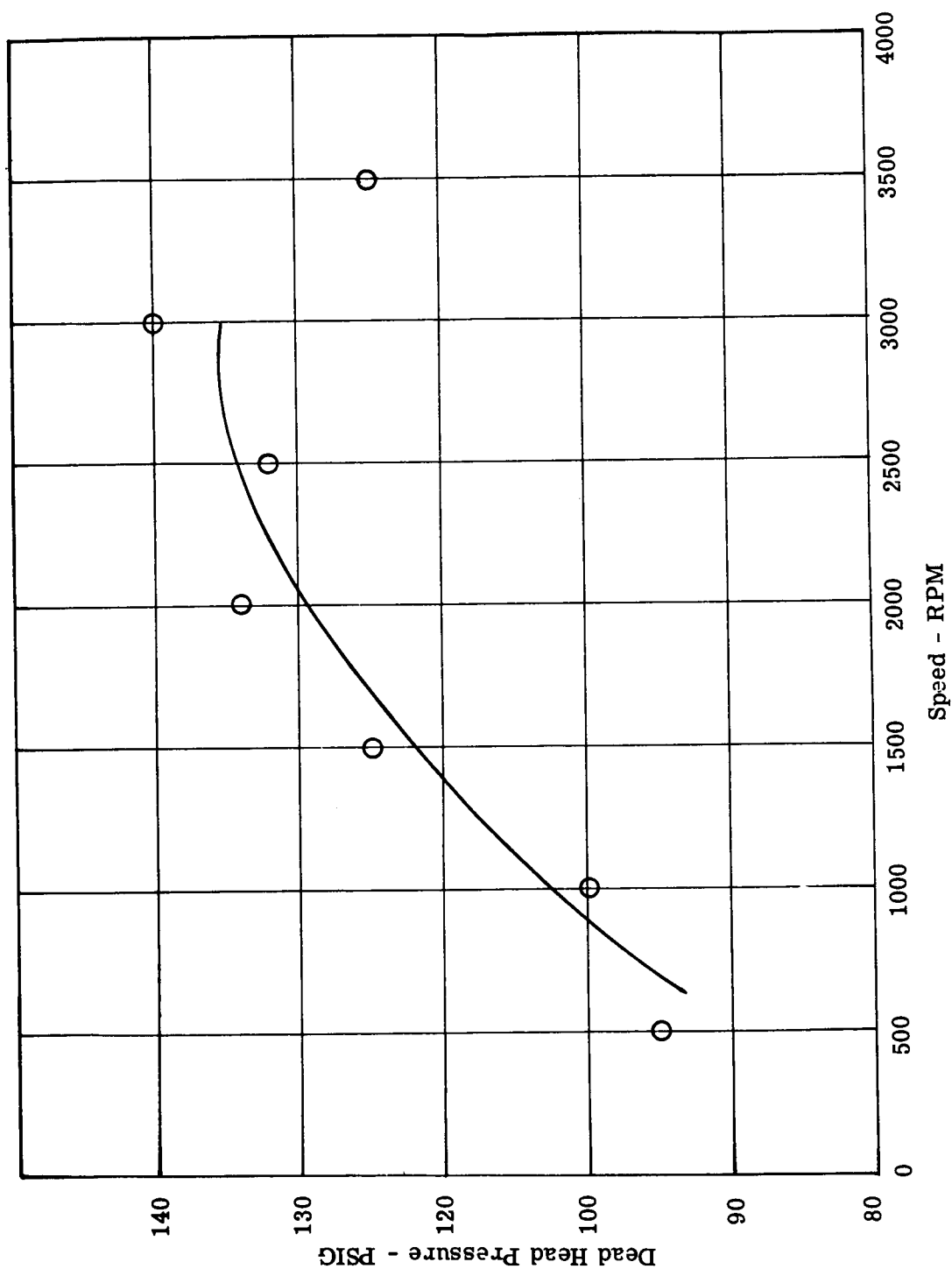


Fig. 4-17 - First Stage "Dead Head" Pressure vs. Speed

4.3.2.2 Two-Stage Calibration Results - Figure 4-18 shows η_v/CF versus the pressure ratio of the second stage of the compressor. Figure 4-19 shows η_o versus the pressure ratio across both stages. Figure 4-20 is a nomogram plot showing measured mass flow rate, calculated mass flow rate for a 60°R inlet temperature (assuming volumetric flow rate will not change with inlet temperature), and measured input power; all versus the pressure ratio across both stages of the compressor. The data was taken from test runs at 1500, 2000, 2500, 3000 and 3500 rpm during which:

Inlet pressure was maintained at 19.63 psia.

Inlet temperature was maintained at -108°F $\begin{matrix} -20 \\ +8 \end{matrix}^{\circ}\text{F}$.

Interstage pressure varied between 30 to 95 psig.

Interstage temperature varied between 15 to 70°F.

Outlet pressure varied between 50 to 920 psig.

Outlet temperature varied between 32 to 120°F.

The statically measured clearance volume of the first stage was 4.89% of displacement.

The statically measured clearance volume of the second stage was 5.68% of displacement.

Both cylinders were cooled to an outside temperature of 0°F.

The second stage η_v/CF results shown in Figure 4-18 is not considered to be accurate data because of the effect of cylinder cooling with relatively high gas temperature, the effect of pressure pulsation in transfer line between stages, and the effect of clearance changes due to high discharge pressure. These effects are discussed in more detail in Section 4.3.3. The wide scatter of the data in Figure 4-18 is attributed to variations in valve performance with speed, and to the fact that particular pressure ratios were obtained with different inlet

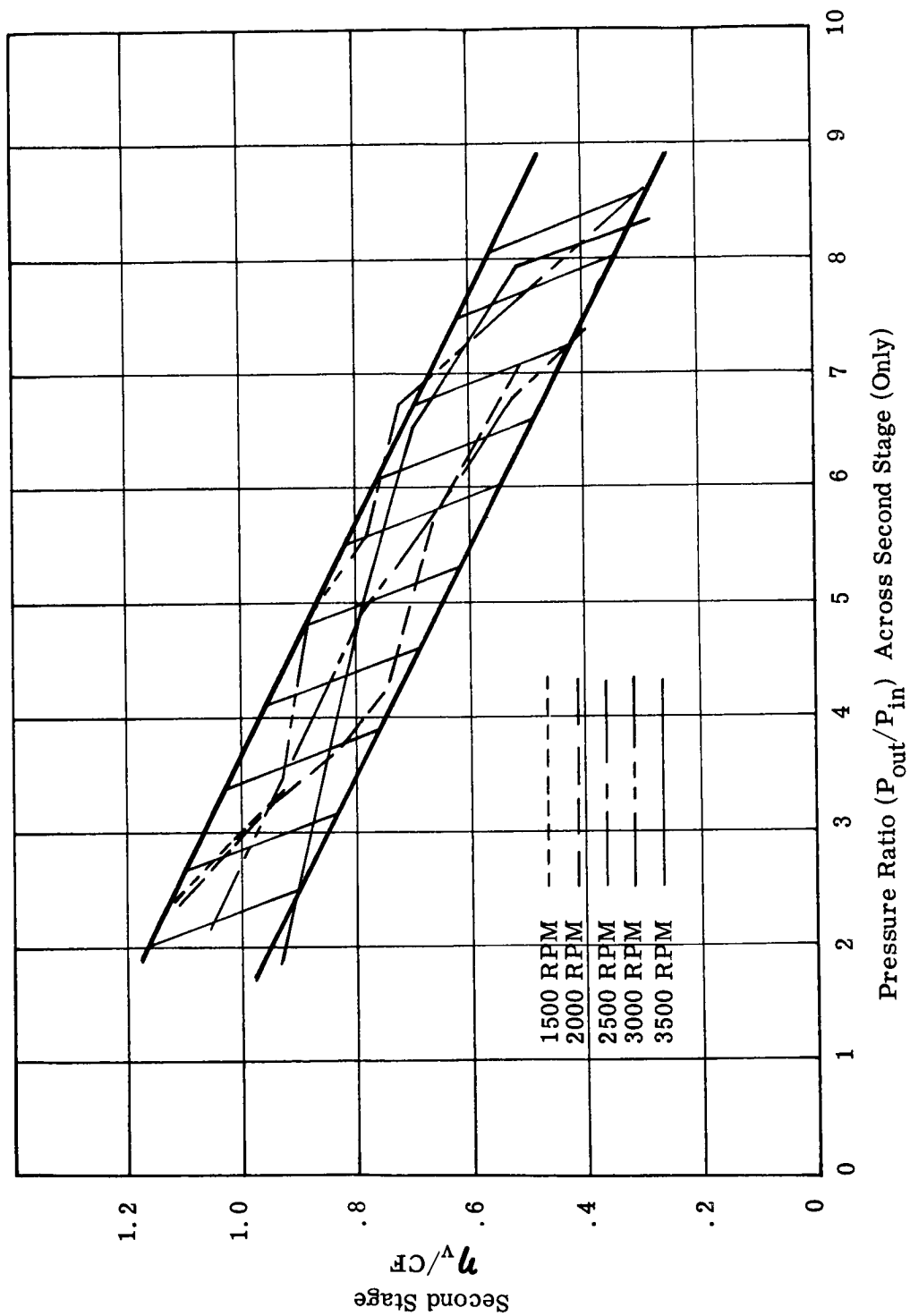
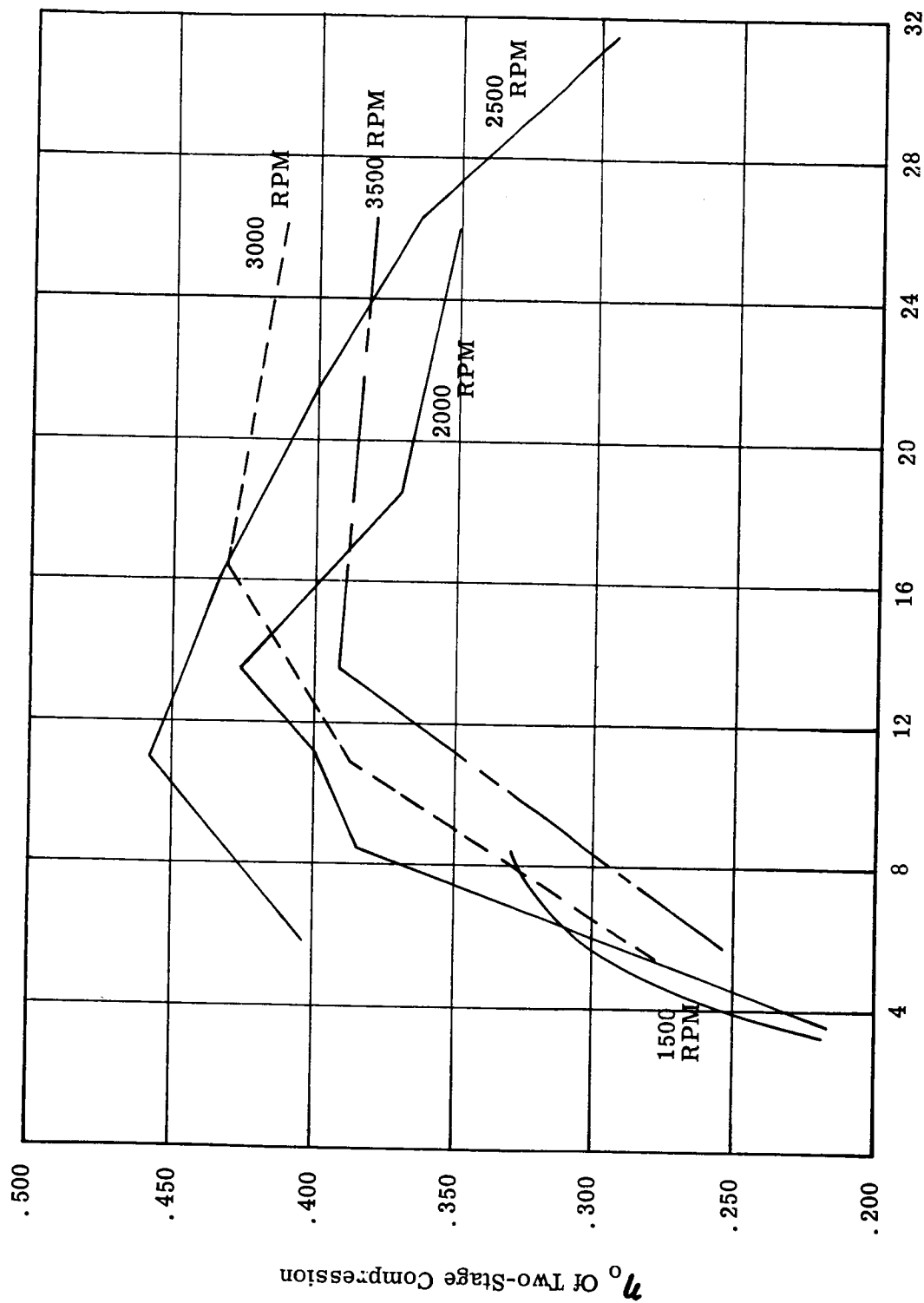


Fig. 4-18 - Second Stage η_v/CF vs. Pressure Ratio



Pressure Ratio (P_{out}/P_{in}) Across Both Stages

Fig. 4-19 - Two-Stage η_0 vs. Pressure Ratio

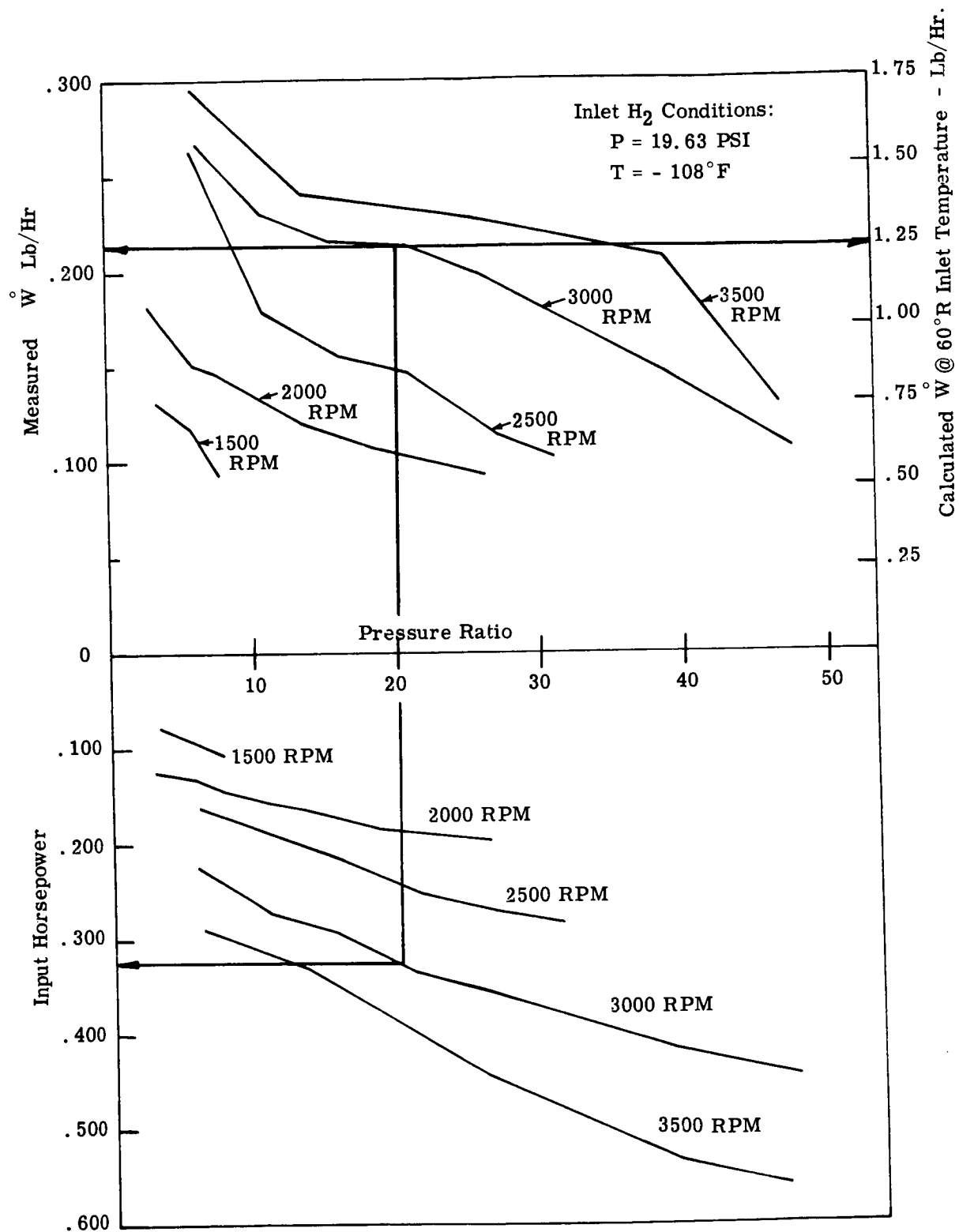


Fig. 4-20 - Two-Stage Calibration Nomogram of Weight Flow and Input Power vs. Pressure Ratio

pressures as well as different speeds during different runs , and this resulted in different amounts of clearance change due to deflections.

Though the second stage η_v/CF results are less accurate than the first stage results, it is believed that actual second stage η_v/CF performance is higher than that for the first stage because a given pressure drop across the inlet valve has less degrading effect on the performance when the magnitude of the inlet pressure is high.

The η_o curves shown in Figure 4-19 show that overall efficiency is higher with two-stage compression than with single-stage compression (see Figures 4-13 and 4-16 for comparison).

The higher η_o results mainly from the fact that more work was done on the gas in proportion to the friction work. In addition, the first stage was operating at low pressure ratios (from 1.5 to 4.8) where its η_v/CF is very high.

The effect of decreasing η_o with increasing speed is also present. Compare the 3000 and 3500 rpm curves. The drop-off in overall efficiency of the 2000 and 2500 rpm curves at high pressure ratios is attributed to the fact that their η_o/CF efficiencies drop with increased pressure ratio at these speeds.

The conclusion drawn in Section 4.3.2.1, that the drop-off in first stage overall efficiency was due to low η_v/CF and not to increased friction due to pressure loading of the piston sealing lip, is supported by the fact that the two-stage overall efficiency is relatively high, while the peak pressure acting on the second stage piston is much higher (up to 35 times) than

the peak pressure acting on the first stage piston during the single-stage test.

By using these flow values and the power versus pressure ratio curves in Figure 4-20, the power required to deliver one pound per hour at a given ratio at 60°R, assuming that the overall efficiency does not change with temperature, can be calculated. For example, with a pressure ratio of 20 and a speed of 3000 rpm, 1.26 lb/hr of hydrogen would be delivered and .315 horsepower would be required. The power per flow rate would be .25 hp/lb-hr (or 4 lb/hp-hr). This value still leaves a good margin of engine shaft power for useful work with an overall compressor performance of 42.5%.

- 4.3.3 Accuracy of Compressor Test Results - The type of results presented in Sections 4.3.1 and 4.3.2 are listed below in the order of decreasing accuracy:

Mass Flow Rate

Power

η_o

First Stage η_v/CF

Second Stage η_v/CF

The mass flow rates were obtained with a certified Rotometer flow meter discharging to ambient. The meter was located a sufficient distance away from the compressor so that the gas temperature reached ambient temperature and such that pressure pulsations were damped out.

The accuracy of the power results was limited by the necessity of working in the lower part of the 1000 in-oz. torque pick-up scale so that the pick-up would not be destroyed during speed

transients.

The accuracy of the η_o results was limited by any power inaccuracy and by the extent to which the actual cycle deviated from the assumed isentropic cycle. The isentropic assumption was least accurate with reference to the second stage during two-cycle compression because inlet gas temperature was near ambient, and the cylinder was cooled to 0°F. It was necessary to cool the cylinder to protect the Rulon material because with the inlet temperatures used (approximately - 200°F) the heat capacity of the gas was not sufficient to carry away the friction heat.

The present test hardware and instrumentation appears to have produced erroneous η_v/CF test results. For a given speed, η_v/CF results are too high at low pressure ratios and too low at high pressure ratios. Note that Figures 4-12, 4-15 and 4-18 show η_v/CF values above 100 percent at low pressure ratios. The erroneous results are due to the way measurements are taken, the dynamic properties of the compressor, and the way volumetric performance is calculated.

In essence, η_v/CF , which has a maximum possible value of one, is calculated by dividing the measured discharge weight flow by a calculated maximum possible weight flow. The maximum possible weight flow is calculated with measured inlet temperature, the measured inlet pressure, the measured speed, the static measurement of the cylinder swept volume, clearance volume, and assuming isentropic re-expansion of residues from measured discharge pressure to measured inlet pressure.

At low pressure ratios, it is believed that the actual temperature of the gas entering the first stage cylinder is lower than

the measured inlet temperature and that at high pressure ratios, the actual temperature of gas entering the cylinder is higher than the measured inlet temperature. For example, the first stage inlet temperature is below ambient and is measured a finite distance away from the inlet valve. At low pressure ratios the actual flow is high; the head temperature is not increased greatly by compressing the gas. Therefore, the actual gas temperature at the point of measurement is lower than the measured temperature indication due to heat leak from ambient, and gas flows from the point of measurement into the cylinder without picking up much heat due to its high flow rate and because of the low temperature of the head. At high pressure ratios, the flow is low due to re-expansion of residuals, and the head temperature is high due to the compression work done on the gas. Therefore, the gas can increase in temperature as it moves from the point of measurement into the cylinder, due to heat transfer from the head and because of its low flow rate.

The second argument is that due to balance between the piston pressure loads and the inertia forces of the piston and drive linkage, the drive linkage deflects so as to increase the stroke and to reduce the clearance volume at low pressure ratios, and to reduce the stroke and increase the clearance volume at high pressure ratios.

During a static load test of the internal linkage only, the piston moved about .04 inch under a 45-pound load (equivalent to a pressure of 60 psi on the first stage piston). When working with statically set clearances of .020 inch and with a stroke of .5 inch, a .04 inch change will greatly affect performance.

The deflection argument and the temperature argument, at high pressure ratios, also apply to the second stage during two-stage operation. In addition, two other effects are present. At low pressure ratios, when the head is cool and when the cylinder is colder than the inlet gas, there is a tendency for the gas to cool below the measured inlet temperature upon entering the cylinder and thus cause the efficiency to be high. Also, the fact that first stage discharge and second stage inlet occur at the same time, and the fact that the transfer tube diameter and volume is small compared to that of the cylinders, causes the total pressure in the tube to be higher than the measured static pressure, and results in a higher η_v/CF indication of all pressure ratios.

4.3.4 Discussion of Compressor Test Results - The following conclusions were drawn from the compressor test results:

1. It was demonstrated by endurance and performance testing that Rulon A is a suitable bearing material for rubbing contact between the piston and cylinder and between the parts of the internal drive linkage. Since testing was limited to a temperature range between liquid nitrogen temperature to a temperature slightly above ambient, further evaluation of the compressor should be made at lower temperatures.
2. The Rulon capped piston design provided a good seal with the cylinder bore. The effectiveness of the seal was not affected by dimension changes due to temperature. A comparison between the efficiency curves for single and two-stage operation shows that the ratio of the friction loss of the seal to the work done on the gas is smaller at higher discharge pressures. This fact indicates that

when volumetric efficiency is increased by improving the valving and drive linkage, the overall thermal efficiency at high pressure ratios will be high. The high performance of the piston design is attributed to the following: most of the piston length was used for bearing area with the cylinder; the clearance between the basic piston diameter and the cylinder bore was sufficient to provide for thermal expansion; the thin sealing lip was flexible enough to conform to the cylinder bore during changing conditions; the sealing lip had the following advantage compared to piston rings which were tested: no ring gap leakage losses; no leakage loss at BDC when a piston ring must move from one side of its groove to the other; no leakage loss from a ring sticking down in its groove; no high friction loss encountered when a ring was sufficiently spring loaded with an expander ring to prevent it from sticking in its groove. Performance of the Rulon A capped piston design at lower temperatures than those used during the tests will depend upon the properties of the Rulon A materials.

3. The final internal drive linkage design was unique and was an expedient means of using existing hardware which was fabricated for an earlier, unsatisfactory internal drive linkage design. The drive linkage functioned sufficiently well to allow the development of the piston-to-cylinder seal to evaluate the metallic bellows and to evaluate Rulon A bearing material. Were more space available, larger bearing area would have been provided for the Rulon bearing surfaces. However, the bearings did not fail during two-stage operations when they were loaded to higher bearing pressures than recommended by the material manufacturer. The fact that the bearing

area was less than desired, provided for more fair evaluation during the 100-hour endurance test which was run at less than maximum specified pressure ratios.

Because of failures of the metallic bellows, and because lowered volumetric efficiency, and the inability to achieve high pressure ratios in a single stage due to changes in clearance volume and stroke resulting from the combined deflection of the internal and the external drive linkage, and because a single stage unit may ultimately be evolved, it is not recommended that the drive linkage design should be considered for a final flight type configuration. Design studies should be made to re-evaluate the drive linkage concept. A drive concept in which few friction generating parts are in contact with or conducting heat to the gas will tend to reduce the compressor size and increase overall efficiency.

Though the present drive linkage is not recommended for the final design, the hardware can be used effectively during the next stage of development. By reworking the first stage piston for an inlet valve-in-piston design, and by making the discharge valve poppet the same diameter as the cylinder so it may be hit by the piston without damage to either the valve or the piston, the drive linkage could be adjusted statically for a stroke which extends beyond the discharge end of the cylinder. In this way, operation at high pressure ratios can be accomplished at high volumetric efficiency because effective clearance volume will not be greatly reduced by pressure load deflection of the drive linkage.

4. It is felt that further effort should be exerted to develop a single-stage compressor. One reason for this is that unless surplus boil-off gas is available which can be used to cool the gas in the transfer line between stages, there is no thermodynamic advantage in using a two-stage compressor because ambient temperature is above the gas temperature. Another reason for using a single-stage is that a safer operating temperature for the Rulon capped piston can be achieved. For any particular compressor stage, the mean hardware temperature (assuming perfect external insulation and equal temperature distribution in the material) will be equal to the mean effective temperature, with respect to time, somewhere between the inlet temperature and the outlet temperature. The discharge temperature will depend upon the mass flow, the specific heat of the fluid, the friction heat, and the inlet pressure and temperature. During two-stage compression the second stage operates at higher temperature level than the first. Under a limiting set of conditions which would cause the second stage of a two-stage compressor to be at the maximum operating temperature of the Rulon piston material, a single-stage compressor could deliver the same mass flow at the same pressure ratio with mean operating temperature well below the maximum temperature limit of the piston material.

If the possibility of cooling the second stage cylinder with incoming fluid to prevent overheating is considered, it should be remembered that increasing the temperature of the fluid before it enters the compressor will increase the compressor size and the amount of energy required to compress a unit mass of fluid. An additional advantage of single over two-stage compression is that the loss due

to the pressure drop of two valves is eliminated.

5. The compressor valving limited compressor performance in two major ways and indirectly, in a third way. First, having both the inlet and discharge valves in the cylinder head allowed heat to transfer from the discharge port to the inlet valve and down the inlet line to the incoming fluid, thus decreasing its density and resulting in increased power requirements. Secondly, the small flow area in conjunction with the spring loading of the poppet necessary to closing of the first stage inlet valve caused η_v/CF , η_o , HP/lb-hr to be higher than necessary. By examining the expression for ideal work of compression,

$$W_K = \frac{n}{1-n} P_1 V_1 \left[\left(\frac{P_2}{P_1} \right)^{\frac{n-1}{n}} - 1 \right]$$

it can be seen that as the absolute value of the inlet pressure is reduced, the percentage of loss due to a given pressure drop across the inlet valve increases. The expression also shows that a given pressure drop at the inlet valve does more harm than the same pressure drop across the discharge.

The third and indirect way in which valving reduced performance during the test program is that if an inlet valve-in-piston design and a full piston diameter discharge valve design had been used, the η_v/CF losses due to drive linkage deflection could have been compensated for by statically setting small or interference clearance.

For the above reasons it is believed that the inlet valve should be placed in the piston. With the inlet valve in the

piston, less heat would be transferred to the incoming gas because the inlet valve is not contained in the same piece of material through which the higher temperature discharge gas is flowing. The pressure drop across the valve would be reduced by allowing valve diameter to be increased and because the piston would move into a standing column of gas during the intake stroke, rather than having to accelerate a column of gas. In addition, it would be possible to increase the area of and thus reduce the pressure drop of the discharge valve. Two preliminary layout drawings of proposed inlet valve-in-piston designs for which the present compressor piston could be reworked are shown in Figures 4-21 and 4-22. With the design shown in Figure 4-21 it will be necessary to optimize the balance between inertia force and spring force for the desired operating speed. The spring must be designed to perform within the anticipated temperature range. The design shown in Figure 4-22 has two basic advantages over the design shown in Figure 4-21. The first advantage is that it has no spring and therefore, has no low temperature spring forces problem to contend with. The second advantage is that it will dynamically function properly at any speed up to the lower of two possible critical speed limits. One critical speed limit is the speed at which the inertia force of the annular sliding portion of the piston becomes greater than the combined force of cylinder wall friction and the force due to pressure acting on the annular area outside the seating diameter when the driven portion of piston is being decelerated as it approaches TDC. This critical speed will increase as the discharge pressure is increased and it can be accurately calculated. When the critical speed is reached during test, the inlet valve will open before TDC and an abrupt change in performance will

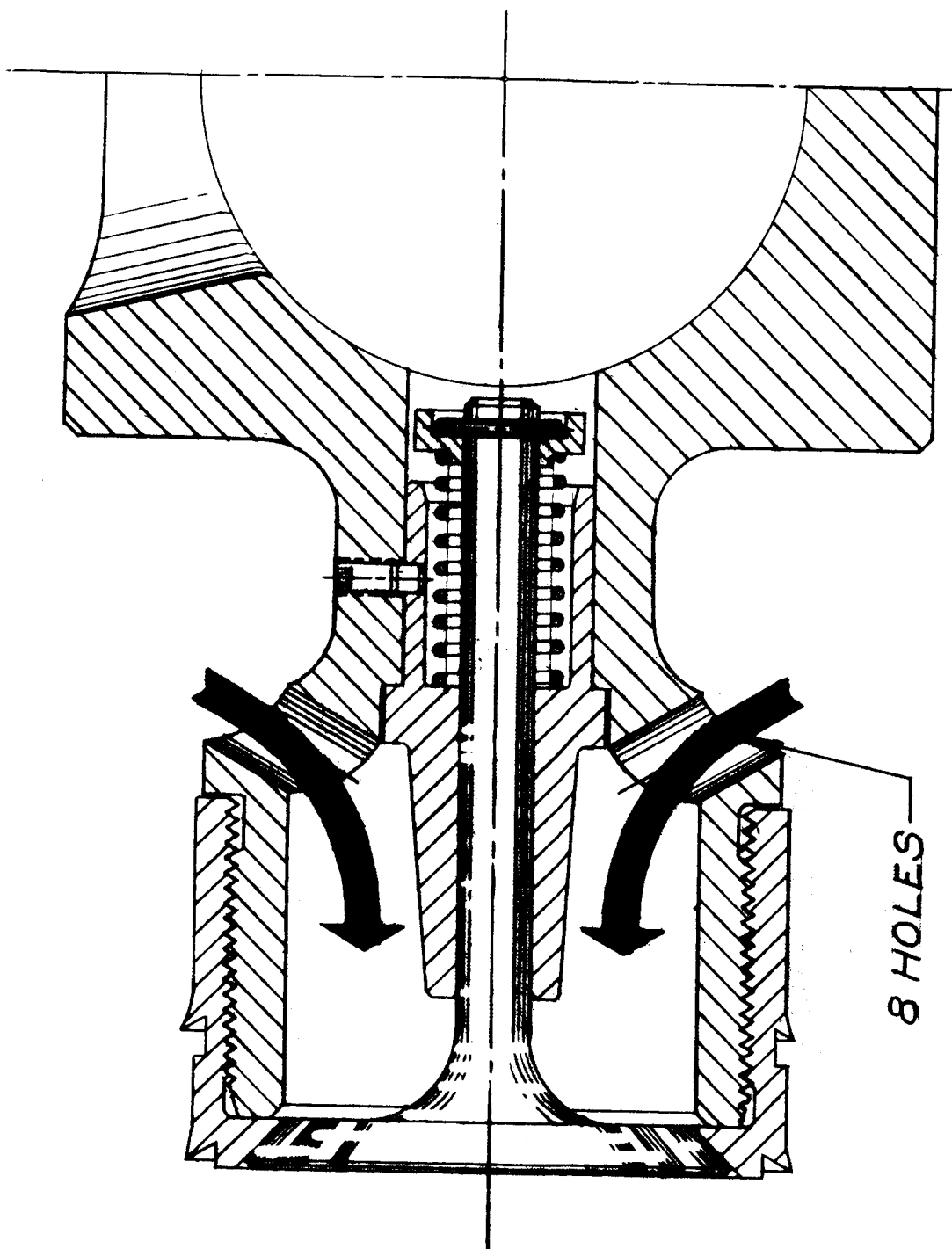


Fig. 4-21 - Spring Loaded First Stage Inlet Valve-in-Piston

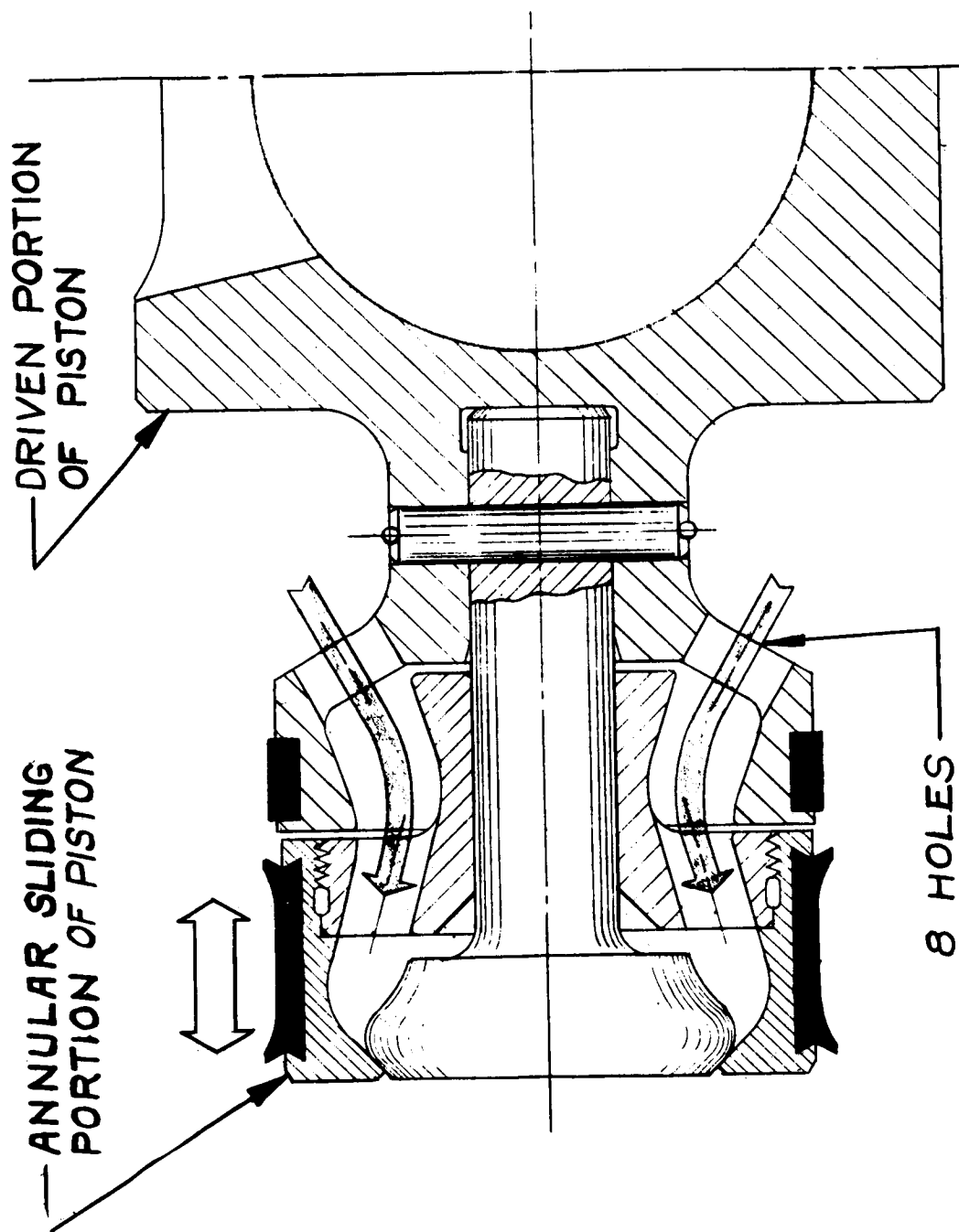


Fig. 4-22 - Friction Actuated First Stage Inlet
Valve-in-Piston

be detected.

The second critical speed will not be as abrupt as the one just described. If the clearance is small, thus causing residual pressure to decay rapidly, with respect to volume increase, the valve will be opened during the inlet stroke a short distance from TDC by the combined forces of cylinder friction and inertia acting on the annular sliding portion of piston. The valve will remain open until the driven portion of the piston reaches BDC. The open valve dwell time at BDC will allow for further filling by pressure equalization. These last statements are true until a critical speed is reached at which the inertia force tending to close the valve becomes greater than the friction force tending to hold it open. After this speed has been reached, the performance will slowly decrease as speed is further increased. The accuracy of calculated values for this critical speed will depend upon how well friction force is defined.

REFERENCES

1. NASA Contractor Report CR-55060, Phase Report on NASA Contract NAS 3-2550. "Development of a Hydrogen-Oxygen Internal Combustion Engine Auxiliary Power Supply System" by N. E. Morgan, September 30, 1963.
2. ASD-TDR-62-961 Final Report on Air Force Contract AF33(616)8406 "Hydrogen-Oxygen Internal Combustion Engine" by R. C. Thomas, W. A. Bass, N. E. Morgan, January 15, 1963.
3. H. M. Cameron and N. E. Morgan "Development of a Hydrogen-Oxygen Fueled 3 KW Internal Combustion Engine." AIAA Paper 64-756, September 4, 1964, Philadelphia.
4. N. E. Morgan "Hydrogen-Oxygen Space Power Internal Combustion Engine" ASME Paper 64-WA/AV-9, November 30, 1964, New York.
5. J. D. McCullough: "Engine Cylinder Pressure Measurements" SAE Transactions Volume 61, 1953, Pp 557-567.

APPENDIX A

FAILURE REPORT AND SUMMARY SHEETS

ENGINE FAILURE MODES

1. Oxygen Injector
 - A. Broken flex pivot
 - B. Static seal leak
 - C. Bushing to shaft seizure
 - D. Leaf spring retainer deformed
 - E. Flame-plated valve worn
 - F. Rocker shaft Brinelled
 - G. Rocker shaft galled
 - H. O₂ injector rocker arm and poppet wear
 - I. Leaf spring broke
 - J. Retainer broke
2. Engine
 - A. H₂ valve assembly leakage
 - B. Catalyst plug gasket leak
 - C. H₂ valve retainer ring broke
 - D. Piston dome retaining screw broke
 - E. Piston seized in cylinder
 - F. Top cylinder-to-cooling jacket
"O" ring failure
 - G. Copper, head-to-cylinder gasket
 - H. Haskel "K" seal leakage
 - I. Top of cylinder cracked
 - J. Broken H₂ valve spring (inner)
 - K. Broken H₂ valve spring (outer)
 - L. H₂ valve spider broke
 - M. Lockwire piston body bolts
 - N. Piston dome stud braze

VICKERS INCORPORATED
FAILURE REPORT & SUMMARY SHEET
FOR NASA CONTRACT NASA 3-2787
MARK I H₂ - O₂ ENGINE MODEL EA-1570-515

Sheet 1 of 6

Failure No.	Data Sheet No. Time & Date of Failure	Part Name	Part No. & Serial No.	Description of Failure (The Part Condition)	Description of Conditions (Active on Part prior to Failure)	Failure Mode No.	Cumulative Time on Part in Hours	Action Taken
1	D. S. 18	O ₂ Injector Flex Pivot	X610104	Broken Flex Pivot	Engine shut down due to tendency of oxygen valve to stick open.	1A	1.17 Cold 0.7 Hot	New flex pivot installed
2	D. S. 21	O ₂ Injector Flex Pivot	X610104	Broken flex pivot	Engine cylinder head temperature was low and could not be increased.	1A	4.3 Cold 1.25 Hot	New flex pivot installed; poppet refinished and lapped; seat guide lapped.
3	D. S. 23	O ₂ Injector Face Seal	X610113	Leaking haskel seal	Engine stopped because O ₂ ΔP gauge showed increased flow.	1B		New seal installed.
4	D. S. 23	O ₂ Injector Flex Pivot	X610104	Flex pivot broken	Cylinder head temperature could not be raised to 1400° F and O ₂ flow fluctuated excessively	1A	1.47 Hot	Pivot removed and replaced with a new stainless flex pivot.
5	D. S. 27, 28-10-12-63	O ₂ Injector Flex Pivot	X610104	All three bands of O ₂ injector flex pivot broken.	Engine stopped when O ₂ flow fluctuated excessively.	1A	2.36 Hot	New flex pivot installed
6	10-18-63	O ₂ Injector Bushing	X611376	Flame plated bearing seized in bushing. Bushing had started to come out of body.	Engine started and O ₂ flow increased to full flow.	1C	1.13 Cold 1 Min Hot	Bushing pressed back into body.
7	D. S. 33	O ₂ Injector Bushing	X611376	O ₂ Injector was sticking. Flame plated bushing and shaft seized together.	Engine stopped when O ₂ flow became erratic.	1C	6.15 Hot	Bushing honed out for an 0.0008 to 0.001 clearance and counter-bored to prevent end of shaft from rubbing on bushing.
8	11-1-63	O ₂ Injector Retainer	X611378	Leaf spring had been deformed around end of valve.	Normal inspection of O ₂ injector.	1D	4.12 Hot	New retainer installed.

VICKERS INCORPORATED
FAILURE REPORT & SUMMARY SHEET
FOR NASA CONTRACT NASA 3-2787
MARK I H₂ - O₂ ENGINE MODEL EA-1570-515

Sheet 2 of 6

Failure No.	Data Sheet No. Time & Date of Failure	Part Name	Part No. & Serial No.	Description of Failure (The Part Condition)	Description of Conditions (Active on Part prior to Failure)	Failure Mode No.	Cumulative Time on Part in Hours	Action Taken
9	11-13-63	O ₂ Valve	X611402	Some flame plated material came off seat area.	Test stand used for test valve run using cold gas.	1E	1.13 Cold	Valve sent to NASA Lewis for examination.
10	11-16-63	O ₂ Injector Retainer	X611378	Leaf spring had been deformed around end of valve.	Normal inspection of O ₂ injector.	1D	3.87 Hot	New retainer installed.
11	11-19-63	H ₂ Valve Assembly	X611414	Seals in H ₂ valve assembly leaking.	Engine stopped when flames were observed coming from H ₂ valve assembly.	2A	3.83 Hot	New H ₂ valve assembly seals installed. One copper seal made. H ₂ manifold brazed.
12	12-7-63	O ₂ Injector Valve	X611402	Some flame plated material came off seat area.	Test stand used for test valve run using cold gas.	1E	0.50 Cold	Valve to be returned to Linde Co. for examination and recommendation.
13	11-21-63	H ₂ Valve Assembly	X611414	Seals in H ₂ valve assembly leaking.	Engine stopped when flames came out of H ₂ valve assembly.	2A	0.10 Hot	New seals installed.
14	11-23-63	O ₂ Injector Valve	X611402	Excessive wear on guide area of valve (flame plated).	Engine stopped when O ₂ injector could not be controlled.	1E	5.0 Hot	Valve sent to NASA Lewis for metallurgist examination.
15	12-12-63	O ₂ Injector Retainer	X611378	Leaf spring retainer deformed around end of valve.	Normal inspection of injector.	1D	9.2 Hot	New retainer installed.
16	12-12-63	H ₂ Valve Assembly Ring	X610171	H ₂ valve ring worn through.	Normal disassembly for inspection of O ₂ injector.	2C	13.65	New ring installed.
17	12-20-63	H ₂ Valve Assembly		H ₂ valve assembly leakage.	Engine stopped when fire came out of top seal of H ₂ valve assembly. Note: The 3 screws had loosened and may have caused the leak.	2A	0.68 Hot	New seals installed.

VICKERS INCORPORATED
FAILURE REPORT & SUMMARY SHEET
FOR NASA CONTRACT NASA 3-2787
MARK I H₂ - O₂ ENGINE MODEL EA-1570-515

Sheet 3 of 6

Failure No.	Data Sheet No. Time & Date of Failure.	Part Name	Part No. & Serial No.	Description of Failure (The Part Condition)	Description of Conditions (Active on Part prior to Failure)	Failure Mode No.	Cumulative Time on Part in Hours	Action Taken
18	1-17-64	Piston Dome Retaining Screw	X611408	Piston dome retaining screw failed in tension allowing piston dome to jam between piston and cylinder head, thus causing the engine to stop abruptly.	Engine had been run hot for 43 minutes when a strange noise started followed by an abrupt stop of the engine.	2D	9.0 Cold 6.26 Hot	Use new piston design now being fabricated. Interim Corrective Action: 1. Reduce installing torque from 80in-lb to 50in-lb. 2. Design rework to reduce or eliminate leakage and to increase screw diameter.
19	2-6-64	O ₂ injector rocker shaft	X610099	Rocker shaft was Brinelled by needle bearings.	Engine had been run for 14 hours endurance run.	1F	37.8	Evaluate oilite bushing bearing.
20	3-12-64	O ₂ injector rocker shaft	X610099	Rocker shaft was galled by lower iron oilite bearings.	Engine did not run steady and O ₂ injector lift had dropped.	1G	0.68 Hot 0.42 Cold	Shaft polished and hardened. Alternate bearing materials and shaft finishes to be evaluated.
21	3-30-64	Piston Assembly	X612030	Piston seized to cylinder due to local thermal expansion of piston top nearest O ₂ inlet port.	Head insert deflecting O ₂ axially down cylinder onto piston.	2E	1 Min Hot 6.9 Cold	Increase piston-to-cylinder clearance and reposition head insert.
22	3-31-64	Piston Assembly	X612030	Piston rings and top of piston scored cylinder and started to seize in cylinder.	Piston to cylinder and ring gap clearance still insufficient.	2E	3 Min Hot 7.0 Cold	Further increase piston-to-cylinder clearance and increase ring gap.
23	4-10-64	O Ring	X612049	"O" Ring leaked Dowtherm at top of cylinder.	Cylinder wall temperature was higher than expected.	2F	2.1 Hot	New "O" Rings installed. Viton "A" "O"-Rings Ordered

VICKERS INCORPORATED
FAILURE REPORT & SUMMARY SHEET
FOR NASA CONTRACT NASA 3-2787
MARK I H₂ - O₂ ENGINE MODEL EA-1570-515

Sheet 4 of 6

Failure No.	Data Sheet No. Time & Date of Failure	Part Name	Part No. & Serial No.	Description of Failure (The Part Condition)	Description of Conditions (Active on Part prior to Failure)	Failure Mode No.	Cumulative Time on Part in Hours	Action Taken
24	4-13-64	O Ring	X612049	2F		2F	0.7 Hot	New "O" Rings installed. Viton "A" 'O'-Rings ordered
25	4-14-64	O Ring	X612049	2F		2F	0.37 Hot	SK 15822 Viton O Rings installed.
26	4-16-64	Head Seal	X612207	Head seal leaked during run	Flame came out from under head.	2G	0.37 Hot	New seal installed
27	4-21-64	O Ring	SK 15822	2F		2F	1.54 Hot 1.92 Cold	New O Ring installed
28	4-22-64	O Ring	SK 15822	2F		2F	0.93 Hot	New O Ring installed
29	4-27-64	O Ring	SK 15822	2F		2F	2.38 Hot	New O Ring installed
30	4-28-64	O Ring	SK 15822	2F		2F	0.32 Hot	New O Ring installed
31	4-28-64	Head Seal	X612207	2G	Flame came out from under head	2G	0.32 Hot	New seal installed
32	5-1-64	Head Seal	X612207	2G		2G	1.60 Hot	New seal installed
33	5-1-64	Haskel Seal	X609921	Haskel "K" seal leaked	Leaked after run	2H	2.55 Hot	New seal installed
34	5-5-64	Head Seal	X612207	2G		2G	3.58 Cold 0.97 Hot	New seal installed
35	5-5-64	Haskel Seal	X609921	2H		2H	3.58 Cold 0.97 Hot	New seal installed
36	5-12-64	Head Seal	X612207	2G		2G	2.22 Cold 5 Min Hot	New seal installed

VICKERS INCORPORATED
FAILURE REPORT & SUMMARY SHEET
FOR NASA CONTRACT NASA 3-2787
MARK I H₂ - O₂ ENGINE MODEL EA-1570-515

Sheet 5 of 6

Failure No.	Data Sheet No. Time & Date of Failure	Part Name	Part No. & Serial No.	Description of Failure (The Part Condition)	Description of Conditions (Active on Part prior to Failure)	Failure Mode No.	Cumulative Time on Part in Hours	Action Taken
37	5-12-64	Haskel Seal	X609921	2H		2H	2.22 Cold 5 Min Hot	New seal installed
38	5-13-64	Head Seal	X612207	2G		2G	0.7 Hot	New stainless seal installed
39	5-23-64	Haskel Seal	X609921	2H		2H	1.68 Hr. 49 Min Hot	Design study
40	5-23-64	O ₂ Rocker Arm O ₂ Poppet Valve	X612212 SK154154	Seating surfaces worn Poppet seat worn concave	Valve lift reduced after run	1H	1h38m cold 105h8m hot	Design study
41	5-27-64	Haskel Seal	X609921	2H		2H	1hr3m	New seal installed
42	6-2-64	Haskel Seal	X609921	2H		2H	1.2 Hr.	New seal installed
43	6-5-64	Cylinder Assy.	SK15858	Top of cylinder cracked		2I	27 Hr.	New cylinder assy. installed
44	6-11-64	Haskel Seal	X609921	2H		2H	1.75Hr.	New seal installed
45	6-18-64	H ₂ Valve Spring SK15449		H ₂ Valve spring found to be broken	H ₂ flow erratic	2J	91.0Hr.	New spring installed
46	6-28-64	H ₂ Valve Spring SK15450		H ₂ Valve spring found to be broken	H ₂ flow erratic	2K	110.5H	New spring installed
47	6-29-64	O ₂ Leaf Spring		O ₂ spring broke	O ₂ flow excessive	1I	39.4	Spring eliminated from design

VICKERS INCORPORATED
FAILURE REPORT & SUMMARY SHEET
FOR NASA CONTRACT NASA 3-2787
MARK I H₂ - O₂ ENGINE MODEL EA-1570-515

Sheet 6 of 6

Failure No.	Data Sheet No. Time & Date of Failure	Part Name	Part No. & Serial No.	Description of Failure (The Part Condition)	Description of Conditions (Active on Part Prior to Failure)	Failure Mode No.	Cumulative Time on Part in Hours	Action Taken
48	7-3-64	Lockwire		Piston bolts lockwire cut by rod.		2M		Modify assembly procedure and break edge of rod.
49	7-3-64	Piston Assy.	X612029	Piston dome stud braze melted.		2N	179.5	Heliarc weld.
50	7-10-64	O ₂ Retainer	X612216	O ₂ poppet retainer broke.	Erratic O ₂ flow.	1J	80.1	Use thicker retainer.
51	7-21-64	H ₂ Valve Spider	X610162	Spider broken at snap ring groove.		2L	120.0	Use new design.
52	7-22-64	H ₂ Valve Spider	X611416	Spider broken through safety pin hole.		2L	6.0	Replace with o'd design with hardened tips.
53	7-27-64	H ₂ Valve Spider	X610162	Spider broken at snap ring groove.		2L	7.0	Replace
54	8-24-64	H ₂ Valve Spider	X611416	Spider broken through safety pin hole.	Engine #2	2L	1.2	

APPENDIX B

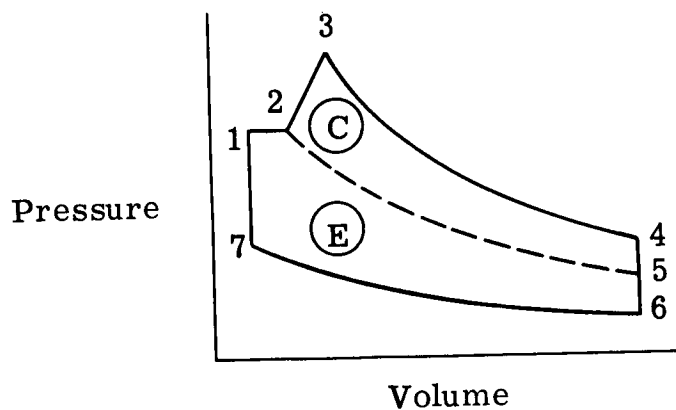
DERIVATION OF ENGINE INPUT ENERGY

The evaluation of the energy input to an internal combustion engine which operates with a high pressure ratio across it must account for the energy available from gas expansion as well as from the heat of combustion.

Thus

$$E_{in_{tot}} = E_{in_{expansion}} + E_{in_{combustion}}$$

Typical P-V diagram of internal combustion expansion engine



P_1 = Inlet (supply) pressure

P_6 = Exhaust pressure

Simplifying Assumptions: Refer to Fig. 1.

1. The expansion energy input is represented by area \textcircled{E} = 1-2-5-6-7-1 on Fig. 1.
2. The combustion energy input is represented by area \textcircled{C} = 2-3-4-5-2 on Fig. 1.
3. Ignore recompression work, i. e. the area under 6-7 on Fig. 1. Recompression work is theoretically zero for engine operating in space with zero absolute exhaust pressure.
4. The pressure ratio (or available expansion ratio) across the engine is infinite when operating in space with zero exhaust pressure.
5. For fuel (H_2) rich operating conditions assume that all of the fuel (H_2) acts as expander working fluid and the oxidizer provides only a source of heat.
6. Thus the input energy consists of:
 - a. Expansion work available from the consumed hydrogen at engine inlet temperature expanding thru an infinite expansion ratio.
 - b. Combustion energy available from burning the oxygen at 6480 Btu per lb of O_2 (LHV) for the $\text{H}_2 + \text{O}_2$ reaction.

EVALUATE HYDROGEN EXPANSION ENERGY

Using assumptions 3 and 4, the energy available from isentropic expansion is

$$E_{\text{exp}} = \frac{\gamma}{\gamma - 1} RT_i \left[1 - \left(\frac{P_e}{P_i} \right)^{\frac{\gamma-1}{\gamma}} \right] \frac{\text{lb} \cdot \text{ft}}{\text{lb}}$$

For an infinite pressure ratio this becomes

$$E_{\text{exp}} = \frac{\gamma}{\gamma - 1} RT_i$$

EVALUATE COMBUSTION ENERGY

Heat release from the hydrogen-oxygen reaction (L. H. V.) is:

$$Q_i = 51800 \text{ Btu/lb of } H_2 \text{ reacted}$$

$$\text{or } Q_i = \frac{51800}{8} = 6480 \text{ Btu/lb of } O_2$$

with excess hydrogen it is assumed that all of the oxygen is consumed.

TOTAL INPUT ENERGY

$$E_{\text{in}_{\text{tot}}} = E_{\text{in}_{\text{exp}}} + E_{\text{in}_{\text{comb}}}$$

$$E_{\text{tot}} = \left(\frac{\gamma}{\gamma - 1} RT_i \right) (w_{H_2}) + Q_i (w_{O_2})$$

where w_{H_2} , w_{O_2} = mass flow per cycle

$$E_{tot} = w_{H_2} \left[\left(\frac{\gamma}{\gamma - 1} RT_i \right) + \frac{w_{O_2}}{w_{H_2}} Q_i \right]$$

Let $\frac{w_{O_2}}{w_{H_2}} = O/F$ (oxidizer/fuel ratio)

$$E_{tot} = w_{H_2} \left[\frac{\gamma}{\gamma - 1} RT + \frac{O}{F} Q_i \right]$$

Let N = engine speed, rpm or cycles/min.

$$\text{Then } w_{H_2} = \frac{\dot{W}_{H_2} \text{ (lb/hr)}}{60N \text{ (cycles/hr)}}$$

$$E_{tot} = \frac{\dot{W}_{H_2}}{60N} \left[\frac{\gamma}{\gamma - 1} RT_{i_{H_2}} + \frac{O}{F} Q_i \right]$$

To evaluate E_{tot} :

$$\left. \begin{array}{l} \gamma = 1.4 \\ R = 772 \frac{\text{ft} \cdot \text{lb}}{\text{lb}^o R} \end{array} \right\} \text{ for } H_2 \quad Q_i = 6480 \text{ Btu/lb of } O_2$$

$$778 \frac{\text{ft} \cdot \text{lb}}{\text{Btu}}$$

$$E_{tot} = \frac{\dot{W}_{H_2}}{60N} \left[\frac{1.4}{.4} \times \frac{772 T_{i_{H_2}}}{778} + 6480 O/F \right] \text{ Btu/cycle}$$

$$E_{\text{tot}} = \frac{\dot{W}_{H_2}}{60N} \left[3.48 T_{iH_2} + 6480 \text{ O/F} \right] \text{ Btu/cycle}$$

$$E_{\text{tot}} = \frac{3.48 \dot{W}_{H_2}}{60N} \left[T_{iH_2} + 1860 \text{ O/F} \right]$$

$$E_{\text{tot}} = \frac{\dot{W}_{H_2}}{17.25N} \left[T_{iH_2} + 1860 \text{ O/F} \right]$$

In order to compare engine output in terms of BMEP, convert input energy to MEP (mean effective pressure) units by:

- (a) Divide by piston displacement
- (b) Convert Btu to lb · in.

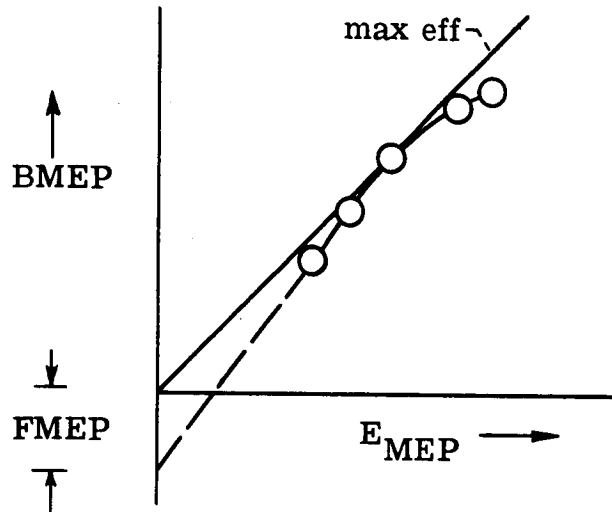
$$E_{\text{MEP}} = \frac{\dot{W}_{H_2}}{17.25N D} \left[T_{iH_2} + 1860 \text{ O/F} \right] \times 12 \times 778 \text{ psi}$$

$$E_{\text{MEP}} = \frac{540 \dot{W}_{H_2}}{ND} \left[T_{iH_2} + 1860 \text{ O/F} \right] \text{ psi}$$

The hydrogen-oxygen internal combustion engine tested in this program has a displacement of 2.72 cu in. Thus for this engine

$$E_{\text{MEP}} = \frac{199 \dot{W}_{H_2}}{ND} \left[T_{iH_2} + 1860 \text{ O/F} \right] \text{ psi}$$

To evaluate overall engine performance plot BMEP vs E_{MEP}



For evaluation of certain engine losses, it may be useful to modify the input energy expression to account for only that portion of the available energy which a given engine configuration could theoretically use.

For example: An engine cannot utilize an infinite pressure ratio because of the mechanical limitations to expansion ratio achievable in the cylinder. Thus, if the expression for E_{MEP} were modified to allow for limited expansion ratio, the unavailable energy in the engine exhaust would not be included in E_{MEP} and other losses might be more readily recognized.

The expansion energy available with a finite expansion ratio is

$$E_{exp} = \frac{\gamma}{\gamma - 1} RT_i \left[1 - \left(\frac{V_1}{V_5} \right)^{\gamma-1} \right]$$

Ref: Fig. 1.

The maximum expansion ratio available in an engine is V_5/V_1

The combustion energy available is also subject to expansion ratio limitations. Thus

$$Q_{iA} = Q_{i\text{comb}} \left[1 - \left(\frac{V_1}{V_5} \right)^{\gamma-1} \right]$$

assuming heat release occurs instantaneously at V_1 .

Thus, with expansion ratio limitations, the available input energy becomes

$$E_{A\text{MEP}} = \frac{540 \dot{W}_{H_2}}{ND} \left[T_{iH_2} + 1860 \text{ O/F} \right] \left[1 - \left(\frac{V_1}{V_5} \right)^{\gamma-1} \right]$$

For the experimental engine tested in this program, most meaningful data were obtained with a clearance volume of 8.5% of piston displacement. Thus

$$\frac{V_1}{V_5} = \frac{C}{1+C} = \frac{0.085}{1.085} = 0.0784$$

$$\text{and } \left[1 - \left(\frac{V_1}{V_5} \right)^{\gamma-1} \right] = 0.638$$

Thus, for 8.5% Cl vol and 2.72 cu in. displ., the available input MEP is

$$E_{A_{MEP}} = \frac{127 W_{H_2}}{N} \left[T_{i_{H_2}} + 1860(O/F) \right]$$

APPENDIX C

ANALYSIS OF EXHAUST GAS

National Engineering Science Company

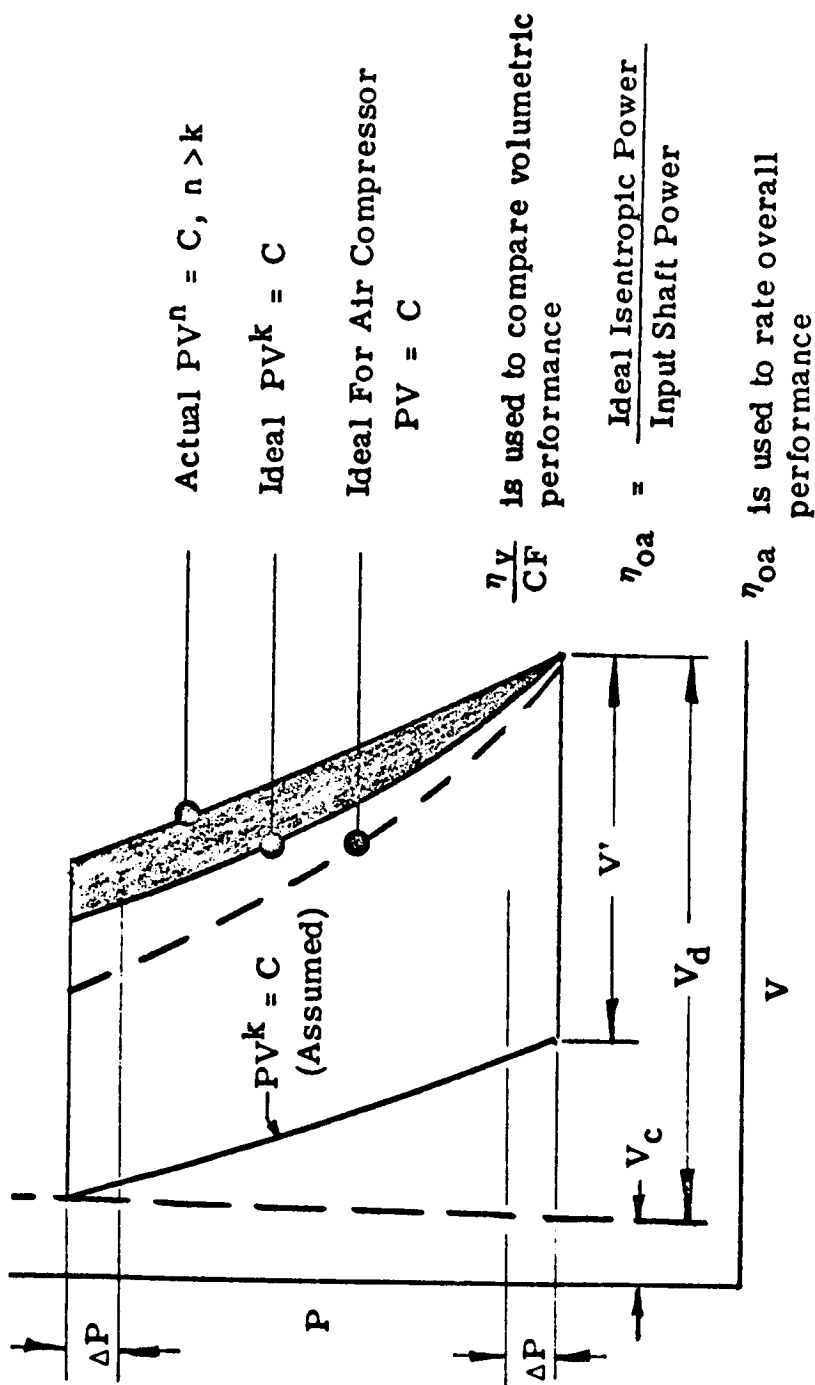
Following are results of analyses on three samples of exhaust gas:

Sample	3000-4:00	3000-3:45	4300-3:50
O ₂	0.092	0.14	0.17
N ₂	0.92	0.95	0.93
H ₂ O	3.2	4.1	5.3
H ₂	Remainder	Remainder	Remainder

The figures are volume percentages; the small oxygen percentages are estimated accurate to 0.05. Air may not have been entirely removed from the space before the stopcock. If this is so, then the oxygen values are higher than they should be. The variation in water analyses may be related to sampling methods but may also be related to water absorption in the mass spectrometer. This instrumental surface absorption of water leads to continued outgasing and progressively higher water analyses with like samples.

APPENDIX D

PERFORMANCE GRAPH



$$CF = \text{Ideal } \eta_v = \frac{V'}{V_d} = 1 + \frac{V_c}{V_d} - \frac{V_c}{V_d} \left\{ \frac{P_{out}}{P_{in}} \right\}^{1/k}$$

$$\eta_v = \frac{\text{Weight of gas discharged per cycle}}{\text{Weight of gas that would occupy piston displacement under intake conditions per cycle}}$$

APPENDIX E

SAMPLE DATA SHEETS AND DATA REDUCTION FORMS

VICKERS INCORPORATED STD TEST DATA SHEET
FOR NASA CONTRACT NASA 3-2787
MARK I H₂ - O₂ ENGINE MODEL NUMBER EA 1570-515
TEST STAND NO. II

Data Sheet No. 29, Test Order No. 59
Build Up Sheet No. ENG NPT II
Test Engr. L. Sheeks Date 6-11-69
Test Objective ENDURANCE

Cyl. Head Type MUSHROOM
Flow Tube Orifice Dia.: H₂ 0.036 in., O₂ 0.023 in.
H₂ Valve Phase 10° B TDC to 35° A TDC
O₂ Valve Phase 15° A TDC to 55° A TDC
Lub. Meter Motor Size N.A.
Starting O₂ Valve Lift 15° ATDC
O₂ Orifice: Type CONICAL

Total Running Time of this Test * Hrs.
Previously Accumulated Time 3 hr. 12 min. Hrs.
Was objective accomplished? YES

Write observations & comments in space below,

Stopped at 3:37 because of oil leak RESTART 8:22 P.M. O₂ Tot 144.0144
at gear case cover line "B" not fitting Set 1.84.0137

Observers:

Item No.	Item	Units	Clock Time of Reading							
			1:00 P	2:00	3:00 P	8:38 P	9:00	9:30	10:00 P	10:22 P
1	Line Current	Amps	50.2	47.5	47	53	51	50.5	51	
2	Excit. Field Current	Amps	3	3	3	3	3	3	3	
3	Arm. Volts	Volts	23	22.5	22.5	22.6	22.9	23.1	23.1	
4	Speed	rpm	3002	3004	3008	3015	2991	2980	3016	
5	H ₂ Inlet Press. to Engine	psig	300	300	300	300	300	300	300	
6	O ₂ Inlet Press. to Engine	psig	680	650	780	540	520	525	540	
7	H ₂ Flow Tube Press.	psig	310	310	310	310	310	310	310	
8	O ₂ Flow Tube Press.	psig	680	650	780	540	520	525	540	
9	H ₂ Flow Tube ΔP	In. of H ₂ O	134	140	140	135	135	130	137	
10	O ₂ Flow Tube ΔP	In. of H ₂ O	73	52	61	100	100	101	102	
11	Cyl. Coolant Flow	gpm	313	314	337	323	329	323	347	
12	Lub. Pressure	psig	43	45	45	45	48	48	48	
13	Lub. Meter Motor Speed	rpm	1425	1444	1265	1348	1482	1530	1528	
14	Vacuum Press.	In. of Hg.	190	202	205	186	181	184	188	
15										
16										
17	H ₂ Flow Tube Temp	°F T ₁	94	93	92	80	85	86	82	
18	O ₂ Flow Tube Temp	°F T ₂	76	76	78	66	68	71	73	
19	H ₂ Engine Inlet Temp	°F T ₁₁	500	500	500	505	500	485	490	
20	O ₂ Engine Inlet Temp	°F T ₉	81	82	81	70	72	73	74	
21	Dyno. Arm. Temp	°F								
22	Dyno Series Field Temp	°F T ₄	68	67	70	60	60	58	59	
23	Cyl. Coolant Inlet Temp	°F T ₅	210	211	210	179	197	208	210	
24	Cyl. Coolant Outlet Temp	°F T ₆	241	241	230	235	240	247	248	
25	Lub. Inlet Temp	°F T ₇	185	185	180	165	180	186	188	
26	Lub. Outlet Temp	°F T ₈	200	200	193	183	195	200	202	
27	Cyl. Wall Temp Top	°F T ₁₃	484	460	450	455	465	485	475	
28	Cyl. Wall Temp Top	°F T ₁₄	460	435	430	470	470	485	480	
29	Cyl. Wall Temp Bot.	°F T ₁₅	290	281	270	285	285	305	305	
30	Head Temp	°F T ₁₇	1495	1428	1415	1435	1425	1430	1415	
31	O ₂ Injector Nose Temp	°F T ₁₆	1025	965	955	1005	1005	1000	995	
32	Eng. Exh.	T ₁₂	425	398	370	455	450	455	465	
33										
34	Acc. Time	*	3 hr. 42 min	4 hr. 42 min	5 hr. 42 min	15 MIN	37 MIN	1 hr 7 min	1 hr 37 min	
35										
36										
37	Cooling Fluid									
38	Peak Cyl. Temp K or B.P.	psig								

VICKERS INCORPORATED DATA REDUCTION SHEET FOR
HYDROGEN-OXYGEN INTERNAL COMBUSTION ENGINE
TEST STAND NO. II

Data Sheet No. 22, Date Data was Taken 6-11-64
This Data was Reduced by R.F.M. on 6-12-64
Instructions: This sheet to be attached to data sheet and placed in data book

Item No.	Calculations to obtain		Clock Time of Reading							
			1:00	3:00	5:00	7:30	9:00	9:30	10:00	
(1) Speed	(4)	rpm	3002	3004	3008	3015	3021	3030	3036	
(2) I Line (I_{dyno})	(1) x 1.04 **	Amps	522	484	489	551	530	525	530	
(3) V Line (V_{dyno})	(3)	Volts	23	22.5	22.5	22.6	22.9	23.1	23.1	
(4) (IV) Line	(2) x (3)	Watts	1201	1112	1120	1245	1244	1213	1234	
(5) Arm. Temp.	(2)	°F								
(6) Series Field Temp	(2)	°F	68	67	70	60	60	58	59	
(7) Ar. & S. Field Resis	Curve (with (5) & (6))	OHMS								
(8) (I _R + BRUSH) Loss	Curve (with (7) & (2))	Watts	122.5	124.0	122.5	141.0	135.0	133.5	135.0	
(9) I Excit. (I_F)	(2)	Amps	3	3	3	3	3	3	3	
(10) Stray Loss	Curve (with (1) & (9))	Watts	540	540	540	573	538	536	543	
(11) Power Elect.	(4) + (8) + (10)	Watts	1873.5	1766.0	1762.5	1929	1807	1802.5	1902	
(12) Shaft H. P.	(11) (0.001341)	H. P.	2512	2382	2363	2587	2430	2404	2551	
(13) O ₂ F. T. Press.	(8) + 15 Psi	psia	675	665	795	555	535	540	555	
(14) O ₂ F. T. ΔP	(13)	in of H ₂ O	73	52	4	100	100	41	42	
(15) O ₂ F. T. Dia.	From Data Sheet	In.	0.203							
(16) O ₂ F. T. CxK	From Chart	--	0.1062	0.1073	0.1062	0.1051	0.0951	0.1046	0.1040	
(17) (13) x (14)	(13) x (14)	--	50235	46570	47475	55890	53500	54570	56110	
(18) (13) x (14)	(17)	--	225.5	186.0	230.7	236.0	231.5	233.8	238.0	
(19) W O ₂	(16) x (18)	--	2395	1886	2339	2480	2433	2472	2475	
(20) O ₂ F. T. Temp	(8) + 460 °R	°R	536	536	538	516	528	531	539	
(21) (20)	(20)	°R	2315	2315	232	2295	2300	2305	2306	
(22) (520/20)	22.8 / (21)	--	985	985	983	982	981	989	987	
(23) W O ₂ Corr for T.	(19) x (22)	lb/hr.	2359	1866	2289	2363	2411	2405	2448	
(24) H ₂ F. T. P	(13) + 15 Psi	psia	725							
(25) H ₂ F. T. 7P	(24)	In. of H ₂ O	124	140	140	135	135	130	132	
(26) H ₂ F. T. CxK	From Chart	--	0.095							
(27) (24) x (25)	(24) x (25)	--	43520	45500	45500	43875	43875	42250	43520	
(28) (24) x (25)	(27)	--	208.8	213.5	213.5	209.8	209.8	205.8	211.0	
(29) W of H ₂	(26) x (28)	lb/hr.	1994	2028	2028	1993	1993	1855	2005	
(30) H ₂ F. T. Temp	(17) + 460 °R	°R	554	553	552	540	545	546	547	
(31) (30)	(30)	°R	2358	2355	235	2235	2238	2240	2240	
(32) (520/30)	22.8 / (31)	--	967	968	970	981	985	974	974	
(33) W H ₂ Corr. for T.	(29) x (32)	--	1919	1963	1967	1955	1943	1894	1953	
(34) W Total	(23) + (33)	lb/hr.	4278	3949	4266	4418	4434	4299	4401	
(35) BSFC Shaft	(34) / (12)	lb/hp-hr.	1.703	1.649	1.805	1.708	1.721	1.707	1.725	
(36) O ₂ /H ₂ Ratio	(23) / (33)	lb/lb	1.629	1.402	1.669	1.260	1.241	1.263	1.253	
(37) Cyl. Flow	X *	gpm								
(38) Cyl. Tout	(2)	°F	241	241	230	225	240	247	248	
(39) Cyl. Tin	(2)	°F	20	21	20	179	187	208	210	
(40) CHAT			21	20	20	46	43	55	38	
(41)										
(42)										
(43) TORQUE	(2) x 63000 / (1)	IN-LB	52.7	50.0	98.5	54.1	59.3	53.4	53.3	
(44) BMEP	2.31 (43)	P.S.I.	122	115	114	125	123	123	123	
(45) BMEP/P	(44) / (3 + 15)	P.S.I./P.S.I.	.387	.365	.361	.396	.390	.390	.390	
(46)										
(47)										

○ Refers to reduction sheet items

△ Refers to data sheet items

* Downtherm Fluid etc.

* 4% METER CORRECTION

VICKERS INCORPORATED DATA REDUCTION SHEET
FOR NASA CONTRACT NAS 3-2787
PROTOTYPE COMPRESSOR MODEL EA-1570-516
DATA REDUCTION SHEET

Data Reduction Sheet No.: 47 Data Sheet No.: 47
Date of Data Reduction 6-25-64 Date Data Was Taken: 5/10/64
Data Was Reduced By: R. Cox
Reduction Was Checked By: _____

Item No.	Item	Calculations to Obtain	Units of	Data Point 1	Data Point 2	Data Point 3	Data Point 4	Data Point 5	Data Point 6	Data Point 7
1	Tare Torque	From Test Curve	in-lb	915	915	915	915	915		
2	Shaft Torque	3 - 1	in-lb	5.085	5.085	7.985	8.385	8.985		
3	Speed	4	rpm	3524	3522	3467	3557	3529		
4	Power	(2) 3 / 63025	H. P.	2.843	3.289	4.293	5.300	5.59		
5	Barometer	From Data Sheet	in. Hg.	29.26						
6	Barometer	(5) x 0.4912	psia	14.72						
7	Gas N ₂ - H ₂ - O ₂	2	--	H ₂	H ₂	H ₂	H ₂	H ₂		
8	Rotameter	8	mm	120	120	84	84	47		
9	144 V/R	From Rotam. Curv.	10 ⁻² °R/hr	10.15	8.5	8.02	7.3	4.62		
10	Rotam. Temp.	12 + 460	°R	517	517	517	517	517		
11	Act. Flow = \dot{W}_A	(9) x (6) / (10)	lb/hr	2070	2120	2283	2070	1315		
12	\dot{W}_A / hp	(11) / (4)	lb/hp-hr	1.065	2.358	5.197	3.921	2.352		
13	1st stg. X *	From Table		4.9210						
14	Stroke = s	From Data	in	519						
15	1st stg. SNX	(14) x (3) x (13)		9.001	8.993	8.853	9.080	9.011		
16	1st stg. P _{1in}	(5) + (5) x .4912	psia	19.63						
17	1st stg. T _{1in}	8 + 460	°R	343	340	343	340	348		
18	1st stg. \dot{W}_{VD}	(15) x (16) / (17)	lb/hr	5131	5192	5467	5247	5083		
19	1st stg. $\eta_v = \dot{W}_A / \dot{W}_{VD}$	(11) / (18)	Ratio	5610	461	4566	3860	2587		
20	1st stg. clearance	From Data	in	8.9						
21	1st stg. Y dead	From Table	in	8.64						
22	1st stg. CL _{tot}	(20) + (21)	in	92.54						
23	1st stg. C = $\frac{CL_{tot}}{s}$	(22) / (14)	Ratio	1809						
24	1st stg. P _{out}	6 + 6	psia	62.72	64.72	72.22	96.72	102.72		
25	1st stg. P _{out} /P _{in}	(24) / (16)	Ratio	3.175	3.297	4.061	4.927	5.589		
26	1st stg. (P _{out} /P _{in}) ^{1/N}	(25) 1/N **	--	2.225	2.247	2.725	3.128	3.421		
27	" C x (P _{out} /P _{in}) ^{1/N}	(23) x (26)	--	1122	1148	1332	1530	1673		
28	" CF	1 + (23) - (27)	Ratio	2.367	2.341	2.457	2.859	3.016		
29	η_v / CF	(19) / (28)	Ratio	2.382	4.990	4.921	4.420	2.834		
30	B* for 25 & 17	From Curve	B/ib°R/cyc	90	95	125	155	178		
31	B x \dot{W}_A x T _{1in}	(30) x (11) x (17)	B/cyc	81.21	76.17	93.80	89.51	81.46		
32	Ideal HP isen.	3.93 x 10 ⁻⁴ x (31)	HP	0.351	0.307	0.385	0.430	0.330		
33	η_{0a}	(32) / (4)	Ratio	1235	0.833	0.876	0.811	1.360		
34	2nd X	From Table	--	1.432						
35	2nd SNX	(14) x (3) x (34)	--	2615	2614	2593	2641	2617		
36	2nd T _{1in}	40 + 460	°R	515	520	530	508	500		
37	2nd \dot{W}_{VD}	(35) x (24) / (36)	lb/hr	3185	3253	3970	5028	5247		
38	2nd η_v	(11) / (37)	Ratio	974	7439	5899	4133	2200		
39	2nd P _{out}	7 + 6	°R psia	11422	26472	31472	76472	84472		
40	2nd P _{out} /P _{in}	(39) / (24)	--	1.8271	4.092	6.4066	7.965	8.3368		
41	2nd (P _{out} /P _{in}) ^{1/N}	(40) 1/N	--	1.522	2.742	3.000	4.390	4.550		
42	2nd Clearance	From Data	in	8190						
43	2nd Y dead	From Table	in	8125						
44	2nd CL _{tot}	(42) + (43)	in	8295						
45	2nd C = CL _{tot} /s	(44) / (14)	Ratio	8568						
46	2nd C x (P _o /P _n) ^{1/N}	(45) x (41)	--	8874	1557	2158	2493	2584		

O Refers to reduction sheet

Δ Refers to data sheet

1st Stage 2nd Stage

* X_{H₂} = 4.92 x 10⁻³ 1.43 x 10⁻³ ** Let 1/N = 0.715 or state reason
X_{N₂} = 6.84 x 10⁻² 1.99 x 10⁻² for other value.
X_{O₂} = 7.81 x 10⁻² 2.28 x 10⁻²

VICKERS INCORPORATED DATA REDUCTION SHEET
FOR NASA CONTRACT NAS3-2787
PROTOTYPE COMPRESSOR MODEL EA-1570-516

Data Sheet Number 47 Date Data Was Taken 5/18/64
 This Data Was Reduced By PEY On 6/25/64
 This sheet is to be attached to Data Sheet and placed in Data Book.

Item No.	Item	Calculations to obtain	Units of	DATA POINTS						
				1	2	3	4	5	6	7
47	2 nd CF	1 + (45) - (46)	Ratio	.9624	.9011	.8410	.8075	.7984		
48	2 nd Q _v /CF	(38) / (47)	Ratio	.9360	.8755	.7914	.5118	.2866		
49	Series P _{out} /P _{in}	(39) / (16)	Ratio	5.844	13.185	26.221	38.957	46.588		
50	B for (49) & (17)	From Curve	B/ab R/cyc	1.88	4.00	8.45				
51	B x T _{in}	(50) x (11) x (17)	B/cyc	106.36	332.12	426.77				
52	Ideal HP _{isen}	3.93 x 10 ⁻⁴ x (51)	HP	.0733	.1294	.1677				
53	η _{oa}	(52) / (4)	Ratio	.2575	.3934	.3817				

○ Refers to reduction sheet items

△ Refers to data sheet items